Thesis submitted for the degree of
Doctor of Philosophy

Exact and Numerical Methods in (Super)Conformal Field Theories

Gergely Kántor

Supervisor

Dr Constantinos Papageorgakis

June 27, 2022

Centre for Theoretical Physics
School of Physical and Chemical Sciences
Queen Mary University of London

This thesis is dedicated to my family,
for always being there for me in the hardest of times,
and helping me pursue my passions, no matter the distance.

Ezt a disszertációt a családomnak ajánlom,
akik mindig ott voltak a legnehezebb időkben is,
akármilyen távol voltak, és segítettek követni az álmaimat.

To see a World in a Grain of Sand
And a Heaven in a Wild Flower
Hold Infinity in the palm of your hand
And Eternity in an hour

– William Blake, *Auguries of Innocence*

Abstract

In this thesis we aim to study a variety of problems in (super)conformal field theories in various dimensions using both analytical and numerical techniques.

In the first chapter we hope to set the context in which this work appears by giving an account of the main historical events, both in theoretical physics and computer science which led up to this point, in a non-technical fashion.

In the second chapter we give a quick run-down of the prerequisite knowledge of conformal field theories, which will play a pivotal role in all the succeeding chapters.

The third chapter will start the core part of thesis where we present our findings. Here we will set up a novel algorithm using reinforcement learning (a subset of machine learning) to study conformal field theories in two dimensions, but without the use of Virasoro symmetry. A detailed description of the algorithms used will be presented as well as the numerical results obtained for some minimal models such as the: Ising model and the tri-critical Ising model. We also present numerical results for the free boson on a circle.

The fourth chapter uses a prescribed free-field realisation to recover the structure of 2D $\mathcal{N} = 2$ superconformal algebras. We present two algorithms which can derive the vacuum characters corresponding to these algebras. We calculate the vacuum characters for the algebras with underlying symmetry $\mathbb{Z}_3$, $\mathbb{Z}_4$, $\mathbb{Z}_6$ and $G(3, 1, 2)$ and explain their importance through the 2D/4D duality.

In the fifth chapter, forming the last of the core chapters, we look at the $\mathrm{AdS}_7/\mathrm{CFT}_6$ correspondence. Using a specific 7D supergravity black hole solution with 3 equal rotations and 2 equal charges, we determine its thermodynamic properties and establish the metric on the boundary. Using this boundary metric we evaluate the partition function of the circle reduced (2,0) theory on S^5 in the large N and Cardy-like limit, where we get the expected N^3 scaling and match with the supergravity side.

In the final chapter we present a summary of results and an overview of the tools used throughout the thesis. We conclude by justifying the use of numerical methods in theoretical physics and argue that all of these methods should be used in conjunction.

Acknowledgements

First and foremost my thanks go out to my supervisor, Dr Constantinos Papageorgakis. It is with fondness I recall all the time I spent in his office trying to explain to him some of my crazy revelations or listening to him share complex ideas with such ease. I could not have asked for more freedom in my PhD to explore my interests, which constituted a lot of my personal and academic growth. Even though we had this laissez-faire approach, he was always more than happy to provide guidance and tips along my journey.

There was never a dull day in my day-to-day life in academia thanks to the fellow PhD students and staff in the G.O. Jones building at QMUL. All the discussions, seminars, projects and inside jokes (of which there were too many) were indispensable for a fun and productive work place. I would like to personally thank some of the past and present students: Manuel Accettulli Huber, Rashid Alawadhi, Enrico Andriolo, George Barnes, Graham Brown, Stefano De Angelis, Josh Gowdy, Adrian Padellaro, David Peinador Veiga, Rajath Radhakrishnan, Lewis Sword, Sam Wikeley, Shun-Qing Zhang, Marcel Hughes, Ricardo Stark-Muchão, Nejc Čeplak, Rodolfo Panerai, Arnau Koemans Collado, Zoltán Laczkó, Joseph Hayling, Christopher Lewis-Brown, Ray Otsuki, Luigi Alfonsi, Nadia Bahjat-Abbas and Linfeng Li.

I would also like to very warmly thank my friends outside academia, who kept me cheerful with their company and endured my occasional physics lectures. I would like to particularly thank Sargam Gurung, Snehan Sighat, Helina Berhane, Nikolakis Palamidas, Elizabeth Violet Christiansen, Oliver Bradley, Jess Ruane, Meg Young, Yoan Stoyanov, David Robertson, Chris Robinson, Alex Hackett and Luke Harris.

I also wish to thank my Master's Essay supervisor Professor David Tong for many enlightening conversations about my project into 3D Bosonisation, as well as his lecture notes, which provided most of my early insight into theoretical physics. I thank Professor Sarben Sarkar who helped me with my postgraduate applications while at King's College London. Last, but not least, I would like to thank my high school teachers Chris and Kerry Gray, and their endless motivation which they passed on to me.

Ugyancsak szeretném megköszönni a segítséget és támogatást magyar barátaimnak, ismerőseimnek, különösen Lengyel Tamásnak, valamint a Karinthy Frigyes ÁMK Általános Iskola tanári karának.

Declaration

I, Gergely Kántor, confirm that the research included within this thesis is my own work or that where it has been carried out in collaboration with, or supported by others, that this is duly acknowledged below and my contribution indicated. Previously published material is also acknowledged below.

I attest that I have exercised reasonable care to ensure that the work is original, and does not to the best of my knowledge break any UK law, infringe any third party's copyright or other Intellectual Property Right, or contain any confidential material.

I accept that the College has the right to use plagiarism detection software to check the electronic version of the thesis.

I confirm that this thesis has not been previously submitted for the award of a degree by this or any other university.

The copyright of this thesis rests with the author and no quotation from it or information derived from it may be published without the prior written consent of the author.

Signature:

Date: June 27, 2022

Details of collaboration and publications:

This thesis describes research carried out with my supervisor Constantinos Papageorgakis, which was published in [1, 2, 3, 4]. We collaborated with Paul Richmond in [1]; with Prarit Agarwal and Enrico Andriolo in [2]; and with Vasilis Niarchos in [3, 4]. It also contains some unpublished material. Where other sources have been used, they are cited in the bibliography.

Contents

Chapter 1

Introduction

Just like experimental physicists rely on their instruments and apparatuses to make measurements, theoretical physicists rely on a set of tools to extract physics from certain mathematical models. One can reasonably continue this analogy further, as the quality of the apparatus improves, so does the ability of the physicist to make experimental observations (in most cases). This is very much the case in theory too, where applying new and or more sophisticated techniques to existing problems might make all the difference. For this very reason the evolution of the subjects of mathematics and physics has been very closely linked. While fundamentally mathematics exists as a self contained subject, physics requires a medium to describe all that we observe around us, and mathematics very much fits that bill. This means that while many physical paradigm shifting ideas might start as empirical observations or ideas of a non-quantitative nature, eventually they are translated into mathematical formulations which serve to fit observations. Perhaps the most curious artifact of this relationship is when this link is used in reverse, and new, but detached mathematical topics are applied to existing physical theorems to extend and push the boundaries of our understanding further using the intrinsic rigour and abstractness of mathematics. The vast unexplored landscape of mathematics, and also numerical mathematics, a computational subarea which we shall explore in great detail too, provide the desired metaphorical toolbox where one can search for the next course-altering revelation to be found.

Perhaps one of the most fitting places to start the tale of the evolution of tools is with calculus. Of course these days not using differentiation or integration is almost unimaginable, but these tools were developed initially by Sir Isaac Newton, Gottfried Liebniz and Bernhard Riemann just to name a select few, and their development continued for centuries, being perfected even to this day. Building on these discoveries, the work on statistical mechanics and thermodynamics in the 1870s by Ludwig Boltzmann and James Clerk Maxwell, among others, left the physical community stunned. It opened up a whole new world of analysing physical systems with enormous amounts of degrees of freedom by looking at the dynamics statistically and considering microstates

of the system and through that the entropy, and so much more. These foundations would then inadvertently pave the way to our modern understanding of physics and also a certain subset of data science called machine learning (ML). Continuing on the trajectory we have started on leads us to the turn of the twentieth century which most would agree hosted some of the largest paradigm shifts physics has ever seen. This period saw the famous Solvay conferences which were devoted to the outstanding problems in physics and chemistry at the time. The participants whose names are widely known these days, (and listing them would exhaust all the space available in the introduction) have developed the tools which we already consider modern physics. This was the time which saw the rise of quantum mechanics (QM), which describes particles as probabilistic distributions, wave functions, previously unheard of. In addition to that, in the first two decades of the twentieth century another set of the most important physical theories was developed: Albert Einstein's special and general theories of relativity (GR). It is almost impossible to say how significant the development of QM and GR was to the world of science. These brand new ideas in theoretical physics allowed for better predictions when comparing with experiments. They revolutionised the way we thought about the structure of the atom, and its subatomic components. GR also allowed us to explain the perihelion precession of the planet Mercury, which until that point was unexplained.

The shiny new tools of QM and GR inspired people to start combining ideas and making use of the link we described before. This resulted in the development of one of the crown jewels of physics besides GR and the spiritual successor to QM, namely, quantum field theory (QFT). It arose from many decades of work by brilliant physicists trying to combine quantum mechanics and special relativity in a mathematically and physically consistent way. It is one of the most prominent frameworks being used to date and people are still trying to figure out its implications and predictions. Along the same lines, coming from the extension of statistical mechanics, the similar subject of statistical field theory (SFT) was discovered. Further analysis of SFTs led to the classifications of the ones that arise from statistical systems and how they change when one starts to coarse grain and look at the physics contained within the initial high energy theory from the perspective of the low energy theory. This way of thinking inspired the concept of the renormalisation group (RG) flows, which was pioneered by Kenneth Wilson around the 1970s. It could describe flows which took theories away from critical points, or back to critical points or even between critical points. These critical points became a massive centre of interest in the realm of theoretical physics. The reason being their very special properties, which include large amounts of invariances, or symmetries, due to their scale invariance, which made them much easier to analyse than their non-restricted counterparts. Theories which describe critical points of these SFTs or even QFTs became known as conformal field theories (CFTs).

One of the biggest ambitions in contemporary theoretical physics is to find the so-called theory of everything, or grand unified theory. Our current best understanding of the quantum world comes from a QFT description known as the Standard Model of Particle Physics (SM). It describes the interactions between almost all the fundamental subatomic particles we currently understand that exist in nature, where these interactions are mediated by gauge bosons, and are responsible for the strong, weak and electromagnetic interactions. It is not all the subatomic interactions, because the SM makes no mention of gravity or GR. Hence the ambition of unification was ignited by trying to reconcile these two theories. The application of the quantum framework to gravity leads to the appearance of divergences, which is not the worrisome part. Infinities appear quite a lot in QFTs, but in the study of quantum gravity they cannot be dealt with by standard renormalisation techniques employed in the study of QFTs. Nevertheless this has not stopped the advance of physics into new realms where we might find a solution. The last half a century saw the rise of supersymmetry, which can be used to extend the existing Poincaré symmetry of QFTs and hence include more particles which can describe the ones missing from the Standard Model. The other novelty introduced was String Theory. These two together form the currently the most investigated framework in theoretical physics besides the previously mentioned quantum field theory. The novelty is that in String Theory particles are swapped with one-dimensional string objects which can be closed or open — describing either gravitational or other interactions —, and only take the shape of strings when observed at high energies, while at low energies they recreate our well known world of particles. These two were brought together to create superstrings, which decrease the spacetime dimension these strings are required to live in (from mathematical and physical constraints) from 26 down to 10 dimensions. This is still quite a bit more than one would find just strolling about at home, but methods of consistent dimensional reductions could eventually lead the way to finding a promising theory out of the countless ones String Theory offers.

The appearance of these modern frameworks of physics inspired countless state-of-the-art tools with which the implications and the physical contents can be analysed in order to gain insight into what such constructions truly mean. Perhaps the most popular tool devised in recent years has been the AdS/CFT correspondence (also referred to as the gauge-gravity duality) conjectured in 1997 by Juan Maldacena [5]. This is a type of holographic duality which means that the information contained in a theory living in the space is encoded in the theory on the boundary of this space. The actual duality describes string theories, or M-theories (unifying superstring theory in 11D) in an anti-de Sitter space with an attached spherical space being dual to a conformal field theory living only on the AdS boundary. One such example of a duality is M-theory living on $\mathrm{AdS}_7 \times S^4$ which is equivalent to the so-called $(2,0)$ theory [6]. This theory is a very

special case of a superconformal field theory (CFTs which are also supersymmetric, SCFTs) as it lacks a Lagrangian description. It is at this point in the trajectory of the story where the work presented in this thesis enters the flow. Through the use of the AdS/CFT correspondence and also the superconformal index [7, 8], which is another tool one can use to analyse SCFTs, analogous to the vacuum characters of 2D CFTs, one can infer the spectrum of these theories. Another device which has potentially only gained significant traction in the analysis of SCFTs is the method of supersymmetric localisation [9]. Its origins come from mathematics, perfectly fitting the reverse link between mathematics and physics, and its potential is vast. In the successive chapters we tell the story of the cross-applications of these formidable tools and the results they managed to extract from open problems.

As it may be, during all the commotion caused by the impressive advances in theoretical physics we overlooked the similar progress in a subject which has now grown to be one of the most influential areas in the world — computer science, data science, and eventually machine learning. While we were focused on the quantum revolution, in the 1930s and 40s Alan Turing formulated the idea of the modern computer and also built his famous Bombe machine which cracked the Enigma code in World War 2. Building machines which could perform calculations as well as logical operations was a huge breakthrough not only in computer science, but also the rest of the sciences. Even the most simple of numerical methods the "brute force" method has become somewhat within arms reach. In this method one would attempt to do a calculation in a straight forward way without any (or moderate) simplifications, also known as the exhaustive search. Also in the 1940s, started the area of machine learning (ML) when the first mathematical foundations for neural networks were laid down by Walter Pitts and Warren McCulloch [10]. The aim of ML being to create computer algorithms which can make decisions without the prompt of a pre-written code. An example would be classification algorithms, where the algorithm would build its own intuition on how to discriminate between the classes, rather than using logic statements written by humans in code. At the time, with the computing power available this would have been a dream, but as we shall see, that dream will come very close to reality.

In the following decades, as people and corporations realised the power of computers, their processing power has exploded exponentially. In 1965 an American engineer called Gordon Moore based on empirical observations declared that the number of transistors (related to processing power) doubles every year [11]. This as we saw turned out to be very much the case and would lead to the rise of numerical computations in science. In the branch of experimental physics the increase of computational power was fast integrated, since processing and storing the large amounts of data arising from experiments demanded it. Theoretical physics is a bit more stubborn, which is of course due to the fact that an analytic solution to a problem is considered much more powerful

than a numerical one. On the other hand numerical solutions to theoretical problems have the opportunity to offer the insight to otherwise unapproachable problems. One of these has been the emergent area of numerical relativity in the late 1980s and early 90s [12] which to this days shows much potential in analysing solutions to Einstein's equations. The outlook has been steadily improving for the application of numerical approaches to theoretical physics arriving into the 21st century. As we established before, the importance of CFTs is immeasurable and their analysis warrants all available tools, and to that end the algorithm of numerical conformal bootstrap was born [13] in 2008. Using this one could constrain the parameters of CFTs.

Finally, we arrive at the re-ignition of machine learning and data science. The initial problems of ML were that it demanded large amounts of memory and processing power. Nowadays, power and memory which can already train machine learning algorithms exists for anyone to use. This availability caused the subject to gain immense popularity and be applied to an endless amount of subjects. In more recent years algorithms from ML have begun to manifest in theoretical physics as well. Some recent interesting ones include applications to the string landscape and vacua with different approaches [14, 15], among other inspiring works [16, 17, 18, 19]. This thesis aims to join the pioneering works presented by the aforementioned applications of ML to theoretical physics, and venture towards establishing new machinery in the world of conformal field theories.

1.1 Outline

The structure of this thesis might take an unorthodox format, nevertheless we aim to present an overarching story connecting the works presented across three seemingly unrelated chapters. The theme of developing and perfecting the tool set of theoretical physics, both analytical and numerical, is the ultimate aim of this thesis. Each of the chapters in this thesis contains enough information to be understood alone, and some contain their own reviews and contextual introductions.

In Chapter 2 we aim to give a short summary of all the relevant information on conformal field theories (CFTs) required to understand the research in this thesis. In Sections 2.1-2.2 we describe the conformal algebra, which is relevant to all the topics discussed later in the thesis. In Sec. 2.3 we introduce facts for CFTs in various dimensions along with Sec. 2.4, where we focus more on the 2D crossing equations. They will be relevant for Chapter 3. Sections 2.5-2.6 describe 2D algebras and focus on Kac-Moody and vertex operator algebras, which will be used mostly in Chapter 4.

In Chapter 3 we introduce the use of reinforcement-learning (RL) techniques to the conformal-bootstrap programme. We then move on to presenting a short recap of modern numerical bootstrap techniques in Sec. 3.3, which will then allow us to contrast it with the RL algorithm. In Sec. 3.4 we present the theoretical background required to

understand how RL algorithms work and also give detailed examples on how the algorithm can be implemented and run in Sec. 3.4.4 and 3.4.5. We then demonstrate that suitable soft Actor-Critic RL algorithms can perform efficient, relatively cheap high-dimensional searches in the space of scaling dimensions and OPE-squared coefficients that produce sensible results for tens of CFT data from a single crossing equation. Later in this chapter we test this approach in well-known 2D CFTs, with particular focus on the Ising and tri-critical Ising models in Sec. 3.5 and the free compactified boson CFT in Sec. 3.6. We present results of as high as 36-dimensional (number of free parameters) searches, whose sole input is the expected number of operators per spin in a truncation of the conformal-block decomposition of the crossing equations. Our study of 2D CFTs in this chapter uses only the global $\mathfrak{so}(2,2)$ part of the conformal algebra, and our methods are equally applicable to higher-dimensional CFTs. When combined with other, already available, numerical and analytical methods, we expect our approach to yield an exciting new window into the non-perturbative structure of arbitrary (unitary or non-unitary) CFTs.

In Chapter 4 we start by presenting a short literature review on the subject of vertex operator algebras. Equipped with this knowledge, in Sec. 4.2 we aim to define all relevant superconformal algebras which will form the backbone of our research. Sec. 4.3.1 serves as a guide to the recipe provided by [20] and we give a detailed step-by-step guide showing how it can be implemented. Following closely the prescription of [20], in Sec. 4.4-4.5 we will meticulously build from the ground up $\mathcal{N}=2$ and small $\mathcal{N}=4$ algebras using this novel free-field realisation. Now that we have the algebras in the free-field representations at our disposal, in Sec. 4.7, we will introduce two algorithms for calculating the vacuum characters for the previously introduced vertex operator algebras. In addition to that we will also provide a source to download our codes and use them. In sections 4.7.3-4.7.6 we brute-force evaluate the vacuum character for $\mathcal{N}=2$ vertex operator algebras labelled by crystallographic complex reflection groups $G(k,1,1)=\mathbb{Z}_k$, $k=3,4,6$, and $G(3,1,2)$. For $\mathbb{Z}_{3,4}$ and $G(3,1,2)$ these vacuum characters have been conjectured to respectively reproduce the Macdonald limit of the superconformal index for rank one and rank two S-fold $\mathcal{N}=3$ theories in four dimensions. For the $\mathbb{Z}_3$ case, and in the limit where the Macdonald index reduces to the Schur index, we find agreement with predictions from the literature.

In Chapter 5 our aim is to generalise the work of [21] for the case of $\mathrm{AdS}_7/\mathrm{CFT}_6$. In order to build up to that, we first introduce the concept of localisation. First in Sec. 5.2.1-5.2.2 we present the mathematical background, and Atiyah-Bott-Berline-Vergne Localisation. This serves as a mathematical framework for the physics analogue: supersymmetric localisation. Sec. 5.3 serves as a toy example based on [22] in order to show in simple terms the capabilities of the localisation procedure. From Sec. 5.4 we begin to present our findings, starting from the 2-equivalent charge, 3-equivalent

rotation non-extremal black-hole solution in 7D gauged supergravity. In Sections 5.4.4-5.4.5 we consider the supersymmetric and then the extremal limit and evaluate the associated thermodynamic quantities. Away from extremality, the black-hole solution becomes complex. The entropy is then given by the Legendre transform of the on-shell action with respect to two complex chemical potentials subject to a constraint. In Sec. 5.5, at the conformal boundary of AdS_7 we look at the dual background and evaluate the corresponding partition function for the A_{N-1} 6D (2,0) theory at large N in a Cardy-like limit. This is carried out in Sec. 5.5.2, via a 5D $\mathcal{N} = 2$ super Yang–Mills calculation on S^5. The gravitational on-shell action is found to be exactly reproduced by the boundary partition function at large N.

In the final chapter we will start by briefly summarising all the major results which were presented in each of the preceding chapters and commenting on the methodology employed to arrive at the results, and also where applicable highlighting the shortcomings and advantages of such an approach. In the ultimate section of this chapter we will aim to further discuss what one can learn from applying such a variety of tools in modern theoretical physics, and also to hypothesise where they might be heading to in the future.

Chapter 2

A Brief Review of Conformal Field Theories

In what follows we assume some familiarity with the basic concepts of conformal field theory. For a review of conformal field theory we refer the reader to the standard textbook [23] and the recent overviews in [24, 25, 26], which summarise the more modern perspective on CFTs above two dimensions. In Sec. 2.1-2.2 we state the fundamental constituents and properties of conformal symmetries and the conformal algebra in diverse dimensions. Sec. 2.3 provides a general, but more in depth overview of useful properties for CFTs in any spacetime dimension. In Sec. 2.4 we specialise the discussion to 2D CFTs, which will be the main focus of the computations in the later parts of this thesis. Some extra computations will be discussed later on in Sec. 3.2.

2.1 The Global Part of the Conformal Algebra

This is the part of the CFT algebra in two dimensions which makes contact with the other dimensions. By this we mean that this part of the algebra exists analogously in higher dimensions due to the fact that it is a global symmetry. There are four fundamental parts of this global symmetry. The first two—rotations ($M_{\mu\nu}$) and translations (P_μ)—actually form a subgroup which is the well-known Poincaré algebra or the algebra of the Euclidean group depending on the signature of the space. The third one is dilations (D), which scale distances. The ultimate part is the most mysterious, called special conformal transformations (K_μ), but it can be imagined as an inversion ($x^\mu \to \frac{x^\mu}{x^2}$) followed by a translation, and then by another inversion. Formally one can summarise their actions written in terms of space(-time) coordinates as:

$$\begin{aligned} P_\mu &= -i\partial_\mu \\ L_{\mu\nu} &= -i\left(x_\mu\partial_\nu - x_\nu\partial_\mu\right) \end{aligned}$$

$$\begin{aligned} D &= x^\mu \partial_\mu \\ K_\mu &= i\left(2x_\mu x^\nu \partial_\nu - x^2 \partial_\mu\right). \end{aligned} \tag{2.1}$$

These generators obey the well-known commutation relations:

$$\begin{aligned} [D, P_\mu] &= P_\mu \\ [D, K_\mu] &= -K_\mu \\ [K_\mu, P_\nu] &= 2\left(\delta_{\mu\nu} D - i M_{\mu\nu}\right) \\ [K_\rho, M_{\mu\nu}] &= i\left(\delta_{\rho\nu} K_\mu - \delta_{\rho\mu} K_\nu\right) \\ [P_\rho, M_{\mu\nu}] &= i\left(\delta_{\rho\nu} P_\mu - \delta_{\rho\mu} P_\nu\right) \\ [M_{\mu\nu}, M_{\rho\sigma}] &= i\left(\delta_{\mu\rho} M_{\nu\sigma} + \delta_{\nu\sigma} M_{\mu\rho} - \delta_{\nu\rho} M_{\mu\sigma} - \delta_{\mu\sigma} M_{\nu\rho}\right). \end{aligned} \tag{2.2}$$

Using this algebra one could go down the usual representation theory route and start classifying the representations of this algebra by the rotational subgroup and also the dilation operator by assigning a spin and a conformal dimension to the representations. While this is very important, we will mostly keep to discussing the function of the algebra itself and just declare the spin and the dimension to be the usual eigenvalues of the Cartans of the relevant rotation group and dilation operators.

As we mentioned before, this algebra is actually valid in any number of dimensions, but we will stick to two dimensions specifically. We will make this manifest by explicitly changing our coordinates to complex coordinates

$$z = x^1 - i x^2, \quad \bar{z} = x^1 + i x^2, \quad \partial_z = \frac{1}{2}\left(\partial_1 + i\partial_2\right), \quad \partial_{\bar{z}} = \frac{1}{2}\left(\partial_1 - i\partial_2\right). \tag{2.3}$$

It is important to note that in Euclidean signature these will obey that $z^* = \bar{z}$, while in Lorentzian signature they will take the form of independent real variables. The star here means the usual complex conjugation. From here on we will find it most useful to view z and $\bar{z}$ as independent complex coordinates, with the constraint $z^* = \bar{z}$ implying a particular physical Euclidean slice.

Using this complex notation we can reparametrise our global algebra as

$$\begin{aligned} L_{+1} &= \frac{1}{2}\left(K^1 - iK^2\right), & \bar{L}_{+1} &= \frac{1}{2}\left(K^1 + iK^2\right), \\ L_0 &= \frac{1}{2}\left(D - iM_{12}\right), & \bar{L}_0 &= \frac{1}{2}\left(D + iM_{12}\right), \\ L_{-1} &= \frac{1}{2}\left(P_1 + iP_2\right), & \bar{L}_{-1} &= \frac{1}{2}\left(P_1 - iP_2\right). \end{aligned} \tag{2.4}$$

From this we can clearly see that the holomorphic and anti-holomorphic parts form

separate algebras, with the only non-zero commutators being:

$$\begin{aligned}[L_m, L_n] &= (m-n)L_{m+n}, \text{ for } m,n = 0, \pm 1 \\ \left[\bar{L}_m, \bar{L}_n\right] &= (m-n)\bar{L}_{m+n}, \text{ for } m,n = 0, \pm 1\end{aligned} \tag{2.5}$$

This format allows us to clearly see that our global algebra is actually $\mathfrak{sl}(2) \times \overline{\mathfrak{sl}(2)}$.

2.2 The Infinite Dimensional Conformal Algebra

The global algebra above does not exhaust the full list of symmetries one has available when dealing with 2D conformal field theories. As it turns out there is a huge freedom which allows us to reparametrise the complex coordinates we defined above in any analytic way we like as such,

$$z \to f(z), \quad \bar{z} \to \bar{f}(\bar{z}). \tag{2.6}$$

Due to the analiticity of these functions, we can take a look at the infinitesimal transformations instigated by f and $\bar{f}$:

$$z \to z + \epsilon(z), \quad \bar{z} \to \bar{z} + \bar{\epsilon}(\bar{z}) \tag{2.7}$$

And making further use of the analytical nature of these transformations

$$\epsilon(z) = \sum_{n=-\infty}^{+\infty} z^{n+1}\epsilon_n. \tag{2.8}$$

The local nature of the theories we are considering allows us to define an energy-momentum tensor, $T_{\mu\nu}$. In these theories (coming from usual CFT constraints) the energy-momentum tensor is conserved and traceless. In the coordinates we defined these two constraints manifest as

$$T_{z\bar{z}} = T_{\bar{z}z} = 0 \tag{2.9}$$

$$\partial_{\bar{z}} T_{zz} = \partial_z T_{\bar{z}\bar{z}} = 0. \tag{2.10}$$

The first line implies that we only have two non-zero components in the energy-momentum tensor, while the second line tells us that one is holomorphic and the other is anti-holomorphic. Let us define these two objects as

$$T(z) = -2\pi T_{zz}, \quad \overline{T}(\bar{z}) = -2\pi T_{\bar{z}\bar{z}} \tag{2.11}$$

Where the strange coefficients are a convention.

The next step is to integrate over a boundary enclosing the energy-momentum tensor to obtain the charge relating to the conformal transformation (2.7).

$$Q_\epsilon = \frac{1}{2\pi i}\oint dz\epsilon(z)T(z) \tag{2.12}$$

Using complex analysis we can Laurent expand both T and $\overline{T}$ and define the so-called Virasoro L, $\bar{L}$ modes.

$$T(z) = \sum_{n=-\infty}^{+\infty} z^{-n-2}L_n, \quad L_n = \frac{1}{2\pi i}\oint dz z^{n+1}T(z) \tag{2.13}$$

For the sake of brevity we did not show the expansion for $\overline{T}$, but it is virtually the same, with its own modes $\bar{L}_n$. This allows us to rewrite equation (2.12) as

$$Q_c = \sum_{n=-\infty}^{+\infty} \epsilon_n L_n, \quad Q_{\bar{\epsilon}} = \sum_{n=-\infty}^{+\infty} \bar{\epsilon}_n \bar{L}_n, \tag{2.14}$$

which means that the charges are actually linear combinations of an infinite amount of generators of local conformal transformations. Of course these operators obey an algebra which is given by

$$\begin{aligned}
[L_m, L_n] &= (m-n)L_{m+n} + \frac{c}{12}\left(m^3 - m\right)\delta_{m+n,0} \\
\left[\bar{L}_m, \bar{L}_n\right] &= (m-n)\bar{L}_{m+n} + \frac{c}{12}\left(m^3 - m\right)\delta_{m+n,0} \\
\left[L_n, \bar{L}_m\right] &= 0.
\end{aligned} \tag{2.15}$$

This is the famous Virasoro algebra. One can observe that for $m, n = 0, \pm 1$ one gets back to the global algebra defined in equation (2.5).

2.3 General Aspects of CFTs

The $\mathfrak{so}(D, 2)$ conformal algebra of a CFT in D spacetime dimensions organises the spectrum of local operators/states of the theory in corresponding representations. A primary operator $\mathcal{O}_i$ has scaling dimension Δ_i and spin (under the $SO(D)$ Lorentz group) s_i. As we saw in the case $D = 2$ is special, since the $\mathfrak{so}(2, 2)$ part of the conformal algebra extends to the infinite-dimensional Virasoro algebra. It is, therefore, customary in 2D CFTs to refer to the operators that are highest-weights in Virasoro representations as primaries, while operators that are highest-weights in representations of the global part $\mathfrak{so}(2, 2)$ are called quasi-primary. Since we will be using only the $\mathfrak{so}(2, 2)$ structure of 2D CFTs, the reader should anticipate a clear distinction between primary and quasi-primary operators in the context of our applications.

A central object in the analysis of CFTs is the Operator Product Expansion (OPE), which allows one to recast the product of two conformal primaries $\mathcal{O}_i$, $\mathcal{O}_j$ as a sum over single conformal primaries and their descendants

$$\mathcal{O}_i(x_1)\mathcal{O}_j(x_2) = \sum_k C_{ij}^k \hat{f}_{ij}^k\,(x_1, x_2, \partial_{x_2})\,\mathcal{O}_k(x_2)\ . \tag{2.16}$$

The OPE coefficients C_{ij}^k are c-numbers that are closely connected to the three-point function coefficients C_{ijk} of the conformal primaries $\mathcal{O}_i, \mathcal{O}_j, \mathcal{O}_k$. For example, the two- and three-point functions of three conformal primary scalar operators are given by the expressions

$$\langle \mathcal{O}_i(x_1)\mathcal{O}_j(x_2)\rangle = \frac{g_{ij}}{|x_{12}|^{2\Delta}}\ ,\quad \text{for}\quad \Delta_i = \Delta_j \equiv \Delta\ , \tag{2.17}$$

$$\langle \mathcal{O}_i(x_1)\mathcal{O}_j(x_2)\mathcal{O}_k(x_3)\rangle = \frac{C_{ijk}}{|x_{12}|^{\Delta_{ij,k}}|x_{23}|^{\Delta_{jk,i}}|x_{13}|^{\Delta_{ik,j}}}\ , \tag{2.18}$$

with $\Delta_{ij,k} \equiv \Delta_i + \Delta_j - \Delta_k$ and $x_{ij} = x_i - x_j$. In this case, $C_{ijk} = \sum_k C_{ij}^m g_{mk}$. The conformal symmetry forces the two-point functions in (2.17) to vanish if $\Delta_i \neq \Delta_j$ and fixes the spacetime dependence of both the two- and three-point functions. For spinning operators the expressions in (2.17), (2.18) generalise to include the tensor structure of the spins. The quantity $\hat{f}_{ij}^k$ in the sum (2.16) is a differential operator that incorporates the contributions of all the conformal descendants in the conformal multiplet of $\mathcal{O}_k$. Its form is fixed by conformal symmetry.

The OPE (2.16) can be used to reduce a generic n-point function to a sum of products of three-point functions. Hence, the full dynamical content of local correlation functions in a CFT can be captured by the knowledge of two- and three-point functions. Equivalently, the solution of the local structure of a CFT entails the computation of the full spectrum of scaling dimensions Δ_i at each spin s_i and of the corresponding OPE coefficients C_{ij}^k.[1]

Four-point functions $\langle \mathcal{O}_{i_1}(x_1)\mathcal{O}_{i_2}(x_2)\mathcal{O}_{i_3}(x_3)\mathcal{O}_{i_4}(x_4)\rangle$ provide a powerful demonstration of this reduction. Unlike (2.17), (2.18), conformal symmetry does not completely fix the spacetime dependence of four-point functions. Solely from the viewpoint of conformal symmetries we can write

$$\langle \mathcal{O}_{i_1}(x_1)\mathcal{O}_{i_2}(x_2)\mathcal{O}_{i_3}(x_3)\mathcal{O}_{i_4}(x_4)\rangle = \boldsymbol{K}(\Delta_i, x_i)\, g(u,v)\ , \tag{2.19}$$

where the factor $\boldsymbol{K}(\Delta_i, x_i)$ has a fixed form (that will be written explicitly in two dimensions below), and $g(u,v)$ is a—typically complicated—theory-specific function of

[1] Another special feature of CFTs is the operator/state correspondence. We will frequently use it to interchange language between states and operators.

the cross-ratios

$$u = \frac{x_{12}^2 x_{34}^2}{x_{13}^2 x_{24}^2} \ , \quad v = \frac{x_{14}^2 x_{23}^2}{x_{13}^2 x_{24}^2} \ , \tag{2.20}$$

which are invariant under conformal transformations. The OPE expansion (2.16) of the products $\mathcal{O}_{i_1}\mathcal{O}_{i_2}$ and $\mathcal{O}_{i_3}\mathcal{O}_{i_4}$ allows us to recast (2.19) as

$$\langle \mathcal{O}_{i_1}(x_1)\mathcal{O}_{i_2}(x_2)\mathcal{O}_{i_3}(x_3)\mathcal{O}_{i_4}(x_4)\rangle = \boldsymbol{K}(\Delta_i, x_i) \sum_{k_1,k_2} C_{i_1 i_2}^{k_1} g_{k_1 k_2} C_{i_3 i_4}^{k_2} g_{\mathcal{O}_k}^{(i_1 i_2 i_3 i_4)}(u,v) \ , \tag{2.21}$$

where $g_{\mathcal{O}_k}^{(i_1 i_2 i_3 i_4)}(u,v)$ is the conformal block that captures the contribution of intermediate operators $\mathcal{O}_{k_1}$, $\mathcal{O}_{k_2}$ with equal scaling dimension Δ_k. The conformal blocks are theory-independent and, as already mentioned earlier, in many cases are either known analytically in closed form, or can be determined using convenient relations. Specific expressions for two-dimensional conformal blocks will be given momentarily.

It is customary (in the context of the so-called conformal frame) to re-express the cross-ratios in terms of two variables $z, \bar{z}$ as

$$u = z\bar{z} \ , \quad v = (1-z)(1-\bar{z}) \ . \tag{2.22}$$

In Euclidean CFT z and $\bar{z}$ are complex conjugate.

It is also customary to work in a basis of conformal primaries that diagonalises the two-point functions (2.17). This is a convenient choice in general, but it can be subtle in conformal manifolds for degenerate protected operators because of operator-mixing effects. In what follows we denote the OPE-squared sum at fixed scaling dimension Δ_k as

$$\mathfrak{C}_{i_1 i_2 i_3 i_4}^{k} \equiv \sum_{k_1,k_2 \,|\, \Delta_{k_1}=\Delta_{k_2}=\Delta_k} C_{i_1 i_2}^{k_1} g_{k_1 k_2} C_{i_3 i_4}^{k_2} \ . \tag{2.23}$$

In the absence of degeneracies in the spectrum of operators that run in this sum, the sum (2.23) comprises a single term. This is not, however, the only possibility and in some of the applications of the main text we will encounter cases where degeneracies do exist.

Obviously, the OPE expansion in (2.21) is not unique. Instead of using the OPEs $\mathcal{O}_{i_1}\mathcal{O}_{i_2}$ and $\mathcal{O}_{i_3}\mathcal{O}_{i_4}$ one can use the OPEs $\mathcal{O}_{i_3}\mathcal{O}_{i_2}$ and $\mathcal{O}_{i_1}\mathcal{O}_{i_4}$ to obtain a different looking, but equivalent, expansion of the four-point function. These two approaches yield respectively the so-called s- and t-channel expansions of the four-point function.[2] To distinguish the OPE-squared coefficients in each channel, we will denote the s-channel coefficients as ${}_s\mathfrak{C}_{i_1 i_2 i_3 i_4}^{k}$ and the t-channel coefficients as ${}_t\mathfrak{C}_{i_1 i_2 i_3 i_4}^{k}$. The t-channel

[2] It is also possible to consider the $(1,3)-(2,4)$ OPEs that yield the u-channel expansion. We will not be considering the u-channel expansion. We note that the s, t and u channel expansions do not converge simultaneously at all cross-ratio values. For further comments we refer the reader to the review [25].

can be obtained from the s-channel by exchanging the insertions $1 \leftrightarrow 3$ and equivalently the cross-ratios $u \leftrightarrow v$, or $z \leftrightarrow 1-z$ and $\bar{z} \leftrightarrow 1-\bar{z}$. The equality of the two expansions leads to the crossing symmetry constraints

$$\sum_k {}_s\mathfrak{C}^k_{i_1 i_2 i_3 i_4} g^{(i_1 i_2 i_3 i_4)}_{\Delta_k}(u,v) - \sum_{k'} {}_t\mathfrak{C}^{k'}_{i_1 i_2 i_3 i_4}\, h(\Delta_i; u, v) g^{(i_3 i_2 i_1 i_4)}_{\Delta_k}(v,u) = 0 \ , \tag{2.24}$$

where the factor $h(\Delta_i; u, v)$ accounts for the contribution of the prefactor $\boldsymbol{K}$.

In general, the operators that appear in the s-channel k-sum are different from the operators that appear in the t-channel k'-sum. Moreover, note that the crossing equations (2.24) have to be satisfied as functions of u, v at any values of u, v. This imposes stringent constraints on the CFT data of scaling dimensions and OPE coefficients.

2.4 Crossing Equations in 2D CFTs

It will be useful for our purposes to spell out the above results in the more specific case of two-dimensional CFTs.

The analysis of the crossing equations (2.24) requires explicit knowledge of the conformal blocks $g^{(i_1 i_2 i_3 i_4)}_{\Delta_k}(u,v)$. Over the years significant progress in the computation of conformal blocks (see [25] for a guide to the literature) has provided important input in the development of the conformal-bootstrap programme. In even-dimensional CFTs the conformal blocks in four-point functions of scalar operators are known analytically in closed form. In two-dimensional CFTs, in particular, they are also known analytically for any four-point function of spinless or spinning conformal primary operator [27]. The latter is one of the basic reasons why we will focus on 2D CFTs. We stress again that the aforementioned conformal blocks in two dimensions are conformal blocks for the global $\mathfrak{so}(2,2)$ part of the Virasoro algebra. We will not be using Virasoro conformal blocks.[3]

Concretely, consider four quasi-primary operators in a (Euclidean) 2D CFT denoted as $\mathcal{O}_i$ $(i = 1, 2, 3, 4)$ with left- and right-moving conformal weights $(h_i, \bar{h}_i)$. The corresponding scaling dimensions and spins of these operators are $\Delta_i = h_i + \bar{h}_i$ and $s_i = h_i - \bar{h}_i$. We insert the operators at four distinct spacetime points denoted in complex coordinates as $(z_i, \bar{z}_i)$. The s-channel conformal-block expansion of the four-point function of these operators is

[3] In two dimensions it would have been more efficient, in general, to work with the full Virasoro blocks. However, this would be problematic for us for two reasons. First, the general Virasoro conformal blocks are not known in closed analytic form (see, however, [28] for useful expansions of these quantities). Second—and more important—this would limit the direct applicability of our approach to the special features of two-dimensional CFTs.

$$\langle \mathcal{O}_1(z_1,\bar{z}_1)\mathcal{O}_2(z_2,\bar{z}_2)\mathcal{O}_3(z_3,\bar{z}_3)\mathcal{O}_4(z_4,\bar{z}_4)\rangle = \frac{1}{z_{12}^{h_1+h_2}z_{34}^{h_3+h_4}}\frac{1}{\bar{z}_{12}^{\bar{h}_1+\bar{h}_2}\bar{z}_{34}^{\bar{h}_3+\bar{h}_4}}$$
$$\times \left(\frac{z_{24}}{z_{14}}\right)^{h_{12}}\left(\frac{\bar{z}_{24}}{\bar{z}_{14}}\right)^{\bar{h}_{12}}\left(\frac{z_{14}}{z_{13}}\right)^{h_{34}}\left(\frac{\bar{z}_{14}}{\bar{z}_{13}}\right)^{\bar{h}_{34}}\sum_{\mathcal{O},\mathcal{O}'} C_{12}^{\mathcal{O}} g_{\mathcal{O}\mathcal{O}'} C_{34}^{\mathcal{O}'}\, g_{h,\bar{h}}^{1234}(z,\bar{z}) \ , \quad (2.25)$$

where $z_{ij} = z_i - z_j$,

$$g_{h,\bar{h}}^{1234}(z,\bar{z}) = z^h \bar{z}^{\bar{h}}\, {}_2F_1(h-h_{12}, h+h_{34}; 2h; z)\, {}_2F_1(\bar{h}-\bar{h}_{12}, \bar{h}+\bar{h}_{34}; 2\bar{h}; \bar{z}) \quad (2.26)$$

and

$$z = \frac{z_{12}z_{34}}{z_{13}z_{24}} \ , \quad \bar{z} = \frac{\bar{z}_{12}\bar{z}_{34}}{\bar{z}_{13}\bar{z}_{24}} \quad (2.27)$$

the complex parameters $z, \bar{z}$ that express the cross-ratios u, v in (2.22). We are also using the notation $h_{ij} = h_i - h_j$, while ${}_2F_1(a,b;c;z)$ is the ordinary hypergeometric function. Adapting (2.23), we also set

$$\sum_{\mathcal{O},\mathcal{O}' \,|\, \Delta_{\mathcal{O}}=\Delta_{\mathcal{O}'}=h+\bar{h}} C_{12}^{\mathcal{O}} g_{\mathcal{O}\mathcal{O}'} C_{34}^{\mathcal{O}'} \equiv {}_s\mathfrak{C}_{h,\bar{h}} \quad (2.28)$$

suppressing the reference to the operators $\mathcal{O}_i$.

In the above notation the crossing equations (2.24) take the form

$$\sum_{h,\bar{h}} {}_s\mathfrak{C}_{h,\bar{h}}\, g_{h,\bar{h}}^{(1234)}(z,\bar{z}) =$$
$$= (-1)^{(h_{41}+\bar{h}_{41})}\frac{z^{h_1+h_2}}{(z-1)^{h_2+h_3}}\frac{\bar{z}^{\bar{h}_1+\bar{h}_2}}{(\bar{z}-1)^{\bar{h}_2+\bar{h}_3}}\sum_{h',\bar{h}'} {}_t\mathfrak{C}_{h',\bar{h}'}\, g_{h',\bar{h}'}^{(3214)}(1-z,1-\bar{z}) \ . \quad (2.29)$$

At this point it is useful to make the following observations.

First, when one sums over the conformal block of a spinning quasi-primary operator (i.e. an operator with conformal weights $(h,\bar{h})$ and $h \neq \bar{h}$) in either channel, one is also summing over a quasi-primary with conformal weights $(\bar{h}, h)$. When we exchange h and $\bar{h}$, the spin $s \to -s$, and the corresponding OPE-squared coefficients $\mathfrak{C}_{h,\bar{h}}$ and $\mathfrak{C}_{\bar{h},h}$ are not in general equal. However, when the external operators are spinless, the OPE-squared coefficients are equal, $\mathfrak{C}_{h,\bar{h}} = \mathfrak{C}_{\bar{h},h}$, and we can collect together the $(h,\bar{h})$ and $(\bar{h},h)$ contributions to form a single conformal block of the form

$$\tilde{g}_{h,\bar{h}}^{(1234)}(z,\bar{z}) = \frac{1}{1+\delta_{h,\bar{h}}}\Big[z^h\bar{z}^{\bar{h}}\, {}_2F_1(h-h_{12}, h+h_{34}; 2h; z)$$
$$\times\, {}_2F_1(\bar{h}-\bar{h}_{12}, \bar{h}+\bar{h}_{34}; 2\bar{h}; \bar{z}) + (z \leftrightarrow \bar{z})\Big] \ . \quad (2.30)$$

In this manner, we can restrict the sums in (2.29) to only run over operators with $h \geq \bar{h}$, hence reducing by half the number of intermediate quasi-primary operators that we need to consider later in the thesis.

Second, it is useful to single-out the contribution of the identity operator, when this is present in a given channel, by setting $\mathfrak{C}_{0,0}\, g_{0,0}^{(1234)}(z,\bar{z}) = g_{12}g_{34}$.

2.5 Primaries versus Quasi-Primaries in More Detail

Primaries are a vital part of the group theoretic construction of CFTs. They form the set of *highest-weight states*, which annihilate a subset of the operators we defined above, and hence are used as fundamental building blocks of CFTs. However, as we have found out above, in two dimensions the algebra expands to an infinite dimensional group, so we have to be a bit careful. This is where the distinction of primaries versus quasi-primaries enters.

We established before that the operators $L_{-1,0,1}, \bar{L}_{-1,0,1}$ form the $\mathfrak{sl}(2)$ subalgebras of the Virasoro algebra. Quasi-primaries are states which are annihilated by the action of L_1 or $\bar{L}_1$, and have the eigenvalues h and $\bar{h}$ under the action of L_0 and $\bar{L}_0$ respectively. h and $\bar{h}$ are referred to as the holomorphic and anti-holomorphic conformal dimension. In terms of the $T(z)$ OPE this translates to

$$T(z)\phi(0) \sim \underbrace{\dots}_{\text{not constrained}} + \overbrace{\frac{0}{z^3}}^{\text{must vanish}} + \frac{h_\phi \phi(0)}{z^2} + \frac{\partial\phi(0)}{z} + \dots \tag{2.31}$$

Essentially the few constraints we described above are reflected in what we can see in this OPE. We took the operator $\phi(z)$ to be our primary, and the constraints make the order z^{-3} term vanish and constrain the form of the z^{-2} and z^{-1} terms. Most importantly however they do not restrict the form of the smaller powers in the Laurent expansion.

Now that we have explained quasi-primaries, primaries are very simple to motivate. If we move to the whole Virasoro algebra, we will have a whole set of L_n and $\bar{L}_n$ operators. The premise is similar to what we did before, but now we constrain our state such that it is annihilated by all $n > 0$ for both barred and unbarred L's. As one can imagine, this is an infinitely more powerful constraint as the one we had for quasi-primaries, and it actually reads like this for the $T(z)$ OPE

$$T(z)\phi(0) \sim \underbrace{0}_{\text{must vanish}} + \frac{h_\phi \phi(0)}{z^2} + \frac{\partial\phi(0)}{z} + \dots \tag{2.32}$$

As we can see, the new constraints completely remove all the coefficients of any powers smaller than -2 and constrain the form of the remaining ones.

2.6 Vertex Operator and Affine Kac-Moody Algebras

In Chapter 4, we will be studying the 4D/2D correspondence [29] and this correspondence states that any four-dimensional $\mathcal{N} = 2$ SCFT possesses a subsector which can be identified with a two-dimensional chiral algebra. These two-dimensional chiral algebras are defined as the holomorphic parts of a 2D CFT, otherwise also called *meromorphic CFTs*, or even more commonly in mathematical context, *vertex operator algebras* (VOAs). We shall briefly introduce Affine Kac-Moody (AKM) algebras in this subsection, because they will be very relevant to the results we will present in the following sections. AKMs are an extension of the algebras presented above (in two dimensions) with an additional flavour symmetry. This symmetry adds a conserved current operator $J^A_\mu(z, \bar{z})$ which is in the adjoint representation of the flavour group, the index A being in the adjoint [30].

Just like in the case of the energy-momentum tensor, the conservation of this current implies that it will factorise into holomorphic and anti-holomorphic parts. The OPE of the holomorphic $J^A(z)$ is given as

$$J^A(z)J^B(0) \sim \frac{k}{z^2} + \frac{if^{AB}_C J^C(0)}{z} + \dots \tag{2.33}$$

There are two unknown quantities here: the *level*, denoted by k and also the *structure constants* of the Lie algebra f^{AB}_C. Of course for this to be an algebra we must close it on the OPE of T and J (and their anti-holomorphic pairs). This is very simple to do because $J(z)$ is actually a Virasoro primary with $h = 1$ and $\bar{h} = 0$, so we know exactly what the OPE will look like. The anti-holomorphic bits are analogous, and the cross-OPEs vanish. One can also expand the currents into modes and integrate them in order to obtain their commutation relations. We present them here for the sake of completeness:

$$\left[J^A_m, J^B_n\right] = if^{AB}_C J^C_{m+n} + km\delta^{AB}\delta_{m+n,0}. \tag{2.34}$$

One can observe that the zero modes recreate the flavour Lie algebra.

Chapter 3

Conformal Bootstrap with Reinforcement Learning

3.1 Introduction

The non-perturbative formulation of a generic Quantum Field Theory (QFT) and the analytic, or numerical, solution of its dynamics remains an extremely challenging conceptual and computational problem with important theoretical and experimental implications.

The problem becomes more tractable in Conformal Field Theories (CFTs): a special class of QFTs that describe typically the short and large-distance behaviours of generic QFTs. Most notably, in a unitary, relativistic CFT in D spacetime dimensions, the local structure of the theory is characterised by a set of discrete data: the scaling dimensions Δ_i of local conformal primary operators $\mathcal{O}_i$ and their Operator Product Expansion (OPE) coefficients C_{ij}^k. Once these data are known, the generic correlation function of any local operator in the theory can be determined.

Unitarity implies certain well-known constraints on these data. For example, a conformal primary operator with scaling dimension Δ and spin s must satisfy the inequalities

$$\Delta \geq \frac{D-2}{2} \ , \quad \text{for } s = 0 \tag{3.1}$$

$$\Delta \geq s + D - 2 \ , \quad \text{for } s > 0 \ . \tag{3.2}$$

The equality $\Delta = s + D - 2$ occurs only for conserved currents.

More elaborate, and powerful, constraints on the CFT data arise from crossing symmetry: the property that a correlation function is the same irrespective of the channel used in its OPE decomposition. These constraints (consistency conditions) form the basis of the *conformal bootstrap approach*. Since the 1970s (see e.g. [31, 32]) it was hoped that by solving the conformal bootstrap equations, one would be able to

solve CFTs non-perturbatively, without the need for a Lagrangian formulation. For many years the complexity of the conformal bootstrap equations, and the fact that they admit an infinite set of solutions for an infinite set of unknowns, did not allow the programme to evolve beyond a limited set of cases in 2D conformal field theory.

3.1.1 Brief Background on the Modern Conformal Bootstrap

Significant progress was instigated in 2008 by the seminal paper [13], which shifted the focus away from the search of exact solutions of the conformal bootstrap equations and towards the following approach: *Make an assumption about the spectrum of the CFT and ask if the bootstrap equations can be satisfied; if the equations cannot be satisfied, then this assumption can be successfully eliminated.* With suitable truncations on the infinite-dimensional CFT spectrum, this programme can be implemented numerically, and powerful linear and semidefinite programming methods[4] have been employed in recent years to obtain many significant results in this direction. It is impossible to list here all the results and different applications of this approach. Later in this chapter we will present a review of relevant facts from modern CFT bootstrap in order to better present the comparison between our algorithm and the current standard. For a separate concise review, and orientation to the relevant literature, we refer the reader to [24, 25, 26].

The assumptions that drive this approach are selected blindly; in the words of [35], the bootstrap computations in this context are performed in an "oracle mode". Nevertheless, suitable assumptions not only carve out significant parts of the space of potential CFTs, but one interestingly finds in many cases that known theories lie at cusps of the boundary of allowed possibilities. Even more efficiently, sometimes one discovers that the allowed region is an isolated "island". When this happens, the oracle-mode can be used to compute the scaling dimensions and OPE coefficients remarkably well. A beautiful application of this method is encountered in the 3D Ising model [36, 37]. Theories at the boundary of the allowed and disallowed regions are obviously special from this perspective and have been the primary target of standard applications of the conformal bootstrap. Efficient computational methods, like the Extremal Functional Method [38, 39], can be used to enhance the arsenal of the conformal bootstrap in this context.

Nevertheless, some obvious shortcomings of this approach include:

(a) For theories inside the allowed region one cannot, in general, tell how far they are located away from the boundary.

(b) With generic assumptions in oracle mode it is hard to identify and solve specific pre-selected CFTs, such as one's favourite gauge (conformal field) theory, that

[4] A commonly used package is the Semidefinite Program Solver (SDPB) [33, 34].

may not lie on the boundary of allowed and disallowed regions of the search.

(c) Higher-dimensional searches that would facilitate the study of more general classes of CFTs are computationally expensive and difficult to implement with the existing techniques. Typically, with current standard techniques one is restricted to searches of a couple of parameters.

There have been some recent approaches [35][40] trying to solve these issues. These methods and the one we introduce below, are phrased as optimisation problems. A distinctive feature of what we do is that instead of minimising directly the quantity of interest, we optimise a Neural Network (NN) that predicts a probability distribution, which is then sampled to make the actual predictions. This approach has several advantages. When directly optimising a function, one needs to compute partial derivatives, which can become expensive in high-dimensional searches.[5] In contrast, we use fixed optimisation algorithms for the NNs (already implemented at high efficiency), simplifying the details and complexity of the specific problem. Moreover, when one optimises the function of interest directly, one has to first pick a point in state-space to initialise the process, and then the derivatives guide the search towards the closest minimum. In order to flow to the minimum, one has to pick a small enough learning rate, but that inevitably restricts the flow to the closest minimum, even if it is not the global one. Our approach is efficient at trying to find the global minimum, because the probing scale varies and it detects minima at varying distances from the original starting point. The price we have to pay for these advantages is that our computations become less "exact", i.e. less direct and more statistical.

3.1.2 A Novel Study of Truncations Based on Artificial Intelligence

In the present work we study truncated crossing equations as an optimisation problem and develop methods to find approximate numerical solutions taking advantage of recent developments in Machine Learning (ML) and the wider availability of associated techniques. Similar to [40, 41], our approach is more akin to the original philosophy of the 1970s, which aimed at a *direct solution* of the conformal bootstrap equations. We will explain momentarily how we set up and implement a multi-dimensional search of approximate solutions and how this search benefits from artificial intelligence-techniques.

Introductory Comments on ML Terminology

Designing architectures and algorithms which one day could surpass human performance has been a long-running goal in the field of ML. Although a significant part

[5] In [35] this problem is avoided with a general SDP gradient formula and the efficient use of a quasi-Newton method.

of the theoretical (statistical and probabilistic) groundwork had been laid down for more than half a century, ML has only recently started to truly flourish. Decades ago algorithms which beat professional chess players had already been designed, but these approaches involved codes that were rigid and non-dynamic, meaning that once written their knowledge would be capped. In contrast, all of the modern developments in having machines learn how to solve problems include dynamic programming and a statistical approach to learning. The latter has only become practically feasible of late with the rapid development of and easier access to powerful central processing units (CPUs) and graphics processing units (GPUs).

The three best-known categories of ML algorithms are: *supervised*, *unsupervised* and *reinforcement learning*. In supervised learning some of the data are tagged and contain both the input and desired output. The algorithm trains on the tagged data and learns how to produce a sensible output from any input. Typical applications of supervised learning are classification and regression problems. In unsupervised learning there are no externally provided tagged data for training; the algorithm recognises on its own structure in a given set of data. In Reinforcement Learning (RL) [42]—or Deep Reinforcement Learning (DRL), that employs Deep Neural Networks (DNNs) in the learning steps of the "agent"—one knows the goals but does not know how to achieve them. The algorithm interacts with a dynamic environment and receives feedback based on its performance that guides it towards the desired result.

In recent years, ML has had a rising number of applications in High Energy Physics.[6] In this chapter, we will showcase a study of the conformal-bootstrap programme using RL techniques. This is the first study of conformal field theory of this kind.[7]

RL Setup in the Conformal Bootstrap

Ultimately, a successful RL algorithm should be able to *identify* a proper CFT, by converging to a configuration of CFT data that satisfy the crossing equations within a prescribed accuracy. It should similarly be able to *exclude* improper CFTs by failing to converge to a configuration that satisfies the crossing equations within the prescribed accuracy.

The basic scenario of our approach includes the following ingredients:

- Consider a specific four-point function with operators that have fixed symmetry properties, scaling dimensions and spins. If the scaling dimensions of the external

[6] See [43, 44] for a compendium of reviews ranging from the more experimental to the more computational aspects, and [45] for a summary of applications to String Theory. RL implementations have appeared in the context of String Theory even more recently in [15, 46, 47, 48]. See also [49] for a nice introduction to deep learning from a physics-motivated viewpoint.

[7] An alternative ML approach towards certain aspects of CFT, using supervised learning, appeared in [50]. The methodology, focus and scope of [50] are very different from the one that we introduce below.

operators are unknown, one can include them, as unknown variables, into the search.

- The crossing equations are truncated with a specific assumption about the number of operators per spin that appear in each channel. We call this assumption the *spin-partition* of the truncated conformal-block expansion. For example, if the truncation of the conformal block expansion in a given channel is assumed to include only operators of integer spin, and we truncate at maximum spin 3, then the spin-partition specifies the number of operators at spin 0, 1, 2 and 3. The spin-partition, which is an input to the RL algorithm, specifies the dimensionality of the vector of unknown scaling dimensions and OPE-squared coefficients $(\vec{\Delta}, \vec{\mathfrak{C}})$, that we aim to determine.

- We assume that the conformal blocks are known analytically, or numerically, [24, 25, 26]. The crossing equations, which are functions of the cross-ratios (see Sec. 2.3 for details), are reduced to a set of algebraic equations for the unknown scaling dimensions and OPE-squared coefficients $(\vec{\Delta}, \vec{\mathfrak{C}})$. The reduction can be achieved by Taylor expanding the conformal blocks around a particular point (as in standard applications of the numerical conformal bootstrap), or by evaluating the conformal blocks on a set of different points in cross-ratio space. We will be implementing the latter approach. Naturally, the number of algebraic crossing equations obtained in this manner should be larger than the number of unknowns. In compact vector form, the reduced algebraic crossing equations are

$$\vec{\mathbf{E}}(\vec{\Delta}, \vec{\mathfrak{C}}) = 0 \ . \tag{3.3}$$

  Since we truncate the crossing equations, it is not guaranteed (or expected) that Eqs. (3.3) have an exact solution. Our aim is to find approximate solutions to (3.3) that minimize $\vec{\mathbf{E}}$. Approximate solutions are expected to flow towards exact solutions of the exact crossing equations as one adds more and more operators to the truncation.

- One can specify the width of the search either individually for each unknown scaling dimension and OPE-squared coefficient, or collectively. For example, one can set a common upper cutoff, Δ_{max}, on the unknown scaling dimensions. Clearly, because of the unitarity constraints, (3.1)-(3.2), if the maximum spin in the spin-partition is s_{max}, then $\Delta_{\text{max}} \geq s_{\text{max}} + D - 2$.

- With these specifications in mind, we set up a soft Actor-Critic RL algorithm, [51], that performs a multi-dimensional search on the vector space of the unknown scaling dimensions and OPE-squared coefficients $(\vec{\Delta}, \vec{\mathfrak{C}})$ and returns configura-

tions that minimise the norm of the crossing-equation vector $\vec{\mathbf{E}}$. The operation and key components of the RL algorithm will be discussed in Sec. 3.4.

3.1.3 Overview and Discussion of Results

Our main goal here is to show that suitable RL algorithms can be applied to the conformal-bootstrap programme to efficiently perform multi-dimensional searches, and (when appropriately guided) to detect and solve arbitrary CFTs. We test the RL algorithms against results that can be obtained independently using analytic methods.

We choose to analyse 2D CFTs, as in this case it is straightforward to write exact conformal blocks for operators of arbitrary spin. Throughout our computations, we will only use the global $\mathfrak{so}(2,2)$ part of the 2D conformal algebra, without making any reference to the Virasoro algebra, which is a special feature of two dimensions. Consequently, every tool that we set up is directly generalisable and applicable to higher-dimensional CFTs, which will be treated elsewhere. For concreteness, we will focus separately on the two leading unitary minimal models (the Ising and tri-critical Ising model) and the free boson CFT on a circle.

Key Results

We highlight the following results:

- In all the cases we analysed, the algorithm was able to detect the CFT whose spin-partition we used as input. This is extremely promising. It suggests that Reinforcement Learning has a great potential as a tool in conformal-bootstrap studies of generic pre-selected CFTs. Our approach is not limited to special theories, e.g. CFTs on cusps of parameter spaces, or CFTs with enhanced symmetries.

- Even with a relatively small upper cutoff on the scaling dimensions our algorithm produces sensible numerical results that satisfy the truncated crossing equations at good accuracy. The details depend on the theory and the four-point function that we are analysing. For instance, for simple CFTs like the 2D Ising model, a run with only 5 quasi-primary operators yields scaling dimensions and OPE-squared coefficients comparable with their analytic values within the order of 1%. In the free compactified boson CFT we obtain sensible results even with 4 quasi-primary operators and cutoff $\Delta_{\text{max}} = 2$. As one might expect, the results of our RL algorithm are generically more accurate for lower scaling dimensions, and less accurate for quasi-primaries close to the cutoff when compared with the analytic answers.

- We can probe the dependence of CFTs on closely spaced discrete parameters, or continuous parameters like exactly marginal couplings. We present examples of

such a study in the context of the 2D free boson on a circle. In that case, the continuous parameter is the radius of the circle. Being applicable in such scenarios, our method could readily be combined with analytic results in convenient parameter regimes (e.g. at weak-coupling points) to solve the theory at generic points by adiabatically changing the parameters.

- We can perform efficient high-dimensional searches; our current algorithm can do direct searches with tens of operators. In the context of the 2D compactified boson CFT, we present results of a run with 36 parameters. We can, in principle, go to even higher spins and scaling dimensions with multiple sequential runs that start with a smaller number of operators and gradually introduce more.

Numerical Uncertainties

An important aspect of our approach, which is not addressed in detail in the preliminary investigations here, has to do with the systematic treatment of errors. As emphasised at the beginning of this subsection, the main goal of the present work is to establish that our algorithm detects the intended CFT and produces sensible numbers. We achieve this goal by comparing said numbers with the available exact analytic results. A preliminary discussion of errors and uncertainties, and how they can be incorporated systematically in the future, is relegated to the concluding Sec. 6.1.1. In the rest of this subsection, we flesh out an important aspect of our approximations that affects the implementation of our approach.

As already noted, the truncated crossing equations that we are trying to solve do not admit, in general, any exact solutions. Therefore, our main task is to find configurations that minimise the violation of the truncated equations. What is the minimal violation of the truncated equations that we should be aiming for? This is not a priori known and the answer can depend strongly on the specifics of the CFT, the four-point function that we are considering, the type of truncation that we are implementing on the spectrum and the way we reduce the crossing equations as functions in cross-ratio space to a number of algebraic equations. The answer to this question has obvious practical implications. Most notably, it determines when a run should be terminated and affects the decision of whether a given output should be accepted as a solution to an actual CFT, or whether it should be rejected as a false minimum.

In Sec. 3.2 we define a measure of relative accuracy $\mathbb{A}$ (see Eqs. (3.6), (3.7)) that quantifies a % violation of the truncated crossing equations. $\mathbb{A}$ has a minimum value $\mathbb{A}_{\text{min}}$ for searches in a compact subspace of parameter space. It is expected that $\mathbb{A}_{\text{min}} \to 0$ as we incorporate more and more operators, but it is not obvious, in general, how to determine $\mathbb{A}_{\text{min}}$ as a function of all the factors that were listed in the previous paragraph. If there is a regime, where the analytic solution is known, $\mathbb{A}_{\text{min}}$ can be estimated with a

direct RL-algorithm run in the vicinity of the known solution. This estimate can then be used as a guide in other regimes of parameters where the analytic solution is not known.

We have empirically found that in all computations performed in our investigation a solution has been properly identified for values of $\mathbb{A}$ below 0.1% irrespective of the spin truncation. Once $\mathbb{A}$ is below this empirical threshold *and* $\mathbb{A}$ stops improving *and* the agent has visibly converged to a configuration, we terminate the run and record the result. We have implemented this triple selection rule in all the runs that are reported in this chapter.

To obtain further evidence for the acceptance, or rejection, of a configuration one can study the dependence of the best $\mathbb{A}$ obtained by the algorithm as more and more operators are included. Once a configuration has been accepted as a valid approximation to the exact problem, one can define individual uncertainties for each CFT datum that is being computed. We present preliminary results of statistical errors in specific examples in Sec. 3.6. We discuss general uncertainties and their sources further in the concluding Sec. 6.1.1.

3.1.4 Outline

The rest of this chapter is organised as follows. In Sec. 3.2 we present the truncation scheme that we use, the associated spin partitions and a measure of accuracy that plays a key role in the numerical computations of the main text. In Sec. 3.3 we present a concise introductory review of the current numerical bootstrap methods as a contrast to our own algorithms. In Sec. 3.4 we give a mathematical and conceptual introduction to Markov Decision Processes and Reinforcement Learning in general. We then move on to describe the key components of specific RL algorithms and eventually work our way to the soft Actor-Critic algorithm and outline three practical modes of how we chose to implement it. Secs 3.5 and 3.6 are the central sections of the chapter. In Sec. 3.5 we present an RL study of four-point functions of the spin and energy-density operators in the 2D Ising and tri-critical Ising models. In Sec. 3.6 we study four-point functions of primary operators in the momentum/winding sector of the compactified boson CFT and four-point functions of the conserved $U(1)$ current. We discuss the dependence of the results on the scaling dimension cutoff Δ_{max} and the exactly marginal coupling of the theory. We conclude in Sec. 6.1.1 with a brief synopsis of the main results and an outlook on future directions.

3.2 Truncations, Spin-partitions and Measures of Accuracy

We view the exact crossing equations (2.29) as non-linear equations for the unknown positive[8] conformal scaling dimensions $\Delta = h + \bar{h}$ and the corresponding OPE-squared coefficients $\mathfrak{C}_{h,\bar{h}}$ in both channels. The spin $s = h - \bar{h}$ of the intermediate operators and the conformal weights $(h_i, \bar{h}_i)$ $(i = 1, 2, 3, 4)$ of the external operators are assumed to be given. However, in their current form, the *exact* crossing equations (2.29) are impractical both for analytic and numerical methods. As already mentioned in Sec. 3.1.2, we need to implement a truncation.

For numerical methods the first obvious obstacle is the appearance of a typically infinite number of contributions to the conformal-block expansion. We address this problem by truncating the spectrum of intermediate quasi-primary operators, by setting some upper cutoff $\Delta_{\max}$ on the scaling dimensions. The convergence properties of the conformal-block expansion [52] imply that one does not have to consider very large values of $\Delta_{\max}$ for sensible numerical results, but the precise value of an optimal $\Delta_{\max}$ is not easy to determine a priori and is, in general, theory-dependent. We will later make the surprising observation that in some examples values of $\Delta_{\max}$ as low as 2 can already yield good approximations.[9]

A second issue has to do with the continuous dependence of the exact crossing equations (2.29) on the cross-ratio parameters $z, \bar{z}$. We shall follow the approach of [53] and evaluate the truncated crossing equations at a finite discrete set of points in the z-plane. We have noticed experimentally that the sampling of z-points suggested in Sec. 3.1 of [53] works well also in our computations. In general, if the number of unknown scaling dimensions and OPE-squared coefficients is, in total, $N_{unknown}$, we choose N_z z-points (with $N_z > N_{unknown}$) to evaluate the truncated crossing equations.

With these specifications, the exact crossing equations (2.29) have been reduced to a finite set of non-linear algebraic equations, where the scaling dimensions of all contributing intermediate quasi-primary operators are bounded from above by $\Delta_{\max}$. This necessarily also puts an upper bound on the allowed spin s of these operators, since $|s| \leq \Delta \leq \Delta_{\max}$.[10] However, despite the above considerable simplifications, the problem remains intractable: there is still a vast space of possibilities that an algorithm can explore associated with the freedom to choose any number of quasi-primaries at each spin. This final issue can be fixed by introducing a *spin-partition*.

[8] The positivity of the conformal weights $h, \bar{h}$ follows from well-known unitarity constraints in two dimensions.

[9] It may be that such behaviour is correlated with the fact that a CFT is easily truncable, in the sense of [40]. In general, however, truncability is not a pre-requisite for the application of our method.

[10] Truncations on the spin of the conformal-block expansion and suitable discretisations in cross-ratio space are also commonplace in standard applications of the numerical conformal bootstrap.

Spin	0	1	2	$\cdots$	$n-1$	n
s-channel	a_0	a_1	a_2	$\cdots$	a_{n-1}	a_n
t-channel	b_0	b_1	b_2	$\cdots$	b_{n-1}	b_n

Table 1: A depiction of the spin-partition for a truncated spectrum of integer-valued spins in a four-point function of spinless operators where the conformal-block expansions can be phrased in terms of only positive spins. In this example, we have chosen to use the same number of maximum spin in both s and t channels. The non-negative integers a_i, b_i specify the number of operators with the corresponding spin, in the corresponding channel. For such a spin-partition the total number of unknowns in our problem is $N_{unknown} = 2\sum_{i=0}^{n}(a_i + b_i)$. For each unknown scaling dimension there is a corresponding unknown OPE-squared coefficient, hence the factor of 2 in this expression for $N_{unknown}$.

The spin-partition is a sequence of positive integers that specifies the number of quasi-primaries per spin contributing to the conformal-block expansions of the truncated crossing equations. The spin-partition is an input to the RL algorithm that we set up in the next section. It fixes the dimensionality $N_{unknown}$ of the vector space of parameters $(\vec{\Delta}, \vec{\mathfrak{C}})$ where the search takes place. We will be listing spin-partitions using the template of Tab. 1.

We have thus arrived at a framework of truncated equations

$$\vec{\mathbf{E}}(\vec{\Delta}, \vec{\mathfrak{C}}) = 0 \ , \tag{3.4}$$

where the dimension of the vector $(\vec{\Delta}, \vec{\mathfrak{C}})$ is $N_{unknown}$ and the dimension of the vector $\vec{\mathbf{E}}$ is N_z. Each entry $\mathbf{E}_i$ $(i = 1, \ldots, N_z)$ of the vector $\vec{\mathbf{E}}$ contains the evaluation of the truncated version of Eq. (2.29) at one of the points $(z_i, \bar{z}_i)$ in our z-sampling

$$\begin{aligned}\mathbf{E}_i = &\sum_{h,\bar{h}}^{trunc} {}_s\mathfrak{C}_{h,\bar{h}}\, g^{(1234)}_{h,\bar{h}}(z_i, \bar{z}_i) \\ &- (-1)^{(h_{41}+\bar{h}_{41})} z_i^{h_1+h_2} \bar{z}_i^{\bar{h}_1+\bar{h}_2} (z_i - 1)^{-h_2-h_3} (\bar{z}_i - 1)^{-\bar{h}_2-\bar{h}_3} \\ &\times \sum_{h',\bar{h}'}^{trunc} {}_t\mathfrak{C}_{h',\bar{h}'}\, g^{(3214)}_{h',\bar{h}'}(1 - z_i, 1 - \bar{z}_i) \ ,\end{aligned} \tag{3.5}$$

where $\sum^{trunc}$ denotes the truncated sum over intermediate operators.

This framework is very similar to the starting point of the approach [40, 41]. Notice, however, that the truncation in the scheme of [40, 41] is arbitrary, whereas here it comes with a further assumption that the unknown scaling dimensions are inside a specific window of scaling dimensions. This detail is an important distinction between our approach/implementation and those of [40, 41]. In particular, our approach entails a probabilistic search in specified parameter windows.

In general, (3.4) is not expected to have any exact solutions. Accordingly, as we explain in the next section, our RL algorithm is designed to minimise the Euclidean norm of $\vec{\mathbf{E}}$ and determine configurations of CFT data that satisfy the truncated crossing equations with the best possible accuracy. Although the Euclidean norm $||\vec{\mathbf{E}}||$ is an important quantity of the computation, it is not straightforward to judge whether its raw value at an optimal configuration is actually small or large. For that reason, we find it useful to define a "relative measure of accuracy", $\mathbb{A}$, defined in the context of (3.5) as

$$\mathbb{A} = \frac{||\vec{\mathbf{E}}||}{\mathbf{E}_{abs}} \tag{3.6}$$

with

$$\mathbf{E}_{abs} = \sum_{i=1}^{N_z} \left[\sum_{h,\bar{h}}^{trunc} \left| {}_s\mathfrak{C}_{h,\bar{h}}\, g^{(1234)}_{h,\bar{h}}(z_i,\bar{z}_i) \right| \right. \tag{3.7}$$

$$\left. + \left| z_i^{h_1+h_2}\bar{z}_i^{\bar{h}_1+\bar{h}_2}(z_i-1)^{-h_2-h_3}(\bar{z}_i-1)^{-\bar{h}_2-\bar{h}_3} \right| \sum_{h',\bar{h}'}^{trunc} \left| {}_t\mathfrak{C}_{h',\bar{h}'}\, g^{(3214)}_{h',\bar{h}'}(1-z_i,1-\bar{z}_i) \right| \right] .$$

The quantity $\mathbb{A}$ is guaranteed to be a number between 0 and 1. Its value gives a % measure of the accuracy at which we have been able to satisfy the truncated equations (3.4), and this can in turn be compared more straightforwardly between different computations.

3.3 Numerical Bootstrap

As we have established from before, the crossing equation is one of the most important constraints one can impose on the CFT data. This in turn makes it very important in verifying what CFTs are allowed to exist. Say, if we took a random set of numbers, the crossing equation would be able to determine if they could form a consistent CFT.

The crossing equation given in the above form has been known for a very long time, but solving it has been a highly non-trivial task. Crossing equations tend to depend quite simply — most of the time linearly — on the squared OPE coefficients, but they are highly non-linear in the scaling dimensions of the operators. There is also of course the fact that we have to usually deal with an infinite number of operators which sum into this equation, and the fact that this equation is satisfied for all the values of the conformal cross-ratios.

Solving the crossing equations exactly is very much out of the question. However, there are some tools developed roughly a decade ago [13] which have been used to place bounds on CFT data. In this section we will spend some time explaining these ideas and also looking at how one could apply such methods numerically by using computers.

3.3.1 Placing Bounds on Data Analytically

The main revelation of the paper mentioned above [13] is that they look at the crossing equation as a sum of vectors in an infinite dimensional space of functions. In order to demonstrate the method, we will use this 2 dimensional crossing equation:

$$\sum_{\mathcal{O}} f^2_{\phi\phi\mathcal{O}} \left(v^{\Delta_\phi} g_{\Delta,\ell}(u,v) - u^{\Delta_\phi} g_{\Delta,\ell}(v,u)\right) = 0. \tag{3.8}$$

Where above we have the crossing equation coming from the four-point function $\langle\phi\phi\phi\phi\rangle$. The sum is over primaries $\mathcal{O}$ exchanged between the two vertices of the four-point function. Other unknowns in the equations are the OPE squared coefficients $f^2_{\phi\phi\mathcal{O}}$, the dimensions Δ_ϕ, the conformal blocks g and their inputs, the cross-ratios u, v, as well as the scaling dimension of the exchanged primary Δ.

Now let us re-examine this equation, but from the perspective of a summation of different vectors $\overrightarrow{F}^{\Delta_\phi}_{\Delta,\ell}$. These vectors are taken straight from the cross ratio (3.8).

$$\overrightarrow{F}^{\Delta_\phi}_{\Delta,\ell} = v^{\Delta_\phi} g_{\Delta,\ell}(u,v) - u^{\Delta_\phi} g_{\Delta,\ell}(v,u) \tag{3.9}$$

This is quite an abstract way to think about this problem, but the geometrical ideas coming from visualising these as vectors will be sufficient to place bounds on the CFT data. If we rewrite equation (3.8) so that the OPE coefficients are all positive then we can define this sum of vectors:

$$\sum_{\Delta,\ell} p_{\Delta,\ell} \overrightarrow{F}^{\Delta_\phi}_{\Delta,\ell} = 0. \tag{3.10}$$

Where, $p_{\Delta,\ell} \geq 0$. As it turns out, looking at the problem from this angle, we can already infer some important information, knowing that these vectors have to sum to zero. To put this simply, the vectors which are being summed cannot all be "pointing in the same direction". This is just a statement that for all the components of these vectors to cancel, they have to be spread out with respect to each other. The simplest example would be the case of two vectors, where in order for them to be able to cancel, they would have to be pointing in the opposite direction — i.e. they would be the most spread out.

Hence the criterion for the CFT existing rests on the ability of these vectors to cancel. One can show that this is impossible if these vectors all lie on one side of a plane α running through the origin, cutting the space in half. Now we have abstracted the problem from adding functions to looking at the existences of specific planes. In the next few sections we shall explain how one can fabricate algorithms to place bounds on CFT data.

Bounds on Scaling Dimensions

Placing the bounds on the scaling dimensions is relatively straightforward. The first step would be to make a guess (ansatz) at the operators which might appear. At this point, we are only really interested in their spins and their dimensions, which label the operators. The only operators one has to create an ansatz for are the ones that would be present in the OPE of the given external operator (in our case ϕ) that one chose. The next step would be to search for that fabled α plane. In the space of the functions α would take the form of a functional, and based on the discussions above, it would have to be semi-positive acting on all the vectors. This effectively means it has to be non-negative on all but one operator, which has to be strictly positive:

$$\alpha\left(\overrightarrow{F}^{\Delta_\phi}_{\Delta,\ell}\right) \geq 0. \tag{3.11}$$

As we stated above, if α exists for these values, then we have reached an inconsistency and the given values cannot form a CFT. The full algorithm would be to repeat this with different ansatze until one reaches a division point between the consistent and non-consistent theories.

At the moment one might recall that we are still in the analytical mindset and we are dealing with an infinite set of primaries as well as the infinite space of α's to consider. How one shifts this problem over to the numerical regime will be discussed after presenting all the algorithms in section 3.3.2.

Bounds on OPE Coefficients

The process for bounding the OPE coefficients $f^2_{\phi\phi\mathcal{O}} = p_{\Delta,\ell}$ is a bit more involved [54]. First and foremost, we have to separate the contribution from the identity operator

$$\sum_{\Delta,\ell} p_{\Delta,\ell}\overrightarrow{F}^{\Delta_\phi}_{\Delta,\ell} = 1. \tag{3.12}$$

Here we have to make sure that all the coefficients $p_{\Delta,\ell} \geq 0$. This is because we will interpret equation (3.12) as the identity function being inside a convex cone. This can be seen from the right-hand side of the equation which if the coefficients are allowed to change, would fill a convex cone. Let us now pick another operator from the right-hand side and move it to the left:

$$\sum_{\Delta,\ell} p_{\Delta,\ell}\overrightarrow{F}^{\Delta_\phi}_{\Delta,\ell} = 1 - p_{\bar{\Delta},\bar{\ell}}\overrightarrow{F}^{\Delta_\phi}_{\bar{\Delta},\bar{\ell}}. \tag{3.13}$$

The right-hand side is a linear combination of two vectors from our space, and if we change $p_{\bar{\Delta},\bar{\ell}}$ it will move it to align more or less with $\overrightarrow{F}^{\Delta_\phi}_{\bar{\Delta},\bar{\ell}}$. There could exist a critical

value of p^* above which the vector will leave the cone. This is very similar to the logic we used with the scaling dimensions where we tried to construct an inconsistency. The goal here is the same — to find a bound on the OPE coefficients which makes equation (3.10) contradicting.

The next step is to find the value of p^*. For this we will reach back to the previous section and grab the functional α which we defined. We define it to be linear and impose the condition (3.11). We will also normalise the functional on the unit operator

$$\alpha[1] = 1. \tag{3.14}$$

Applying this to both sides of equation (3.13) we get the constraint:

$$\alpha\left[1 - p_{\bar{\Delta},\bar{\ell}}\overrightarrow{F}^{\Delta_\phi}_{\bar{\Delta},\bar{\ell}}\right] = 1 - p_{\bar{\Delta},\bar{\ell}}\,\alpha\left[\overrightarrow{F}^{\Delta_\phi}_{\bar{\Delta},\bar{\ell}}\right] \geq 0. \tag{3.15}$$

Which we can then rearrange to give

$$p_{\bar{\Delta},\bar{\ell}} \leq 1/\alpha\left[\overrightarrow{F}^{\Delta_\phi}_{\bar{\Delta},\bar{\ell}}\right]. \tag{3.16}$$

Note that this bound is dependent on the functional that is chosen. The right-hand side of the equation can then be defined as the object we have been seeking

$$p^* \equiv 1/\alpha\left[\overrightarrow{F}^{\Delta_\phi}_{\bar{\Delta},\bar{\ell}}\right]. \tag{3.17}$$

This would already impose a bound, but in order to get the most out of this relation we need to take the extremal value of the right side. This concludes the analytical way of determining the bounds for the OPE coefficients.

3.3.2 From Analytical to Numerical

Changes Demanded by Numerical Techniques

In the previous section we described algorithms to try to bound the values of the CFT data. In practice these algorithms as described are not actually very useful as it is very rare that a problem is so simple that it can be bounded analytically. In such cases numerical solutions tend to be the next most accurate and efficient method to obtain a good approximation of the analytical solution. We have drawn attention to some of the potential issues which would arise when porting these methods to work with computers in the sections leading up to this, but it is worthwhile to collect them here and address them individually. The most important drawbacks:

- The are endless possibilities for the functional α.
- The infinite number of operators whose labels ℓ and Δ range from 0 to ∞, while

Δ can also technically take any real value.

The points raised above can be relatively easily bypassed in order to move into the domain of numerical computations. Both issues have to be solved by understanding that most computer algorithms cannot search an infinite range or deal with continuous variables. Hence, the logical approach is to truncate the space we are searching and to discretise the continuous variables.

The issue of the infinity arising from the space of functionals can be solved by taking linear combinations of derivatives at a given point — usually taken to be the point $z = \bar{z} = \frac{1}{2}$, which is where the crossing equations converge exponentially.

$$\alpha(F) = \sum_{m+n \leq \Lambda} a_{mn} \partial_z^m \partial_{\bar{z}}^n F(z, \bar{z})|_{z=\bar{z}=\frac{1}{2}} \tag{3.18}$$

We have already introduced almost all of the symbols in the equation above (for $F(z, \bar{z})$ we just dropped the labels for clarity), the notable exception being Λ. This is the value which controls the total number of derivatives being applied to the functions appearing in the crossing equation. We can see that now the space of functionals is described by the values a_{mn} of which there is a finite amount by virtue of the cutoff Λ.

For the other issue at hand, we can do a large variety of things, but here we will just detail the simplest approach. We need to discretise the scaling dimensions Δ (the smaller spacing between them, the better), and also impose an upper bound for the search Δ_{max}. The same approach can be applied to ℓ, keeping in mind that it is already discrete by default.

3.4 A Review of Reinforcement Learning

In many physical settings it is very common to have access to large amounts of data (e.g. collider physics), where supervised/unsupervised ML techniques find direct application. However, in scenarios often found in theoretical physics this is not usually the case. This is where RL comes in handy because the learning agent is able to generate its own data.

Reinforcement Learning, in brief, is an algorithm consisting of two parts with equal importance. The first is the so-called "agent", which is the brain of the algorithm. The second is the "environment": what the agent interacts with. The basic setup of the algorithm is the process of the agent making decisions as it explores the provided environment, while the environment gives feedback on the agent's actions. One wants the agent to explore the environment towards finding an ideal solution, while exploiting the best solution it finds (explore-exploit dilemma). One also has to find a suitable algorithm for how the agent (the neural network) "learns" and retains its experiences.

There exists a considerable amount of previous work on DRL algorithms, which have been applied to a large variety of problems, both theoretical and real-world. There are examples of agents which can beat video games, drive cars, guide robots, solve mathematical equations and—possibly the most famous one—AlphaGo, which beat professional Go champions using a combination of supervised learning and DRL [55, 56], and the improved AlphaGo Zero, which relied completely on DRL [57].

Such algorithms can be split into two main sets and can be distinguished by whether the actions (defined by numbers) taken by the agent are discrete or continuous. Algorithms such as Deep Q-Learning [58] or Actor-Critic methods [59] use a discrete action space (convenient when one can take only a finite amount of actions), while algorithms such as the soft Actor-Critic method [51] and the Deep Deterministic Policy Gradient method [60] were developed for when the actions can take any real value.

In the research presented in this thesis we will be making use of the soft Actor-Critic algorithm and implementing it using the PyTorch package for Python 3.7, but one could have equivalently chosen the Deep Deterministic Policy Gradient or any of the other Machine Learning libraries (TensorFlow etc.). We will not go into the details of most of the aforementioned algorithms, since these can be found in the original papers (with pseudo code), and there exist plenty of additional online resources showcasing their implementations. We will however build up the prerequisites to understand how the algorithm we use —soft Actor-Critic— works in practice.

This section is fully dedicated to setting the scene and explaining the state-of-the-art technology of reinforcement learning (RL). We will try to set up some basic mathematical ideas behind RL and also deep reinforcement learning (DRL). Note that the latter will be done without formally introducing machine learning (ML) and deep neural networks (DNNs). While it is desirable to know these topics in order to discuss RL, it is possible to treat them as "black boxes" and still understand how RL algorithms work.

3.4.1 Fundamental Components of RL

What constitutes a reinforcement learning algorithm? That is the question we will try to elaborate upon in this section. Perhaps the two most well known subalgorithms would be the agent and the environment. Beyond those two, there are also three other elements which are just as vital for RL to function: a policy, a reward and a value function.

- **Agent.** Roughly speaking this part of the code would act like the "brain" of the algorithm. This is where the decisions are made based on the current state the agent is in. A good example which we will be bringing up throughout the rest of the sections will be the example of a player playing a game. The agent would

then take the role of the player.

- **Environment.** This part of the algorithm is where the agent makes contact with the problem at hand. The job of the environment is to effectively tell the agent what its current situation is. This can be very abstract sometimes, but using our analogy of a game, this would translate to the rules and the space in which this game is played. The environment also reacts to any actions made by the agent.

- **Policy.** Now that we have a player and a game, time to actually play the game. The policy tells us how the agent will make decisions based on a specific state it occupies in the environment. Effectively this is just a function which maps perceived states from the environment to actions to perform in those given states. The policy forms the basis of the agent.

- **Reward.** Any game must have and end goal, or a particular way of being successful. The reward or reward signal, is a way of quantifying that. For every step the agent takes in the environment it must be told the reward that step invoked. This gives the agent a sense of how it did and also how it can improve in the future. This makes the maximisation of the reward the single most important objective of the agent.

- **Value Function.** The reward is useful for determining how well an agent is doing at an instant, but sadly it misses the global information about a specific environment. What we mean by this is that maximising the reward in the short-term might not always be the optimal way to win a game. What might happen is that in order to reach the highest reward, the agent has to travel through an undesirable area of the state space. This requires more long-term thinking by the agent. The implementation of this is done through the so-called value function which estimates the "value" of a state which translates to how much reward we can get in the future. This means that in reality we want an agent which maximises the value function which in turn will maximise the future reward.

We have now introduced the fundamental aspects of reinforcement learning. In the next section we will go into detail about how the agent explores the environment and tries to retrieve the information stored within.

3.4.2 Finite Markov Decision Processes

Notation and Definitions

In this section we will be defining RL more mathematically rigorously through the use of finite Markov Decision Processes (MDPs). Just as a word of warning looking ahead, MDPs are a purely theoretical construction for ideal RL cases so the later application

to solve problems, will need some modifications (transition to DRL), as one usually does with numerical/machine learning problems.

Let us call upon the ideas of Sec. 3.4.1 and recall that the two main components of an RL algorithm are the agent and the environment. The most important thing to note about these two is that they are continuously interacting with one another, they are stuck in a cycle. To be a bit more concrete, at each step of the algorithm —when the agent makes a decision on what to do— the environment receives that information and outputs what the agent needs to make the next decision. That is one step. The algorithm will run over many many steps, which we can label as time steps $t = 0, 1, 2, \ldots$.

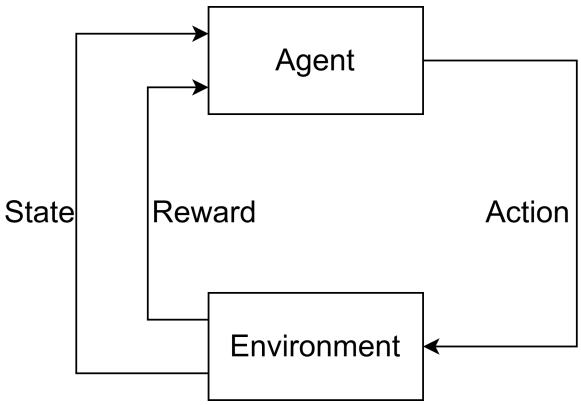

Figure 1: A flowchart describing how the Agent-Environment loop works.

Let us introduce more notation. As shown in Fig. 1, at each instance t the agent will be fed a certain representation of the state of the environment, $S_t \in \mathcal{S}$, where $\mathcal{S}$ is the space of all possible states. Using this state, the agent will make an action, $A_t \in \mathcal{A}(s)$, where $\mathcal{A}(s)$ is the set of all actions possible from the state s. In some cases (like the ones we will be using later in this thesis) the action space is the same for all states. Once the action has been performed, the environment will change to state S_{t+1}, and the reward for the action taken will be dispensed, given as $R_{t+1} \in \mathcal{R} \subset \mathbb{R}$. An important thing to note at this point is that here the space of states, actions and rewards is finite, hence the use of finite MDPs.

If we start treating the new state s' and the reward r arising from the previous states s and action a then it is possible to define a probability distribution $p(s', r|s, a)$ which theoretically contains the information of all the transitions through the entire state and action spaces. By grace of it being a probability distribution, it has to obey the following condition:

$$\sum_{s' \in S} \sum_{r \in \mathcal{R}} p\left(s', r \mid s, a\right) = 1, \text{ for all } s \in \mathcal{S}, a \in \mathcal{A}(s). \tag{3.19}$$

The fact that the probability p describes all the information of this process means that this process must be a Markov Decision Process. This fact stems from the way the probability was defined to only depend on the previous time step and no earlier. This means that the previous state itself must contain enough information about the past such that it is useful for the future.

We can marginalise over the reward in the joint conditional probability distribution in order to obtain the state-transition probability

$$p\left(s' \mid s, a\right) = \sum_{r \in \mathcal{R}} p\left(s', r \mid s, a\right). \tag{3.20}$$

It is also possible to compute the expected reward going from a specific state with a specific action

$$r(s, a) \equiv \mathbb{E}\left[R_t \mid S_{t-1} = s, A_{t-1} = a\right] = \sum_{r \in \mathcal{R}} r \sum_{s' \in \mathcal{S}} p\left(s', r \mid s, a\right). \tag{3.21}$$

Furthermore using the rules of conditional probability to fix the next state, the expected reward in terms of the other three variables can be given as

$$r\left(s, a, s'\right) = \mathbb{E}\left[R_t \mid S_{t-1} = s, A_{t-1} = a, S_t = s'\right] = \sum_{r \in \mathcal{R}} r \frac{p\left(s', r \mid s, a\right)}{p\left(s' \mid s, a\right)} \tag{3.22}$$

Now that we have laid down some of the groundwork for MDPs, time to go back to studying reinforcement learning. As we have described before, in RL the agent should try to optimise the *total* amount of reward it is obtaining. This is much harder than maximising the most immediate reward, as it requires thinking ahead. In order to quantify this idea, let us define the expected return, which is something we would like to maximise at each point in time

$$G_t \equiv R_{t+1} + R_{t+2} + R_{t+3} + \cdots + R_T. \tag{3.23}$$

T here denotes the final time step. Note that this is the expected reward from any point in time t. This seems like a simple enough definition, but there is a slight issue. What happens when there is no end to the process? There is no reason to assume that the rewards would converge and so we could easily end up with optimising an infinite value. As it turns out there is a much more convenient approach to take which in turn also offers a satisfactory explanation. Introduce the notion of *discounting*. What this means is that each reward which is later than the most immediate one will be weighted by an increasing power of a discount factor which is between 0 and 1. This ensures that the sum converges and also implies that the value of the most immediate decisions is

more important than the ones very far in the future.

$$G_t \equiv R_{t+1} + \gamma R_{t+2} + \gamma^2 R_{t+3} + \cdots = \sum_{k=0}^{\infty} \gamma^k R_{t+k+1}. \tag{3.24}$$

Here γ is the discount parameter. This parameter effectively controls the agent's far-sightedness. From this definition of the expected return immediately follows the recursion relation

$$G_t = R_{t+1} + \gamma G_{t+1}. \tag{3.25}$$

For a finite series $G_T = 0$, since there are no rewards after the process has terminated.

Policies and Value Functions

Back in Sec. 3.4.1 we introduced some basic aspects of an RL algorithm and one of these was the value function. Just to summarise exactly what we mean by this, we mean the functions which take the state alone or the state-action pair and try to quantify how good it is to be in a specific state or to perform a specific action from the state. In the previous section we defined this notion of "good" to be related to the reward and later on we started to use the expected return at a specific instance. It is immediately obvious that since the agent has a choice, these value functions should be different depending on what the agent's policy is. Recall that the policy, which we will denote $\pi(a|s)$ at the instance t, is the probability that the agent selects the action a given the original state $s = S_t$. As the agent will experience more and more of the state and action spaces we expect this policy to change in order to optimise the value function.

Now we will relate the value function to the expected return we defined in Eq. 3.24. The definition of the value function of a state s with a policy π is defined to be

$$v_\pi(s) \equiv \mathbb{E}_\pi \left[G_t \mid S_t = s \right] = \mathbb{E}_\pi \left[\sum_{k=0}^{\infty} \gamma^k R_{t+k+1} \mid S_t = s \right] \quad \forall\ s \in \mathcal{S}. \tag{3.26}$$

Here we took the expectation value of G_t with the agent following a given policy π at the step t. An important trait which it inherits from the expected return is that for the last step of the process the value of that state is zero. This happens for the same reason as for G_T, as there are no more steps to be taken and hence no more reward to be earned. The official name assigned to v_π is the *state-value function* for the policy π. Definitely note this name because it is one of the prominent functions in RL literature.

Just like before, in Eq. (3.21) where we took the expectation value with the action a given, we can do a similar thing for the state-value function. This would give the value of performing the action a from the state s and then obeying the policy π, which

we will denote $q_\pi(s, a)$.

$$q_\pi(s,a) \equiv \mathbb{E}_\pi \left[G_t \mid S_t = s, A_t = a \right] = \mathbb{E}_\pi \left[\sum_{k=0}^{\infty} \gamma^k R_{t+k+1} \mid S_t = s, A_t = a \right]. \tag{3.27}$$

This function also enjoys a huge following in recent literature and it has been dubbed the *action-value function*. From the definitions of these two functions, the latter being for a specific action, follows the following property which relates the two

$$v_\pi(s) = \sum_a \pi(a|s)\ q_\pi(s,a). \tag{3.28}$$

Which is just a statement that the q-value function's expected value based on the policy is the state-value function.

Here we have defined the two most important functions we will be using in our RL construction. Note that these are all analytical and one would require the knowledge of the distribution which governs the reward space in order to calculate these exactly. In most cases that will be completely unfeasible and we will actually end up approximating both v_π and q_π by probing the state and action spaces in order to gain insight into the distribution of the rewards. This will build a data set we can use to train our neural networks, which will approximate these functions in deep reinforcement learning.

The Bellman Equations

Before we move on to approximating the value functions explained in Sec. 3.4.2 we need to find an equation that imposes a constraint on them. The Bellman equation does exactly this. The recursion of the expected return shown in Eq. (3.24) actually imposes a consistency condition on the functions we defined before. Using the definition of the state-value function we get:

$$\begin{aligned} v_\pi(s) &\equiv \mathbb{E}_\pi \left[G_t \mid S_t = s \right] \\ &= \mathbb{E}_\pi \left[R_{t+1} + \gamma G_{t+1} \mid S_t = s \right] \\ &= \sum_a \pi(a \mid s) \sum_{s'} \sum_r p\left(s', r \mid s, a\right) \left[r + \gamma \mathbb{E}_\pi \left[G_{t+1} \mid S_{t+1} = s' \right] \right] \\ &= \sum_a \pi(a \mid s) \sum_{s', r} p\left(s', r \mid s, a\right) \left[r + \gamma v_\pi\left(s'\right) \right], \quad \forall\ s, s' \in \mathcal{S}. \end{aligned} \tag{3.29}$$

In the second line we substituted in Eq. (3.24). The third line is tricky, but we essentially just use some conditional probability rules and also use Eq.(3.21) for the first half, but for the second we have to use the law of iterated expectations:

$$\mathbb{E}_\pi \left[v_\pi\left(S_{t+1}\right) \mid S_t \right] = \mathbb{E}_\pi \left[\mathbb{E}_\pi \left[G_{t+1} \mid S_{t+1} \right] \mid S_t \right] = \mathbb{E}_\pi \left[G_{t+1} \mid S_t \right] \tag{3.30}$$

This is also how we then finally get to the third line of Eq. (3.29). This line is known as the *Bellman equation* for the state-value function. It relates the values of two successive states. The reason we introduced this equation is that it introduces a significant constraint, which is solved by the state-value function. We can repeat the process for the action-value function too:

$$q_\pi(s,a) = \sum_{s'}\sum_{r} p\left(s', r \mid s, a\right)\left[r + \gamma \sum_{a'} \pi\left(a' \mid s'\right) q_\pi\left(s', a'\right)\right] \tag{3.31}$$

This is known as the Bellman equation for the action-value function.

Let us now take a broader perspective and ask: how does one solve an MDP? There is a consensus that we can consider an MDP solved if we can find something called the *optimal policy*. This is essentially the same statement we made before about trying to build an agent which maximises the value functions. Let us now define quantitatively what we want. Our statement translates to the requirement that we have a $v_\pi(s) \geq v_{\pi'}(s)$ for all $s \in \mathcal{S}$. We are guaranteed to have at least one policy like this, but it does not have to be unique. Let us denote all optimal policies by π_* and they are given to be

$$v_*(s) \equiv \max_\pi v_\pi(s) \;\forall s \in \mathcal{S}. \tag{3.32}$$

A convenient fact is that all optimal policies also possess the same optimal action-value function too

$$q_*(s,a) \equiv \max_\pi q_\pi(s,a) \;\forall s \in \mathcal{S} \text{ and } a \in \mathcal{A}. \tag{3.33}$$

We want to start solving for the optimal policy. We shall do this by maximising over our optimal action-value function $q_*(s,a)$. For this we need to solve for $q_*(s,a)$ and then pick the action which gives us the most optimal $q_*(s,a)$. This effectively collapses our policy to be fully deterministic

$$\pi_*(a \mid s) = \begin{cases} 1 & \text{if } a = \underset{a \in \mathcal{A}}{\operatorname{argmax}}\; q_*(s,a) \\ 0 & \text{otherwise.} \end{cases} \tag{3.34}$$

This means that in the optimal policy we pick the action with the largest $q_*(s,a)$. Before we might think the problem is solved, we still need to find $q_*(s,a)$, but once we have it we can construct our optimal policy out of it.

The Bellman Optimality Equations

Now that we have a way to work out the optimal policy, all that remains is to find the optimal value functions. Like the title suggests we will do this by recalling the Bellman equations (3.29) and (3.31). Let us also consider the relationship between the two value functions given by Eq. (3.28). We can derive a similar relationship, but between the optimal versions of these two functions.

$$v_*(s) = \max_{a \in \mathcal{A}(s)} q_{\pi_*}(s, a) \tag{3.35}$$

The main thing to note here is that the expectation turned into a maximum over the action which can be traced back to the statement of Eq. (3.34). From here we can start deriving the so-called *Bellman optimality equations*.

$$\begin{aligned} v_*(s) &= \max_a \mathbb{E}_{\pi_*} \left[G_t \mid S_t = s, A_t = a \right] \\ &= \max_a \mathbb{E}_{\pi_*} \left[R_{t+1} + \gamma G_{t+1} \mid S_t = s, A_t = a \right] \\ &= \max_a \mathbb{E} \left[R_{t+1} + \gamma v_* \left(S_{t+1} \right) \mid S_t = s, A_t = a \right] \\ &= \max_a \sum_{s', r} p \left(s', r \mid s, a \right) \left[r + \gamma v_* \left(s' \right) \right] \end{aligned} \tag{3.36}$$

Here in the first line we just took (3.35) and substituted in (3.31), but written as an expectation value. In the second line we reused the manipulation (3.25). Then the last two lines are the same manipulations we used to derive the original Bellman equations for the state-value function in Eq. (3.29). The ultimate and penultimate lines in this calculation are two forms in which the Bellman optimality equation is expressed for the optimal state-value function. We can do a similar process for q_*:

$$q_*(s, a) = \mathbb{E} \left[R_{t+1} + \gamma \max_{a'} q_* \left(S_{t+1}, a' \right) \mid S_t = s, A_t = a \right] \tag{3.37}$$

$$= \sum_{s', r} p \left(s', r \mid s, a \right) \left[r + \gamma \max_{a'} q_* \left(s', a' \right) \right]. \tag{3.38}$$

Here we have presented the two relevant Bellman optimality equations which one has to consider when solving a Markov Decision Process and hence a reinforcement learning problem. As we said before in order to derive the optimal policy, one has to find one of the optimal value functions. This of course is very difficult to do in practice, especially with processes which have enormous state and action spaces. In order to surmount this problem, we will try to use computational methods to approximate these functions. The next sections will focus on placing the solutions into context and also providing details on which algorithms we used in the course of this thesis.

3.4.3 Deep Reinforcement Learning

In this section we will use all the knowledge we have acquired while investigating Markov Decision Processes and try to solve them using computational algorithms. In recent years there have been many research papers on solving finite action space problems — the agent can only do a limited number of things, such as move up and down — using highly varying approaches [61, 62, 63, 64]. Another class of reinforcement learning algorithms developed quite recently were continuous action space algorithms [65, 60], which will be the most relevant to the research presented in later sections.

All of these algorithms attempt to solve the equations posed in the previous sections, and the literature is quite vast. For simplicity we will only focus on explaining algorithms which are directly related to our work. We will begin by focusing on Actor-Critic (AC) methods for DRL, and this will then lead us to consider the final stop for our review: the Soft Actor-Critic algorithm, which we shall make heavy use of.

Policy Gradient

In our quest to eventually discuss Actor-Critic methods, first we have to discuss Policy Gradient (PG) methods on which AC is based. These methods (just like a lot of RL) actually trace their origin back to almost 3 decades ago [64, 66]. The significance of PG methods is that they start making the relationship between RL and ML manifest. This is done through the introduction of a function requiring optimisation

$$J(\theta) = \mathbb{E}_\pi[r(\tau)]. \tag{3.39}$$

Here we just set up the machine learning problem to solve the maximisation of the expected reward as in reinforcement learning. The variable θ is the set of parameters which define the function we are trying to optimise. They are usually grouped into a vector, but we will omit the vector notation because in the context of this literature their nature is clear all the time. The only difference from the notation we used in the previous sections is the use of $r(\tau)$, which is just a more general expected reward (extended to continuous time), but we can replace it with our G_t and then we'll arrive at the so-called REINFORCE algorithm [66]. If the reader has had exposure to machine learning techniques then they can guess what we will use equation (3.39) for. In ML we use the function $J(\theta)$ to perform the optimisation. Usually however we are trying to minimise the function, but in this instance we will be maximising it to solve the RL problem. We will do this by gradient ascent which defines an update rule for the parameters

$$\theta_{t+1} = \theta_t + \alpha \nabla J(\theta). \tag{3.40}$$

Here the gradient is taken with respect to the parameters θ and α is referred to as the learning rate (it measures how quickly we move towards an optimum). This procedure is used to find the parameters which optimise the function $J(\theta)$. The next very important result of the policy gradient method is that the derivative of the expectation of $r(\theta)$ is the expectation of the product of the reward and gradient of the log of the policy π_θ, parametrised by the θs

$$\nabla \mathbb{E}_{\pi_\theta}[r(\tau)] = \mathbb{E}_{\pi_\theta}\left[r(\tau)\nabla \log \pi_\theta(\tau)\right]. \tag{3.41}$$

Here we just condensed the probabilities into $\pi_\theta(\tau)$ as such,

$$\pi_\theta(\tau) = \Pi_{t=1}^{T} \pi_\theta\left(a_t \mid s_t\right) p\left(s_{t+1}, r_{t+1} \mid s_t, a_t\right). \tag{3.42}$$

After some manipulation this will allow us to rewrite (3.41) as

$$\nabla \mathbb{E}_{\pi_\theta}[r(\tau)] = \mathbb{E}_{\pi_\theta}\left[\left(\sum_{t=1}^{T} G_t \nabla \log \pi_\theta\left(a_t \mid s_t\right)\right)\right]. \tag{3.43}$$

This last equation, which we will refer to as the update equation, is the take-away message from the REINFORCE-GP method. This is what one would use to update the θ parameters in Eq. (3.40). This relationship between the gradient of the expected reward and the log probabilities is what we will use to build the actor-critic methods in the next section.

Actor-Critic Algorithm

In relatively simple terms, the actor-critic algorithm is a *temporal difference* (TD) version of policy gradient (which just means it will compare values at different time steps), and it has two important entities within it: the actor and the critic. In deep reinforcement learning, both of these will be approximated by their own individual neural networks. The actor will contain the policy function and will decide what action to take at each step, while the critic, as the name suggests will try to inform the actor of the value of the action taken and how to improve.

In the previous section we introduced the REINFORCE algorithm. The reason for this was because the actor follows a very similar algorithm, but with a small extension called the baseline function, which just replaces $G_t \to G_t - b(s_t)$. This was done to improve on the REINFORCE algorithm, which without this has very high variance for the gradients and hence the learning can be noisy and lacking stability. In the AC algorithm this function is picked to be the state-value function $v_{\pi_\theta}(s_t)$.

$$A_{\pi_\theta}(s_t, a_t) = r(s_t, a_t) + \gamma v_{\pi_\theta}(s_{t+1}) - v_{\pi_\theta}(s_t) \tag{3.44}$$

To obtain the equation above we place the baseline function into (3.43) and then perform the same manipulation as we did when deriving the state-value function Bellman equation in (3.29). We then group the three terms together and call it the *advantage function*. This is also sometimes referred to as the TD error δ.

There is a slight problem with expression (3.44). The state-value function is defined in terms of the policy π_θ, which in an ideal scenario would be fine, but we cannot exactly calculate this value function, which leads us back to what we said above about the use of two neural networks. We have already approximated π_θ with parameters θ and now we will approximate the value function for this policy with parameters ω, $v_\omega(s)$. The advantage function defined above can now be rewritten in terms of this approximation.

$$A_\omega(s_t, a_t) = r(s_t, a_t) + \gamma v_\omega(s_{t+1}) - v_\omega(s_t) \tag{3.45}$$

This now allows us to define the "errors" for the two neural networks. First for the **actor**, coming from approximating the policy gradient expression:

$$J(\theta)_t \approx A_\omega\left(s_t, a_t\right) \log \pi_\theta\left(a_t, s_t\right). \tag{3.46}$$

Here, note the subscript on the error since this is at a specific time step. The definition of the error for the **critic** is much more straightforward since it is only the advantage function squared, $\frac{1}{2}A_\omega^2$. A very important thing to note here is that when taking the gradient of the advantage function with respect to ω there are two value functions, but the $v_\omega(s_{t+1})$ function is taken to be constant [67].

Now we are fully ready to give a small rundown of how the algorithm works. We will do this by writing what is known as a pseudocode which outlines how one would structure the code to perform the AC algorithm.

Algorithm 1: Actor-Critic

Initialise parameters s_0, θ, ω and also learning rates α_θ, α_ω;
Sample an action a from the distribution $\pi_\theta(a|s_0)$;
for $t = 1$ **to** T **do** ;
  Sample reward r_t;
  Sample next action and next state, a_{t+1} and s_{t+1};
  Update the policy parameters: $\theta \leftarrow \theta + \alpha_\theta v_\omega(s_t) \nabla_\theta \log \pi_\theta\left(a_t, s_t\right)$;
  Calculate the advantage at instance t: $A_\omega(s_t, a_t)$;
  Use it to update value parameters: $\omega \leftarrow \omega + \alpha_\omega A_\omega \nabla_\theta A_\omega$;
  Advance $a_t \rightarrow a_{t+1}$ and $s_t \rightarrow s_{t+1}$;
end for

The pseudocode above describes how this algorithm should be constructed. The deep reinforcement learning procedure will be to iterate over this loop and tune the

two sets of parameters of the neural networks until the agent learns the best strategy for navigating the environment. As a final remark we will say that all of the above analysis can also be done by using the action value function instead of the state value.

Soft Actor-Critic

Now that we have explained the crucial background for the algorithm we use in our research, let us motivate the reason for choosing this algorithm. First of all, almost all the algorithms which we described or mentioned in this DRL section work only for when the action space is discrete and finite. This, to reiterate, just means that at each step we can only select from a finite pool of distinguishable actions (they need not be the same for each state). We will not be able to make use of these algorithms when we apply machine learning to estimating the scaling dimensions and OPE coefficients of CFTs in the following sections as they can take continuous values. Luckily for us there have been algorithms developed for when actions take values in the real numbers. To clarify this, we still have a finite amount of actions, but each action is not just picked, but gives a real number. Let us give an example here to make the difference obvious. For the discrete action one could have the agent move up, down, left, right in an environment by a unit distance. At each step the agent will have to choose which action to make (i.e. choose which of the actions is allocated a 1 and all the rest 0), hence the discreteness. In the case of the continuous, the agent doesn't choose which action to turn on but chooses what number to assign to each action. To run with the example of 4 actions, the agent might pick 0.36 for the first, -0.001 for the second and so on.

Soft Actor-Critic [65] is part of a group of algorithms which are called entropy-regularised. What this means is that we will be altering the RL problem in Eq. (3.39) by adding a term which accounts for the entropy of the policy

$$J = \mathbb{E}_\pi \left[\sum_{t=0}^{\infty} \gamma^t \left(R\left(s_t, a_t, s_{t+1}\right) + \alpha H\left(\pi\left(\cdot \mid s_t\right)\right)\right)\right] \tag{3.47}$$

Here we are already using the expanded and discounted version of the expected return and hence assuming an infinite horizon. The dot in the expression for the policy is a placeholder for the random action variable indicating that the entropy H takes the probability distribution function itself at a state as an input (i.e. not the value of the probability at a specific a). There is one extra parameter which we have introduced which may look like a learning rate, but it is actually a parameter controlling the exploration of the agent. Note that since this is a shift to the expected return, both the value functions and their Bellman equations will change accordingly.

Let us now start introducing the algorithm itself. The soft actor-critic algorithm

aims to train four neural networks at the same time: the policy π_θ and two Q-value functions Q_{ϕ_1}, Q_{ϕ_2}, and a state-value function v_ψ. A huge innovation from the AC algorithm we introduced in the previous section is that SAC has something known as the replay buffer. It is like a memory for the agent and at every step it will sample from this pool of memories and use that to update the networks. This means that the networks are not necessarily updated using the action which the stochastic policy samples when deciding the agent's action to move in the environment. This is a huge difference from the AC algorithm, and is referred to as *off-policy* RL, while actor-critic follows an *on-policy* algorithm.

We will proceed in the same fashion as we did for the previous algorithm by introducing the error terms for each of the networks and explaining them and then laying the algorithm out in a pseudocode. An important thing to understand when dealing with such algorithms is that all of the expectation values which we have defined before will have to be approximated from the observations of the environment. The errors:

1. The error used to train the state-value function is:

$$J_V(\psi) = \frac{1}{2}\left(V_\psi\left(s_t\right) - \left[\min_{\phi_{1,2}} Q_{\phi_{1,2}}\left(s_t, a_t\right) - \log \pi_\theta\left(a_t \mid s_t\right)\right]\right)^2 \tag{3.48}$$

   The most important thing to note here is the minimum over the two Q-functions, which just means that the smaller of the two should be taken. It is there in order to avoid overestimating the action-value.

2. The error used to train the action-value functions is:

$$J_Q(\phi_{1,2}) = \frac{1}{2}\left(Q_{(\phi_{1,2}}\left(s_t, a_t\right) - \hat{Q}\left(s_t, a_t\right)\right)^2. \tag{3.49}$$

   Where $\hat{Q}$ is known as the target and is given as

$$\hat{Q}\left(s_t, a_t\right) = r\left(s_t, a_t\right) + \gamma V_{\bar{\psi}}\left(s_{t+1}\right). \tag{3.50}$$

   Here, the only thing requiring an explanation is the state-value function with parameters $\bar{\psi}$. This is odd since we said we would only be training 4 neural networks. In the strictest sense this is still true, but we did sweep quite a bit under the rug. Technically this is a neural network of its own, but we are actually not training it. There are no gradients for its parameters and no optimisation. It is called the target value network and it is updated periodically by copying the parameters ψ onto $\bar{\psi}$. Introducing a new network like this might seem like an arbitrary thing to do, but this actually helps to stabilise the learning.

3. The last is the error used to train the policy:

$$J_\pi(\theta) = \log \pi_\theta\left(a_t \mid s_t\right) - \min_{\phi_{1,2}} Q_{\phi_{1,2}}\left(s_t, a_t\right). \tag{3.51}$$

This equation is a bit less simple than it seems because the action a_t actually comes from the policy network so actually both terms will be nonzero in the θ gradient. The reason for that is that the network used to approximate the policy actually approximates the parameters to a probability distribution rather than the distribution itself. This is usually done by using a Gaussian and the output of the policy network will be the means and the standard deviations for the individual actions. This is then sampled for a_t. This is what is referred to as a stochastic action.

Note that just like we mentioned above, none of the expressions have expectations in them and that is because we are already approximating them with the sampling.

The next step is to lay out the pseudocode so we can see how the algorithm would flow in practice, shown in Alg. 2.

There are a couple of things worth noting in this pseudocode. We introduced the parameter ρ which controls how strongly the parameters are copied onto the target network. The other point is that we summed over the batches of the sampled tuples in the replay buffer when doing the gradient step. This comes as an artefact of the expectation values which now we have replaced by sampling, hence also the division by the batch size, which will give us the arithmetic mean.

We display the details of the NNs that we used for our searches in Tab. 2.

NN Hyperparameter	Value
learning rates	0.0005
γ (discount factor)	0.99
replay buffer size	100000
batch size	64
τ (smoothing coefficient)	0.001
layer 1 size	128
layer 2 size	64
reward scale	0.005

Table 2: Hyperparameter values for the NNs used in our calculations, presented in the format of [51].

Algorithm 2: Soft Actor-Critic

Initialise parameters s, θ, ϕ_1, ϕ_2, and ψ and also their learning rates α_θ, α_{ϕ_1}, α_{ϕ_2}, α_ψ;
Initialise empty replay buffer $\mathcal{B}$;
Set the target parameters equal to the state-value parameters $\bar{\psi} \leftarrow \psi$;
repeat
  Observe the state s and sample the action a;
  Implement the action in the environment;
  Observe the next state s', the reward r and also the done signal which indicates whether if s' is a terminal state;
  Store the tuple (s, a, r, s', d) in $\mathcal{B}$;
  If terminal state was reached, reset environment;
  if *need to update NNs* **then**
    for *number of times NNs need to be updated* **do**
      Sample a batch $B = \{(s, a, r, s', d)\} \subset \mathcal{B}$;
      Update state-value function by one gradient step using;

$$\frac{1}{|B|} \sum_{(s,a,r,s',d) \in \mathcal{B}} \nabla_\psi J_V(\psi)$$

      Update action-value functions by one gradient step using;

$$\frac{1}{|B|} \sum_{(s,a,r,s',d) \in \mathcal{B}} \nabla_{\phi_i} J_Q(\phi_i), \quad \text{for } i = 1, 2$$

      Update policy by one gradient step using;

$$\frac{1}{|B|} \sum_{(s,a,r,s',d) \in \mathcal{B}} \nabla_\theta J_\pi(\theta)$$

      Update the target value network with;

$$\bar{\psi} \leftarrow \rho\psi + (1 - \rho)\psi$$

    end
  end
until *convergence*;

3.4.4 Environment

Here we summarise some of the most salient features of the environment implementation. The latter guides the agent's learning on how to predict the CFT data. Since implementations of RL agents can be easily adapted for use in a large variety of problems, setting the environment becomes the most important part of the implementation. The environment must provide an interface that the agent can interact with, calculate the constraints, come up with a quantitative notion of success and define a terminal state.

The environment in which our agent "moves" is the space of parameters $(\vec{\Delta}, \vec{\mathfrak{C}})$. Every value for the scaling dimensions/OPE-squared coefficients defines a different theory. For our purposes, a point $(\vec{\Delta}, \vec{\mathfrak{C}})$ in parameter space is judged based on how well it satisfies the numerical constraints of truncated crossing equations $\vec{\mathbf{E}}(\vec{\Delta}, \vec{\mathfrak{C}}) = 0$, (3.4).

The agent's predictions feed into these numerical constraints. Since we have truncated the equations and are numerically approximating the values (and the number of constraints is larger than the number of unknowns) it is unlikely that there will be a solution that exactly satisfies all constraints in (3.4). In fact, one ends up with deviations from zero for each constraint, which then have to be minimised so that the constraints are satisfied to as good a numerical approximation as possible. These deviations are individual numbers that form the observations of the agent.

One can now straightforwardly define the reward function. Clearly, the agent should be encouraged to pick values for the parameters which minimise all the constraints. The simplest choice for such a reward is

$$R := -||\vec{\mathbf{E}}|| \tag{3.52}$$

The use of the Euclidean norm of the vector $\vec{\mathbf{E}}$ is natural (but not unique) as it quantifies the distance from the origin where the truncated equations (3.4) are satisfied exactly. The negative sign punishes larger distances away from the origin more than smaller ones. It would be interesting in the future to further explore how the efficiency of the algorithm depends on the choice of reward and to examine other options, e.g. the possibility of different weights in the definition of the Euclidean norm.

The very last section of the environment checks for final states. In our case this is simply a flag checking if the current solution is better than the current best from previous runs. If, indeed, it is, then the code overwrites the previous best, and supplies the flag to the agent. The agent needs to know whether or not the step led to a final state, as this directly feeds into the approximation of the probability distribution.

We summarise these steps in Alg. 3, where A stands for an action by the agent and R^* for the current best reward.

3.4.5 Three Modes of Running the Algorithm

The RL algorithm can be implemented in several different ways depending on the scope and focus of the search. In this subsection, we outline three different modes that were employed in producing the results of Secs 3.5 and 3.6. In summary, these are:

- **Mode 1.** Specify the spin-partition and Δ_{max} and search for scaling dimensions within the unitarity bound and Δ_{max}. For OPE-squared coefficients there are very few constraints, e.g. they may only be restricted by unitarity to be positive.
- **Mode 2.** There is a specific expectation for the scaling dimensions, for which the search is contained within a narrow window. There are no expectations for the OPE-squared coefficients, where the search is initially as wide as in mode 1.
- **Mode 3.** Both scaling dimensions and OPE-squared coefficients are within a specified, known narrow window. This mode could be implemented as a supplementary run after a mode 1 or mode 2 run, or it could be relevant in cases where we are verifying an analytic solution in the context of the truncated crossing equations, or in cases where the solution is known in some regime of parameters and we are changing these parameters adiabatically.

Algorithm 3: Basic Reinforcement-Learning Routine

Input: A, R^*
Output: individual constraints, R, R^*
Env calculate constraints using A;
Env calculate R;
Env check if $R > R^*$;
Agent observe individual constraints;
Agent store memory in buffer;
Agent learn;
if $R > R^*$ **then**
  overwrite previous best reward $R^* = R$;
end

Clearly, the range of the search becomes more narrow as we go from mode 1 to mode 3. The computational time is expected to be larger, in general, in mode 1.

Our algorithm gives the user two key dials that can be tuned at will at the beginning, or multiple times in the middle of a run. The first is a lower bound for each parameter (we will call it the "floor"). The second dial is a separate size for the search window of each parameter, in each action of the agent (we will call this dial the "guess-size"). As a rule of thumb, the initial window should at first be set large enough to minimise the probability of the agent getting trapped at a local minimum. Once the presence of a potential global minimum has been established, one can then start to hone in by gradually reducing its size. We next provide a more detailed description of each mode.

Mode 1

Since this mode involves the widest search windows, a blind search may be hindered by the existence of multiple false vacua, or may lead to an approximate solution that represents a CFT that is not of immediate interest. As a result, this mode can be assisted by additional preparation that partially restricts the search. For example, one could start with a rough preliminary exploration of the minima of $||\vec{\mathbf{E}}||$ using Mathematica, or obtain a rough estimate of some of the scaling dimensions using the approach of [40]. This preparation can help significantly facilitate the subsequent search.

To commence the search we initially run the algorithm in "guessing mode" where the RL agent only tries to improve on its own guess in the current cycle. This allows for the random exploration of configuration space and generates some initial profiles of CFT data.

Then, we enter the "normal mode", where the agent initially takes the final state from the guessing mode and tries to find small corrections so as to better satisfy the constraints. Once it finds such a correction, it replaces the final state and proceeds with a new correction iteratively. Here one can set specific values for the floor and guess-sizes. It helps to set the guess-size at a magnitude comparable to the expected order of parameter change as the agent hits the next final state. In most cases, the user can easily detect this size by observing how the agent generates configurations in real time.

The algorithm continues the search ad infinitum and the crucial question is when to stop and record the result. We have observed in the context of different theories that in actual solutions the agent reaches in reasonable time (of the order of an hour on a modern laptop) a value of the relative measure of accuracy $\mathbb{A}$ below 0.5%. In addition, when the search window is set near actual solutions the agent keeps reducing $\mathbb{A}$ significantly below the threshold of 0.5% with an apparent convergence on the values of the parameters $(\vec{\Delta}, \vec{\mathfrak{C}})$. Based on this observation, we have always aimed for runs that drop $\mathbb{A}$ below 0.1%.

Mode 2

In this mode we conduct, from the beginning, a narrow search in scaling dimensions. We have found that the following protocol produces good results.

We set the floor of the scaling dimensions to the expected values and the corresponding guess-sizes to 0. This freezes the scaling dimensions and reduces the dimensionality of the search by half, since we are conducting a search by varying only the OPE-squared coefficients. After exiting the guessing mode, we conduct the search for the optimal OPE-squared coefficients using the same procedure as in mode 1.

Once the relative accuracy $\mathbb{A}$ drops to the order of 1%, we unfreeze the scaling

dimensions by reducing their floor and opening their guess-size. The size of the search window around the expected values of the scaling dimensions can be controlled freely by the user. If the agent is already in the vicinity of a solution, the scaling dimensions will not move significantly once unfrozen, and the full set of parameters $(\vec{\Delta}, \vec{\mathfrak{C}})$ will now be adjusted by the agent to reduce $\mathbb{A}$ even further. We continue the search until we achieve an acceptably small value of $\mathbb{A}$ and observe an apparent convergence following the general procedure outlined in mode 1.

During this process it may happen that some scaling dimensions are driven towards the boundary of the prescribed window of search. In that case, the user can slightly increase the corresponding window to explore whether the approximate solution lies nearby. As long as the agent keeps improving the accuracy $\mathbb{A}$, the window can be kept in place. If there is, however, a stage in the run where the agent stops improving at an unacceptably high $\mathbb{A}$, and the adjustment of guess-sizes does not help, then this can be viewed as a strong signal that a solution does not exist in the prescribed windows.

Mode 3

In this case, we are conducting a narrow search in all components of the parameters $(\vec{\Delta}, \vec{\mathfrak{C}})$. We can run the algorithm as in mode 2 without the initial run to approximate the configuration of the OPE-squared coefficients, since this is already approximately known.

Enlarging the Spin-Partition

After having obtained results for a given spin-partition one can implement a shortcut for subsequent searches with an enlarged spin-partition (e.g. when Δ_{max} is increased). Instead of re-running the algorithm for all parameters, it is more economical to instead implement a strategy akin to that of mode 2:

- Perform the search with the least number of parameters using the steps outlined previously.
- Freeze these parameters.
- Start adding the new dynamical parameters to the set of frozen ones to approximately find the new global minimum.
- Unfreeze all parameters and let the agent determine how these new parameters change the old ones to find a better solution.

This type of implementation opens up the exciting possibility of reconstructing considerable amounts of CFT data without a full, specific, a priori given spin-partition.

Algorithm 4: Reinforcement-Learning CFT Data Search

```
Input: spin partition, floor, guess-size
Output: (Δ⃗, c⃗)
initialise Agent (memory buffer + NN weights);
initialise file for overall best reward R*;
while running guessing mode do
    Agent choose action;
    Env calculate constraints;
    Env calculate R;
    Env check if R > R*;
    Agent observe current state;
    Agent store memory in buffer;
    Agent learn;
    if R > R* then
        overwrite previous best result, R* = R;
    end
end
while not accurate enough do
    reinitialise Agent (memory buffer + NN weights);
    while running normal mode do
        Agent choose action;
        Env calculate constraints;
        Env calculate R;
        Env check if R > R*;
        Agent observe current state;
        Agent store memory in buffer;
        Agent learn;
        if R > R* then
            overwrite previous best result, R* = R;
        end
        if Agent trapped then
            break normal mode loop;
        end
    end
end
if adding new parameters then
    rerun above code first freezing then unfreezing;
end
```

Comments on User Input

To summarise, our overall approach is sketched in Alg. 4. It should be apparent from the description of the above three modes that, although the RL algorithm is set up to run independently without the input of an external user, in actual runs user intervention can help in significantly speeding up the search. A suitable real-time adjustment of the guess-size for individual parameters helps the agent focus faster around a region of potential interest. In the future, this is an aspect of the algorithm we would like to improve—or better automate—in order to facilitate more efficient parallel runs. At this stage, the mode with the minimal user input is mode 3, which involves the smallest search windows.

3.5 Application I: Minimal Models

We now pass on to explicit applications of our algorithm, starting with minimal models. The unitary minimal models are, in the appropriate sense, the simplest possible 2D CFTs and benchmarks of the original conformal bootstrap programme from the 1970s. Here we revisit them from the perspective of the global part of the Virasoro algebra, completely disregarding the Virasoro enhancement of the $\mathfrak{so}(2,2)$ conformal algebras.

In this section we search for approximate solutions to the crossing equations that we listed in Sec. 2.4, which describe minimal models. The consistency of the crossing equations in this well-known class of 2D CFTs was understood analytically early on. It is therefore a good starting point to verify that our method recovers known facts about these theories correctly. We focus on the two leading representatives in the series of unitary minimal models, the Ising and tri-critical Ising models.

3.5.1 Analytic Solution

We next briefly recall some of the salient features of the Ising and tri-critical Ising models (see [23] for a comprehensive review).

Ising Model

The Ising model, $\mathcal{M}(4,3)$, is the simplest model in the unitary minimal series $\mathcal{M}(p+1,p)$. It has central charge $c=\frac{1}{2}$ and it is equivalent to the CFT of a free Majorana fermion. Besides the identity operator $\mathbb{I}$, its spectrum contains two more primary operators: the spin operator σ with conformal weights $(h,\bar{h})=(\frac{1}{16},\frac{1}{16})$, and the energy-density operator (also called thermal operator) ε with conformal weights $(h,\bar{h})=(\frac{1}{2},\frac{1}{2})$. The corresponding OPEs are

$$\sigma\times\sigma=[\mathbb{I}]+[\varepsilon] \tag{3.53}$$

$$\sigma \times \varepsilon = [\sigma] \tag{3.54}$$

$$\varepsilon \times \varepsilon = [\mathbb{I}] \ , \tag{3.55}$$

where $[\mathcal{O}]$ denotes the Virasoro conformal family of the primary $\mathcal{O}$. In what follows, we will study the four-point functions

$$\langle \sigma(z_1,\bar{z}_1)\sigma(z_2,\bar{z}_2)\sigma(z_3,\bar{z}_3)\sigma(z_4,\bar{z}_4)\rangle \ , \tag{3.56}$$

$$\langle \varepsilon(z_1,\bar{z}_1)\varepsilon(z_2,\bar{z}_2)\varepsilon(z_3,\bar{z}_3)\varepsilon(z_4,\bar{z}_4)\rangle \ . \tag{3.57}$$

The conformal-block decomposition of these correlation functions contains, according to the first and third OPEs in (3.53), (3.55), the quasi-primaries in the Virasoro conformal family of the identity and energy-density operators. By definition, a quasi-primary state (in the holomorphic sector) is annihilated by the $L_1 = \frac{1}{2\pi i}\oint dz\, z^2\, T(z)$ conformal generator. Equivalently, the OPE between the energy-momentum tensor $T(z)$ and a quasi-primary should have no z^{-3} pole. It is straightforward to construct these quasi-primaries by acting on the primary state with the Virasoro raising operators L_{-k}, $(k \geq 1)$ but one needs to take into account the structure of the Virasoro algebra and the presence of null states in the corresponding Verma modules. States of the form $L_{-1}|\text{state}\rangle$ are, by definition, descendants in the sense of the $\mathfrak{so}(2,2)$ global part of the conformal algebra.

For example, by focusing on the holomorphic part of the theory, we obtain at the first few levels the following quasi-primaries in the Virasoro conformal families of the identity and energy-density operators.[11] In the conformal family of the identity, the states

$$L_{-2}|0\rangle \ , \quad \left(L_{-2}^2 - \frac{3}{10}L_{-1}L_{-3}\right)|0\rangle, \quad \left(L_{-2}L_{-3} - \frac{1}{2}L_{-1}L_{-2}^2 - \frac{1}{6}L_{-1}L_{-4}\right)|0\rangle \tag{3.58}$$

are the only quasi-primaries up to level 5. In the conformal family of the energy-density, the states

$$|\varepsilon\rangle \ , \quad \left(L_{-3} - \frac{4}{9}L_{-1}L_{-2}\right)|\varepsilon\rangle \ , \quad \left(L_{-4} + \frac{10}{27}L_{-2}^2 - \frac{5}{9}L_{-1}L_{-3}\right)|\varepsilon\rangle \ ,$$

$$\left(L_{-5} - \frac{2}{3}L_{-1}L_{-4} + \frac{5}{24}L_{-1}^2L_{-3} - \frac{1}{40}L_{-1}^5\right)|\varepsilon\rangle \tag{3.59}$$

are the only quasi-primaries up to level 5. A potential quasi-primary at level 2 does not exist, because it is one of the characteristic null states of the Ising model.

When combined with the anti-holomorphic sector, these results yield the spin-partitions that will be employed in the analysis of Sec. 3.5.2 below.

[11] This computation is greatly facilitated by the Mathematica package **FeynCalc9.3.1** [68, 69, 70, 71].

Tri-critical Ising Model

The tri-critical Ising model, $\mathcal{M}(5,4)$, is the next minimal model in the unitary series.[12] It has central charge $c = \frac{7}{10}$, and besides the identity operator, its conformal primary spectrum comprises three energy-density operators

$$\begin{aligned}
\varepsilon \quad &\text{with} \quad (h,\bar{h}) = \left(\frac{1}{10},\frac{1}{10}\right) \ , \\
\varepsilon' \quad &\text{with} \quad (h,\bar{h}) = \left(\frac{3}{5},\frac{3}{5}\right) \ , \\
\varepsilon'' \quad &\text{with} \quad (h,\bar{h}) = \left(\frac{3}{2},\frac{3}{2}\right) \ ,
\end{aligned}$$

and two spin operators

$$\begin{aligned}
\sigma \quad &\text{with} \quad (h,\bar{h}) = \left(\frac{3}{80},\frac{3}{80}\right) \ , \\
\sigma' \quad &\text{with} \quad (h,\bar{h}) = \left(\frac{7}{16},\frac{7}{16}\right) \ .
\end{aligned}$$

The OPEs of these operators are listed in Tab. 7.4 of [23]. We will be interested in four-point functions of the tri-critical Ising model that resemble those of the Ising model, and the way our algorithm differentiates between the two CFTs. We will therefore focus on the primary operators σ' and ε'', which satisfy

$$\sigma' \times \sigma' = [\mathbb{I}] + [\varepsilon''] \ , \quad \varepsilon'' \times \varepsilon'' = [\mathbb{I}] \ . \tag{3.60}$$

Notice the similarity with the OPEs (3.53), (3.55). Accordingly, in the next subsection we will study the four-point functions

$$\langle \sigma'(z_1,\bar{z}_1)\sigma'(z_2,\bar{z}_2)\sigma'(z_3,\bar{z}_3)\sigma'(z_4,\bar{z}_4)\rangle \ , \tag{3.61}$$

$$\langle \varepsilon''(z_1,\bar{z}_1)\varepsilon''(z_2,\bar{z}_2)\varepsilon''(z_3,\bar{z}_3)\varepsilon''(z_4,\bar{z}_4)\rangle \ . \tag{3.62}$$

Similar to the case of the Ising-model primary ε, we find that the conformal family of ε'' in the tri-critical Ising model contains the following quasi-primary states, up to level 4 in the holomorphic sector:

$$\left(L_{-2} - \frac{3}{8}L_{-1}^2\right)|\varepsilon''\rangle \ , \quad \left(L_{-2}^2 + \frac{43}{2240}L_{-1}^4 - \frac{15}{56}L_{-1}^2 L_{-2}\right)|\varepsilon''\rangle \ ,$$

$$\left(L_{-4} + \frac{31}{672}L_{-1}^4 - \frac{5}{28}L_{-1}^2 L_{-2}\right)|\varepsilon''\rangle \ . \tag{3.63}$$

[12] One of the beautiful features of the tri-critical Ising model is that it is secretly endowed with supersymmetry [72], but this feature will not play any role in our analysis.

Spin	0	1	2	3	4	5	6
	2	-	1	-	1	-	1

Table 3: A spin-partition informed by the conformal block decomposition of the four-point function $\langle\sigma(z_1,\bar{z}_1)\sigma(z_2,\bar{z}_2)\sigma(z_3,\bar{z}_3)\sigma(z_4,\bar{z}_4)\rangle$ in the Ising model with $\Delta_{\text{max}} = 6.5$.

To obtain this result we had to use that the Verma module of the state $|\varepsilon''\rangle$ contains the following null state at level 3 (in the holomorphic sector):

$$\left(L_{-3} - \frac{4}{7}L_{-1}L_{-2} + \frac{4}{35}L_{-1}^3\right)|\varepsilon''\rangle \ . \tag{3.64}$$

3.5.2 Reinforcement-Learning Results

The above analytic data can now be compared with those obtained from our RL algorithms. The current state-of-the-art numerical bootstrap methods currently impose bounds on the CFT data. Sometimes in simple theories like these, one can find isolated regions where the CFT data can be determined extremely well. In these cases our method verifies these results quite well, but our method truly shines in the cases when the bounds cannot restrict the CFT data enough. This exercise is helpful in checking the efficiency of our code before proceeding to the more complicated example of the $c = 1$ compactified boson CFT.

$\langle\sigma\sigma\sigma\sigma\rangle$ in Ising Model

The exact crossing equation for the four-point function (3.56) in the Ising model is

$$\sum_{h\geq\bar{h}}{}' \mathfrak{C}_{h,\bar{h}}\left(|z-1|^{2\Delta_\sigma}\tilde{g}^{(\sigma\sigma\sigma\sigma)}_{h,\bar{h}}(z,\bar{z}) - |z|^{2\Delta_\sigma}\tilde{g}^{(\sigma\sigma\sigma\sigma)}_{h,\bar{h}}(1-z,1-\bar{z})\right) + |z-1|^{2\Delta_\sigma} - |z|^{2\Delta_\sigma} = 0 \ . \tag{3.65}$$

As this correlator involves four identical spinless operators, both channels, s and t, exchange the same intermediate operators with even spin. In the last two terms we have singled out the contribution of the identity operator and hence the sum $\sum'$ does not contain it.

Using the crossing equation (3.65) to determine our reward function, we performed the following computation with the RL algorithm. We set $\Delta_\sigma = \frac{1}{8}$, for the external spin operator σ, and searched in mode 2 for solutions with the spin-partition of Tab. 3, which is informed by the analytic solution with a cutoff $\Delta_{\text{max}} = 6.5$. A more agnostic search in mode 1, with more limited information about the initial profile of the scaling dimensions, is also feasible. Such runs are presented in the next Sec. 3.6. Here, the mode-2 runs are computing independently the OPE-squared coefficients and confirm the analytic values of the scaling dimensions that were used to initiate the runs. In the

$\Delta_\sigma = \frac{1}{8}$				
spin	analytic Δ	RL Δ	analytic $\mathfrak{C}$	RL $\mathfrak{C}$
0	4	3.9331603	2.44141×10^{-4}	3.657538×10^{-4}
0	1	0.9881525	0.25	0.25254947
2	2	1.9802496	0.015625	0.015717817
4	4	3.9497	2.19727×10^{-4}	2.4715587×10^{-4}
6	6	5.971367	1.36239×10^{-5}	0.54007314×10^{-5}
$\mathbb{A} = 3.31618\times10^{-6}$				

Table 4: Analytic and numerical solutions for scaling dimensions and OPE-squared coefficients in the conformal-block decomposition of the four-point function $\langle\sigma(z_1,\bar{z}_1)\sigma(z_2,\bar{z}_2)\sigma(z_3,\bar{z}_3)\sigma(z_4,\bar{z}_4)\rangle$ for $\Delta_\sigma = \frac{1}{8}$ and the spin-partition of Tab. 3 with $\Delta_{\max} = 6.5$. The numerical results were obtained with a mode-2 run of the RL algorithm.

implementation of the algorithm we enforced the unitarity constraint that the OPE-squared coefficients are positive.

This is a search in a 10-dimensional space of unknowns (5 for the scaling dimensions and 5 for the corresponding OPE-squared coefficients). The results of a run with 29 crossing equations—that is, (3.65) evaluated at 29 different points on the z-plane—appear in Tab. 4. This particular run took approximately half an hour on a modern laptop machine to yield the relative accuracy $\mathbb{A} = 3.31618\times10^{-6}$.[13] When unfrozen, the scaling dimensions were allowed to vary with a guess-size 0.1. It is worth noting that the agent started the run with a random profile of OPE-squared coefficients (some of which were orders of magnitude away from those of the Ising model) and gradually converged to the results of Tab. 4.

We observe that the relative accuracy at which we can satisfy the truncated crossing equations is impressively strong, even with a very rough truncation of only 5 quasi-primary operators. When compared against the analytic expectations, the numerical results for the scaling dimensions agree at the order of 1%. For the OPE-squared coefficients, the agreement is equally impressive for the two lower-lying operators ε and L_{-2} with scaling dimensions 1 and 2 respectively, but (as might be expected) becomes worse for the higher scaling dimension operators at $\Delta = 4, 6$ that lie closer to $\Delta_{\max}$.

Notice that the exact unitarity bound for the spin-2, 4 and 6 operators requires their scaling dimensions satisfying $\Delta \geq 2, 4$ and 6 respectively. Since we have truncated the crossing equations, we do not expect the results to obey the strict unitarity bounds, and, as a result, we have allowed the agent to explore solutions with a small violation of these bounds.

[13] Originally we used the MPMATH numerical PYTHON library, which is 24 times slower, and the calculation of results similar to those of Tab. 4 took around 12 hours.

Spin	0	1	2	3	4	5	6
	2	-	3	-	1	-	1

Table 5: A spin-partition informed by the conformal-block decomposition of the four-point function $\langle\sigma'(z_1,\bar{z}_1)\sigma'(z_2,\bar{z}_2)\sigma'(z_3,\bar{z}_3)\sigma'(z_4,\bar{z}_4)\rangle$ in the tri-critical Ising model with $\Delta_{\max}=6.5$.

$\langle\sigma'\sigma'\sigma'\sigma'\rangle$ in Tri-critical Ising Model

Similarly, in the tri-critical Ising model we study the four-point function (3.61) whose crossing equation is

$$\sum_{h\geq\bar{h}}{}'\mathfrak{C}_{h,\bar{h}}\Big(|z-1|^{2\Delta_{\sigma'}}\tilde{g}^{(\sigma'\sigma'\sigma'\sigma')}_{h,\bar{h}}(z,\bar{z})-z^{2\Delta_{\sigma'}}\tilde{g}^{(\sigma'\sigma'\sigma'\sigma')}_{h,\bar{h}}(1-z,1-\bar{z})\Big)+|z-1|^{2\Delta_{\sigma'}}-|z|^{2\Delta_{\sigma'}}=0\,. \tag{3.66}$$

Once again, the sum over $h,\bar{h}$ does not include the contribution of the identity operator, which has been singled out in the last two terms of the equation. In this case we ran the RL algorithm in mode 2 by setting $\Delta_{\sigma'}=\frac{7}{8}$ for the external operator σ', and using the spin-partition of Tab. 5 informed by the analytic solution of the tri-critical Ising model with $\Delta_{\max}=6.5$.

It may be instructive to compare this spin-partition with the corresponding spin-partition for the Ising model in Tab. 3. The only difference is 3 versus 1 spin-2 quasi-primary operators. In the analytic solution there is another difference, which is not apparent in Tab. 5. At spin-6 the tri-critical Ising model has 2 degenerate quasi-primary states

$$\left(L_{-2}^3+\frac{10}{7}L_{-6}-\frac{1}{2}L_{-1}L_{-2}L_{-3}\right)|0\rangle\ ,\quad \left(L_{-3}^2+\frac{92}{63}L_{-6}-\frac{4}{9}L_{-1}L_{-2}L_{-3}\right)|0\rangle\ , \tag{3.67}$$

instead of just one, whose contribution combines as a single term in the crossing equations. The degeneracies are, therefore, invisible to the spin-partition and consequently not detectable from our analysis.

In this context, we performed a search in a 14-dimensional space of scaling dimensions and OPE-squared coefficients. The RL algorithm was run with 29 different points on the z-plane. The results that appear in Tab. 6 were obtained after a run that lasted approximately 20 minutes and yielded a configuration with relative accuracy $\mathbb{A}=0.000705966$ (significantly larger than that in Tab. 4 for the Ising model).

The comparison between the numerical and analytic results follows a pattern similar to that in the Ising model. The agent has clearly located the CFT data of the tri-critical Ising model, and the agreement with the analytic results is better for the low-lying operators at spin-0 and spin-2 with expected scaling dimensions 3 and 2 respectively.

$\Delta_{\sigma'} = \frac{7}{8}$				
spin	analytic Δ	RL Δ	analytic $\mathfrak{C}$	RL $\mathfrak{C}$
0	4	3.8950076	0.299072	0.63403654
0	3	2.9969018	0.285171	0.29550505
2	2	1.97196	0.546875	0.6054145
2	6	5.97496	0.0238323	0.041339442
2	5	5.0424104	0.0270531	0.040516548
4	4	4.051943	0.0435791	0.06928008
6	6	5.9997706	0.00589177	0.0047707544
$\mathbb{A} = 0.000705966$				

Table 6: Analytic and numerical solutions for scaling dimensions and OPE-squared coefficients in the conformal-block decomposition of the four-point function $\langle\sigma'(z_1,\bar{z}_1)\sigma'(z_2,\bar{z}_2)\sigma'(z_3,\bar{z}_3)\sigma'(z_4,\bar{z}_4)\rangle$ for $\Delta_\sigma = \frac{7}{8}$ and the spin-partition of Tab. 5 with $\Delta_{\max} = 6.5$. The numerical results were obtained with a mode-2 run of the RL algorithm.

4-point Functions with the Identity as the Single Virasoro Conformal Block

Several minimal models have 4-point functions of a single conformal primary with the identity as the only Virasoro conformal block. In the Ising model, $\mathcal{M}(4,3)$, this feature appears in the four-point function $\langle\varepsilon(z_1,\bar{z}_1)\varepsilon(z_2,\bar{z}_2)\varepsilon(z_3,\bar{z}_3)\varepsilon(z_4,\bar{z}_4)\rangle$, in the tri-critical Ising model, $\mathcal{M}(5,4)$, in the four-point function $\langle\varepsilon''(z_1,\bar{z}_1)\varepsilon''(z_2,\bar{z}_2)\varepsilon''(z_3,\bar{z}_3)\varepsilon''(z_4,\bar{z}_4)\rangle$, in the three-state Potts model, $\mathcal{M}(6,5)$, and also in the relevant four-point function $\langle Y(z_1,\bar{z}_1)Y(z_2,\bar{z}_2)Y(z_3,\bar{z}_3)Y(z_4,\bar{z}_4)\rangle$ etc. The operators $\varepsilon, \varepsilon'', Y$ are all spinless with different scaling dimensions: $1, 3, 6$, respectively. In this subsection, we compare the first two cases: $\langle\varepsilon\varepsilon\varepsilon\varepsilon\rangle$ in the Ising model, and $\langle\varepsilon''\varepsilon''\varepsilon''\varepsilon''\rangle$ in the tri-critical Ising model.

In all these cases the crossing equations are similar,

$$\sum_{h\geq\bar{h}}{}' \mathfrak{C}_{h,\bar{h}}\Big(|z-1|^{2\Delta_\mathcal{O}}\tilde{g}^{(\mathcal{O}\mathcal{O}\mathcal{O}\mathcal{O})}_{h,\bar{h}}(z,\bar{z}) - z^{2\Delta_\mathcal{O}}\tilde{g}^{(\mathcal{O}\mathcal{O}\mathcal{O}\mathcal{O})}_{h,\bar{h}}(1-z,1-\bar{z})\Big) + |z-1|^{2\Delta_\mathcal{O}} - |z|^{2\Delta_\mathcal{O}} = 0\,, \tag{3.68}$$

and the spin-partition is the same. $\mathcal{O}$ is the spinless external operator and $\Delta_\mathcal{O}$ its scaling dimension.

Using the spin-partition of Tab. 7, which contains the expected number of quasi-primary operators in the identity Virasoro block up to scaling dimension 6.5, we varied the scaling dimension $\Delta_\mathcal{O}$ of the external operator and searched for solutions to the crossing equations (3.68). Our main purpose in this subsection was to verify the expected analytic solutions of the Ising and tri-critical Ising models and that the algorithm could distinguish solutions with different external scaling dimensions but the same spin-partition. For these purposes a mode-3 run was deemed sufficient.

The results of Tab. 8 were obtained with $\mathcal{O} = \varepsilon$. Indeed, they verify quite clearly the expected structure of the Ising model. The run reported in Tab. 8 took only 5 minutes to reach the relative accuracy $\mathbb{A} = 0.000862723$ in mode 3.

Spin	0	1	2	3	4	5	6
	1	-	2	-	1	-	1

Table 7: A spin-partition for the conformal block contribution of the identity operator with $\Delta_{\max} = 6$.

$\Delta_\varepsilon = 1$				
spin	analytic Δ	RL Δ	analytic $\mathfrak{C}$	RL $\mathfrak{C}$
0	4	4.0683885	1	1.0427935
2	2	1.9544389	1	1.1926383
2	6	5.926708	0.1	0.1150967
4	4	3.904911	0.1	0.20634486
6	6	5.9300733	0.0238095	0.022085898
$\mathbb{A} = 0.000862723$				

Table 8: Analytic and numerical solutions for scaling dimensions and OPE-squared coefficients in the conformal block decomposition of the four-point function $\langle\varepsilon(z_1,\bar{z}_1)\varepsilon(z_2,\bar{z}_2)\varepsilon(z_3,\bar{z}_3)\varepsilon(z_4,\bar{z}_4)\rangle$ for $\Delta_\varepsilon = 1$ and the spin-partition of Tab. 7 with $\Delta_{\max} = 6.5$. The numerical results were obtained with a mode-3 run of the RL algorithm.

A similar mode-3 run with $\mathcal{O} = \varepsilon''$ produced the results of Tab. 9 with a comparable relative accuracy $\mathbb{A} = 0.000668002$. The general features of the expected structure of the tri-critical Ising model are present, but some of the numbers (depicted in magenta in Tab. 9) exhibit significant discrepancies with the analytic results. A possibly related feature in the analytic solution is the presence of sizeable OPE-squared coefficients at higher scaling dimensions. In order to probe this feature further, we repeated the computation with a higher cutoff, $\Delta_{\max} = 8.5$, which involves a spin-partition with 8 different operators. The resulting 16-dimensional search in mode 3 produced the numbers listed in Tab. 10, which exhibit a definite improvement compared to the previous $\Delta_{\max} = 6.5$ run. For the convenience of the reader we have highlighted with a magenta color the corresponding numbers in Tabs 9 and 10.

In the above computations we fixed the scaling dimension of the external operator and tried to determine the remaining data. It would be interesting to perform a more general computation, where the scaling dimension of the external operator is one of the unknowns of the search. In mode 1, this search should be able to identify, solely from the input of the spin-partition, different solutions corresponding to the data of each CFT in the minimal series. We do not perform this computation here, but present results of a very similar computation in Sec. 3.6.2 in the case of the compactified boson CFT.

$\Delta_{\varepsilon''} = 3$				
spin	analytic Δ	RL Δ	analytic $\mathfrak{C}$	RL $\mathfrak{C}$
0	4	5.3342843	41.3265	43.009876
2	2	2.586108	6.42857	6.317041
2	6	5.900023	23.4184	23.202938
4	4	4.8769903	3.64286	16.4788
6	6	6.0306115	1.23387	1.7063767
$\mathbb{A} = 0.000668002$				

Table 9: Analytic and numerical solutions for scaling dimensions and OPE-squared coefficients in the conformal block decomposition of the four-point function $\langle\varepsilon''(z_1,\bar{z}_1)\varepsilon''(z_2,\bar{z}_2)\varepsilon''(z_3,\bar{z}_3)\varepsilon''(z_4,\bar{z}_4)\rangle$ for $\Delta_{\varepsilon''} = 3$ and the spin-partition of Tab. 7 with $\Delta_{\max} = 6.5$. The numerical results were obtained with a mode-3 run of the RL algorithm.

$\Delta_{\varepsilon''} = 3$				
spin	analytic Δ	RL Δ	analytic $\mathfrak{C}$	RL $\mathfrak{C}$
0	4	4.505229	41.3265	40.726093
0	8	7.9896655	13.2704	13.0988035
2	2	2.3935893	6.42857	5.4763665
2	6	7.1316943	23.4184	21.824356
4	4	4.362866	3.64286	4.9283843
4	8	7.9502306	5.89678	6.0844507
6	6	6.0996165	1.23387	2.7852516
8	8	8.006613	0.251744	0.0013012796
$\mathbb{A} = 0.000771919$				

Table 10: A $\Delta_{\max} = 8.5$ version of Tab. 9.

3.6 Application II: $c = 1$ Compactified Boson

With an eye towards more general applications, it is important to explore the performance of our approach beyond the restricted class of rational conformal field theories, of which minimal models are a special case. In this section, we study the $c = 1$ compactified boson CFT. This is a free scalar CFT. Free CFTs are the benchmark of the Lagrangian QFT approach and the basis of perturbative methods in quantum field theory, readily solved by traditional methods and an entry-level litmus test for the generalisation of our method to more challenging settings.

The reader should appreciate that by rediscovering the compactified boson CFT as a solution to the crossing equations, one would be able to solve it without the use of the standard Lagrangian methods, e.g. they would be able to determine correlation functions without using Wick's theorem. Despite its simplicity, the free scalar CFT has a rich spectrum of primary operators with momentum and winding around the target circle and scaling dimensions that depend non-trivially on an exactly marginal

coupling—the radius of the circle. This is therefore an interesting toy model where our methods can be used to compute non-trivial CFT data across a continuous family of CFTs connected by exactly marginal deformations, namely across a conformal manifold. Conformal manifolds are ubiquitous in four-dimensional supersymmetric QFTs, e.g. in 4D $\mathcal{N} = 4$ SYM theory, which would be one of the natural subsequent applications of the RL approach presented here.

We study two examples of four-point functions in the compactified boson CFT: four-point functions of vertex operators with momentum or winding, and four-point functions of the conserved $U(1)$ current. We discover that even with a very small cutoff, as low as $\Delta_{\text{max}} = 2$, the algorithm can detect correctly the 2D compactified boson CFT and returns rather accurate approximate values for scaling dimensions and OPE-squared coefficients.

3.6.1 Analytic Solution

Before delving into the results of the RL exercise, it is useful to recall briefly the analytic solution of the 2D S^1 scalar theory that we want to rediscover from a conformal bootstrap/RL perspective.

Consider the 2D CFT of a compact boson X with radius R:

$$S = \frac{1}{4\pi}\int d^2z\ \partial X \bar{\partial} X\ , \quad X \simeq X + 2\pi R\ . \tag{3.69}$$

Since this is a free theory, it is straightforward to analytically compute all its data. Let us summarise some of the pertinent details following closely the conventions of [73] with $\alpha' = 2$.

The basic conformal primaries of the theory are the $U(1)$ currents

$$j(z) = \frac{i}{2}\partial X(z)\ , \quad \bar{j}(\bar{z}) = \frac{i}{2}\partial X(\bar{z}) \tag{3.70}$$

and the vertex operators[14]

$$V_{p,\bar{p}}(z,\bar{z}) = e^{ipX(z)+i\bar{p}\bar{X}(\bar{z})}\ , \quad p = \frac{n}{R} + \frac{wR}{2}\ , \quad \bar{p} = \frac{n}{R} - \frac{wR}{2}\ , \tag{3.71}$$

where n and w are the integer momentum and winding quantum numbers of the corresponding states. j, $\bar{j}$ have respectively conformal scaling dimensions $(h,\bar{h}) = (1,0),(0,1)$, while $V_{p,\bar{p}}$ has $(h,\bar{h}) = (\frac{p^2}{2},\frac{\bar{p}^2}{2})$. The spin of an operator is $s = h - \bar{h}$. As a result, the vertex operator $V_{p,\bar{p}}$ has spin $s = \frac{1}{2}(p^2 - \bar{p}^2) = nw$. Corresponding states with only momentum, or only winding, are spinless.

The remaining spectrum of operators can be organised using the Virasoro algebra,

[14] All the operators appearing below should be understood as being normal ordered.

but since we only want to use the global $\mathfrak{so}(2,2)$ part of the 2D conformal algebra, we need to also identify all the quasi-primary operators. All quasi-primaries of the theory can be obtained by combining any quasi-primary operator from the left-moving (holomorphic) sector with any quasi-primary operator from the right-moving (anti-holomorphic) sector. There are no factors with mixed holomorphic-antiholomorphic derivatives in an operator because of the equations of motion $\partial\bar{\partial}X = 0$. Hence, let us focus momentarily on the holomorphic sector.

As already noted in our minimal-model discussion, a quasi-primary state (in the holomorphic sector) is annihilated by the $L_1 = \frac{1}{2\pi i}\oint dz\, z^2\ T(z)$ conformal generator. This requires that the OPE between the energy-momentum tensor $T(z)$ and a quasi-primary should have no z^{-3} pole. The general vertex operator with holomorphic momentum p has the form

$$\mathcal{O}_{m_1,\ldots,m_r;p} \equiv \prod_{a=1}^{r} (\partial^a X)^{m_a}\, e^{ipX}\ . \tag{3.72}$$

A straightforward computation shows that the z^{-3} pole in the OPE $T(z)\mathcal{O}_{m_1,\ldots,m_r;p}(0)$ is

$$\Big[T(z)\mathcal{O}_{m_1,\ldots,m_r;p}(0)\Big]_3 = \sum_{a=2}^{r}(a-1)a\,\mathcal{O}_{m_1,\ldots,m_{a-1}+1,m_a-1,m_{a+1},\ldots,m_r;p}(0)\ . \tag{3.73}$$

A generic quasi-primary is a linear combination of operators of the form (3.72) with the same conformal dimension. Eq. (3.73) can be used to determine the numerical coefficients in these combinations. For example, the quasi-primaries with up to six derivatives are:

$$\begin{gathered}
\left[(\partial X)^2 + ip\partial^2 X\right]\, e^{ipX}\ ,\quad \left[(\partial X)^3 + \frac{3}{2}ip\partial X\partial^2 X - \frac{p^2}{4}\partial^3 X\right]\, e^{ipX}\ ,\\
\left[(\partial X)^4 + 2ip(\partial X)^2\partial^2 X - p^2(\partial^2 X)^2\right]\, e^{ipX}\ ,\quad \left[\partial X\partial^3 X + \frac{ip}{12}\partial^4 X - \frac{3}{2}(\partial^2 X)^2\right]\, e^{ipX}\ ,\\
\left[(\partial X)^5 + \frac{5ip}{2}(\partial X)^3\partial^2 X - \frac{p^2}{4}\left((\partial X)^2\partial^3 X + ip\partial^2 X\partial^3 X + 6\partial X(\partial^2 X)^2\right)\right]\, e^{ipX}\ ,\\
\left[(\partial X)^2\partial^3 X - \frac{3}{2}\partial X(\partial^2 X)^2 + \frac{p}{4}\left(\frac{5i}{6}\partial X\partial^4 X - \frac{1}{24}\partial^5 X - i\partial^2 X\partial^3 X\right)\right]\, e^{ipX}\ ,\\
\left[(\partial X)^6 + 3ip(\partial X)^4\partial^2 X - 3p^2\left((\partial X)^2(\partial^2 X)^2 + \frac{ip}{3}(\partial^2 X)^3\right)\right]\, e^{ipX}\ ,\\
\left[(\partial X)^3\partial^3 X - \frac{3}{2}\left((\partial X)^2(\partial^2 X)^2 + \frac{ip}{3}(\partial^2 X)^3\right)\right.\\
\left. + \frac{3ip}{2}\left(\partial X\partial^2 X\partial^3 X - (\partial^2 X)^3 + \frac{ip}{12}(\partial^3 X)^2\right)\right]\, e^{ipX}\ ,
\end{gathered}$$

$$\left[\partial X\partial^5 X + \frac{ip}{30}\partial^6 X - 10\partial^2 X\partial^4 X + 10(\partial^3 X)^2\right] e^{ipX} \ ,$$
$$\left[(\partial X)^3\partial^3 X - \frac{3}{2}(\partial X)^2(\partial^2 X)^2 + \frac{3p^2}{8}(\partial^3 X)^2 - \frac{p^2}{3}\partial^2 X\partial^4 X \right.$$
$$\left. + \frac{ip}{3}(\partial X)^2\partial^4 X - \frac{ip}{2}\partial X\partial^2 X\partial^3 X\right] e^{ipX} \ . \tag{3.74}$$

Putting together the holomorphic and anti-holomorphic parts, general quasi-primaries can be obtained as linear combinations of the operators

$$\mathcal{O}_{\{m_a\},\{\bar{m}_{\bar{a}}\};p,\bar{p}} \equiv \prod_{a=1}^{r} (\partial^a X)^{m_a} \prod_{\bar{a}=1}^{\bar{r}} \left(\partial^{\bar{a}}\bar{X}\right)^{\bar{m}_{\bar{a}}} e^{ipX + i\bar{p}\bar{X}} \ . \tag{3.75}$$

The conformal dimensions of these operators are

$$h = \ell + \frac{1}{2}p^2 = \ell + \frac{1}{2}\left(\frac{n}{R} + \frac{wR}{2}\right)^2 \ , \tag{3.76}$$
$$\bar{h} = \bar{\ell} + \frac{1}{2}\bar{p}^2 = \bar{\ell} + \frac{1}{2}\left(\frac{n}{R} - \frac{wR}{2}\right)^2 \ , \tag{3.77}$$

where $\ell = \sum_{a=1}^{r} a\, m_a$, $\bar{\ell} = \sum_{\bar{a}=1}^{\bar{r}} \bar{a}\, \bar{m}_{\bar{a}}$ and $p, \bar{p}$ are expressed in terms of the momentum and winding quantum numbers.

The two- and three-point functions involving the above quasi-primaries can be computed straightforwardly using Wick contractions. Explicit results, that will be compared against those from the RL output, will be listed in the next subsection.

3.6.2 Reinforcement-Learning Results

We will now attempt to rediscover the S^1 theory from the conformal-bootstrap perspective. We consider two kinds of four-point functions. The first one is the four-point function of four spinless conformal primaries with arbitrary, but fixed, scaling dimensions. The zero-spin assumption is not necessary; we only make it here for convenience and illustration purposes. We further assume that these operators are charged under a conserved $U(1)$ symmetry. We denote them as V_p and parametrise their scaling dimension Δ_p by the real variable p using the relation

$$\Delta_p \equiv p^2 \ . \tag{3.78}$$

We emphasise that this equation should be viewed as the definition of the real number p. At this point we do not specify how p relates to the $U(1)$ charge of V_p and hence (3.78) is *not* a dynamical statement about the scaling dimension Δ_p in terms of some

	Spin	0	1	2	3	4	5
$\Delta_{\max} = 2$	s-channel	1	–	–	–	–	–
	t-channel	1	1	1	–	–	–
$\Delta_{\max} = 3.5$	s-channel	1	–	1	1	–	–
	t-channel	1	2	1	1	–	–
$\Delta_{\max} = 4.5$	s-channel	2	–	1	1	1	–
	t-channel	2	2	2	1	1	–
$\Delta_{\max} = 5.5$	s-channel	2	1	1	1	1	1
	t-channel	2	3	2	2	1	1

Table 11: Spin-partitions for the conformal-block decomposition of the four-point function $\langle V_p(z_1,\bar{z}_1)V_p(z_2,\bar{z}_2)\bar{V}_p(z_3,\bar{z}_3)\bar{V}_p(z_4,\bar{z}_4)\rangle$ at four different values of the cutoff $\Delta_{\max}$.

other quantum number.

Keeping the above in mind, we consider the four-point function

$$\langle V_p(z_1,\bar{z}_1)V_p(z_2,\bar{z}_2)\bar{V}_p(z_3,\bar{z}_3)\bar{V}_p(z_4,\bar{z}_4)\rangle \ , \tag{3.79}$$

where $\bar{V}_p$ denotes the complex conjugate of V_p. Since V_p and $\bar{V}_p$ have opposite $U(1)$ charge, the four-point function (3.79) is neutral under the assumed global $U(1)$ symmetry. V_p is expected to capture the primary vertex operator $V_{p,p}(z,\bar{z}) = e^{ip(X(z)+\bar{X}(\bar{z}))}$ with $p = \bar{p} = \frac{n}{R}$ and winding $w = 0$, or the T-dual $V_{p,-p}(z,\bar{z}) = e^{ip(X(z)-\bar{X}(\bar{z}))}$ with $p = \bar{p} = \frac{w}{R}$ and momentum $n = 0$. Only a minimal part of this information will be incorporated indirectly into the algorithm via the spin-partition. Using this partial information, the agent will have to uncover that V_p is indeed part of the S^1 theory and that p is related to the $U(1)$ charge.

The second kind of four-point function that we will consider is the correlator of the conserved spin-1 operator j,

$$\langle j(z_1)j(z_2)j(z_3)j(z_4)\rangle \ . \tag{3.80}$$

We next display the results of the RL algorithm for each case.

Momentum/winding Sector

The crossing equation for the four-point function (3.79) can be written as

$$\sum_{h\geq\bar{h}} {}_s\mathfrak{C}_{h,\bar{h}}|z-1|^{2\Delta_p}\tilde{g}^{(VV\bar{V}\bar{V})}_{h,\bar{h}}(z,\bar{z}) - {\sum_{h'\geq\bar{h}'}}' {}_t\mathfrak{C}_{h',\bar{h}'}|z|^{2\Delta_p}\tilde{g}^{(\bar{V}VV\bar{V})}_{h,\bar{h}}(1-z,1-\bar{z}) - |z|^{2\Delta_p} = 0 \ . \tag{3.81}$$

In the t-channel block decomposition we have separated the contribution of the identity operator and have used the normalisation convention $\langle V_p\,\bar{V}_p\rangle = 1$.

Let us fix for concreteness the scaling dimension Δ_p of V_p to some specific value, e.g. $\Delta_p = 0.1$. This value is deliberately small to allow for spin-partitions with relatively small cutoff Δ_{max}. In Tab. 11 we collect four spin-partitions that will be used to study the truncated version of the crossing equations (3.81). These spin-partitions are inspired by the analytic solution of the S^1 theory when imposing the cutoff $\Delta_{\text{max}} = 2, 3.5, 4.5, 5.5$, respectively, in the OPEs of the s- and t-channels. In each of these spin-partitions the number of unknowns (scaling dimensions plus OPE-squared coefficients) that we are solving for is 8, 16, 26, 36.

In Tabs 12-14 we have collected the expected analytic results of the S^1 theory for $V_p = V_{p,\pm p}$ and $|p| = \sqrt{0.1}$ together with the best results of the runs we performed. In contrast to Sec. 3.5, where we presented results based mainly on mode-2 and mode-3 runs (guided by partial prior information about the CFT data in the initialisation of the code), in this section we present results of genuine mode-1 runs based only on the information provided by the spin-partition.

One of the first observations in Tab. 12 is that already in the simplest case of $\Delta_{\text{max}} = 2$ the RL algorithm predicts the corresponding CFT data to very good accuracy. The run reported in Tab. 12 for $\Delta_{\text{max}} = 2$ used 30 z-points and took approximately 5 minutes to yield the relative accuracy $\mathbb{A} = 0.000197442$. The results for the higher cutoffs, that incorporate further operators with higher conformal scaling dimensions (and spin), were obtained by building on the $\Delta_{\text{max}} = 2$ data with the use of the incremental mode-1 procedure of Sec. 3.4.5.

The results at $\Delta_{\text{max}} = 3.5$ in Tab. 12 exhibit a noticeable decrease in $\mathbb{A}$ (which translates to a smaller violation of the truncated-reduced crossing equations) and agreement between the numerical and analytic results for the low-lying spectrum, which is comparable with the $\Delta_{\text{max}} = 2$ run. Notice that there are two deliberate features complicating the $\Delta_{\text{max}} = 3.5$ run. First, the fact that the spin-3 operator is absent in the s-channel was not an input. The agent had to discover this feature (as it does), but this complicates the search. Interestingly, although the spin-3 operator is absent in the exact conformal decomposition, the agent manages to identify its scaling dimension with remarkable accuracy. Apparently, this is not an accident; similar results are obtained in the higher cutoff runs of Tabs 13-14. Second, in the runs of Tab. 12 we are not using any information about the signs of the OPE-squared coefficients. As a result, some of the OPE-squared coefficients obtained in the $\Delta_{\text{max}} = 3.5$ run have the wrong sign in the t-channel. Once again, this complicates the search and prevents the agent from improving the agreement between the numerical and analytic results.

The data reported in Tabs 13-14 are based on multi-dimensional searches with an even larger number of operators (13 and 18 respectively). To increase the accuracy (namely, reduce the value of $\mathbb{A}$) we used the results of the incremental mode-1 procedure of Sec. 3.4.5 to initialise an additional, subsequent mode-2 run with 49 z-points. The

$\Delta_{\max} = 2$					
Channel	spin	analytic Δ	RL Δ	analytic $\mathfrak{C}$	RL $\mathfrak{C}$
s	0	0.4	0.38694087	1	0.99479413
t	0	2	2.1108415	0.01	0.010378244
	1	1	0.9485743	-0.1	-0.10135128
	2	2	2.1295118	0.005	0.004827103
$\mathbb{A} = 0.000197442$					

$\Delta_{\max} = 3.5$					
Channel	spin	analytic Δ	RL Δ	analytic $\mathfrak{C}$	RL $\mathfrak{C}$
s	0	0.4	0.39011472	1	0.999143
	2	2.4	2.2029796	3.57143×10^{-3}	2.2229333×10^{-3}
	3	3.4	3.203875	0	4.971186×10^{-7}
t	0	2	2.1141205	0.01	0.008170344
	1	1	0.95283717	-0.1	-0.09884554
	1	3	2.8024354	-5×10^{-4}	9.701283×10^{-4}
	2	2	2.1266346	0.005	0.003557264
	3	3	2.8005629	-1.66667×10^{-4}	4.3958283×10^{-4}
$\mathbb{A} = 0.00000225745$					

Table 12: Analytic and numerical solutions for scaling dimensions and OPE-squared coefficients for $\Delta_p = 0.1$ and spin-partitions with $\Delta_{\max} = 2, 3.5$ and 30 z-points respectively. The numerical results were obtained using the mode described in Sec. 3.4.5.

mode-2 run began with a search on the OPE-squared coefficients alone, while the scaling dimensions were kept fixed at the values obtained from the prior mode-1 search. At a second stage of the run, the scaling dimensions were unfrozen and the agent was allowed to search in the complete space of scaling dimensions and OPE-squared coefficients to find the results reported in Tabs 13-14. In the $\Delta_{\max} = 4.5$ run we kept the signs of the OPE-squared coefficients free (as in Tabs 12). With the exception of the OPE-squared coefficients for the second spin-0 operator in the s-channel, the agent managed to predict the correct signs. To illustrate what happens when we input the correct signs, we performed the more complicated $\Delta_{\max} = 5.5$ run by fixing the signs of the OPE-squared coefficients at their expected analytic values. The combined mode-1 and mode-2 runs at $\Delta_{\max} = 4.5$ took approximately 2 hours and the runs at $\Delta_{\max} = 5.5$ 4 hours.

Comparing the numerical and analytic results in Tabs 13-14 we observe that the agent has performed impressively well for the scaling dimensions (even for the odd-spin operators that do not contribute to the s-channel in the exact result). It performed decently for the OPE-squared coefficients of the low-lying $\Delta_{\max} = 2$ operators, but poorly for many of the remaining, numerically smaller coefficients. From the single

$\Delta_{\max} = 4.5$					
Channel	spin	analytic Δ	RL Δ	analytic $\mathfrak{C}$	RL $\mathfrak{C}$
s	0	0.4	0.4185128	1	0.98406625
	0	4.4	4.229518	1.27551×10^{-5}	$-5.3023865 \times 10^{-5}$
	2	2.4	2.4269097	3.57143×10^{-3}	4.041962×10^{-3}
	3	3.4	3.2022634	0	$-1.0026526 \times 10^{-3}$
	4	4.4	4.574162	1.96039×10^{-3}	2.7667696×10^{-4}
t	0	2	2.0097528	0.01	0.0025764485
	0	4	3.8530886	2.5×10^{-5}	4.1462967×10^{-4}
	1	1	0.9313935	-0.1	-0.10908633
	1	3	2.9478629	-5×10^{-4}	-7.262531×10^{-3}
	2	2	2.0496795	0.005	0.013589153
	2	4	3.8056073	1.66667×10^{-5}	6.19941×10^{-5}
	3	3	2.9541698	-1.66667×10^{-4}	-4.592793×10^{-3}
	4	4	4.0146556	4.16667×10^{-6}	4.924626×10^{-3}
$\mathbb{A} = 0.0000206548$					

Table 13: Analytic and numerical solutions for scaling dimensions and OPE-squared coefficients for $\Delta_p = 0.1$ and spin-partitions with $\Delta_{\max} = 4.5$ and 49 z-points. The numerical results were obtained using a mode-2 run on top of the mode described in Sec. 3.4.5.

runs reported in Tabs 13-14 we can immediately deduce that the algorithm works, because it managed to minimise the violation of the truncated crossing equations and identified CFT data with a very low value of $\mathbb{A}$. To obtain a better understanding of the values predicted by the algorithm, and record a more solid result, one needs (at the very least) to perform multiple runs and determine the statistical variation of the obtained results. We expect the smallest statistical variations for the low-lying scaling dimensions and the corresponding OPE-squared coefficients. It would also be interesting to explore further how these data are affected by the choice of the z-sampling and the precise form of the reward function. As a preliminary check, we examined a derivative expansion of the crossing equations around the fully symmetric point $u = v = 1$ (see Ref. [41]), using the quoted scaling dimensions in Tab. 14 as an input. Truncating to the appropriate order we solved the resulting linear system to obtain the corresponding OPE-squared coefficients. Interestingly, we observed numerical values comparable to the ones obtained in Tab. 14 with the use of the RL algorithm.

As an illustration, we performed a preliminary analysis of the statistical errors with multiple runs for the $\Delta_{\max} = 2$, $\Delta_p = 0.1$ case by completing 12 runs with 20 z-points. The results, collected in Tab. 15, provide a more complete picture of the final output of the computation. We note that the errors in Tab. 15 do not include systematic errors associated with the truncation or the choice of the z-points.

Finally, we performed the following exercise. Using the fixed spin-partition for $\Delta_{\max} = 2$ from Tab. 11, we varied Δ_p from 0.1 to 0.6 with a step of 0.1. As Δ_p

$\Delta_{\max} = 5.5$					
Channel	spin	analytic Δ	RL Δ	analytic $\mathfrak{C}$	RL $\mathfrak{C}$
s	0	0.4	0.40006787	1	1.0057276
	0	4.4	4.336432	1.27551×10^{-5}	$0.43016876 \times 10^{-5}$
	1	5.4	5.307818	0	$-2.2633198 \times 10^{-4}$
	2	2.4	2.4060674	3.57143×10^{-3}	5.486169×10^{-3}
	3	3.4	3.446559	0	$-0.4480493 \times 10^{-5}$
	4	4.4	4.410344	1.96039×10^{-3}	$0.27796367 \times 10^{-3}$
	5	5.4	5.3354797	0	-9.976282×10^{-5}
t	0	2	2.001293	0.01	0.0056684865
	0	4	4.0166564	2.5×10^{-5}	4.8836926×10^{-4}
	1	1	1.040068	-0.1	-0.085237
	1	3	3.0494268	-5×10^{-4}	-2.271628×10^{-2}
	1	5	4.9848695	-8.33333×10^{-7}	-9.268466×10^{-4}
	2	2	2.00707	0.005	0.0018059064
	2	4	4.045016	1.66667×10^{-5}	7.282457×10^{-4}
	3	3	3.0331514	-1.66667×10^{-4}	-2.894943×10^{-4}
	3	5	4.9544168	-4.16667×10^{-7}	$-3.3044117 \times 10^{-3}$
	4	4	3.9395354	4.16667×10^{-6}	6.668457×10^{-4}
	5	5	5.0390368	-8.33333×10^{-8}	$-4.3607014 \times 10^{-4}$
$\mathbb{A} = 0.0000321653$					

Table 14: Analytic and numerical solutions for scaling dimensions and OPE-squared coefficients for $\Delta_p = 0.1$ and spin-partitions with $\Delta_{\max} = 5.5$ and 49 z-points. The numerical results were obtained using a mode-2 run on top of the mode described in Sec. 3.4.5.

$\Delta_{\max} = 2$					
Channel	spin	analytic Δ	RL Δ	analytic $\mathfrak{C}$	RL $\mathfrak{C}$
s	0	0.4	0.38941 ± 0.00862	1	0.99546 ± 0.00335
t	0	2	1.96776 ± 0.11673	0.01	0.01151 ± 0.00359
	1	1	0.96145 ± 0.04084	-0.1	-0.10180 ± 0.00435
	2	2	2.06592 ± 0.17467	0.005	0.00497 ± 0.00156
$\mathbb{A} = 0.000298727 \pm 0.0000960205$					

Table 15: Analytic and numerical solutions from 12 runs for the mean and standard deviations of the scaling dimensions and OPE-squared coefficients for $\Delta_p = 0.1$, spin-partitions with $\Delta_{\max} = 2$ and 20 z-points. The numerical results were obtained in mode 1.

increases so do the scaling dimensions in the s-channel. As a result, in the s-channel we increase appropriately the upper cutoff in the search and the fixed spin-partition is no longer that of $\Delta_{\max} = 2$. At the same time, the t-channel scaling dimensions remain within the $\Delta_{\max} = 2$ window. In Fig. 2 we plot the scaling dimension Δ_s of the lowest scalar in the s-channel OPE of V_p as a function of Δ_p. The slope of the best-fit line, $\Delta_s = -0.0127 + 3.99345\Delta_p$, is 0.16% close to the analytically expected value of

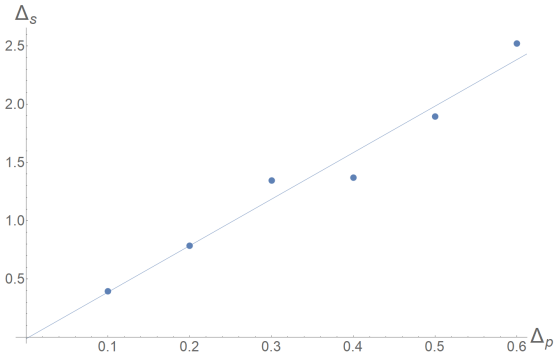

Figure 2: A plot of the numerically obtained values of Δ_s for the lowest scalar in the s channel as a function of Δ_p. The solid line is the line of best fit.

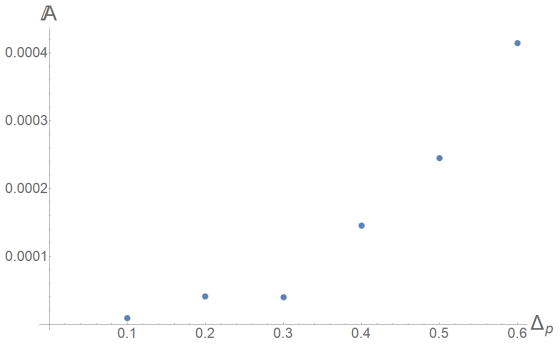

Figure 3: A plot of the relative accuracy $\mathbb{A}$ for the runs leading to Fig. 2 as a function of Δ_p.

$\Delta_s = 4\Delta_p$, although the relative accuracy $\mathbb{A}$ of the corresponding search increases for higher Δ_p, as can be seen from Fig. 3. This result suggests that the fixed spin-partition in the top entry of Tab. 11 is inadequate as we increase the scaling dimension of the external operators and that more operators need to be included for large external scaling dimensions in both channels. It would be useful to develop a better understanding of the optimal use of cutoffs and search windows in such situations.

One can also infer some additional information from Fig. 2. Had one been agnostic about the CFT, Fig. 2 would provide evidence that the variable p is proportional to the $U(1)$ charge of the operator V_p, since the scalar appearing in the OPE V_pV_p has twice the $U(1)$ charge of V_p (the $U(1)$ charge is additive) and the scaling dimension Δ_s is found to be $\Delta_s = (2p)^2$. A sharper argument along these lines could be obtained by studying the four-point function $\langle V_{p_1}V_{p_2}\bar{V}_{p_1}\bar{V}_{p_2}\rangle$ for a generic pair of p_1, p_2. The four-point function $\langle jjV_p\bar{V}_p\rangle$ would also yield related information.

At this point, it is interesting to ask whether the RL results allow us to conclusively determine that the CFT in question has a one-dimensional conformal manifold (namely an exactly marginal operator). The uncharged, spinless operator of scaling dimension 2 that appears in the t-channel is an obvious candidate that indicates the existence of a

Spin	0	1	2	3	4	5	6	7	8
	-	-	1	-	1	-	1	-	1

Table 16: A spin-partition inspired by the conformal-block decomposition of the four-point function $\langle j(z_1)j(z_2)j(z_3)j(z_4)\rangle$ with $\Delta_{\max} = 8$.

$\Delta_j = 0.993577 \pm 0.00528402$				
spin	analytic Δ	RL Δ	analytic $\mathfrak{C}$	RL $\mathfrak{C}$
2	2	2.01688 ± 0.0242115	2	1.94164 ± 0.0426005
4	4	3.96686 ± 0.0419861	1.2	1.15899 ± 0.0351261
6	6	5.95325 ± 0.0438046	0.23809524	0.22054 ± 0.00729978
8	8	7.97585 ± 0.0767531	0.03263403	0.0240609 ± 0.00121834
$\mathbb{A} = 0.000213657 \pm 0.00000819217$				

Table 17: Analytic and numerical solutions from 10 runs for the mean and standard deviation of scaling dimensions and OPE-squared coefficients in the conformal-block decomposition of the four-point function $\langle j(z_1)j(z_2)j(z_3)j(z_4)\rangle$. Δ_j is also an unknown and the spin-partition is that of Tab. 16. The numerical results were obtained with 16 z-points and a mode-1 run of the RL algorithm.

one-dimensional conformal manifold. Moreover, if there is some additional information that the spectrum of the CFT is discrete, the fact that we can solve the crossing equations for a continuous set of scaling dimensions Δ_p for the operators V_p, signals the fact that the theory has an exactly marginal deformation and that the scaling dimension of V_p can be used as a proxy for the value of the exactly marginal coupling.

Spin-1 correlation functions

A characteristic feature of the S^1 theory is the existence of a conserved holomorphic (and separately an anti-holomorphic) $U(1)$ current $j(z)$, under which many of the operators of the theory are charged. In this subsection, we study the four-point function of this current, (3.80). The holomorphic current $j(z)$ has spin 1 and (since it is conserved) scaling dimension $\Delta_j = 1$. Keeping its scaling dimension Δ_j free for the moment, we find that the four-point function (3.80) yields the crossing equation

$$\sum_{h\geq\bar{h}}{}' \mathfrak{C}_{h,\bar{h}}\Big((z-1)^{2\Delta_j} g^{(jjjj)}_{h,\bar{h}}(z,\bar{z}) - z^{2\Delta_j} g^{(jjjj)}_{h,\bar{h}}(1-z,1-\bar{z})\Big) + \frac{1}{16}\Big((z-1)^2 - z^2\Big) = 0\,. \quad (3.82)$$

The 1/16 factor in the last term, capturing the contribution of the identity, originates from the normalisation condition $\langle jj\rangle = \frac{1}{4}$.

The quasi-primaries that one needs in (3.82) come from the $j(z_1)j(z_2)$ OPE of the S^1 theory and can be straightforwardly obtained following the discussion around (3.72),

$\Delta_j = 1$				
spin	analytic Δ	RL Δ	analytic $\mathfrak{C}$	RL $\mathfrak{C}$
2	2	2.0080483	2	1.9766322
4	4	4.0273294	1.2	1.1675011
6	6	6.014957	0.23809524	0.21928822
8	8	8.0047245	0.03263403	0.023595015
$\mathbb{A} = 0.00018822$				

Table 18: Analytic and numerical solutions for scaling dimensions and OPE-squared coefficients in the conformal-block decomposition of the four-point function $\langle j(z_1)j(z_2)j(z_3)j(z_4)\rangle$ for $\Delta_j = 1$ and the spin-partition of Tab. 16. The numerical results were obtained with 16 z-points and a mode-2 run of the RL algorithm.

by isolating contributions of the type $\partial^m X \partial^n X$ and setting $p \to 0$. These read

$$(\partial X)^2 \ , \qquad \partial X \partial^3 X - \frac{3}{2}(\partial^2 X)^2 \ , \qquad \partial X \partial^5 X - 10\partial^2 X \partial^4 X + 10(\partial^3 X)^2 \ ,$$
$$\frac{1}{21}\partial X \partial^7 X - \partial^2 X \partial^6 X + 5\partial^3 X \partial^5 X - \frac{25}{6}\left(\partial^4 X\right)^2 \ , \tag{3.83}$$

and lead to the spin-partition of Tab. 16 with $\Delta_{\text{max}} = 8$.

With this spin-partition we ran the RL algorithm 10 times in mode 1 using 16 z-points. In this case, we kept the conformal scaling dimension of the external operator j as one of the unknowns to be determined by the agent. Overall, this was a 9-dimensional search. The results, collected in Tab. 17, include statistical errors and exhibit the relative accuracy $\mathbb{A} = (2.13657 \pm 0.0819217) \times 10^{-4}$. It is very rewarding to see that the agent determined the scaling dimension of the conserved $U(1)$ current to excellent accuracy just from the knowledge of the spin partition, and reproduced sensibly the low-lying spectrum and OPE data of the quasi-primary operators that appear in the OPE of the current with itself. For comparison, we also performed a single, independent mode-2 run with 16 z-points, where the scaling dimension of the current was fixed from the beginning at the analytic value $\Delta_j = 1$. The results, at relative accuracy $\mathbb{A} = 0.00018822$, are summarised in Tab. 18. They are nicely consistent with the mode-1 results of Tab. 17.

Chapter 4

Vacuum Characters of 2D VOAs

4.1 Introduction

In recent years there has been intense activity pertaining to the study of superconformal theories (SCFTs) that do not admit a Lagrangian description. Theories with $\mathcal{N} \geq 2$ superconformal symmetry are ideal for such explorations. Despite the lack of perturbative control, one can still extract nontrivial data by exploiting the large amount of symmetry, e.g. by employing the power of dualities [74, 69, 75], implementing the bootstrap programme [13, 76], or evaluating superconformal indices [7].

In this context, "pure" $\mathcal{N} = 3$ SCFTs—$\mathcal{N} = 3$ theories which do not automatically enhance to $\mathcal{N} = 4$—were envisioned in [77, 78] and engineered in string theory through the S_k-fold constructions of [79, 80]. These are isolated, holographic SCFTs ($a_{4\mathrm{D}} = c_{4\mathrm{D}}$) with an F-theory dual on an $\mathrm{AdS}_5 \times (\mathrm{S}^5 \times \mathrm{T}^2)/\mathbb{Z}_k$ background. The gravity description was used in [81, 82] to evaluate the superconformal index in the large-rank limit. Candidates for additional rank-one and rank-two $\mathcal{N} = 3$ examples were presented in [83, 84], by constructing corresponding Coulomb-branch geometries via gaugings of $\mathcal{N} = 4$ theories by a discrete subgroup of the R-symmetry and electromagnetic duality groups. The "Coulomb" limit of the superconformal index [85] and the Higgs-branch Hilbert series for these models were evaluated in [86]; see also [87].

As $\mathcal{N} = 3$ theories are automatically $\mathcal{N} = 2$, a concrete computational handle can be established through the description of a "Schur" Bogomol'nyi–Prasad–Sommerfield (BPS) subsector of any $\mathcal{N} = 2$ 4D theory [85] by a (non-unitary) vertex operator algebra (VOA) [29]. VOAs for $\mathcal{N} = 3$ theories were initially constructed in [88, 89] culminating in the work of [20]. In that reference, it was conjectured that certain VOAs labelled by non-Coxeter crystallographic complex reflection groups encode the Schur subsector of the known $\mathcal{N} = 3$ S-fold theories. In particular, [20] gave a prescription for an elegant free-field realisation of such VOAs, along the lines of [90]. By constructing the latter, one is able to recover the "Macdonald" limit of the superconformal index [85] for $\mathcal{N} = 3$ S-fold theories, from the VOA vacuum character. See also [91] for an alternate

prescription on implementing a Macdonald grading of the chiral algebra.

Albeit concrete, implementing the findings of [20] in practice quickly becomes computationally intensive. It is difficult to write down the explicit free-field realisations of the relevant VOAs in all but the simplest of cases, and also to evaluate the corresponding vacuum characters in a fugacity expansion for increasing conformal weights. The goal of this chapter is to show how far one can get by implementing a brute-force approach using mathematical software, for the VOAs labelled by the complex reflection groups $G(k,1,1) = \mathbb{Z}_k$, $k = 3,4,6$ ($\mathbb{Z}_{3,4}$ label rank-one S-fold models) and $G(3,1,2)$ (labels a rank-two S-fold model). We employ the $G(k,p,N)$ notation of [92], where p is a divisor of k; general complex reflection groups are denoted as G. $G(k,p,N)$ can be defined as the semi-direct product of an abelian group of order k^N/p with the symmetric group, $\mathrm{Sym}(N)$.

Towards that end, we reconstruct and explicitly exhibit the free-field realisations of [20] for the theories of interest. We then provide algorithms for automating the process of finding null states and for evaluating the VOA vacuum characters. Our code, appended to this letter, can in principle be executed to obtain the corresponding Macdonald index at arbitrary orders in a fugacity expansion. Note however that the vacuum character computation time increases exponentially as a function of the conformal weight. Our code is also customisable—and we have clearly signposted how to do so—for the reader interested in extending it to the evaluation of vacuum characters for VOAs labelled by other complex reflection groups, once the complete free-field realisation of the VOA has been found.

Our results, all of which have been collected in the ancillary files here for quick reference, can be used to check the conjecture of [20] against independent calculations of the Macdonald index of 4D $\mathcal{N} = 3$ S-fold theories and vice versa. For example, a proposal for the Schur limit of the superconformal index—a special case of the Macdonald index—for the rank-one $\mathbb{Z}_3$ S-fold theory was put forward in [93]. In that limit, their and our findings are in complete agreement.

4.1.1 Outline

In this section we aim to give a guide as to how the rest of this chapter is structured. In Chapter 2 we gave a brief overview of some basic aspects of conformal field theories and defined the conventions we will be employing. In Sec. 4.2 we aim to first build up the $\mathcal{N} = 2$ and small $\mathcal{N} = 4$ superconformal algebras (SCAs) to then later be used to calculate the vacuum characters. In Sec. 4.3 we present the prescription of [20]. Sec. 4.4 and 4.5 are the sections in which we build the free-field realisations of the VOAs up from scratch. Then in Sec. 4.6 we present a new $\mathcal{R}$-filtration charge which can be used to label the free-fields in order to make contact with the 4D Macdonald indices. In Sec. 4.7 we explain two algorithms which can be used in order to calculate the vacuum

characters efficiently, before moving on to presenting all the vacuum characters we obtained as results. The conclusion for the chapter with a brief summary and potential outlooks will be in Sec. 6.1.2.

4.2 $\mathcal{N} = 2$ and Small $\mathcal{N} = 4$ Superconformal Algebras

The $2D/4D$ duality implies that every 4D $\mathcal{N} \geq 2$ has a subsector which is isomorphic to a VOA. These VOAs will take the form of extended $\mathcal{N} = 2$ or small $\mathcal{N} = 4$ superconformal algebras (SCAs). By extended we mean that suitable operators will be added. All of these VOAs will be chiral algebras, which is an extra constraint on the algebras which we introduced before in Chapter 2. It says that all the operators must be holomorphic, and hence conserved. This in turn of course implies that all the OPEs will be only in terms of z. Unitarity will constrain the weight h to be non-negative, which will also put a cutoff on the largest singularity on the OPEs.

In this section we will describe both the $\mathcal{N} = 2$ and small $\mathcal{N} = 4$ superconformal algebras in detail, listing all their operators and giving the OPEs of the algebra. We will first start with the latter because the former can be defined as its subalgebra.

The small $\mathcal{N} = 4$ SCA comprises of the AKM $\mathfrak{sl}(2)$ currents $J^{0,\pm}$, the energy-momentum tensor and also four fermionic generators $G^{\pm}$ and $\tilde{G}^{\pm}$ — the superpartners of the currents. The bosonic generators' OPEs are given as

$$J^0(z_1)\,J^0(z_2) \sim \frac{2k}{(z_1-z_2)^2} \tag{4.1}$$

$$J^0(z_1)\,J^{\pm}(z_2) \sim \frac{\pm 2J^{\pm}}{(z_1-z_2)} \tag{4.2}$$

$$J^+(z_1)\,J^-(z_2) \sim \frac{-k}{(z_1-z_2)^2} + \frac{-J^0}{(z_1-z_2)} \tag{4.3}$$

$$T(z_1)\,T(z_2) \sim \frac{c/2}{(z_1-z_2)^4} + \frac{2T(z_2)}{(z_1-z_2)^2} + \frac{\partial T(z_2)}{(z_1-z_2)}. \tag{4.4}$$

For simplicity we will stop adding the ellipses to represent the remaining non-singular terms as it should be understood when they are present from context. There should be nothing too surprising among these OPEs, it is just a Virasoro algebra with an AKM extension. There is however an important fact to note about this theory, and that is that the central charge and the level of the AKM are related by

$$c = 6k. \tag{4.5}$$

Now we present the fermionic part of the algebra. The OPEs behave the same way, but one has to keep in mind that these generators are Grassmann odd, which means

they pick up a negative sign when commuted.

$$G^+(z_1)\widetilde{G}^-(z_2) \sim \frac{2k}{(z_1-z_2)^3} + \frac{J^0(z_2)}{(z_1-z_2)^2} + \frac{T(z_2)+\frac{1}{2}\partial J^0(z_2)}{z_1-z_2} \tag{4.6}$$

$$G^\pm(z_1)\widetilde{G}^\pm(z_2) \sim \frac{2J^\pm(z_2)}{(z_1-z_2)^2} + \frac{\partial J^\pm(z_2)}{z_1-z_2} \tag{4.7}$$

All the other OPEs which were left out are regular. The only OPEs left are the ones which are between the bosonic and fermionic generators.

$$J^\pm(z_1)G^\mp \sim \mp\frac{G^\pm(z_2)}{z_1-z_2} \tag{4.8}$$

$$J^\pm(z_1)\widetilde{G}^\mp \sim \mp\frac{\widetilde{G}^\pm(z_2)}{z_1-z_2} \tag{4.9}$$

Which concludes the list of all relevant OPEs for this algebra. We omitted the OPEs with T and J^0 because these OPEs will just reveal the eigenvalues under T and J^0. We list these eigenvalues in the table below:

Generator	Charge under T (h)	Charge under J^0 (j)
T	2	0
J^0	1	0
$J^\pm$	1	± 1
$G^\pm$	$\frac{3}{2}$	$\pm\frac{1}{2}$
$\widetilde{G}^\pm$	$\frac{3}{2}$	$\pm\frac{1}{2}$

Table 19: Charges of all the Generators in the small $\mathcal{N}=4$ SCA.

Now that we have completely presented the small $\mathcal{N}=4$ superconformal algebra, we will define the $\mathcal{N}=2$ SCA as a subalgebra of the above generators. This can be done by the simple identification

$$\mathcal{J} = J^0, \quad \mathcal{G} = G^-, \quad \widetilde{\mathcal{G}} = \widetilde{G}^+, \quad \mathcal{T} = T. \tag{4.10}$$

The benefit of first doing the larger algebra is that we have already presented all the OPEs and one can just pick out the relevant ones which are inherited by the $\mathcal{N}=2$ SCA without having to list them again.

This concludes the review into the CFTs and VOAs which will be required for the remainder of this chapter. In the following sections we will be presenting a free-field realisation which reproduces the algebras shown in this section and also moving on to extend these algebras to eventually use them to calculate the vacuum characters of

these VOAs and make contact with the 4D theories.

4.3 The Free-Field Realisation

In this section we will present the free-field realisation for $\mathcal{N}=2$ and small $\mathcal{N}=4$ SCAs as proposed in [20]. We will first present the generators in the $\mathcal{N}=2$ superconformal algebra and then in the subsequent subsections we will describe how further generators can be added using this realisation.

4.3.1 The $\mathcal{N}=2$ SCA in the Free-Field Realisation

Our first order of business is to introduce a group G. This might seem like a bit of a random decision, and from the perspective of the two dimensional theories it will be, until we make contact with the four dimensional side. For the moment it is enough to say that in 4D this will be related to the gauge group of the superconformal theory, and in 2D this will translate to the definition of a so-called W-algebra labelled by G. We will not explore this terminology any further and just focus on the fact that this group defines a specific VOA, denoted by $\mathcal{W}_{\mathsf{G}}$. What happens when the 4D theory does not have a gauge group? In the case of $\mathcal{N}=3$ theories in 4D we can still relate the theory to a specific crystallographic complex reflection (CCR) group and hence identify a corresponding 2D VOA. In general we shall refer to the CCR of $\mathcal{N}=2$ SCAs in two dimensions as G and the CCR of $\mathcal{N}=4$ ones as Γ. In the case of the latter, the CCR is actually upgraded to a Coxeter group.

The proposal for the free-field realisation is the following: there are as many free $\beta\gamma bc$ systems as the rank of G, $r=\text{rank}(\mathsf{G})$, or equivalently, the number of fundamental invariants in the CCR. These systems have the OPEs:

$$\beta_{\ell_1}(z_1)\,\gamma_{\ell_2}(z_2)=-\frac{\delta_{\ell_1\ell_2}}{z_{12}},\quad b_{\ell_1}(z_1)\,c_{\ell_2}(z_2)=\frac{\delta_{\ell_1\ell_2}}{z_{12}}. \tag{4.11}$$

Here the indices $\ell_{1,2}$ run from 1 to r. Using these free fields we can put the generators of the $\mathcal{N}=2$ superconformal algebra into a new form

$$\mathcal{J}=\sum_{\ell=1}^{\mathrm{r}}\left[p_\ell\beta_\ell\gamma_\ell+(p_\ell-1)\,b_\ell c_\ell\right] \tag{4.12}$$

$$\mathcal{G}=\sum_{\ell=1}^{\mathrm{r}}b_\ell\gamma_\ell,\quad \widetilde{\mathcal{G}}=\sum_{\ell=1}^{\mathrm{r}}\left[p_\ell\beta_\ell\partial c_\ell+(p_\ell-1)\,\partial\beta_\ell c_\ell\right], \tag{4.13}$$

$$\mathcal{T}=\sum_{\ell=1}^{\mathrm{r}}\left[-\frac{1}{2}p_\ell\beta_\ell\partial\gamma_\ell+\left(1-\frac{1}{2}p_\ell\right)\partial\beta_\ell\gamma_\ell-\frac{1}{2}(p_\ell+1)\,b_\ell\partial c_\ell+\frac{1}{2}(1-p_\ell)\,\partial b_\ell c_\ell\right]. \tag{4.14}$$

Note that here we swept the normal-ordering and the z-dependence under the rug. All the operators here are meant to be normal-ordered and defined at the same point z, i.e. $:b_l c_l:(z) := \lim_{w\to z}(b_l(z)c_l(w) - \text{singular terms})$.

There is also a relationship between the degrees of the fundamental invariants of the CCR and the central charge of the $\mathcal{N}=2$ theory

$$c = -3\sum_{\ell=1}^{r}(2p_\ell - 1)\,. \tag{4.15}$$

As we can see the central charge of the two dimensional theory is negative, hence this theory is non-unitary. Not to worry! This is acceptable since the two dimensional theory is not the physical one, but the four dimensional ones are and the relationship between their central charges is $c_{2\mathrm{D}} = -12c_{4\mathrm{D}}$ [29]. Furthermore, the weights of the generators (of the abstract algebra) are non-negative so we are all good to go.

Just as we did for the abstract algebra generators, let us summerise the charges of the free fields under various symmetries. The global symmetry group of the $\mathcal{N}=2$ superconformal algebra is $\mathfrak{osp}(2|2)$, with the bosonic subalgebra being $\mathfrak{sl}(2)_z \oplus \mathfrak{gl}(1)$ and there is also an outer automorphism $\mathfrak{gl}(1)_r$.

	h	m	$h-m$	$h+m$	r
β_ℓ	$\frac{1}{2}p_\ell$	$\frac{1}{2}p_\ell$	0	p_ℓ	0
b_ℓ	$\frac{1}{2}(p_\ell+1)$	$\frac{1}{2}(p_\ell-1)$	1	p_ℓ	$\frac{1}{2}$
c_ℓ	$-\frac{1}{2}(p_\ell-1)$	$-\frac{1}{2}(p_\ell-1)$	0	$1-p_\ell$	$-\frac{1}{2}$
γ_ℓ	$1-\frac{1}{2}p_\ell$	$-\frac{1}{2}p_\ell$	1	$1-p_\ell$	0
∂	1	0	1	1	0

Table 20: Charges of all the free fields [20].

4.3.2 Extension to Small $\mathcal{N}=4$

In the subsection above we have constructed a free field realisation for an $\mathcal{N}=2$ SCA corresponding to a specific crystallographic complex reflection group G. In order to construct the small $\mathcal{N}=4$ SCA, we have to construct the remaining generators in the $\mathcal{N}=4$ case. These will be the operators which are charged under the extra $\mathfrak{sl}(2)$ in the global part of the $\mathcal{N}=4$ SCA, $\mathfrak{psl}(2|2)$, in addition to the symmetries in $\mathfrak{osp}(2|2)$. Thankfully in [20] we find a whole recipe on how to construct such an algebra and close it. The free-field realisation gives us these generators for free:

$$J^+ = \beta_1, \quad G^+ = b_1, \tag{4.16}$$

$$W_\ell = \beta_\ell, \quad G_{W_\ell} = b_\ell, \tag{4.17}$$

where again the index $\ell = 2, \ldots, r$. We have introduced two new sets of generators: W_ℓ and G_{W_ℓ}. They only appear in rank 2 or higher $\mathcal{N} = 4$ superconformal algebras. At each ℓ they form an $\mathcal{N} = 2$ chiral multiplet, just like J^+ and G^+.

It is quite plain to see that we have not defined all of the generators needed for this SCA. This is because not everything can be as easily defined when moving to the free-field realisation. The rest of the generators must be constructed through proposing an ansatz and then constraining their coefficients though consistency conditions arising from the closure of the algebra. One would take the simplest generator first and work their way through the rest of the algebra. We will present a step-by-step guide of the prescription of [20] which incorporates the above information and summarises the whole procedure.

1. From the prescription we are told that there is a one-to-one correspondence between the degrees (of the fundamental invariants) of Γ and the chiral strong generators (generators which cannot be expressed as normal ordered products of other operators) of the VOA. This means that for each degree we can write down the highest weight states of the algebra — these would be the operators in (4.16) — and always assign β_l and b_l as the free field realisation to the bosonic and fermionic generators respectively. (In our small $\mathcal{N} = 4$ $SU(2)$ case, this would be equivalent to assigning $J^+ = \beta$ and $G^+ = b$). We shall call these new generators W_l and they actually enter with their $\mathcal{N} = 2$ multiplets, which as mentioned before are chiral, so they only consist of $\{W_l,\ G_{W_l}\}$. This is the equivalent statement of putting β_l and b_l into a chiral multiplet.

2. There are other generators which are not highest weight. There are two types of these: anti-chiral and non-chiral. Let us first discuss the former which is simpler. These multiplets are anti-chiral and the charge conjugates of the W_l multiplet we introduced before. Let us denote the multiplet as $\{\overline{W}_l,\ G_{\overline{W}_l}\}$. $\overline{W}_l$ do not have a prescribed form and the way to determine them is to create an ansatz using the free-field realisation and its quantum numbers. This will result in a finite amount of terms which can potentially enter the ansatz.

3. Using these ansatze, enforce the closure of the VOA. This will introduce linear constraints from the OPEs of generators with other generators and non-linear constrains from the OPEs of the same generator.

4. Impose that the generators introduced in step 1 are primary.

5. Impose that these generators have non-zero norms.

6. Above we also mentioned a case where we have generators which are neither chiral nor anti-chiral. With the other two types of generators one is guaranteed to know about their existence since they come in pairs which correspond to the degrees of the complex reflection group, but could there be extra generators? Yes, there can be extra generators which can be exchanged in the OPEs of the existing generators. As far as we can tell, rank one cases are way too constraining and have weights for the generators too small for these new types of generators to appear in OPEs — they tend to have large weights. There is a methodical way to determine their existence through an extended analysis of the complex reflection group, but the most straightforward way is to note them when trying to close the algebra.

7. Verify that the algebra closes on **all** the strong generators discussed above.

At the moment this may all seem very abstract, but later in section 4.4 we will give explicit examples of VOAs derived using this procedure and hopefully it will become clearer. Just as a word of caution, we will once again note: *for higher rank VOAs, be acutely aware that extra operators can appear, which are essential to closing the algebra and evaluating the vacuum character correctly.*

We will not make a separate section on how to apply this prescription in the case of the extended $\mathcal{N} = 2$ SCAs. It suffices to say that the procedure is virtually the same, but when closing the algebra one has to be aware that the supersymmetry multiplets in $\mathcal{N} = 2$ are smaller.

4.4 Examples of $\mathcal{N} = 4$ VOAs

4.4.1 Rank 1 Example: $\Gamma = S_2$

This is the two-dimensional small $\mathcal{N} = 4$ superconformal algebra with the central charge $c = -9$. In terms of the 2D/4D correspondence this would correspond to the subsector of the 4D $\mathcal{N} = 4$ gauge theory with gauge group $SU(2)$, since the Weyl group of $SU(2)$ is $S_2 \cong \mathbb{Z}_2$. This is by far one of the simplest theories to construct because there are no hidden extra generators, and there is only one set of $\beta\gamma bc$ operators since it is a rank one theory.

Let us write down the operators we get for free from the prescription:

$$\begin{aligned} J^+ &= \beta \\ J^0 &= bc + 2\beta\gamma \\ G^+ &= b \\ G^- &= b\gamma \end{aligned}$$

$$\widetilde{G}^+ = c\partial\beta + 2\partial c\beta$$
$$T = -\frac{3}{2}b\partial c - \beta\partial\gamma - \frac{1}{2}\partial bc \tag{4.18}$$

So far we have not done anything worth noting besides substituting in the value of c and also the degree $p_1 = 2$. Since this is quite a simple case, and we know what the algebra looks like, we know that we are only looking for the operators J^- and $\widetilde{G}^-$.

We construct an ansatz for the operator J^- using its quantum numbers from the table 19 and the quantum numbers of the free-fields from 20. Since this is quite a simple case, it will not have a large amount of terms. We assign an unknown coefficient for each of the terms, except for the term $\beta\gamma\gamma$ whose coefficient we will fix to be one. This will actually fix a special rescaling invariance these algebras enjoy. After using this normalisation and also imposing the constraints arising from the algebra, we end up with

$$J^- = \beta\gamma\gamma + \gamma bc - \frac{3}{2}\partial\gamma. \tag{4.19}$$

Now that we have found this operator, it is quite easy to find the remaining generator $\widetilde{G}^-$ which is in the $\mathcal{N} = 2$ multiplet of J^- just by the action of $\widetilde{G}^+$ on J^-. This gives:

$$\widetilde{G}^- = -b\partial cc + 2\beta\gamma\partial c + \partial\beta\gamma c - \frac{3}{2}\partial^2 c. \tag{4.20}$$

And there we have the whole algebra. One can check by doing all the OPEs that this algebra indeed closes. Below we shall include a small summary of the generators.

Generator	h	m	r	Generator	h	m	r
J^0	1	0	0	T	2	0	0
J^+	1	+1	0	J^-	1	-1	0
G^+	$\frac{3}{2}$	$+\frac{1}{2}$	$+\frac{1}{2}$	G^-	$\frac{3}{2}$	$-\frac{1}{2}$	$+\frac{1}{2}$
$\widetilde{G}^+$	$\frac{3}{2}$	$+\frac{1}{2}$	$-\frac{1}{2}$	$\widetilde{G}^-$	$\frac{3}{2}$	$-\frac{1}{2}$	$-\frac{1}{2}$

Table 21: Charges of all the strong generators of the S_2 extension of the small $\mathcal{N} = 4$ superconformal algebra.

4.4.2 Rank 2 Example: $\Gamma = S_3$

Now we present the first rank 2 algebra of this chapter. This is the VOA labelled by the Coxeter group S_3 which is the Weyl group of $SU(3)$. As we explained before, since this is a rank 2, we expect an increase in the difficulty of finding the free-field representation and also closing the algebra. This will be very clear once we present the generators

which appear in this VOA. This is also the simplest rank 2 algebra where generators which are not chiral or anti-chiral appear.

Let us now take a look at the free-field realisation. Since we are dealing with a rank 2 algebra, we will have to employ two sets of the $\beta\gamma bc$ systems, with the degrees of the fundamental invariants of S_3 being 2 and 3. From these degrees we find the central charge to be $c = -24$.

As per the prescription, our first order of business is to write down the small $\mathcal{N} = 4$ generators in terms of these $\beta\gamma bc$ systems.

$$\begin{aligned}
J^+ &= \beta_1 \\
J^0 &= b_1c_1 + 2\beta_1\gamma_1 + 2b_2c_2 + 3\beta_2\gamma_2 \\
G^+ &= b_1 \\
G^- &= b_1\gamma_1 + b_2\gamma_2 \\
\widetilde{G}^+ &= c_1\partial\beta_1 + 2\partial c_1\beta_1 + (p-1)c_2\partial\beta_2 + p\partial c_2\beta_2 \\
T &= -\frac{3}{2}b_1\partial c_1 - \frac{1}{2}\partial b_1c_1 - \beta_1\partial\gamma_1 - 2b_2\partial c_2 - \partial b_2c_2 - \frac{3}{2}\beta_2\partial\gamma_2 - \frac{1}{2}\partial\beta_2\gamma_2
\end{aligned} \tag{4.21}$$

This is analogous to the part we introduced for the rank 1 case in the previous subsection, but this time the prescription allows us to introduce more operators

$$\begin{aligned}
W &= \beta_2 \\
G_W &= b_2
\end{aligned} \tag{4.22}$$

This is all we get from the initial prescription. The rest is up to us to determine by closing the algebra. We will start the same way, by making an ansatz for J^- and solving it, which will result in:

$$\begin{aligned}
J^- = {} & b_1c_1\gamma_1 + \beta_1\gamma_1\gamma_1 + 2\gamma_1b_2c_2 + 3\gamma_1\beta_2\gamma_2 - c_1b_2\gamma_2 - 4\partial\gamma_1 \\
& + (\beta_1)^2(\gamma_2)^2 + 2\Lambda b_1\beta_1c_2\gamma_2.
\end{aligned} \tag{4.23}$$

Where we used a very specific normalisation. Now that we have J^-, we can generate some extra operators by using supersymmetry and its OPEs. From the $(\widetilde{G}^+J^-)$ OPE we get

$$\begin{aligned}
\widetilde{G}^- = {} & -b_1\partial c_1c_1 + 2b_2\partial c_1c_2 + 2\beta_1b_1\partial c_2c_2 - 2\beta_1^2\gamma_2\partial c_2 \\
& - 2\beta_1\gamma_1\partial c_1 - 3\beta_2\gamma_1\partial c_2 - 3\beta_2\gamma_2\partial c_1 - 2\partial\beta_1\beta_1\gamma_2c_2 \\
& + 2b_1\partial c_1c_1 - 2\partial\beta_1\gamma_1c_1 - \partial\beta_1\gamma_1c_1 + 2\partial\beta_{21}c_2 - b_2c_1\partial c_2 \\
& - \partial\beta_2\gamma_2c_1 + 4\partial^2c_1.
\end{aligned} \tag{4.24}$$

From (WJ^-) we get our first obscure non-chiral or anti-chiral (with respect to SUSY)

generator, which we will call O:

$$O = -b_2c_1 - 2\beta_1 b_1 c_2 - 2\beta_1^2\gamma_2 - 3\beta_2\gamma_1 \tag{4.25}$$

Then we can start building the O multiplet by acting with G^-

$$G_O = -2\beta_1\gamma_2 b_1 - 2\gamma_1 b_2. \tag{4.26}$$

Then we act with $\tilde{G}^+$ on O to get

$$\widetilde{G}_O = 2\beta_1^2\partial c_2 + 3\beta_2\partial c_1 + 2\partial\beta_1^2 c_2 + \partial\beta_2 c_1. \tag{4.27}$$

These are all the generators we can easily get from J^- through the algebra. To fully close the algebra we have to create an ansatz for the $\overline{W}$ operator and solve it just like for J^-. The result is quite long and complicated so it will be shortened here, but the full results are available here, in the ancillary files.

$$\overline{W} = \frac{2}{3}\beta_1^3\gamma_2^3 - 2\beta_1^2\gamma_1^2\gamma_2 + \ldots + 10\partial\gamma_2 b_2 c_2 - \frac{20}{3}\partial^2\gamma_2 \tag{4.28}$$

Now just as we did with the previous operators, we start acting with the supersymmetry generator $\widetilde{G}^+$

$$\widetilde{G}_{\overline{W}} = 4b_1 b_2 c_1\partial c_2 c_2 - 5b_1 c_1\partial^2 c_2 + \ldots - \partial^2\beta_1\gamma_2 c_1 + \frac{20}{3}\partial^3 c_2 \tag{4.29}$$

Here we can also define two new generators (one for W and one for $\overline{W}$), with the OPEs $(\widetilde{G}^- G_W)$ and $(G^+\widetilde{G}_{\overline{W}})$:

$$\begin{aligned} T_W = &-3b_2\partial c_1 - 4\beta_1 b_1\partial c_2 - 2\beta_1^2\partial\gamma_2 - 2\beta_1\partial b_1 c_2 - 3\beta_2\partial\gamma_1 \\ &- \partial b_2 c_1 - 2\partial\beta_1 b_1 c_2 - 2\partial\beta_1\beta_1\gamma_2 - \partial\beta_2\gamma_1, \end{aligned} \tag{4.30}$$

$$\begin{aligned} T_{\overline{W}} = &-4b_1 b_2\partial c_2 c_2 - 5b_1\partial^2 c_2 + 2\beta_1\gamma_1 b_1\partial c_2 + 2\beta_1\gamma_2 b_1\partial c_1 \\ &- 2\beta_1\gamma_2 b_2\partial c_2 + \beta_1\partial\beta_2\gamma_2^2 + 6\beta_2\gamma_2 b_1\partial c_2 + 2\gamma_1 b_2\partial c_1 - \partial b_1\partial c_2 \\ &- 2\partial\beta_1\beta_1\gamma_1\gamma_2 - 3\partial\beta_1\beta_2\gamma_2^2 - 4\partial\beta_1\gamma_2 b_2 c_2 + \partial\beta_1\partial\gamma_2 - \partial\beta_2\gamma_1^2 \\ &+ 4\partial\beta_2\gamma_2 b_1 c_2 + \partial^2\beta_1\gamma_2. \end{aligned} \tag{4.31}$$

We are almost done, we have three more generators to introduce. These will come as the charge conjugates of the O's above. This time we use $(J^+\overline{W})$,

$$\begin{aligned} \overline{O} = &-5b_1\partial c_2 + 4\beta_1^2\gamma_1\gamma_2 + 3\beta_1\beta_2\gamma_2^2 + 4\beta_1\gamma_1 b_1 c_2 + 2\beta_1\gamma_2 b_1 c_1 \\ &+ 4\beta_1\gamma_2 b_2 c_2 - 10\beta_1\partial\gamma_2 + 3\beta_2\gamma_1^2 + 2\gamma_1 b_2 c_1 - 2\partial b_1 c_2 - 3\partial\beta_1\gamma_2. \end{aligned} \tag{4.32}$$

Now the action of G^- on it gives

$$G_{\overline{O}} = 2\beta_1\gamma_1\gamma_2 b_1 - \beta_1\gamma_2^2 b_2 + 3\beta_2\gamma_2^2 b_1 + \gamma_1^2 b_2 + 4\gamma_2 b_1 b_2 c_2 - \gamma_2\partial b_2 - 5\partial\gamma_2 b_1. \tag{4.33}$$

And lastly we have the action of $\widetilde{G}^+$ on O:

$$\begin{aligned}\widetilde{G}_{\overline{O}} =& 2b_2\partial c_1 c_1 - 2\beta_1 b_1 c_1 \partial c_2 + 4\beta_1 b_1 \partial c_1 c_2 + 4\beta_1 b_2 \partial c_2 c_2 - 4\beta_1^2\gamma_1\partial c_2 \\ &- 4\beta_1^2\gamma_2\partial c_1 - 6\beta_1\beta_2\gamma_2\partial c_2 - 4\beta_1\partial\beta_2\gamma_2 c_2 + 10\beta_1\partial^2 c_2 - 6\beta_2\gamma_1\partial c_1 \\ &- 4\partial\beta_1\beta_1\gamma_1 c_2 - 2\partial beta_1\beta_1\gamma_2 c_1 + 8\partial\beta_1\partial c_2 - 2\partial\beta_2\gamma_1 c_1 + 2\partial^2\beta_1 c_2.\end{aligned} \tag{4.34}$$

This is the whole small $\mathcal{N} = 4$ SCA with the S_3 extensions. Of course if one had the patience and the tenacity they could verify that indeed all the OPEs close and the algebra is valid. In order to summarise all that was derived in this section, we will present table below which details all the relevant information about the generators which appear in the VOA, grouped by their derivations.

Generator	h	m	r	Generator	h	m	r
J^+	1	+1	0	J^-	1	-1	0
G^+	$\frac{3}{2}$	$+\frac{1}{2}$	$+\frac{1}{2}$	G^-	$\frac{3}{2}$	$-\frac{1}{2}$	$+\frac{1}{2}$
$\widetilde{G}^+$	$\frac{3}{2}$	$+\frac{1}{2}$	$-\frac{1}{2}$	$\widetilde{G}^-$	$\frac{3}{2}$	$-\frac{1}{2}$	$-\frac{1}{2}$
W	$\frac{3}{2}$	$+\frac{3}{2}$	0	$\overline{W}$	$\frac{3}{2}$	$-\frac{3}{2}$	0
G_W	2	+1	$+\frac{1}{2}$	$\widetilde{G}_{\overline{W}}$	2	-1	$-\frac{1}{2}$
T_W	$\frac{5}{2}$	$+\frac{1}{2}$	0	$T_{\overline{W}}$	$\frac{5}{2}$	$-\frac{1}{2}$	0
O	$\frac{3}{2}$	$+\frac{1}{2}$	0	$\overline{O}$	$\frac{3}{2}$	$-\frac{1}{2}$	0
G_O	2	0	$+\frac{1}{2}$	$G_{\overline{O}}$	2	-1	$+\frac{1}{2}$
$\widetilde{G}_O$	2	+1	$-\frac{1}{2}$	$\widetilde{G}_{\overline{O}}$	2	0	$-\frac{1}{2}$
T	2	0	0	J^0	1	0	0

Table 22: Charges of all the strong generators of the S_3 extension of the small $\mathcal{N} = 4$ superconformal algebra.

As one can observe, the step up from rank one to rank two is quite a significant one. At the moment we can only speculate as to how difficult it might be to derive such a free-field representation for a rank three theory. Later in this chapter, in Sec. 4.5.4, we will derive another rank two case, but in the context of $\mathcal{N} = 2$ SCAs, but for now we shall take a step back and analyse some more rank one theories.

4.5 Examples of $\mathcal{N} = 2$ VOAs

In these subsections we will be analysing the structure of rank 1 $\mathcal{N} = 2$ superconformal algebras which correspond to certain $\mathcal{N} = 3$ theories in four dimensions. The simplest one to start with is the $\mathbb{Z}_3$ case.

4.5.1 Rank 1 Example: $\mathsf{G} = \mathbb{Z}_3$

It is a rank 1 theory, which means a single copy of the free-field systems and the degree of the invariant is $p = 3$, and hence the central charge is $c = -15$. Just as always, we begin with writing down the free-field representation of the underlying algebra (note that in this case it will be $\mathcal{N} = 2$)

$$\begin{aligned}\mathcal{J} &= 2bc + 3\beta\gamma \\ \mathcal{G} &= \gamma b \\ \widetilde{\mathcal{G}} &= 2\partial\beta c + 3\beta\partial c \\ \mathcal{T} &= -2b\partial c - \frac{3}{2}\beta\partial\gamma - \partial bc - \frac{1}{2}\partial\beta\gamma\end{aligned} \tag{4.35}$$

Note that since here we only have a single $\beta\gamma bc$ system, we will drop the index.

The operators $\mathcal{W}$ and $\mathcal{G}_{\mathcal{W}}$ are given by the prescription to be

$$\begin{aligned}\mathcal{W} &= \beta \\ \mathcal{G}_{\mathcal{W}} &= b\end{aligned} \tag{4.36}$$

The next step is to create an ansatz for the operator $\overline{\mathcal{W}}$ and impose the constraints from section 4.3.2. The result is

$$\begin{aligned}\overline{\mathcal{W}} =& \beta^2\gamma^3 + 2\beta\gamma^2 bc - 4\beta\partial\gamma\gamma - \frac{4}{3}\gamma b\partial c + \frac{2}{3}\gamma\partial bc + \frac{2}{3}\partial\beta\gamma^2 \\ &- \frac{8}{3}\partial\gamma bc + \frac{10}{9}\partial^2\gamma\end{aligned} \tag{4.37}$$

Note that here we have used the normalisation we described earlier in section 4.4.1. Now we are only left with the superpartner of $\overline{\mathcal{W}}$ (rank 1 algebras do not tend to have hidden generators) which can be easily coerced to appear from the OPE of $(\widetilde{\mathcal{G}}\overline{\mathcal{W}})$. It will take the form

$$\begin{aligned}\widetilde{\mathcal{G}}_{\overline{\mathcal{W}}} =& \frac{8}{3}b\partial^2 cc + 3\beta^2\gamma^2\partial c - 4\beta\gamma b\partial cc - 4\beta\gamma\partial^2 c - 4\beta\partial\gamma\partial c \\ &- \frac{2}{3}\partial b\partial cc + 2\partial\beta\beta\gamma^2 c - \frac{8}{3}\partial\beta\partial\gamma c + \frac{2}{3}\partial^2\beta\gamma c + \frac{10}{9}\partial^3 c\end{aligned} \tag{4.38}$$

This exhausts the list of strong generators we have to find. One can once again show

that the algebra above closes. Just as with the previous algebras we will summarise the generators in the table below.

Generator	$\mathcal{G}_{\mathcal{W}}$	$\mathcal{W}$	$\mathcal{G}$	$\mathcal{J}$	$\mathcal{T}$	$\widetilde{\mathcal{G}}$	$\overline{\mathcal{W}}$	$\widetilde{\mathcal{G}}_{\overline{\mathcal{W}}}$
h	2	$\frac{3}{2}$	$\frac{3}{2}$	1	2	$\frac{3}{2}$	$\frac{3}{2}$	2
m	$+1$	$+\frac{3}{2}$	$-\frac{1}{2}$	0	0	$+\frac{1}{2}$	$-\frac{3}{2}$	-1
r	$+\frac{1}{2}$	0	$+\frac{1}{2}$	0	0	$-\frac{1}{2}$	0	$-\frac{1}{2}$

Table 23: Charges of all the strong generators of the $\mathbb{Z}_3$ extension of the $\mathcal{N} = 2$ superconformal algebra.

4.5.2 Rank 1 Example: $\mathsf{G} = \mathbb{Z}_4$

This one is also a rank 1 theory, which means that again we use a single copy of the free-field systems. The degree of the invariant is $p = 4$, and the central charge is $c = -21$. Following the same procedure, we begin with writing down the free-field representation of the underlying algebra (note that in this case it will be $\mathcal{N} = 2$)

$$\begin{aligned}
\mathcal{J} &= 3bc + 4\beta\gamma \\
\mathcal{G} &= \gamma b \\
\widetilde{\mathcal{G}} &= 3\partial\beta c + 4\beta\partial c \\
\mathcal{T} &= -\frac{5}{2}b\partial c - 2\beta\partial\gamma - \frac{3}{2}\partial bc - \partial\beta\gamma
\end{aligned} \tag{4.39}$$

The operators $\mathcal{W}$ and $\mathcal{G}_{\mathcal{W}}$ are given by the usual prescription forms. The next step is to create an ansatz for the operator $\overline{\mathcal{W}}$ and impose the constraints from section 4.3.2. The result is

$$\overline{\mathcal{W}} = \beta^3\gamma^4 + 3\beta^2\gamma^3 bc + \ldots + \frac{45}{16}\partial^2\gamma bc - \frac{35}{64}\partial^3\gamma \tag{4.40}$$

Note that here we have used the normalisation we described earlier in section 4.4.1. Due to the number of terms we had to truncate what we show here, but the full versions are available to view in the ancillary files here. Comparing this realisation to the one in section 4.5.1 one can see that the complexity starts to increase with the growing degree. The simple reason for this is that more terms are allowed in the ansatz as the weights of the abstract algebra generators increase.

Now we need to find the superpartner of $\overline{\mathcal{W}}$, which can be easily found from the OPE of $(\widetilde{\mathcal{G}}\overline{\mathcal{W}})$. It will take the form

$$\widetilde{\mathcal{G}}_{\overline{\mathcal{W}}} = \frac{15}{4}b\partial^2 c\partial c + \frac{45}{16}b\partial^3 cc + \ldots + \frac{3}{16}\partial^3\beta\gamma c + \frac{35}{64}\partial^4 c \tag{4.41}$$

Again, we truncated it due to the sheer length of this operator. This exhausts the list of strong generators we have to find. One can once again show that the algebra above closes. Just as with the previous algebras we will summarise the generators in the table below.

Generator	$\mathcal{G}_{\mathcal{W}}$	$\mathcal{W}$	$\mathcal{G}$	$\mathcal{J}$	$\mathcal{T}$	$\widetilde{\mathcal{G}}$	$\overline{\mathcal{W}}$	$\widetilde{\mathcal{G}}_{\overline{\mathcal{W}}}$
h	$\frac{5}{2}$	2	$\frac{3}{2}$	1	2	$\frac{3}{2}$	2	$\frac{5}{2}$
m	$+\frac{3}{2}$	$+2$	$-\frac{1}{2}$	0	0	$+\frac{1}{2}$	-2	$-\frac{3}{2}$
r	$+\frac{1}{2}$	0	$+\frac{1}{2}$	0	0	$-\frac{1}{2}$	0	$-\frac{1}{2}$

Table 24: Charges of all the strong generators of the $\mathbb{Z}_4$ extension of the $\mathcal{N} = 2$ superconformal algebra.

4.5.3 Rank 1 Example: $\mathsf{G} = \mathbb{Z}_6$

This is the last rank 1 theory we will be presenting, the degree of the invariant in this theory is $p = 6$, and the central charge is $c = -33$. We only study this theory out of interest, because unlike the other two $\mathcal{N} = 2$ theories we presented in this section, this one is proposed to not have a 4D partner [80].

We begin with writing down the free-field representation of the underlying algebra:

$$\begin{aligned}
\mathcal{J} &= 5bc + 6\beta\gamma \\
\mathcal{G} &= \gamma b \\
\widetilde{\mathcal{G}} &= 5\partial\beta c + 6\beta\partial c \\
\mathcal{T} &= -\frac{7}{2}b\partial c - 3\beta\partial\gamma - \frac{5}{2}\partial bc - 2\partial\beta\gamma
\end{aligned} \tag{4.42}$$

The operators $\mathcal{W}$ and $\mathcal{G}_{\mathcal{W}}$ are given by the usual prescription forms. The next step is to create an ansatz for the operator $\overline{\mathcal{W}}$ and impose the usual constraints

$$\overline{\mathcal{W}} = \beta^5\gamma^6 + 5\beta^4\gamma^5 bc + \ldots + \frac{175}{216}\partial^4 bc - \frac{77}{1296}\partial^5\gamma. \tag{4.43}$$

Due to the number of terms we had to truncate what we show here, but the full versions are available to view in the ancillary files here. The last term in the VOA takes the form

$$\widetilde{\mathcal{G}}_{\overline{\mathcal{W}}} = \frac{1225}{324}b\partial^3 c\partial^2 c + \frac{35}{8}b\partial^4 c\partial c + \ldots - \frac{5}{1296}\partial^5\beta\gamma c + \frac{77}{1296}\partial^6 c \tag{4.44}$$

This is the full list of the strong generators. One can once again show that the algebra above closes. The summary of the generators is below.

Generator	$\mathcal{G}_{\mathcal{W}}$	$\mathcal{W}$	$\mathcal{G}$	$\mathcal{J}$	$\mathcal{T}$	$\widetilde{\mathcal{G}}$	$\overline{\mathcal{W}}$	$\widetilde{\mathcal{G}}_{\overline{\mathcal{W}}}$
h	$\frac{7}{2}$	3	$\frac{3}{2}$	1	2	$\frac{3}{2}$	3	$\frac{7}{2}$
m	$+\frac{5}{2}$	$+3$	$-\frac{1}{2}$	0	0	$+\frac{1}{2}$	-3	$-\frac{5}{2}$
r	$+\frac{1}{2}$	0	$+\frac{1}{2}$	0	0	$-\frac{1}{2}$	0	$-\frac{1}{2}$

Table 25: Charges of all the strong generators of the $\mathbb{Z}_6$ extension of the $\mathcal{N} = 2$ superconformal algebra.

4.5.4 Rank 2 Example: $\mathsf{G} = G(3, 1, 2)$

In this subsection we will be taking a look at the final theory which will be presented in this chapter. This vertex operator algebra is by far the most complicated one out of all of the ones we present here. Similar to the approach with the previous rank 2 algebra, we will first aim to present all the generators which are given to us for free by the prescription, and then slowly build up more generators using ansatze and constraints from the abstract algebra. This of course requires the knowledge of the abstract algebra, but we will not be presenting that here due to the lack of space. One can find a list of some of the relevant OPEs in [20].

The underlying symmetry group for this VOA will be $G(3, 1, 2)$ which is a rank 2 complex crystallographic reflection group in the notation of Shephard and Todd [92]. The degrees of the fundamental invariants of this CCR are $p_1 = 3$ and $p_2 = 6$. From this we can identify the central charge as being $c = -48$.

Let us now examine the free-field realisation. Just as in the S_3 case, we will have to employ two sets of the $\beta\gamma bc$ systems. Using the prescription, our $\mathcal{N} = 2$ generators in terms of these $\beta\gamma bc$ systems are

$$\begin{aligned}
\mathcal{J} &= 2b_1c_1 + 5b_2c_2 + 3\beta_1\gamma_1 + 6\beta_2\gamma_2 \\
\mathcal{G} &= \gamma_1 b_1 + \gamma_2 b_2 \\
\widetilde{\mathcal{G}} &= 3\beta_1\partial c_1 + 6\beta_2\partial c_2 + 2\partial\beta_1 c_1 + 5\partial\beta_2 c_2 \\
\mathcal{T} &= -2b_1\partial c_1 - \frac{7}{2}b_2\partial c_2 - \frac{3}{2}\beta_1\partial\gamma_1 - 3\beta_2\partial\gamma_2 - \partial b_1 c_1 - \frac{5}{2}\partial b_2 c_2 \\
&\quad - \frac{1}{2}\partial\beta_1\gamma_1 - 2\partial\beta_2\gamma_2.
\end{aligned} \tag{4.45}$$

The extra operators from the prescription:

$$\begin{aligned}
\mathcal{W}_1 = \beta_1, \quad \mathcal{W}_2 = \beta_2, \\
\mathcal{G}_{\mathcal{W}_1} = b_1, \quad \mathcal{G}_{\mathcal{W}_2} = b_2.
\end{aligned} \tag{4.46}$$

Now that we have gone through all the predetermined operators, it is time to start

evaluating the algebra properly. Just as a warning, this algebra was very difficult to close and a lot of the generators are too large to be properly shown here. We will still present the derivation of the operators and some of their terms, but we will mostly relegate the detailed presentation to the ancillary files of this link. As it should be well known by now, we will first create an ansatz for the first generator we shall investigate, which is $\mathcal{W}_1$. There are 88 eligible terms in its ansatz, so this should show the non-triviality of this problem.

As it happens, using all the constraints arising from the $\mathcal{N}=2$ SCA is not enough to fix all the coefficients in the $\mathcal{W}_1$ ansatz. This presents an issue, since this does not allow us to progress in the usual way to close the algebra — by only relying on the ansatze and the OPEs. The space of possible solutions is way too big, which means we will actually need the form of the abstract algebra we discussed a few lines ago. The reason for this is because this allows us to rearrange certain OPEs to form equations for the unknowns. Of course if we are looking at the abstract algebra, we will also have access to the list of generators:

$$\begin{aligned}&\{\mathcal{J},\mathcal{G},\widetilde{\mathcal{G}},\mathcal{T}\},\\&\{\mathcal{W}_{1,2},\mathcal{G}_{\mathcal{W}_{1,2}}\},\{\overline{\mathcal{W}}_{1,2},\widetilde{\mathcal{G}}_{\overline{\mathcal{W}}_{1,2}}\},\\&\{\mathcal{O},\mathcal{G}_{\mathcal{O}},\widetilde{\mathcal{G}}_{\mathcal{O}},\mathcal{T}_{\mathcal{O}}\},\{\overline{\mathcal{O}},\mathcal{G}_{\overline{\mathcal{O}}},\widetilde{\mathcal{G}}_{\overline{\mathcal{O}}},\mathcal{T}_{\overline{\mathcal{O}}}\},\{\mathcal{U},\mathcal{G}_{\mathcal{U}},\widetilde{\mathcal{G}}_{\mathcal{U}},\mathcal{T}_{\mathcal{U}}\}\end{aligned}\tag{4.47}$$

Here we presented all the 24 operators in this algebra beforehand in order to follow the steps laid out later on. The operators above are actually organised into multiplets with the top one being the $\mathcal{N}=2$ current multiplet, the second are the chiral and anti-chiral multiplets (they double up), and the last line is for the non-chiral multiplets (non-anti-chiral also). Note that $\mathcal{U}$ is self-dual, which is why it appears without a barred version.

The way we present this derivation will be a bit different in style to the way we did the S_3 case. It will also take the form of an outline, a recipe which one can follow to re-derive the numbers we got. The recipe is as follows:

1. Substitute in the ansatze for $\overline{\mathcal{W}}_1$ and fix as many unknowns as possible with the $\mathcal{N}=2$ subalgebra constraints.

2. Use the first order pole terms in the OPE $(\mathcal{W}_1\overline{\mathcal{W}}_1)$ to write $\mathcal{U}$ in terms of the unknowns.

3. Use the fourth and third order pole terms in the $(\overline{\mathcal{W}}_1\mathcal{U})$ OPE — which should be zero — in order to solve for some of the unknown coefficients. There will be multiple solutions to the equations unfortunately, but there will be a solution which fixes four of the coefficients, and the rest only three. Pick that solution. This will fix more of the coefficients in $\mathcal{U}$ and $\overline{\mathcal{W}}_1$.

4. In order to fix more coefficients we have to look at another operator and other OPEs. We will impose an equation using the $(\mathcal{W}_1\mathcal{U})$ OPE as we did in step 1, but this time the first order pole will relate $\mathcal{O}$ to $\mathcal{U}$ and $\mathcal{W}_1$. There is a slight complication this time though, because some of the terms mix at this order and we have to introduce two extra unknowns, but this is acceptable.

5. Now use the first order of $(\mathcal{W}_1\mathcal{O})$ and this should fix one of the new coefficients as well as one of the old ones.

6. Look at the coefficient of the second order term in the expansion of $(\mathcal{O}\mathcal{O})$. From the coefficient of the β_1^2 term we can obtain a quadratic equation for the last old unknown. However, it is a quadratic so there will be two solutions. This is not a problem because the third order term in $(\mathcal{U}\mathcal{O})$ will show us which of the two solutions to pick.

7. Once the above is set, the second order term in the expansion of $(\mathcal{O}\mathcal{O})$ can be used to fix the second of the unknown coefficients introduced in step 4. This series of steps should in practice determine all the unknowns in $\overline{\mathcal{W}}_1$ and also $\mathcal{U}$ and $\mathcal{O}$.

8. Now that we possess the form of the above operators things will be easier. We can obtain $\overline{\mathcal{O}}$ from the coefficient of the second order term in $(\overline{\mathcal{W}}_1\mathcal{U})$.

9. Here is the major difference between this VOA and S_3. In a general case we would have to employ the ansatz method for $\overline{\mathcal{W}}_2$, but here we are lucky because the OPE $(\overline{\mathcal{W}}_1\overline{\mathcal{O}})$ closes on this operator, so by finding the other operators in the above steps, we have inadvertently fixed this one too.

10. The supersymmetric partners can be found in the relevant OPEs with the supercurrents.

Following this procedure should allow one to derive the exact free-field realisation of the $\mathcal{N} = 2$ superconformal algebra VOA with the $G(3, 1, 2)$ underlying symmetry. In the other subsections we have tried to explicitly show all the generators in their free-field forms, but this will not be possible in this case and the generators will be given in the ancillary files of this link. Below we have a table summarising the information of the strong generators.

This concludes the derivations of all the relevant superconformal algebras we will be calculating the vacuum characters of. The intricate information contained within the construction of these algebras is indispensable for calculating the vacuum characters. In the following sections we will go on to discuss quantum numbers of operators which are very useful labels from the perspective of the 4D theories, and then we will present two ways of calculating the vacuum characters.

Generator	h	m	r	Generator	h	m	r
$\mathcal{W}_1$	$\frac{3}{2}$	$+\frac{3}{2}$	0	$\overline{\mathcal{W}}_1$	$\frac{3}{2}$	$-\frac{3}{2}$	0
$\mathcal{G}_{\mathcal{W}_1}$	2	$+1$	$+\frac{1}{2}$	$\widetilde{\mathcal{G}}_{\overline{\mathcal{W}}_1}$	2	-1	$-\frac{1}{2}$
$\mathcal{W}_2$	3	$+3$	0	$\overline{\mathcal{W}}_2$	3	-3	0
$\mathcal{G}_{\mathcal{W}_2}$	$\frac{7}{2}$	$+\frac{5}{2}$	$+\frac{1}{2}$	$\widetilde{\mathcal{G}}_{\overline{\mathcal{W}}_2}$	$\frac{7}{2}$	$-\frac{5}{2}$	$-\frac{1}{2}$
$\mathcal{O}$	$\frac{5}{2}$	$+\frac{3}{2}$	0	$\overline{\mathcal{O}}$	$\frac{5}{2}$	$-\frac{3}{2}$	0
$\mathcal{G}_{\mathcal{O}}$	3	$+1$	$\frac{1}{2}$	$\mathcal{G}_{\overline{\mathcal{O}}}$	3	-2	$\frac{1}{2}$
$\widetilde{\mathcal{G}}_{\mathcal{O}}$	$+2$	$+1$	$-\frac{1}{2}$	$\widetilde{\mathcal{G}}_{\overline{\mathcal{O}}}$	3	-1	$-\frac{1}{2}$
$\mathcal{T}_{\mathcal{O}}$	$\frac{7}{2}$	$+\frac{3}{2}$	0	$\mathcal{T}_{\overline{\mathcal{O}}}$	$\frac{7}{2}$	$-\frac{3}{2}$	0
$\mathcal{U}$	2	0	0	$\mathcal{T}_{\mathcal{U}}$	3	0	0
$\mathcal{G}_{\mathcal{U}}$	$\frac{5}{2}$	$+\frac{1}{2}$	$\frac{1}{2}$	$\widetilde{\mathcal{G}}_{\mathcal{U}}$	$\frac{5}{2}$	$-\frac{1}{2}$	$-\frac{1}{2}$
$\mathcal{G}$	$\frac{3}{2}$	$+\frac{1}{2}$	$-\frac{1}{2}$	$\widetilde{\mathcal{G}}$	$\frac{3}{2}$	$+\frac{1}{2}$	$+\frac{1}{2}$
$\mathcal{T}$	2	0	0	$\mathcal{J}$	1	0	0

Table 26: Charges of all the strong generators of the $G(3,1,2)$ extension of the $\mathcal{N}=2$ superconformal algebra.

4.6 $\mathcal{R}$-Filtration

As we have seen in the sections leading up to this one, the VOAs we are considering are realised as a subalgebra of $\beta\gamma bc$ systems. We say subalgebra since not all combinations of free fields will appear and some will be null states, but more on this in Sec. 4.7. For now it suffices to know that we can define a filtration $\mathcal{R}$ at the level of the free-fields. The motivation for this will be to identify a new quantum number which can be used to make contact with a special set of 4D superconformal indices known as *Macdonald indices*. This will be a relatively brief subsection where we will construct the details of this filtration. We present the $\mathcal{R}$-filtration weight ($\mathcal{R}$-weight) in the table below. It is important to note that these charges are not fully "conserved". To elaborate on

	β_ℓ	γ_ℓ	b_ℓ	c_ℓ	∂
$\mathcal{R}$	$\frac{1}{2}p_\ell$	$1-\frac{1}{2}p_\ell$	$\frac{1}{2}p_\ell$	$1-\frac{1}{2}p_\ell$	0
$h-\mathcal{R}$	0	0	$+\frac{1}{2}$	$-\frac{1}{2}$	1

Table 27: The $\mathcal{R}$-weights of all the elements of the $\beta\gamma bc$ systems [20].

this, the monomials constructed from the elements detailed in Tab. 27 will have the $\mathcal{R}$-charges of the individual components summed. However, this is not the case with

polynomials. With polynomials one has to define the $\mathcal{R}$-weight as the largest $\mathcal{R}$-weight out of the monomials which comprise it. This non-conservation gives a larger freedom to what operators are allowed to appear in the OPE of two operators. If one has charge $\mathcal{R}_1$ and the other $\mathcal{R}_2$, the only operators which can appear are ones with $\mathcal{R} \leq \mathcal{R}_1 + \mathcal{R}_2$. Alone this is not very restricting, but we will not be using this for solving algebras, only to grade them.

4.7 Vacuum Characters

4.7.1 From Vacuum Characters to Indices

4D $\mathcal{N} = 2$ SCFTs, $\mathcal{T}$, contain a BPS subsector that is isomorphic to a VOA, $\chi[\mathcal{T}]$ [76]. In this correspondence, the VOA central charge c is related to the type-B Weyl-anomaly coefficient in four dimensions as $c = -12c_{4\mathrm{D}}$, while the VOA vacuum character reproduces the Schur limit of the 4D superconformal index. The Schur subsector of pure $\mathcal{N} = 3$ 4D S-fold SCFTs was conjectured to be isomorphic to "$\mathcal{N} = 2$ VOAs"—i.e. VOAs containing the 2D $\mathcal{N} = 2$ superconformal algebra (SCA) as a subalgebra—$\mathcal{W}_{\mathsf{G}}$ labelled by non-Coxeter crystallographic complex reflection groups.

A nice feature of the free-field description, which we will use extensively in the evaluation of the vacuum characters, is that null states built out of strong generators are identically zero. The free-field realisation also facilitates the introduction of a corresponding $\mathcal{R}$-filtration (Sec. 4.6), inherited from the R-symmetry of the 4D $\mathcal{N} = 2$ SCFT.

The vacuum character of the $\mathcal{R}$-filtered VOA is

$$\chi_{\mathcal{W}_{\mathsf{G}}}(q, \xi, z) := \mathrm{Tr}(-1)^F q^h \xi^{\mathcal{R}+r} z^m \,, \tag{4.48}$$

where F is the fermion number, h is the conformal dimension, and r, m are associated with the $\mathfrak{gl}(1)$ outer automorphism and $\mathfrak{gl}(1)$ subalgebra of the 2D $\mathcal{N} = 2$ SCA $\mathfrak{osp}(2|2)$ respectively. $\mathcal{R}$ is the weight under the $\mathcal{R}$-filtration and the vacuum character is normalised so as to start with a "1" in its q expansion. This vacuum character can be further refined by taking $\xi^{\mathcal{R}+r} \to y^{\mathcal{R}} v^r$. In the free-field realisation the $\beta\gamma bc$ fields carry the quantum numbers presented in Tab. 20. The trace is taken to be over the Hilbert space of states built out of the generators of the VOA acting on the $\mathfrak{sl}(2)$ invariant vacuum.

Eq. (4.48) was conjectured to correspond to the Macdonald limit of the 4D superconformal index of a theory for which $\mathcal{W}_{\mathsf{G}}$ is the associated VOA, $\mathcal{W}_{\mathsf{G}} = \chi[\mathcal{T}]$. This is defined through [85]

$$\mathcal{I}^{\mathcal{T}}_{\mathrm{Macdonald}}(q, t, z) := \mathrm{Tr}(-1)^F q^{E-2R-r} t^{R+r} z^m \,, \tag{4.49}$$

where the trace is taken over the set of Schur operators of the 4D SCFT. Here E is the 4D conformal dimension, while R and r are charges for the Cartan generators of the $SU(2)_R$ and $U(1)_r$ R-symmetry groups respectively. Note that while from the point of view of this 4D $\mathcal{N}=2$ Macdonald index m is a quantum number for a global $U(1)_F$, in the full $\mathcal{N}=3$ description it is part of the $U(3) \supset SU(2)_R \times U(1)_r \times U(1)_F$ R-symmetry group. We should emphasise that in order to connect with (4.48) one needs to redefine $t \to \xi q$ so that

$$\mathcal{I}^{\mathcal{T}}_{\text{Macdonald}}(q,\xi,z) = \text{Tr}(-1)^F q^{E-R} \xi^{R+r} z^m \,. \tag{4.50}$$

4.7.2 Implementation

The derivation of the vacuum character expansion is a very laborious and time consuming process when done by hand. One has to take into account all the possible operators which can arise at a certain level, and the number of these operators proliferates rapidly as one moves higher in the expansion. We instead propose the use of computer algorithms which are optimised to perform these calculations in reasonable time, even for quite complicated algebras mentioned in sections 4.4.2 or 4.5.4.

We shall introduce two independent, complementary methods and describe the strategy behind our codes, while detailed results for each case are presented in subsequent subsections. We are interested in the evaluation of the vacuum character for VOAs labelled by crystallographic, non-Coxeter complex reflection groups $\mathbb{Z}_{3,4,6}$ and $G(3,1,2)$, and interpreting them as Macdonald indices for 4D $\mathcal{N}=3$ S-fold theories. To do so one needs to consider (4.48) and trace over all the states created by acting only with normal-ordered products and derivatives of the strong generators of the VOA on the $\mathfrak{sl}(2)$-invariant vacuum, up to a given conformal weight, while removing the contributions from null states. To speed up the calculation, we have taken advantage of the symmetry of the spectrum under conjugation, by only constructing positively-charged states under the two $\mathfrak{gl}(1)$ symmetries of the VOA.

The Null-States Algorithm

In this section we will be describing how the 2D VOA Null States Code works. First things first, let us describe the main objectives of this code. This code aims to brute force search for the null states occurring at every single level. The number of these null states then determine the correct degeneracies of the states at every level of the expansion of the vacuum character. Hence this code calculates the character one level at a time.

Naively, the action of the creation operators which create a ladder of states should be enough, but as it turns out when we go to a specific theory — setting the central charge to a specific value — this results in certain states turning null.

In order to get the physical set of states, one has to mod out the null ones. This is where the true challenge of calculating the vacuum character lies, since listing all possible states is just the tip of the iceberg. The underlying method of this code start differing from the other one at this stage, but we will discuss that in the following subsection. Due to the operator-state map in a CFT we can just consider the operator side of our CFT and avoid all the mode expansions of the operators etc. This means that at every level we have to generate all the possible operators we can construct out of the original strong generators listed in sections 4.4 and 4.5, using only normal ordered products and derivatives. For example $\mathcal{T}$ is a level (weight) 2 operator, but we can also construct $:\mathcal{J}\mathcal{J}:$ as well as $\partial\mathcal{J}$ for example (the weights of these never change because they are part of the underlying $\mathcal{N}=2$ SCA).

Once we have constructed all the allowed operators at a specific level, the code substitutes in the free-field representation. The reason to do this is because one incredible merit of using the free-field realisation is that all the null states are zero [20]. This step requires manipulating normal-ordered products of $\beta\gamma bc$ ghosts, making heavy use of the OPEdefs [94] and ope.math [95] Mathematica packages. This allows our code to try and create an ansatz for null states at each level, and produce a gigantic matrix of all the coefficients of the operators. The rank of this matrix is then found which reveals information about the number of independent operators at each level.

As one goes down the ladder the number of states proliferates at an increasing rate, and their normal orders and derivatives become increasingly more complicated in terms of the free-fields. The algorithm has been optimised a lot in order to increase the speed at which the degeneracies at each level are calculated. One of the things the algorithm can do in order to speed up the calculation by a lot is to pre-process the potential operators and group them into different categories based on quantum numbers. This of course makes it much easier to solve for the ansatze because terms with different charges will not combine into null states.

Another implementation takes advantage of the $\mathfrak{gl}(1)$ charge symmetry which is present in all of the vacuum characters calculated with this method. This means that if the code finds a degeneracy n for a state with charges $(h,m)=(4,2)$ then there will be the exact same degeneracy for the state $(4,-2)$. Using this we only need to calculate half of the character at a level (half + 1 for odd number of charges). As it turns out, the negative side of the character tends to be much more complicated (due to the ansatze in terms of the free fields being long), amounting to a very significant part of the calculation of the character at a level. Ditching that side and calculating on the other can massively boost the code's performance. The other side of the character can then be inferred by charge conjugation. The code is available to download as an ancillary file here.

The Screening Charge Algorithm

In addition to the method introduced in the preceding section, we have cross-checked our rank 1 results using a second algorithm that makes no connection with the VOA presentation — it uses only the free-fields. Just like with the other algorithm we will give a small overview detailing how it works and what its aim is.

This free-field realisation code is actually radically different from the previous one. In the previous section we described how the code builds the allowed operators at a certain level using the abstract generators. This code does exactly the same thing at this stage, but using the free-fields. This means that the theory has to be specified from the very beginning since the free-fields need to be told what their weights are. Furthermore since we start in the realm of the free-fields we are already guaranteed to be null state free, since they are identically zero.

Now one might think that we are done, but as it turns out there is a complication on this side of the calculation too. Not all the states that we generate using the free fields are actually physical, and some must be discarded in order to make contact with the algebra that it is supposed to be representing. This can be done by constructing the VOA spectrum using all states in rank(G) copies of the $\beta\gamma bc$ ghost system that lie in the kernel of a screening operator, $\mathbb{S}$. This operator is defined as $\mathbb{S} = \int \mathsf{J}$, given a screening current J. Its action is through the first order pole of the OPE. For $\mathsf{G} = \mathbb{Z}_k$ this current is given by [20]

$$\mathsf{J} = b\, e^{\left(k^{-1}-1\right)(\chi+\phi)} \,, \tag{4.51}$$

where χ, ϕ are chiral bosons

$$\beta = e^{\chi+\phi}, \quad \gamma = \partial\chi\, e^{-\chi-\phi} \,, \tag{4.52}$$

and all expressions should be considered as normal-ordered. Such an approach is conceptually more straightforward—construct all states using free fields and then keep those in the kernel of $\mathbb{S}$—but as we will discuss in the next section how it is significantly slower than the algorithm above.

Using this information we can start building all the states and then creating ansatze to find the number of independent states, except this time the ansatze will reveal physical states as opposed to null ones. The unknown coefficients of the ansatze will tell us the degeneracies of states within a certain level. Using this our code determines the vacuum character at that level. This code is also available here.

Remarks About the Codes

In this section we will comment on how we implemented the above algorithms by means of Mathematica, and also give insight on how well they work as well as how one can download and use them.

First of all, the codes are available to download as the ancillary files for this publication [2]. All of the codes are fully equipped with the explanatory material to reproduce the results summarised in this chapter, as well as to potentially extend the workings of the codes to other VOAs the user wants to implement. As we have mentioned in the previous sections above, the speed of the codes varies due to many factors. The most prevalent one which differentiates the two codes is the fact that the screening operator code is always more intensive and hence slower than the null-states code. The reason for this is to do with the huge amount of states the former code has to comb through compared to the latter one. E.g. at $h = 9/2$ one already needs to check 941 and 881 terms for $\mathbb{Z}_3$ and $\mathbb{Z}_4$ respectively.

The comparative speed is always fixed, but there are things which influence the speed of both of the codes. Of course higher levels mean more ansatz terms, which translate into more processing times. More complicated theories, i.e. rank 2 theories or theories with $\mathcal{W}_l$ weights being very high also incur higher processing times, again because of the number of free-fields in the calculations. However, as mentioned before, utilising the $\mathfrak{gl}(1)$ charge symmetry can cut down the processing time by a huge amount. This shortcut is natively present in our codes. In Fig. 4 we show how the computational times scale for different theories at different levels.

4.7.3 Results: $\mathsf{G} = \mathbb{Z}_3$

This is a rank-one VOA with central charge $c = -15$. Its VOA presentation is discussed in section 4.5.1. The ansatz for $\mathcal{W}$ contains 8 undetermined coefficients — reported for the sake of calculation complexity. We always count these before imposing the super-Virasoro primary constraint. Using the codes given above, we have calculated the fully-refined vacuum character (4.48) up to $O(q^8)$ and have cross-checked this result using the screening-operator approach up to $O(q^4)$. The full expression can be found in the ancillary file 'vacuum_characters_summary.nb' here.

This VOA is expected to encode the Schur sector of a rank one, 4D S-fold $\mathcal{N} = 3$ SCFT, with a Coulomb-branch operator of dimension $\Delta = 3$ and trace-anomaly coefficient $c_{4\mathrm{D}} = \frac{5}{4}$. Through (4.50) the Macdonald index of this S-fold theory—including the global $U(1)_F$ fugacity—can be identified with the refined vacuum character. Below we only present the simpler, Schur limit of these expressions for brevity, where $\xi \to 1$,

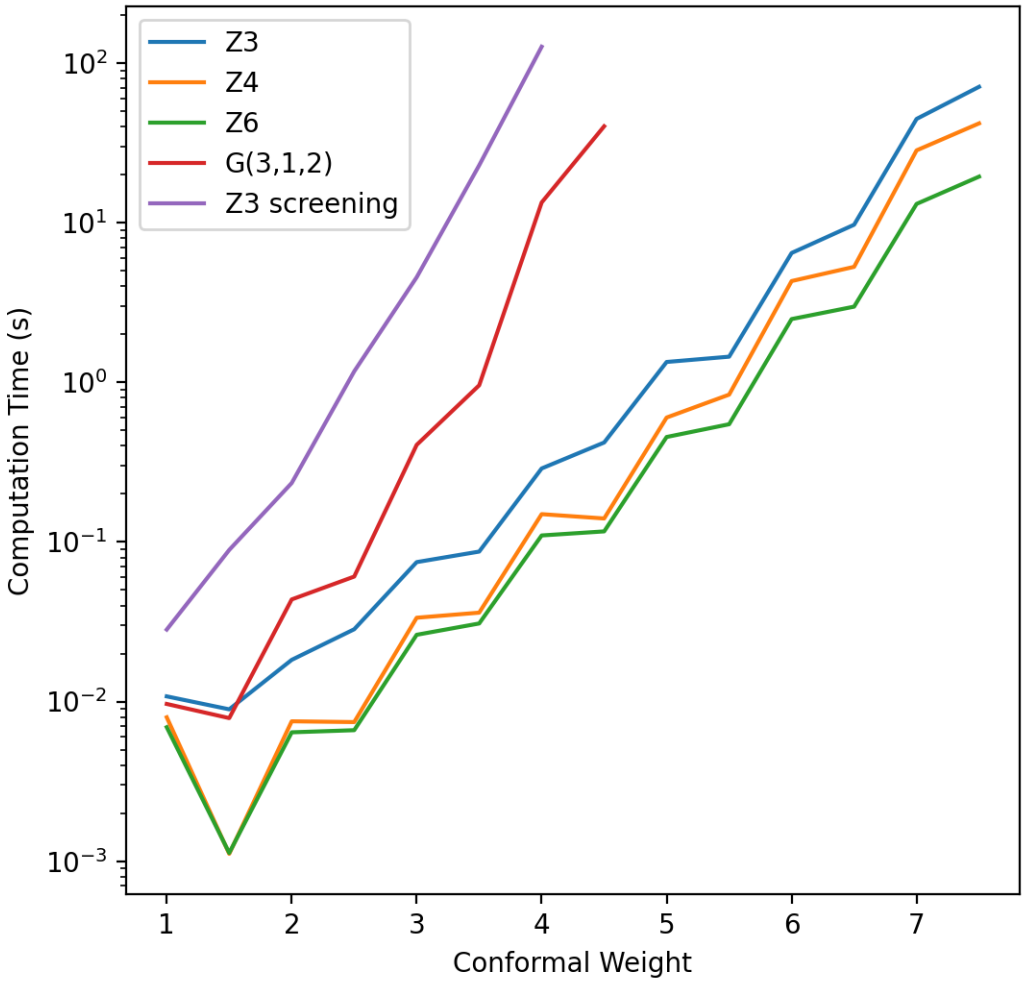

Figure 4: Computation times for carrying out the calculation of the vacuum character for VOAs at different conformal weights. Several different VOAs are shown on the graph for comparison, along with the $\mathbb{Z}_3$ theory computed using the kernel of the screening operator. There are successive dips in the computation time because in general there are less terms at those levels. We used a desktop PC with an Intel Core i7-6700K CPU clocked at 4GHz, and 32GB RAM.

$z \to 1$. Then:

$$\mathcal{I}^{\mathbb{Z}_3}_{\text{Schur}} = 1 + q + q^2 + 2q^3 - 2q^{7/2} + 3q^4 - 2q^{9/2} + 4q^5 - 4q^{11/2} + 6q^6 - 6q^{13/2} + 8q^7 - 8q^{15/2} + 11q^8 + O(q^{17/2}). \tag{4.53}$$

Since the character is counting the independent operators at each level, one can very easily see what operators appear. For example here the first three entries in the expan-

sion correspond to the identity, $\mathcal{J}$ and $\mathcal{T}$. The contributions of $\mathcal{W}$ and $\overline{\mathcal{W}}$ are cancelled by $\mathcal{G}$ and $\widetilde{\mathcal{G}}$ in this limit.

In [93], an independent argument for determining the Schur index of the $\mathsf{G} = \mathbb{Z}_3$ S-fold theory was presented. This entailed starting from an $\mathcal{N} = 1$ 4D UV Lagrangian theory, and flowing to an interacting $\mathcal{N} = 1$ SCFT in the IR, which can also be reached from the $\mathbb{Z}_3$ S-fold theory via an $\mathcal{N} = 1$ preserving marginal deformation. Upon relabelling $q \to p^2$, our result (4.53) agrees with that of [93]—listed to $O(q^7)$—providing a strong consistency check of both calculations.

4.7.4 Results: $\mathsf{G} = \mathbb{Z}_4$

This is a rank-one VOA with central charge $c = -21$. Its VOA presentation is detailed in section 4.5.2. The ansatz for $\mathcal{W}_4$ contains 19 undetermined coefficients. We have calculated the fully-refined vacuum character (4.48) up to $O(q^8)$. We have also cross-checked this result using the screening-operator up to $O(q^4)$.

This VOA is expected to encode the Schur sector of a rank one 4D S-fold $\mathcal{N} = 3$ SCFT, with a Coulomb-branch operator of dimension $\Delta = 4$ and trace-anomaly coefficient $c_{\text{4D}} = \frac{7}{4}$. Through (4.50) the Macdonald index of this S-fold theory can be identified with the vacuum character. The Schur limit of these expressions yields:

$$\begin{aligned}\mathcal{I}^{\mathbb{Z}_4}_{\text{Schur}} = 1 &+ q - 2q^{3/2} + 5q^2 - 6q^{5/2} + 10q^3 - 16q^{7/2} + 27q^4 \\ &- 38q^{9/2} + 56q^5 - 86q^{11/2} + 129q^6 - 178q^{13/2} \\ &+ 251q^7 - 362q^{15/2} + 511q^8 + O(q^{17/2}) \,. \end{aligned} \tag{4.54}$$

In this case the VOA construction is such that the bosonic states always appear with integer while the fermionic ones with half-integer conformal weights. Therefore there are no cancellations between bosonic and fermionic states at each level and the chiral algebra partition function reproduces the partition function of Schur operators in the corresponding 4D $\mathcal{N} = 3$ theory.

4.7.5 Results: $\mathsf{G} = \mathbb{Z}_6$

This is a rank-one VOA with central charge $c = -33$. Its VOA presentation is shown in section 4.5.3. The ansatz for $\mathcal{W}_6$ contains 87 undetermined coefficients. We have calculated the fully-refined vacuum character (4.48) up to $O(q^8)$. We did not crosscheck this result with the screening operator code because it was too time consuming. In the limit $\xi \to 1$, $z \to 1$ this reads:

$$\begin{aligned}\chi_{\mathcal{W}_{\mathbb{Z}_6}} = 1 &+ q - 2q^{3/2} + 3q^2 - 4q^{5/2} + 8q^3 - 12q^{7/2} + 19q^4 \\ &- 26q^{9/2} + 38q^5 - 58q^{11/2} + 85q^6 - 116q^{13/2}\end{aligned}$$

$$+ 165q^7 - 236q^{15/2} + 326q^8 + O(q^{17/2}) \,. \tag{4.55}$$

No known S-fold theory is associated with this VOA [80].

4.7.6 Results: $\mathsf{G} = G(3,1,2)$

This is our only rank 2 example, with central charge $c = -48$. Its VOA presentation is given in section 4.5.4. The ansatz for $\mathcal{W}_1$ contains 84 undetermined coefficients. It turns out that through the OPEs in the W-algebra presentation, one can fix the coefficients of $\mathcal{W}_1$ and by doing so also determine the free-field realisation of all remaining generators. We have calculated the fully-refined vacuum character (4.48) up to $O(q^{9/2})$. We did not crosscheck this result with the screening operator code because we do know the relevant screening charge to be used to restrict the free-field systems. The full result can be found in the ancillary file 'vacuum_characters_summary.nb' here.

This VOA is expected to encode the Schur sector of a rank-two 4D S-fold $\mathcal{N} = 3$ SCFT, with Coulomb-branch operators of dimension $\Delta = 3, 6$ and trace anomaly coefficient $c_{\text{4D}} = 4$. Through (4.50) the Macdonald index of this S-fold theory can be identified with the vacuum character. If for simplicity one considers the limit $z \to 1$:

$$\begin{aligned}
\mathcal{I}^{G(3,1,2)}_{\text{Macdonald}} = 1 &+ q\xi + q^{3/2}\left(-\sqrt{\xi} + \xi^{3/2}\right) + q^2\left(\xi + \xi^2\right) \\
&+ q^{5/2}\left(-\sqrt{\xi} - \xi^{3/2} + 2\xi^{5/2}\right) + q^3\left(\xi - \xi^2 + 2\xi^3\right) \\
&+ q^{7/2}\left(-\sqrt{\xi} - 2\xi^{3/2} + 2\xi^{5/2} + \xi^{7/2}\right) \\
&+ q^4\left(2\xi - \xi^3 + 3\xi^4\right) \\
&+ q^{9/2}\left(-\sqrt{\xi} - 3\xi^{3/2} + \xi^{5/2} + \xi^{7/2} + 2\xi^{9/2}\right) \\
&+ O(q^5) \,.
\end{aligned} \tag{4.56}$$

Chapter 5

AdS_7 Black Hole Entropy from 5D $\mathcal{N} = 2$ Yang-Mills

5.1 Introduction and Summary

Since the introduction of the superconformal index [7, 96, 97] there has been a puzzle pertaining to why it seems to only be capturing supergraviton-state contributions in AdS, and not those of certain BPS black holes as predicted by the AdS/CFT correspondence at large N [98, 99]. Over the years there have been several approaches to this problem. For example, one of the early explanations appealed to the possibility of huge cancellations between bosonic and fermionic states. Later on, the reformulation of the superconformal index in D even spacetime dimensions through the operator-state map as an R-twisted supersymmetric partition function on $S^{D-1} \times S^1_\beta$ revealed that

$$\mathcal{Z}_{S^{D-1}\times S^1_\beta} \;=\; e^{-\mathcal{F}}\mathbb{I}\,, \tag{5.1}$$

where $\mathbb{I}$ is the superconformal index, β the radius of the thermal circle and $\mathcal{F}$ a quantity related to the vacuum Casimir energy [100, 101, 102, 103]. Unlike the index, this "supersymmetric Casimir energy" was shown to exhibit the expected scaling of degrees of freedom at large N. However matching the precise coefficient predicted by AdS/CFT, and corresponding entropy of BPS black holes in the gravity dual, turns out to be subtler, see for example [104]. More recently, the black hole entropy for even D has been recovered from field theory through the extremisation of a quantity closely resembling the supersymmetric Casimir energy [105, 106].

Over the last few years, there has been a significant acceleration of activity in this direction. In [21], a complete gravitational derivation of the field-theoretic entropy function was performed for AdS_5/CFT_4,[15] while in [109, 110] the entropy function was reproduced from field theory in the Cardy limit of large charges, for a variety of bulk

[15] For generalisations see [107, 108].

dimensions. In yet another line of attack, the superconformal index itself (and not the supersymmetric Casimir energy) was shown to be capturing larger than previously thought degeneracies for a particular complexification of chemical potentials, through a formulation that involves solutions for auxiliary Thermodynamic Bethe Ansatz (TBA) equations [111, 112]. Finally, the general behaviour seen in [111, 112] was reproduced for 4D $\mathcal{N}=1$ SCFTs in the Cardy limit without resorting to the TBA equations in [113, 114].

In this chapter we will introduce the concept of localisation, initially in a mathematical setting, and later transitioning to how it works in physics. We will also explain a simple to example following the procedure of [22] which will serve as a light introduction to how localisation is carried out in practice in physics. After this review, we will move on to presenting our research and focusing on the relationship between the AdS$_7$ black hole entropy and the superconformal index of the six-dimensional (2,0) theory.[16] We will first generalise the AdS$_5$ analysis of [21] for the case of 2-equivalent charge and 3-equivalent rotation non-extremal black hole solutions. A study of the regularity conditions for the metric and Killing spinors in the bulk leads to a specific background at the boundary of AdS$_7$. The AdS/CFT correspondence then dictates that the black hole entropy should be related to an R-twisted, supersymmetric partition function for the six-dimensional A_{N-1} (2,0) theory on this particular background in the large-N limit.

As the interacting (2,0) theory does not admit a Lagrangian description one cannot directly employ the method of supersymmetric localisation to evaluate the boundary partition function. We therefore turn to the existing literature, where it has instead been conjectured to arise from a 5D supersymmetric partition function on S^5 for the maximally-supersymmetric ($\mathcal{N}=2$) Yang–Mills theory (MSYM) with $SU(N)$ gauge group [115, 116, 117, 118, 101, 119, 120, 121]—the circle reduction of the (2,0) theory on $S^5 \times S^1_\beta$. A modification of these results at large N and in a Cardy-like limit reproduces a (generalised) supersymmetric Casimir energy that exactly matches the gravitational prediction.[17]

Note also that the statistical entropy of various asymptotically-AdS black holes (not only for D even) can be reproduced microscopically from a different, "topologically-twisted index".[18] The latter can be evaluated through supersymmetric localisation for a topologically-twisted gauge theory along the lines of [122]; see e.g. [123, 124] for applications.

[16] Note that the AdS$_7$ entropy function was first written down in [106], while it was reproduced in the Cardy limit in [109]. However, our scope here will be to provide a microscopic derivation of this quantity from the six-dimensional CFT dual theory.

[17] It would be very interesting to revisit the original work of [97] and investigate the scaling of degrees of freedom directly in the 6D superconformal index along the lines of [111, 112].

[18] In this work, whenever we refer to the "index" we will mean the superconformal index and not its topologically-twisted version.

The rest of this chapter is organised as follows: In Sec. 5.2 we will introduce the mathematical background from where localisation stems — equivariant localisation. In the final part of this section we will explain the dictionary between equivariant and supersymmetric localisation. Sec. 5.3 contains the fully explained derivation of the localisation of the $\mathcal{N} = 2$ Chern-Simons gauge theory on S_3, which results in the full computation of the path integral. This is the review of [22], and it serves as a demonstration of how localisation works. In Sec. 5.4, we analyse the 2-equivalent charge, 3-equivalent rotation black hole solution in AdS$_7$ and determine how it fixes the form of the boundary partition function that is AdS/CFT dual to the corresponding on-shell action at large N. We then discuss the evaluation of this boundary partition function from 5D MSYM using supersymmetric localisation in Sec. 5.5.

5.2 Introduction to Localisation

In this section we will be providing an abstract mathematical basis for the concept of localisation. This will then be applied later on to supersymmetric path integrals. However, in the meantime we would like to become familiar with the concept of abelian equivariant cohomology.

5.2.1 Equivariant Cohomology

Let us say that we would like to calculate an integral over a given manifold, $\mathcal{M}$. If this manifold has a symmetry group G, that is, the integral will not be able to tell apart the points related by the action of G, in order to not overcount naively one would instead define $\mathcal{M}/G$ as the integration manifold. This would be fine if G acted freely on the manifold. Let us suppose that in our case we have fixed points for our group action. This means that $\mathcal{M}/G$ is not a smooth manifold anymore and hence standard cohomology and differential forms will not be applicable.

Enter equivariant cohomology, a generalisation of cohomology to the cases mentioned above. For now, let us define a Riemannian manifold with dimension $2l$ with no boundary (works generally) and an abelian group G. Next we define a Killing vector V corresponding to a $U(1)$ isometry. This means:

$$\mathcal{L}_V g_{\mu\nu} = 0. \tag{5.2}$$

Where the Lie derivative is taken along the flow of V. In this next step we introduce a space of polyforms [125] (polynomials of forms, or rather the sum of forms of different

degrees)

$$\Lambda\mathcal{M} = \left\{ \alpha = \sum_{n=0}^{2l} \alpha_n | \alpha_n \in \Lambda^n \mathcal{M} \right\}. \tag{5.3}$$

Here $\Lambda^n\mathcal{M}$ is the set of forms acting on $\mathcal{T}\mathcal{M}$ In analogy with the exterior differential operator, we also define the so-called equivariant differential d_V:

$$d_V \equiv d - \imath_V. \tag{5.4}$$

d being the exterior differential operator for forms $d : \Lambda^n\mathcal{M} \to \Lambda^{n+1}\mathcal{M}$, and $\imath$ is the inner derivative (otherwise known as contraction with vector field), $\imath : \Lambda^n\mathcal{M} \to \Lambda^{n-1}\mathcal{M}$. An interesting corollary of the above definition is that the square of the equivariant differential is the Lie derivative in the direction of V:

$$d_V^2 = d^2 - d\imath_V - \imath_V d + \imath_V^2 = -\{d, \imath_V\} = \mathcal{L}_V. \tag{5.5}$$

From this property of d_V we can define a set of V-equivariant polyforms which have a vanishing Lie derivative. This means that on this set of polyforms, the equivariant differential behaves exactly like a de Rham operator. Hence if we have $d_V\alpha = 0$, we call α V-equivariantly closed. Similarly, we can define $\alpha = d_V\beta$, which would make α equivariantly exact. Therefore in the same spirit as the nth de Rham cohomology group, one can define the nth V-equivariant cohomology group:

$$H_V^n(\mathcal{M}) = \frac{\text{Ker } d_V|_{\Lambda_V^n\mathcal{M}}}{\text{Im } d_V|_{\Lambda_V^{n-1}\mathcal{M}}}. \tag{5.6}$$

We can now move onto defining integrals of polyforms. Such integrals are defined by only looking at the integral of the top form (highest order)

$$\int_{\mathcal{M}} \alpha \equiv \int_{\mathcal{M}} \alpha_{2l}. \tag{5.7}$$

It is important to note that from the statement that we have no boundaries and Stokes' theorem, we obtain that the integrals of equivariantly exact polyforms vanish:

$$\int_{\mathcal{M}} d_V\beta \equiv \int_{\mathcal{M}} d\beta_{2l-1} = 0. \tag{5.8}$$

This means that we can add exact deformations to this integral without changing the overall value. This is a very important consequence which we will use now to show the localisation argument.

5.2.2 Atiyah-Bott-Berline-Vergne Localisation

In order to start localising we will make use of the property in equation (5.8), and deform our form $\alpha \to \alpha e^{td_V\beta}$. Let t be a real parameter and β a V-equivariant polyform. It can be shown that the integral of this quantity is independent of t since the t derivative of $\alpha e^{td_V\beta}$ will be an exact form, i.e. zero once integrated. This has the impact of letting us take any value of t which we prefer. For example, let us pick the $t \to \infty$ limit. In this limit the integral will be dominated by the minima of $-(d_V\beta)_0$. If we pick β to be dual to the Killing vector V, we get by substituting everything in:

$$\int_{\mathcal{M}} \alpha = \lim_{t\to\infty} \int_{\mathcal{M}} \alpha e^{td\beta} e^{-t|V|^2}. \tag{5.9}$$

We can see that in this limit the second exponential on the RHS turns into a delta function ($\delta(V)$) and localises the integral to the points when $V = 0$ (since we are on Riemannian not pseudo-Riemannian manifolds). We will denote these points where $V = 0$ as $\mathcal{M}_V$ and call it the localisation locus.

In this section we will only discuss localisation for isolated fixed points, however there is a very similar method to derive the formula for a localisation locus which is continuously defined. That is commonly known as the Duistermaat-Heckman formula, but it will not be elaborated upon in this section.

Now that we have made the assumption that our localisation locus is a set of isolated points, $\mathcal{M}_V = \{x_k\}$, we can choose to move to a close vicinity of one of those fixed points (called point P). We zoom so close in fact that we can choose to consider the coordinates of an intertial frame centred at P, with our usual Cartesian metric (with Cartesian and spherical polar coordinates):

$$ds^2 = \sum_{i=1}^{l}(dx_i^2 + dy_i^2) = \sum_{i=1}^{l}(dr_i^2 + r_i^2 d\varphi_i^2). \tag{5.10}$$

In these coordinates locally the Killing vector corresponding to the U(1) action is given by,

$$V = \sum_{i=1}^{l} \omega_{P,i}\left(-y_i\frac{\partial}{\partial x_i} + x_i\frac{\partial}{\partial y_i}\right) = \sum_{i=1}^{l}\omega_{P,i}\frac{\partial}{\partial\varphi_i}. \tag{5.11}$$

Where we have defined $\omega_{P,i}$ to be the angular velocity in a particular plane. From these definitions we can calculate the dual form to V, β

$$\beta = \sum_{i=1}^{l}\omega_{P,i}(-y_i dx_i + x_i dy_i) = \sum_{i=1}^{l}\omega_{P,i} r_i^2 d\varphi_i. \tag{5.12}$$

Then for the equivariant differential of β,

$$\begin{aligned} d_V\beta &= 2\sum_{i=1}^{l}\omega_{P,i}dx_i\wedge dy_i - \sum_{i=1}^{l}\omega_{P,i}^2(x_i^2+y_i^2) \\ &= \sum_{i=1}^{l}\omega_{P,i}\ d(r_i^2)\wedge d\varphi_i - \sum_{i}^{l}\omega_{P,i}^2 r_i^2. \end{aligned} \tag{5.13}$$

Now we are ready to see what the contribution to the integral of α is from this isolated point P

$$\lim_{t\to+\infty}\int_{\text{N.hood of P}}\alpha\ e^{td_V\beta} = \lim_{t\to+\infty}\alpha_0(P)\prod_{i=1}^{l}\left(2t\omega_{P,i}\int_{\mathbb{R}^2}dx_i\wedge dy_i\ e^{-t\omega_{P,i}^2(x_i^2+y_i^2)}\right) \tag{5.14}$$

$$\begin{aligned} &= \lim_{t\to+\infty}\alpha_0(P)\prod_{i=1}^{l}\left(t\omega_{P,i}\int_0^{2\pi}d\varphi_i\int_0^{\infty}d(r_i^2)\ e^{-t\omega_{P,i}^2 r_i^2}\right) \\ &= \alpha_0(P)\frac{(2\pi)^l}{\prod_{i=1}^{l}\omega_{P,i}}. \end{aligned}$$

Already in the first line we have made a drastic simplification, since in the Taylor expansion of the first term in (5.13) we only keep the leading order term in our limit (which is a form of degree $2l$). Remembering that this is the contribution from one of the fixed points, we can do the same analysis for all the others. It turns out that the product of all the $\omega_{P,i}$'s actually corresponds to the Pfaffian of the circle action of V on $T_P\mathcal{M}$. Hence, putting everything together:

$$\int_{\mathcal{M}}\alpha = (2\pi)^l\sum_{x_k\in\mathcal{M}_V}\frac{\alpha_0(x_k)}{\text{Pf}(-\mathcal{L}_V(x_k))}. \tag{5.15}$$

This is the famous Atiyah-Bott-Berline-Vergne localisation formula [126][127]. As one can see, it drastically simplifies the integral in question. As we discussed before, the next step would be to take the fixed points to not be isolated, this would result in the Duistermaat-Heckman formula. The major differences being that now one will integrate over the manifold $\mathcal{M}_V$ and also the transverse fluctuations to $\mathcal{M}_V$. The formula above can be connected to the topic of equivariant index theorems, which are extensions of the Atiyah-Singer index theorem [128] for when there is an action on the compact manifold by a group. However, this is very much beyond the scope of what we need to discuss localisation. Instead of discussing this in detail, we shall move onto drawing similarities between equivariant localisation and supersymmetric localisation.

5.2.3 Supersymmetric Localisation

In this section we will connect the ideas we have introduced so far in the previous sections to supersymmetric path integrals. In SUSY QFT instead of equivariant differentials which square to Lie derivatives of a symmetry, we have the supercharges $\mathcal{Q}$ which square to a bosonic charge B of a symmetry. The bosons and fermions would correspond to even and odd degree polyforms. Equivariantly closed polyforms translate to BPS observables. These observables are annihilated by $\mathcal{Q}$, which means that the action of B on them is also going to give zero. We will now summarise these similarities in a table below for conciseness.

Equivariant Localisation	Supersymmetric Localisation
d_V	$\mathcal{Q}$
$d_V^2 = -\mathcal{L}_V$	$\mathcal{Q}^2 = B$
Even/Odd Polyforms	Bosons/Fermions
$d_V \alpha = 0$	$\mathcal{Q}\mathcal{O} = 0$
$\int_{\mathcal{M}} \alpha = \int_{\mathcal{M}} \alpha e^{t d_V \beta}$	$\int_{\mathcal{F}} \mathcal{D}X \mathcal{O} e^{-S[X]} = \int_{\mathcal{F}} \mathcal{D}X \mathcal{O} e^{-S[X] - t\mathcal{Q}\mathcal{P}_F[X]}$
$L_V \beta = 0$	$B\mathcal{P}_F[X] = 0$
Localisation locus $\mathcal{M}_V$	BPS locus $\mathcal{F}_{\mathcal{Q}}$

Knowing this should allow us to calculate some SUSY partition functions. Before we move onto looking at the 6D/5D theories, we will present a sort of S^3 toy model to warm up with the calculations. In the next section we will start calculating the exact partition function for an $\mathcal{N}=2$ theory on the 3-sphere.

5.3 Localisation on S^3

5.3.1 Setting Up the Path Integral

In this section we will be aiming to perform the path integral of a $\mathcal{N}=2$ SUSY gauge theory defined on a 3-sphere exactly along the lines of [22]. We will be attempting this using the tools of supersymmetric localisation explained in the previous sections. First and foremost we will describe the theory we chose to localise. We will consider a supersymmetric Chern-Simons Lagrangian as the Lagrangian for our gauge theory. We will take the Chern-Simons theory on $\mathbb{R}^3$ first and since it is a conformal theory we will transfer it to S^3 which is how we shall set up our model.

Let us look at the gauge multiplet for an $\mathcal{N}=2$ theory in 3D. As it turns out, this is just the dimensional reduction of an $\mathcal{N}=1$ vector multiplet in 4D. It consists of a gauge field A_μ, two auxiliary scalar fields, D and σ, which are real and an auxiliary fermion λ (a two component complex Dirac spinor). Since these fields are all in the same multiplet they all take values in the same Lie algebra $\mathfrak{g}$ of the Lie group G, whose knowledge is not important at the moment.

The action for our SCS (SUSY Chern-Simons) theory is given by:

$$S = \int_{S^3} d^3x\sqrt{g}\left(\epsilon^{\mu\nu\rho}\left(A_\mu\partial_\nu A_\rho + \frac{2i}{3}A_\mu A_\nu A_\rho\right) - \lambda^\dagger\lambda + 2D\sigma\right). \tag{5.16}$$

As usual, this action is taken to be invariant under the Euclidean $\mathcal{N}=2$ gauge multiplet SUSY transformations:

$$\begin{aligned}
\delta A_\mu &= \frac{i}{2}(\eta^\dagger\gamma_\mu\lambda - \lambda^\dagger\gamma_\mu\varepsilon),\\
\delta\sigma &= -\frac{1}{2}(\eta^\dagger\lambda + \lambda^\dagger\varepsilon),\\
\delta D &= \frac{i}{2}(\eta^\dagger\gamma^\mu(D_\mu\lambda) - (D_\mu\lambda^\dagger)\gamma^\mu\varepsilon) - \frac{i}{2}(\eta^\dagger[\lambda,\sigma] - [\lambda^\dagger,\sigma]\varepsilon)\\
&\quad + \left\{\frac{i}{6}((\nabla_\mu\eta^\dagger)\gamma^\mu\lambda - \lambda^\dagger\gamma^\mu\nabla_\mu\varepsilon)\right\},\\
\delta\lambda &= (-\frac{1}{2}\gamma^{\mu\nu}F_{\mu\nu} - D + i\gamma^\mu D_\mu\sigma)\varepsilon + \left\{\frac{2i}{3}\sigma\gamma^\mu\nabla_\mu\varepsilon\right\},\\
\delta\lambda^\dagger &= \eta^\dagger(\frac{1}{2}\gamma^{\mu\nu}F_{\mu\nu} - D - i\gamma^\mu D_\mu\sigma) - \left\{\frac{2i}{3}\sigma\nabla_\mu\eta^\dagger\gamma^\mu\right\}.
\end{aligned} \tag{5.17}$$

We have separated the transformations which would only be present on S^3 in the curly brackets. They appear as one makes the transition from Euclidean space to S^3. There are two types of covariant derivatives which appear in the expressions above. ∇_μ corresponds to the covariant derivative on S^3 defined in the usual way acting on the Dirac spinors and vectors, whilst D_μ is the full covariant derivative which contains the gauge field terms and also the gravitational terms. Depending on which fields it acts on, it will have a different form (eg. for a spinor in the adjoint it will have the adjoint gauge covariant derivative and the spin connection parts). It is also possible to add matter to the Lagrangian above by introducing a hypermultiplet, but that will not be considered in this report.

Now that the SUSY and the action have been specified, we can move onto performing the localisation.

5.3.2 Localisation of the Gauge Sector

In order to perform supersymmetric localisation we need only to pick one of the supercharges which we have introduced. Using this, we can introduce a $\mathcal{Q}$ exact term into the action which we will then use to perform the localisation. For this we pick:

$$t\delta V = t\delta\mathrm{tr}'\left((\delta\lambda)^\dagger\lambda\right). \tag{5.18}$$

We defined tr$'$ to be some Killing product on $\mathfrak{g}$. We remember from the analysis in section 5.2.3 that V has to be invariant under the bosonic charge of $\mathcal{Q}^2 \sim \delta^2 = B$.

From here we will take the parameter t to go to infinity as prescribed from before. The bosonic part of the variation of V will be $t(\delta\lambda)^\dagger\delta\lambda$, which is positive definite, and hence the fixed points will be given when $\delta\lambda = 0$.

Before moving any further it is important for us to first note that to be able to place any SUSY theory on a curved background one has to be able to solve the Killing spinor equations for the given background [125], in our case for S^3. There are detailed solutions for all the spheres and their Killing spinors, which is why we will not spend much time glossing over them here. Instead we will just state the two Killing spinor equations which are relevant:

$$\nabla_\mu\varepsilon = \pm\frac{i}{2}\gamma_\mu\varepsilon. \tag{5.19}$$

Same for η. Let us choose ε to be the charge with respect to which we localise, and we set $\eta = 0$.

Using these identities we can rewrite the SUSY transformations from equation (5.17) as,

$$\begin{aligned}
\delta A_\mu &= -\frac{i}{2}\lambda^\dagger\gamma_\mu\varepsilon,\\
\delta\sigma &= -\frac{1}{2}\lambda^\dagger\varepsilon,\\
\delta D &= -\frac{i}{2}(D_\mu\lambda^\dagger)\gamma^\mu\varepsilon + \frac{1}{4}\lambda^\dagger\varepsilon + \frac{i}{2}[\lambda^\dagger,\sigma]\varepsilon,\\
\delta\lambda &= (-\frac{1}{2}\gamma^{\mu\nu}F_{\mu\nu} - D + i\gamma^\mu D_\mu\sigma - \sigma)\varepsilon,\\
\delta\lambda &= 0.
\end{aligned} \tag{5.20}$$

It can be seen from these expressions that δ^2 is nilpotent on the relevant fields, and $\delta^2 V = 0$.

Now we will calculate the expression for δV. First of all, we will split the calculation into two parts: a bosonic and a fermionic part. The bosonic part is $\delta V_{bos} = (\delta\lambda)^\dagger(\delta\lambda)$. Substituting in relevant terms (we will drop the trace, but it will still be there in spirit, which is why we will move terms around cyclically):

$$\begin{aligned}
\delta V_{bos} &= (\delta\lambda)^\dagger(\delta\lambda)\\
&= \varepsilon^\dagger\left(\frac{1}{2}\gamma^{\mu\nu}F_{\mu\nu} - D - i\gamma^\mu D_\mu\sigma - \sigma\right)\left(-\frac{1}{2}\gamma^{\alpha\beta}F_{\alpha\beta} - D + i\gamma^\alpha D_\alpha\sigma - \sigma\right)\varepsilon\\
&= \varepsilon^\dagger\Big(-\frac{1}{4}\gamma^{\mu\nu}\gamma^{\alpha\beta}F_{\mu\nu}F_{\alpha\beta} + i\gamma^{\mu\nu}\gamma^\alpha F_{\mu\nu}D_\alpha\sigma + D^2 + 2D\sigma + \sigma^2\\
&\quad + \gamma^\mu\gamma^\alpha(D_\mu\sigma)(D_\alpha\sigma)\Big)\varepsilon\\
&= \frac{1}{2}F_{\mu\nu}F^{\mu\nu} + (D_\mu\sigma)(D^\mu\sigma) + (D+\sigma)^2.
\end{aligned} \tag{5.21}$$

Where in the last line we used 3D gamma matrix identities as well as the fact that we can set our Killing spinor ε to be normalised such that $\varepsilon^\dagger\varepsilon = 1$. Next we will calculate the fermionic part $\delta V_{ferm} = \delta((\delta\lambda)^\dagger)\lambda$:

$$\begin{aligned}\delta V_{ferm} &= \delta((\delta\lambda)^\dagger)\lambda \\ &= \delta\left(\frac{1}{2}\gamma^{\mu\nu}F_{\mu\nu} - D - i\gamma^\mu D_\mu\sigma - \sigma\right)\lambda.\end{aligned}$$

For these, we have to derive how $F_{\mu\nu}$ and $D_\mu\sigma$ transform under these SUSY transformations

$$\begin{aligned}\delta F_{\mu\nu} &= \delta(\partial_\mu A_\nu - \partial_\nu A_\mu + i[A_\mu, A_\nu]) \\ &= D_\mu\delta A_\nu - D_\nu\delta A_\mu \\ &= -\frac{i}{2}(D_\mu\lambda^\dagger)\gamma_\nu\varepsilon + \frac{i}{2}(D_\nu\lambda^\dagger)\gamma_\mu\varepsilon + \frac{1}{2}(\lambda^\dagger\gamma_{\nu\mu}\varepsilon),\end{aligned} \tag{5.22}$$

$$\begin{aligned}\delta(D_\mu\sigma) &= \delta(\partial_\mu\sigma + i[A_\mu, \sigma]) \\ &= D_\mu\delta\sigma + i[\delta A_\mu, \sigma] \\ &= -\frac{1}{2}(D_\mu\lambda^\dagger)\varepsilon - \frac{i}{4}\lambda^\dagger\gamma_\mu\varepsilon + \frac{1}{2}[\lambda^\dagger, \sigma]\gamma_\mu\varepsilon.\end{aligned} \tag{5.23}$$

Now comes the fun bit of plugging it all back into the expression above. Since we have a limited amount of space, we will spare the reader from pages and pages of algebra and just quote the result, and the methods used to get to said result. The fermionic part of the $\mathcal{Q}$-exact bit is given by:

$$\delta V_{ferm} = i\lambda^\dagger\gamma^\mu\nabla_\mu\lambda + i[\lambda^\dagger, \sigma]\lambda - \frac{1}{2}\lambda^\dagger\lambda. \tag{5.24}$$

To get to this result, one has to employ various spinor and gamma matrix identities such as:

$$\gamma^{\mu\nu}\gamma_\nu = 2\gamma^\mu, \tag{5.25}$$

$$\gamma^{\mu\nu}\gamma_\rho\gamma_\nu = -2\delta_\rho{}^\mu. \tag{5.26}$$

For the spinors there is the Fierz identity:

$$(\eta_1^\dagger\eta_2)(\eta_3^\dagger\eta_4) = -\frac{1}{2}(\eta_1^\dagger\eta_4)(\eta_3^\dagger\eta_2) - \frac{1}{2}(\eta_1^\dagger\gamma_\mu\eta_4)(\eta_3^\dagger\gamma^\mu\eta_2). \tag{5.27}$$

We can now write down the full expression for the exact term in the path integral:

$$\delta V = \frac{1}{2}F_{\mu\nu}F^{\mu\nu} + (D_\mu\sigma)(D^\mu\sigma) + (D+\sigma)^2 + i\lambda^\dagger\gamma^\mu\nabla_\mu\lambda + i[\lambda^\dagger, \sigma]\lambda - \frac{1}{2}\lambda^\dagger\lambda. \tag{5.28}$$

That concludes the calculation of the localising term, otherwise in the context of SUSY QFT referred to as the localising action, however we have still not determined the localisation/BPS locus/field configurations. For this we have to see the condition we imposed to minimise the localising action, which was to set $\delta\lambda = 0$. Hence the constraint is:

$$\left(-\frac{1}{2}\gamma^{\mu\nu}F_{\mu\nu} - D + i\gamma^{\mu}D_{\mu}\sigma - \sigma\right) = 0. \tag{5.29}$$

From this equation we can draw two conclusions:

$$\frac{1}{2}\epsilon_{\mu\nu\rho}F^{\nu\rho} = D_{\mu}\sigma, \tag{5.30}$$

$$D = -\sigma. \tag{5.31}$$

The solution to the first line on S^3 is given by setting $F_{\mu\nu} = 0$ (i.e. A_μ is pure gauge), and $\sigma = \sigma_0$ being a constant [22]. Then the second equation just implies that $D = -\sigma_0$. Thus we have our localisation locus, which is the space of constant σ configurations, and all other fields vanishing. One can check that this truly minimises δV, since if we substitute the values derived above into equation (5.28) we get that $\delta V = 0$. This means that we are consistent.

Let us now turn our gaze to the whole path integral. In the saddle point approximation our integral becomes:

$$\mathcal{Z} = \int d\sigma_0 e^{S_{Cl}[\sigma_0]}\mathcal{Z}^g_{1-\text{loop}}[\sigma_0]. \tag{5.32}$$

The first bit of the integrand is our usual classical piece which we got just by taking the classical action on the localisation locus following the localisation procedure. The second term is the piece we did not derive in detail, which results from the transverse oscillations from the locus over which we average and do the path integral to one loop. It is referred to as the 1-loop determinant piece. The expression given above is exact. This is due to the fact that $1/t$ behaves as an auxiliary $\hbar$, but since we are taking the limit $t \to \infty$, it is truly negligible and hence the only leading order term that contributes is the one-loop calculation [125].

The classical piece can be found quite easily through substitution.

$$\begin{aligned} S_{Cl}[\sigma_0] &= 2i\int_{S^3} d^3x\sqrt{g}(D\sigma) \\ &= -2i\int_{S^3} d^3x(\sigma_0^2) \\ &= -4i\pi^2(\sigma_0^2). \end{aligned} \tag{5.33}$$

Where in the last line we have done the volume integral over the 3-sphere.

5.3.3 Gauge Fixing

We include a small interjecting section to explain that the gauge theory that we are localising still has to be gauge fixed. Gauge theory path integrals are ill defined since they are integrating over field configurations which correspond to the same physics, hence vastly overcounting the result of the path integral. To remedy this issue one can use the prescription introduced by Faddeev and Popov. We shall introduce the ghost and antighost fields, respectively $c, \bar{c}$ and the Nakanishi-Lautrup field b. After introducing the gauge fixing terms into the Lagrangian we would like to have the standard BRST transformations (labelled δ_B) which define a new nilpotent fermionic symmetry. Using this symmetry, we combine the SUSY and BRST transformations to give:

$$\delta' = \delta + \delta_B. \tag{5.34}$$

We can then localise with respect to the new shifted charge δ' (since it is also nilpotent), but this requires us to also shift V to V':

$$V' =' \left((\delta\lambda^\dagger)\lambda\right) + \bar{c}\ \nabla^\mu A_\mu. \tag{5.35}$$

Let us look at the variations of this new V with respect to δ'. For the first term the BRST charge does nothing since it is already gauge invariant hence we just get back δV. For the second term the BRST variation gives the usual gauge fixing action: $\bar{c}\ \partial^\mu D_\mu c + b\nabla^\mu A_\mu$. What do we do with the SUSY variation of the second term? The answer is that we are allowed to set $\delta\bar{c} = 0$ and then absorb the rest in the definition of c.

Now that we have tackled the gauge fixing, we can truly move on to performing the path integral.

5.3.4 Performing the 1-loop Determinant

We have set up everything that we require to calculate the path integral exactly, the last thing we require is to calculate the 1-loop determinant of the localising action:

$$\begin{aligned} S = t\int_{S^3} d^3x\sqrt{g}' \Big(&\frac{1}{2}F_{\mu\nu}F^{\mu\nu} + (D_\mu\sigma)(D^\mu\sigma) + (D+\sigma)^2 + i\lambda^\dagger\gamma^\mu\nabla_\mu\lambda + i[\lambda^\dagger,\sigma]\lambda \\ &-\frac{1}{2}\lambda^\dagger\lambda + \partial^\mu\bar{c}D_\mu c + b\nabla^\mu A_\mu\Big). \end{aligned} \tag{5.36}$$

We have changed this up a bit compared to equation (5.28) since we have added the gauge fixing ghost terms. Let us remember that we are taking the limit of $t \to \infty$ so we will redefine the fields to remove it in the integral.

$$\sigma = \sigma_0 + \frac{1}{\sqrt{t}}\sigma',$$
$$D = -\sigma_0 + \frac{1}{\sqrt{t}}D', \tag{5.37}$$
$$\varphi \to \frac{1}{\sqrt{t}}\varphi. \tag{5.38}$$

Where for σ and D we have separated out the zero modes (i.e. the dashed variables do not have zero modes). φ just corresponds to all the other fields. In this scaling of the fields, we can throw away anything which is higher than quadratic in the fields (not zero modes). The action then becomes,

$$S = \int_{S^3} d^3x\sqrt{g'}\left(\frac{1}{2}f_{\mu\nu}f^{\mu\nu} - [A_\mu, \sigma_0]^2 + (\partial_\mu\sigma')(\partial^\mu\sigma') + (D' + \sigma')^2 + i\lambda^\dagger\gamma^\mu\nabla_\mu\lambda\lambda \right.$$
$$\left. + i[\lambda^\dagger, \sigma_0] - \frac{1}{2}\lambda^\dagger\lambda + \partial^\mu\bar{c}\,\partial_\mu c + b\nabla^\mu A_\mu\right). \tag{5.39}$$

We defined $f_{\mu\nu}$ to be the abelian field strength $f_{\mu\nu} = \partial_\mu A_\nu - \partial_\nu A_\mu$. The next step would be to perform the integrals over D' and b. D' is just a Gaussian integral, while b imposes the Lorenz gauge

$$S = \int_{S^3} d^3x\sqrt{g'}\left(-A^\mu\Delta A_\mu - [A_\mu, \sigma_0]^2 + (\partial_\mu\sigma')(\partial^\mu\sigma') + i\lambda^\dagger\gamma^\mu\nabla_\mu\lambda + i[\lambda^\dagger, \sigma_0]\lambda \right.$$
$$\left. - \frac{1}{2}\lambda^\dagger\lambda + \partial^\mu\bar{c}\,\partial_\mu c\right) \tag{5.40}$$

Where we used integration by parts (no boundary terms since S^3 has no boundary). The Laplacian is the standard spherical Laplacian. Let us now separate the vector field into divergenceless and pure divergence components,

$$A_\mu = \partial_\mu\phi + B_\mu. \tag{5.41}$$

B is the divergenceless part since $\nabla_\mu B^\mu = 0$. Using this trick, we can rewrite the Lorenz gauge constraint delta function we obtained by integrating out b, $\delta(\nabla^\mu A_\mu)$ as $\delta(-\Delta\phi)$. Including the contribution coming from the Jacobian of the path integral, we get a factor of $\det(-\Delta)^{-\frac{1}{2}}$. As it turns out, performing the integral over the scalar σ' also results in the same factor. Lucky for us, the ghosts come to the rescue and cancel both of these factors since the result of their Berezin integral will be $\det(-\Delta)$. We are

left with this effective action:

$$S = \int_{S^3} d^3x\sqrt{g}' \left(-B^\mu \Delta B_\mu - [B_\mu, \sigma_0]^2 + i\lambda^\dagger \gamma^\mu \nabla_\mu \lambda + i[\lambda^\dagger, \sigma_0]\lambda - \frac{1}{2}\lambda^\dagger \lambda \right). \quad (5.42)$$

At this stage, we can choose to simplify the path integral further by replacing the integral over the constant matrices of σ_0 in the Lie algebra $\mathfrak{g}$, with some chosen CSA (Cartan subalgebra) [129]. This can be done since the integral is completely gauge invariant. One can then use the Weyl integration formula to rewrite the path integral in the form:

$$\mathcal{Z} = \frac{1}{|\mathcal{W}|} \int da \left(\prod_{\alpha \in \text{roots}} \alpha(a) \right) e^{-4i\pi^2(a^2)} \mathcal{Z}^g_{1-\text{loop}}[a]. \quad (5.43)$$

Where the product runs over the roots of $\mathfrak{g}$ and a are the elements of the CSA. Clearly now we only care about σ_0's which are in the CSA. We shall do a similar anlysis for the gauge field. Let us break up B using the vector space formed by the root spaces (step operators)

$$B_\mu = \sum_\alpha B_\mu{}^\alpha X_\alpha + h_\mu. \quad (5.44)$$

X_α are the step operators normalised such that $tr'(X_\alpha X_\beta) = \delta_{\alpha+\beta}$, and they are labelled by different roots. h_μ is along the direction of the CSA,

$$[\sigma_0, B_\mu] = \sum_\alpha \alpha(\sigma_0) B_\mu{}^\alpha X_\alpha. \quad (5.45)$$

The h_μ term does not appear since CSA elements commute by definition. We can do the exact same thing for the λ's commutation relation. Knowing all of these relations, we substitute them back into the action to get:

$$S = \int_{S^3} d^3x\sqrt{g} \sum_\alpha \left(B^\mu_{-\alpha}(-\Delta + \alpha^2(\sigma_0)) B_{\mu,\alpha} + \lambda^\dagger (i\gamma^\mu \nabla_\mu + i\alpha(\sigma_0) - \frac{1}{2})\lambda \right). \quad (5.46)$$

An important note here is that we chose to leave out the terms proportional to h_μ. The reason for this is that they can all be factorised out and will contribute a term which is not dependent on σ_0, a prefactor for the integral. These prefactors never contribute to expectation values, and hence can be dropped. The integral with the above action can be calculated using the eigenvalues of the Laplacian acting on divergenceless vector fields [130], which are known and can be stated from literature:

$$\det(\text{bosonic}) = \prod_\alpha \prod_{l=1}^{\infty} ((l+1)^2 + \alpha(\sigma_0)^2)^{2l(l+2)}. \quad (5.47)$$

The same can be done for the fermionic determinant:

$$\det(\text{fermionic}) = \prod_{\alpha}\prod_{l=1}^{\infty}((l+i\alpha(\sigma_0))(-l-1+i\alpha(\sigma_0)))^{l(l+1)}\,. \tag{5.48}$$

Therefore if we put together the determinants as they should be:

$$\begin{aligned}\mathcal{Z}^g_{1-\text{loop}} &= \frac{\det(\text{fermionic})}{(\det(\text{bosonic}))^{-\frac{1}{2}}} \\ &= \prod_{\alpha}\prod_{l=1}^{\infty}\frac{(l+i\alpha(\sigma_0))^{l(l+1)}(-l-1+i\alpha(\sigma_0))^{l(l+1)}}{((l+1)^2+\alpha(\sigma_0)^2)^{l(l+2)}} \\ &= \prod_{\alpha}\prod_{l=1}^{\infty}\frac{(l+i\alpha(\sigma_0))^{l+1}}{(l+1-i\alpha(\sigma_0))^{l}} \\ &= \prod_{\alpha}\prod_{l=1}^{\infty}\frac{(l+i\alpha(\sigma_0))^{l+1}}{(l-i\alpha(\sigma_0))^{l-1}}.\end{aligned} \tag{5.49}$$

Because the eigenvalues of the Cartan matrices in the adjoint representation come in positive negative pairs (eigenvalues are the roots) and since we are performing a product over all the roots, it does not matter if we take $\sigma_0 \to -\sigma_0$. Hence:

$$\begin{aligned}\mathcal{Z}^g_{1-\text{loop}}[\sigma_0]\mathcal{Z}^g_{1-\text{loop}}[-\sigma_0] &= \prod_{\alpha}\prod_{l=1}^{\infty}\frac{(l^2+\alpha^2(\sigma_0))^{l+1}}{(l^2+\alpha^2(\sigma_0))^{l-1}} \\ &= \prod_{\alpha}\prod_{l=1}^{\infty}(l^2+\alpha^2(\sigma_0))^2 \\ &= \left(\prod_{l=1}^{\infty}l^4\right)\prod_{\alpha}\prod_{l=1}^{\infty}\left(1+\frac{\alpha(\sigma_0)^2}{l^2}\right)^2.\end{aligned} \tag{5.50}$$

The infinite constant term multiplying the expression can be renormalised away so we will not pay much attention to it. The rest of the product is actually a representation of the hyperbolic sine function

$$\mathcal{Z}^g_{1-\text{loop}}[\sigma_0]\mathcal{Z}^g_{1-\text{loop}}[-\sigma_0] = \mathcal{Z}^g_{1-\text{loop}}[\sigma_0]^2 = \prod_{\alpha}\left(\frac{2\sinh(\pi\alpha(\sigma_0))}{\pi\alpha(\sigma_0)}\right). \tag{5.51}$$

Hence,

$$\mathcal{Z}^g_{1-\text{loop}}[\sigma_0] = \prod_{\alpha}\left(\frac{2\sinh(\pi\alpha(\sigma_0))}{\pi\alpha(\sigma_0)}\right). \tag{5.52}$$

After this, we can simply substitute this result back into the path integral and get the exact result after some cancellations:

$$\mathcal{Z} = \int da\ e^{-4\pi^2 i(a^2)} \prod_{\alpha} (2\sinh(\pi\alpha(\sigma_0))\,. \tag{5.53}$$

5.4 2-equivalent-charge, 3-equivalent-rotation Black Holes in AdS$_7$

We begin with the study of supersymmetric black hole solutions of 7D gauged supergravity (SUGRA). We will follow the AdS$_5$ analysis [21] very closely throughout and discuss two distinct limits, that of supersymmetry and extremality. Generalising the arguments of [21] is conceptually straightforward and we do not encounter any surprises, although the details are more involved. This fact will force us to consider black hole metrics with 2-equivalent charges and 3-equivalent rotations.

5.4.1 Non-extremal AdS$_7$ Black Holes

The low energy limit of M-theory, 11D SUGRA, admits solutions where the geometry is of the form $\mathcal{M}_7 \times S^4$ with the manifold $\mathcal{M}_7$ being asymptotically AdS$_7$. There is a consistent truncation of 11D SUGRA on S^4 such that $\mathcal{M}_7$ is a solution to $\mathcal{N}=4$ $SO(5)$ gauged SUGRA in seven dimensions [131]. Amongst the possible solutions there is an expectation of finding seven-dimensional black holes with two independent parameters (δ_1, δ_2) for the charges of the U$(1)^2$ Cartan subgroup of $SO(5)$ and three independent parameters (a_1, a_2, a_3) for the rotations supported by the $SO(2)^3$ in the maximal compact subgroup of $SO(2,6)$.

For practical purposes charged solutions are sought within a $U(1)^2$ truncation of the maximal $SO(5)$ theory. The bosonic field content of this truncation consists of the metric, two 1-form gauge potentials $A^1_{(1)}, A^2_{(1)}$, one 3-form $A_{(3)}$ which may be traded for a 2-form by utilising an odd-dimensional self-duality relation and two scalars X_1, X_2. The most general black hole solution with generic charges and rotations has not yet been found but solutions with two charges and three equivalent rotations [132] or two equivalent charges and three rotations [133] are known.

5.4.2 2-equivalent-charge, 3-equivalent-rotation Black Hole

For simplicity, we choose to focus on a subclass within the non-extremal AdS$_7$ black holes where all the charges are set to be equal to each other, $\delta_1 = \delta_2 = \delta$, as are all the rotational parameters, $a_1 = a_2 = a_3 = a$. As a result, this family of non-extremal black holes depends on three parameters (m, δ, a). In this scenario the solutions of [132] and [133] must coincide. The solution, incorporating a correction to the original literature

[132], is

$$\begin{aligned}
\mathrm{d}s_7^2 &= H^{\frac{2}{5}}\Big[-\frac{Y}{f_1\Xi_-^2}\mathrm{d}t^2+\frac{\Xi\rho^6}{Y}\mathrm{d}r^2+\frac{f_1}{H^2\Xi^2\rho^4}\Big(\sigma-\frac{2f_2}{f_1}\mathrm{d}t\Big)^2+\frac{\rho^2}{\Xi}\mathrm{d}s^2_{\mathbb{CP}^2}\Big]\,, && (5.54)\\
A^1_{(1)} &= A^2_{(1)} = \frac{2msc}{\rho^4\Xi H}\big(\Xi_-\mathrm{d}t-a\sigma\big)+\frac{\alpha}{\Xi_-}\mathrm{d}t\,, && (5.55)\\
A_{(3)} &= \frac{2mas^2}{\rho^2\Xi\Xi_-}\sigma\wedge(2\mathrm{d}\sigma)\,, && (5.56)\\
X_1 &= X_2 = H^{-1/5}\,. && (5.57)
\end{aligned}$$

As in [21], we have added a pure gauge term, $\Xi_-^{-1}\alpha\mathrm{d}t$, to each of the $U(1)$ gauge fields. The quantities f_1, f_2, H, Y appearing above are all functions of the radial coordinate r through the definition $\rho^2=\Xi r^2$. They are given by

$$\begin{aligned}
H &= 1+\frac{2ms^2}{\rho^4}\,, && (5.58)\\
f_1 &= \Xi\rho^6H^2-\frac{(2\Xi_+mas^2)^2}{\rho^4}+2ma^2\big[\Xi_+^2+c^2(1-\Xi_+^2)\big]\,, && (5.59)\\
f_2 &= -\frac{g\Xi_+\rho^6H^2}{2}+mac^2\,, && (5.60)\\
Y &= g^2\rho^8H^2+\Xi\rho^6-2m\rho^2\big[a^2g^2c^2+\Xi\big]+2ma^2\big[\Xi_+^2+c^2(1-\Xi_+^2)\big]\,, && (5.61)
\end{aligned}$$

with g the gauge coupling parameter and

$$\Xi_\pm = 1\pm ag\,,\qquad \Xi = 1-a^2g^2 = \Xi_-\Xi_+\,,\qquad s = \sinh\delta\,,\qquad c = \cosh\delta\,. \tag{5.62}$$

The black hole outer horizon is located at the largest positive root of $Y(r)$ which we denote by r_+. The remaining data of the solution are given by

$$\sigma = \mathrm{d}\psi+\frac{1}{2}\sin^2\xi l_3\,,\quad \mathrm{d}s^2_{\mathbb{CP}^2} = \mathrm{d}\xi^2+\frac{1}{4}\sin^2\xi(l_1^2+l_2^2)+\frac{1}{4}\sin^2\xi\cos^2\xi l_3^2\,, \tag{5.63}$$

with (l_1,l_2,l_3) a choice of left-invariant 1-forms for $SU(2)$.

The solution given by (5.54)-(5.57), along with its associated Killing vector at the horizon allow for the computation of thermodynamical aspects of the black hole such as its temperature. This is done with respect to the non-rotating Killing vector

$$\ell = \frac{\partial}{\partial t}-g\Omega\frac{\partial}{\partial\psi}\,, \tag{5.64}$$

found by redefining $t\to\Xi_-t$, $\psi\to\psi-gt$. In these new coordinates the temperature,[19]

[19] We have incorporated the corrections to [134] as noted in [106] and [109].

entropy,[20] angular velocity and electrostatic potential are [134]

$$T = \frac{\partial_r Y}{4\pi g\rho^3\sqrt{\Xi f_1}}\,, \tag{5.65}$$

$$S = \frac{1}{G_N}\frac{1}{4}\frac{\pi^3\rho^2\sqrt{f_1}}{\Xi^3}\,, \tag{5.66}$$

$$\Omega = -\frac{1}{g}\left(g+\frac{2f_2\Xi_-}{f_1}\right)\,, \tag{5.67}$$

$$\Phi = \frac{4msc}{\rho^4\Xi H}\left(\Xi_- - a\frac{2f_2\Xi_-}{f_1}\right)\,, \tag{5.68}$$

and are all evaluated at the outer horizon $r=r_+$. G_N denotes the seven-dimensional Newton constant. The conserved charges, namely the energy, angular momentum and electric charge, are:

$$E = \frac{1}{G_N}\frac{1}{g}\frac{m\pi^2}{32\Xi^4}\left[12(ag+1)^2(ag(ag+2)-1)-4c^2\left(a^2g^2(3ag(ag+4)+11)-8\right)\right]\,, \tag{5.69}$$

$$J = -\frac{1}{G_N}\frac{ma\pi^2}{16\Xi^4}\left[4ag(ag+1)^2-4c^2\left(a^3g^3+2a^2g^2+ag-1\right)\right]\,, \tag{5.70}$$

$$Q = \frac{1}{G_N}\frac{1}{2g}\frac{msc\pi^2}{2\Xi^3}\,, \tag{5.71}$$

and are found by integrating the first law:

$$\mathrm{d}E = T\mathrm{d}S + 3\Omega\mathrm{d}J + 2\Phi\mathrm{d}Q\,. \tag{5.72}$$

We will also need the free energy, I, of the black hole solution. The so-called quantum statistical relation gives this as

$$I = \beta(E - TS - 3\Omega J - 2\Phi Q)\,, \tag{5.73}$$

where $\beta = T^{-1}$ and it has been evaluated in [135] to be

$$I = \frac{\beta\pi^2}{8\Xi^3}\Bigg[m - g^2r_+^6 - g^2ms^2(4r_+^2-a^2) - \frac{4g(ms^2)^2[gr_+^4+a^2g(1+ag)r_+^2+2gms^2-a^3(1+ag)^2]}{r_+^6+2ms^2r_+^2-2a^2(1+ag)}\Bigg]\,. \tag{5.74}$$

The free energy is expected to coincide with the on-shell supergravity action evaluated on the black hole solution.[21] The black hole entropy is given in terms of the Legen-

[20] Here we have corrected the expression given in [109].

[21] It would be interesting to derive this explicitly in supergravity without resorting to the quantum statistical relation.

dre transform of the on-shell action with respect to the chemical potentials β, Ω, Φ, conjugate to the charges E, J, Q respectively:

$$E = \frac{\partial I}{\partial \beta}, \qquad J = -\frac{1}{3\beta}\frac{\partial I}{\partial \Omega}, \qquad Q = -\frac{1}{2\beta}\frac{\partial I}{\partial \Phi}, \tag{5.75}$$

hence

$$S = -I + \beta E - 3\beta\Omega J - 2\beta\Phi Q\,. \tag{5.76}$$

5.4.3 Supersymmetry

The non-extremal black hole solution detailed in the previous section is supersymmetric whenever the charge and rotation parameter satisfy one of the following two relations

$$e^{2\delta} = 1 - \frac{2}{3ag}, \tag{5.77}$$

$$e^{2\delta} = 1 - \frac{2}{ag}\,. \tag{5.78}$$

However, when the second condition holds, it is not possible to deal with closed timelike curves (CTCs) [134] and the solution is pathological. On the other hand, naked CTCs can be avoided when (5.77) holds and for this reason it is this condition that we will use in the remainder of this chapter.

The supersymmetric values of the conserved charges are

$$E = \frac{1}{G_N}\frac{1}{g}\frac{m\pi^2}{8}\frac{243\; e^{-2\delta}\left(e^{2\delta}-1\right)^6\left(-21e^{4\delta}+18e^{6\delta}+7\right)}{\left(3e^{2\delta}-5\right)^4\left(3e^{2\delta}-1\right)^3}, \tag{5.79}$$

$$J = \frac{1}{G_N}\frac{m\pi^2}{8g}\frac{81\; e^{-2\delta}\left(e^{2\delta}-1\right)^6\left(18e^{2\delta}+9e^{4\delta}-23\right)}{\left(3e^{2\delta}-5\right)^4\left(3e^{2\delta}-1\right)^3}, \tag{5.80}$$

$$Q = \frac{1}{G_N}\frac{1}{2g}\frac{m\pi^2}{8}\frac{729\; e^{-2\delta}\left(e^{2\delta}-1\right)^7\left(e^{2\delta}+1\right)}{\left(3e^{2\delta}-5\right)^3\left(3e^{2\delta}-1\right)^3}, \tag{5.81}$$

and satisfy

$$E - 3J - 4Q = 0\,. \tag{5.82}$$

The remaining quantities, such as the temperature, can also be evaluated in the supersymmetric limit but the resulting expressions are not compact so we do not present them here. However, the temperature is non-vanishing and consequently, as we will see in the next section, this means the supersymmetric black hole is not necessarily extremal.

5.4.4 Extremality

The black hole is extremal if the outer horizon coincides with another horizon. Since $Y(r)$ is a quartic function of r^2 we expect there to be four distinct horizons in general. We denote the location of these horizons by $(r_+, r_0, \tilde{r}_0, r_-)$ where $r_+^2 \geq r_0^2 \geq \tilde{r}_0^2 \geq r_-^2$. We may write

$$(g^2\Xi^4)^{-1}Y(r) = (g^2\Xi^4)^{-1}(y_0 + y_1 r^2 + y_2 r^4 + y_3 r^6 + y_4 r^8) \tag{5.83}$$
$$\equiv (r^2 - r_+^2)(r^2 - r_0^2)(r^2 - \tilde{r}_0^2)(r^2 - r_-^2)\,, \tag{5.84}$$

so that the extremal limit, reached when $r_+^2 = r_0^2$, corresponds to a double root of $Y(r)$. Comparing coefficients determines

$$(g^2\Xi^4)^{-1}y_4 = 1\,, \tag{5.85}$$
$$(g^2\Xi^4)^{-1}y_3 = -r_+^2 - \tilde{r}_0^2 - r_-^2 - r_0^2\,, \tag{5.86}$$
$$(g^2\Xi^4)^{-1}y_2 = r_+^2\left(\tilde{r}_0^2 + r_-^2 + r_0^2\right) + r_0^2\tilde{r}_0^2 + r_-^2\tilde{r}_0^2 + r_-^2 r_0^2\,, \tag{5.87}$$
$$(g^2\Xi^4)^{-1}y_1 = r_+^2\left(-r_0^2\tilde{r}_0^2 - r_-^2\tilde{r}_0^2 - r_-^2 r_0^2\right) - r_-^2 r_0^2\tilde{r}_0^2\,, \tag{5.88}$$
$$(g^2\Xi^4)^{-1}y_0 = r_+^2 r_-^2 r_0^2\tilde{r}_0^2\,. \tag{5.89}$$

We now show that the double root $r_+^2 = r_0^2$ also corresponds to a zero-temperature solution. Recall that the temperature is given by

$$T = \left.\frac{\partial_r Y}{4\pi g\rho^3\sqrt{\Xi f_1}}\right|_{r=r_+}\,, \tag{5.90}$$

where

$$\partial_r Y|_{r=r_+} = \frac{1}{r_+}(8y_4 r_+^8 + 6y_3 r_+^6 + 4y_2 r_+^4 + 2y_1 r_+^2)\,. \tag{5.91}$$

Substituting for the y's leads to

$$T = \frac{g^2\Xi^4}{4\pi g r_+\rho^3\sqrt{\Xi f_1(r_+)}}\left[2r_+^2(r_+^2 - r_0^2)(r_+^2 - \tilde{r}_0^2)(r_+^2 - r_-^2)\right]\,, \tag{5.92}$$

so that the temperature vanishes when r_0 coincides with r_+, i.e. in the extremal limit. Note that we have not used the supersymmetry condition and hence the extremal black hole is not necessarily supersymmetric.

5.4.5 BPS Limit

As in [21] we will work with supersymmetric black holes and study their behaviour in the extremal limit. When that happens, we use the nomenclature "BPS" (denoting

both supersymmetric *and* extremal solutions) and we label the corresponding quantities with a $*$.

The absence of naked CTCs is a physically sensible requirement and places further constraints on the parameters (m,δ,a) describing the black hole, rendering the supersymmetric solution extremal. One way of ruling out CTCs requires that [134]

$$0 \;=H^{\frac{2}{5}}\left(-\frac{Y}{f_1}+\frac{f_1}{H^2\Xi^2\rho^4}\left(2g+\frac{2f_2\Xi_-}{f_1}\right)^2\right), \tag{5.93}$$

at $r=r_+$. This can be achieved if, in addition to the SUSY condition (5.77), the following relation holds

$$m \;=\; m_* \;=\frac{128e^{2\delta}(3e^{2\delta}-1)^3}{729g^4(e^{2\delta}+1)^2(e^{2\delta}-1)^6}\,. \tag{5.94}$$

When the parameter m takes this value the function Y has a double root as expected at $r_+^2=r_*^2=r_0^2$ given by

$$r_*^2 \;=\frac{16}{3g^2(3e^{2\delta}-5)(e^{2\delta}+1)} \;=\; \frac{4a^2}{(1+ag)(1-3ag)}\,. \tag{5.95}$$

We may invert this expression to write the charge in terms of the BPS radius:

$$e^{2\delta} \;=\; \frac{1}{3}\left(1\pm\frac{4\sqrt{g^2r_*^2(1+g^2r_*^2)}}{g^2r_*^2}\right). \tag{5.96}$$

Evaluating the thermodynamic quantities for these BPS values of m and r_+ gives

$$T^* \;=0\,, \tag{5.97}$$

$$S^* \;=\frac{1}{G_N}\frac{\pi^3}{g^5}\frac{32\sqrt{9e^{2\delta}-7}}{3\sqrt{3}\,(3e^{2\delta}-5)^3\,(e^{2\delta}+1)^{3/2}}\,, \tag{5.98}$$

$$\Omega^* \;=1\,, \tag{5.99}$$

$$\Phi^* \;=2\,, \tag{5.100}$$

$$E^* \;=\frac{1}{G_N}\frac{\pi^2}{g^5}\frac{16\left(18e^{6\delta}-21e^{4\delta}+7\right)}{3\,(3e^{2\delta}-5)^4\,(e^{2\delta}+1)^2}\,, \tag{5.101}$$

$$J^* \;=\frac{1}{G_N}\frac{\pi^2}{g^5}\frac{16\left(9e^{4\delta}+18e^{2\delta}-23\right)}{9\,(3e^{2\delta}-5)^4\,(e^{2\delta}+1)^2}\,, \tag{5.102}$$

$$Q^* \;=\frac{1}{G_N}\frac{\pi^2}{g^5}\frac{8\left(3e^{6\delta}-5e^{4\delta}-3e^{2\delta}+5\right)}{(3e^{2\delta}-5)^4\,(e^{2\delta}+1)^2}\,. \tag{5.103}$$

The supersymmetry relation (5.82) with these expressions can be simply written as

$$E^* - 3J^*\Omega^* - 2Q^*\Phi^* \;=\; 0\,. \tag{5.104}$$

5.4.6 Complexified Solution

We can extract information about the value of the parameter $m = m_+$ at the outer horizon—but away from the extremal limit—by examining $Y(r_+) = 0$. We see that $Y(r_+) = 0$ is equivalent to a quadratic equation for m_+:

$$\begin{aligned} 0 \;&= m_+^2(4g^2s^4) + m_+\Big[2\left(gs^2\left(2g\Xi^2 r_+^4 - a^3(ag+2)\right) - \Xi r_+^2\left(c^2a^2g^2+\Xi\right)+a^2\right)\Big] \\ &\quad + r_+^6(1+g^2r_+^2)\Xi^4\,. \end{aligned} \tag{5.105}$$

Inserting the SUSY condition (5.77), we solve to find

$$\begin{aligned} m_+ \;&= \frac{-2e^{2\delta}\left(3e^{2\delta}-1\right)}{81\left(e^{2\delta}-1\right)^6 g^4}\left(\left(3e^{2\delta}-5\right)g^2r_+^2\left(9e^{2\delta}\left(\left(e^{2\delta}-2\right)g^2r_+^2-2\right)+5g^2r_+^2-2\right)\right. \\ &\quad \left.+32\right) \pm \frac{2e^{2\delta}\left(3e^{2\delta}-1\right)\left(16-3\left(e^{2\delta}+1\right)\left(3e^{2\delta}-5\right)g^2r_+^2\right)}{81\left(e^{2\delta}-1\right)^6 g^2} \\ &\quad \times\sqrt{\left(9e^{2\delta}\left(e^{2\delta}-2\right)+5\right)g^2r_+^2-4}\,. \end{aligned} \tag{5.106}$$

As shown in App. A.1, the parameter m_+ is complex when $r_+ > r_*$ and becomes real (and equal to its BPS value m_*) only at $r_+ = r_*$. Consequently, the thermodynamic quantities in which m_+ appears are generically complex away from the BPS limit. Substituting for this complex m_+ and r_+ gives cumbersome expressions for the thermodynamic quantities, which however can be shown to satisfy the remarkable condition:

$$2\Phi - 3\Omega - 1 \;=\; \pm 2\pi i T\,. \tag{5.107}$$

Using this, one can show that the free energy (5.73) can be expressed very simply in terms of

$$I \;=\; -\frac{\pi^2}{128 g^5 G_N}\frac{\phi^4}{\omega^3}\,, \tag{5.108}$$

where

$$2\phi - 3\omega \;=\; \pm 2\pi i\,. \tag{5.109}$$

Here

$$\omega = \beta(\Omega - \Omega^*) \tag{5.110}$$
$$\phi = \beta(\Phi - \Phi^*)\,. \tag{5.111}$$

In terms of these redefined chemical potentials, the quantum statistical relation (5.73) becomes

$$I = -S - 3\omega J - 2\phi Q\,, \tag{5.112}$$

subject to the condition (5.109), where the energy has disappeared using the relation (5.82). One could formally re-instate it by writing

$$I = \beta(E - 3\Omega^* J - 2\Phi^* Q) - S - 3\omega J - 2\phi Q\,. \tag{5.113}$$

This form of the on-shell action will be useful shortly when establishing the background at the boundary of AdS$_7$.

The results (5.108) and (5.109) obtained here for the free energy reproduce those first written down in [106] following [105]. One sees from (5.112) that a Legendre transform with respect to the chemical potentials ω and ϕ will yield the Bekenstein-Hawking entropy for the AdS$_7$ black hole.

5.4.7 SCFT Background from Bulk Regularity

We will now shift our focus to recovering the form of the background at the conformal boundary located at $r=\infty$.

Metric: We begin by looking at the form of the black hole solution (5.54)-(5.57) in the limit $r\to\infty$. One obtains

$$\begin{aligned} \mathrm{d}s_7^2 &= -g^2r^2\mathrm{d}t^2 + r^2(\sigma + g\mathrm{d}t)^2 + \frac{1}{g^2r^2}\mathrm{d}r^2 + r^2\mathrm{d}s^2_{\mathbb{CP}^2} \\ &= \frac{1}{g^2r^2}\mathrm{d}r^2 + r^2\mathrm{d}s^2_{\text{bdry}}\,, \end{aligned} \tag{5.114}$$

with the boundary metric being

$$\begin{aligned} \mathrm{d}s^2_{\text{bdry}} &= -g^2\mathrm{d}t^2 + (\sigma + g\mathrm{d}t)^2 + \mathrm{d}s^2_{\mathbb{CP}^2} \\ &\to -\mathrm{d}t^2 + \sigma^2 + \mathrm{d}s^2_{\mathbb{CP}^2} \\ &= -\mathrm{d}t^2 + \mathrm{d}s^2_{S^5}\,. \end{aligned} \tag{5.115}$$

In the second line above we performed a scaling of the time coordinate $t\to t/g$ and also absorbed $g\mathrm{d}t$ into σ by sending the fibre coordinate $\psi\to\psi - g\mathrm{d}t$. The boundary metric is therefore just $\mathbb{R}\times S^5$ and does not depend on the chemical potentials defined

in the bulk. This dependence will instead be recovered by looking at the behaviour of the metric at the horizon.

In order to do so, we first analytically continue to Euclidean gravity by letting $t=-i\tau$. One then introduces into (5.54) the shifted radial coordinate $R^2=r-r_+$. At the horizon, the black hole metric takes the following form

$$\mathrm{d}s_7^2 \;=\; h_{RR}\left(\mathrm{d}R^2+R^2\left(\frac{2\pi}{\beta}\mathrm{d}\tau\right)^2\right)+(r_+^2+h_\sigma)\left(\sigma-\frac{2f_2}{f_1}i\mathrm{d}\tau\right)^2+r_+^2\mathrm{d}s^2_{\mathbb{CP}^2}\;, \tag{5.116}$$

where h_{RR} and h_σ are functions of the parameters of the original metric and of some angular coordinates on $\mathbb{CP}^2$, the explicit form of which is not important for the ensuing analysis. By employing similar rescaling transformations as on the boundary metric, $\tau\to\tau/g$ and $\psi\to\psi-i\tau$ and using the definition of Ω from (5.67) we can re-write

$$(r_+^2+h_\sigma)(\sigma+i\Omega\mathrm{d}\tau)^2+r_+^2\mathrm{d}s^2_{\mathbb{CP}^2} \;=\; 2ir_+^2\Omega\sigma\mathrm{d}\tau-r_+^2\Omega^2\mathrm{d}\tau^2+h_\sigma(\sigma+i\Omega\mathrm{d}\tau)^2+r_+^2\mathrm{d}s^2_{S^5}\;. \tag{5.117}$$

At this stage we perform the coordinate transformation detailed in App. A.2,[22] which brings the metric on S^5 as well as the 1-form σ to

$$\begin{aligned}\mathrm{d}s^2_{S^5} \;&=\; \mathrm{d}\theta_1^2+\sin^2\theta_1\mathrm{d}\theta_2^2+\sin^2\theta_1\sin^2\theta_2\mathrm{d}\phi_1^2+\sin^2\theta_1\cos^2\theta_2\mathrm{d}\phi_2^2+\cos^2\theta_1\mathrm{d}\phi_3^2\;,\\ \sigma \;&=\; \sin^2\theta_1\sin^2\theta_2\mathrm{d}\phi_1+\sin^2\theta_1\cos^2\theta_2\mathrm{d}\phi_2+\cos^2\theta_1\mathrm{d}\phi_3\;.\end{aligned} \tag{5.118}$$

Using this fact, we can recast the metric close to the horizon as

$$\begin{aligned}\mathrm{d}s^2 \;&=\; h_{RR}\left(\mathrm{d}R^2+R^2\left(\frac{2\pi}{\beta}\mathrm{d}\tau\right)^2\right)+h_{\theta_1\theta_1}\mathrm{d}\theta_1^2+h_{\theta_2\theta_2}\mathrm{d}\theta_2^2+h_{\phi_1\phi_1}(\mathrm{d}\phi_1+i\Omega\mathrm{d}\tau)^2\\ &\quad+h_{\phi_2\phi_2}(\mathrm{d}\phi_2+i\Omega\mathrm{d}\tau)^2+h_{\phi_3\phi_3}(\mathrm{d}\phi_3+i\Omega\mathrm{d}\tau)^2+h_{\phi_1\phi_2}(\mathrm{d}\phi_1+i\Omega\mathrm{d}\tau)(\mathrm{d}\phi_2+i\Omega\mathrm{d}\tau)\\ &\quad+h_{\phi_1\phi_3}(\mathrm{d}\phi_1+i\Omega\mathrm{d}\tau)(\mathrm{d}\phi_3+i\Omega\mathrm{d}\tau)+h_{\phi_2\phi_3}(\mathrm{d}\phi_2+i\Omega\mathrm{d}\tau)(\mathrm{d}\phi_3+i\Omega\mathrm{d}\tau)\;,\end{aligned} \tag{5.119}$$

where we once again emphasise that the explicit form of the functions h is not important for the remaining discussion.

The metric in Eq. (5.119) describes a warped fibration of S^5 (parametrised by the coordinates $(\theta_1,\theta_2,\phi_1,\phi_2,\phi_3)$) over $\mathbb{R}^2$ (parameterised by R and τ). To ensure the lack of conical singularities at the point $R=0$, one has to introduce the twisted identifications of certain coordinates.

$$(\tau\,,\phi_1\,,\phi_2\,,\phi_3)\;\sim\;(\tau+\beta\,,\phi_1-i\Omega\beta\,,\phi_2-i\Omega\beta\,,\phi_3-i\Omega\beta)\,, \tag{5.120}$$

[22] This coordinate transformation also brings the Killing vector (5.64) to the form $\ell=\partial/\partial t+\Omega\sum_{i=1}^3\partial/\partial\phi_i$.

as one completes a circle around the temporal direction. It is important to point out that the 1-form $i\Omega \mathrm{d}\tau$ is not well defined at $R=0$, but we can remove this dependence from the metric by introducing a "rotating" coordinate frame:

$$\tau \;=\; \hat{\tau}, \quad \phi_1 \;=\; \hat{\phi}_1 - i\Omega\hat{\tau}, \quad \phi_2 \;=\; \hat{\phi}_2 - i\Omega\hat{\tau}, \quad \phi_3 \;=\; \hat{\phi}_3 - i\Omega\hat{\tau}\,. \tag{5.121}$$

We have thus "untwisted" the identifications to recover more canonical ones as we go around the Euclidean time circle

$$(\hat{\tau}\,,\hat{\phi}_1\,,\hat{\phi}_2\,,\hat{\phi}_3) \;\sim\; (\hat{\tau}+\beta\,,\hat{\phi}_1\,,\hat{\phi}_2\,,\hat{\phi}_3)\,. \tag{5.122}$$

We then take the coordinates (5.122) and substitute them into the boundary metric. This results in the following final form

$$\begin{aligned} \mathrm{d}s^2_{\mathrm{bdry}} \;&= \mathrm{d}\hat{\tau}^2 + \mathrm{d}\theta_1^2 + \sin^2\theta_1 \mathrm{d}\theta_2^2 + \sin^2\theta_1 \sin^2\theta_2 (\mathrm{d}\hat{\phi}_1 - i\Omega \mathrm{d}\hat{\tau})^2 \\ &\quad + \sin^2\theta_1 \cos^2\theta_2 (\mathrm{d}\hat{\phi}_2 - i\Omega \mathrm{d}\hat{\tau})^2 + \cos^2\theta_1 (\mathrm{d}\hat{\phi}_3 - i\Omega \mathrm{d}\hat{\tau})^2\,. \end{aligned} \tag{5.123}$$

1-form gauge fields: Next, we will address the remaining fields in the supergravity multiplet, switching momentarily back to Lorentzian signature. The only fields which are non-trivial at the conformal boundary are the 1-form gauge fields which become

$$A|_{\mathrm{bdry}} \;=\; \alpha \mathrm{d}t\,, \tag{5.124}$$

that is, they can only have a pure-gauge dependence. These terms cannot be fixed just by requiring regularity of the bulk metric at the horizon. However, they can be restricted by looking at the action of the Lie derivative with respect to the Killing vector (5.64) on the Killing spinors [21].

The solutions to the Killing spinor equations for the backgrounds [132, 133], or even the special case that we are considering with 2-equal charges and 3-equal rotations are not known. However, the Killing spinors for the background with 2 independent charges and vanishing rotations were given in [136]. For equal charges, this is a subcase of the configuration we are considering with $\Omega = 0$. Fortunately, it is also precisely what we need to fix the asymptotic form of the 1-form gauge fields at the boundary.

When the two charges are set to the same value, the Killing spinor given in [136] is schematically of the form

$$\epsilon \;=\; e^{\frac{1}{4}g(1+2\alpha)t\Gamma^{12}}(\dots)\mathcal{P}\epsilon_0\,, \tag{5.125}$$

where the ellipsis represents the angular and radial terms which commute with Γ^{12}, the $\mathcal{P}$ is a projection operator which also commutes with Γ^{12} and ϵ_0 is a constant spinor.[23]

[23] We note that our normalisations are slightly different when compared to [136], $g_{\mathrm{LM}} = 4g$, $\Gamma^{12}_{\mathrm{LM}} =$

The rank 2 $SO(5)$ Gamma matrix Γ^{12} is such that the Killing spinors have the following eigenvalues, $\frac{i}{2}\Gamma^{12}\epsilon = \pm\epsilon$.

With this information at hand, we proceed with the evaluation of the Lie derivative. For vanishing rotations the Killing vector (5.64) simplifies to $\ell = \frac{\partial}{\partial t}$ and hence we simply need to evaluate $\mathcal{L}_{\frac{\partial}{\partial t}}\epsilon$. Explicit calculation shows that the Lie derivative simplifies dramatically

$$\mathcal{L}_{\frac{\partial}{\partial t}}\epsilon \;=\; \frac{\partial\epsilon}{\partial t} \;=\; \mp\frac{i}{2}(1+2\alpha)g\epsilon\,. \tag{5.126}$$

Keeping in mind that the electrostatic potential is defined as

$$\Phi \;=\; \imath_\ell A|_{r_+} - \imath_\ell A|_{\text{bdry}} = \imath_\ell A|_{r_+} - \alpha\,, \tag{5.127}$$

with $\imath$ the interior product, one can define the gauge parameter as

$$\alpha \;\equiv\; \imath_\ell A|_{r_+} - \Phi\,. \tag{5.128}$$

By also using (5.107), Eq. (5.126) can finally be written as

$$\mathcal{L}_{\partial/\partial t}\epsilon \;=\; \mp\left(-\frac{\pi}{\beta} + i\imath_\ell A|_{r_+}\right) g\epsilon\,. \tag{5.129}$$

Analytically continuing to the Euclidean-signature solution, and using the coordinates (5.122), the circumference of the time circle is β. Transporting the Killing spinor around the time circle generated by ℓ can be done through the exponentiation of the action of the Lie derivative

$$e^{i\beta\mathcal{L}_{i\partial/\partial\hat{\tau}}\epsilon} \;=\; -e^{\pm\beta\imath_\ell A|_{r_+}g}\epsilon\,. \tag{5.130}$$

In order to keep the gauge field well defined, the component in the direction which shrinks as we go to the black hole horizon has to vanish, which sets $A|_{r_+}=0$, while in order to satisfy (5.130) the Killing spinor has to be *anti-periodic* when transported all the way along the time circle. This discussion also fixes the pure gauge parameter once and for all to be

$$\alpha \;=\; -\Phi\,, \tag{5.131}$$

and leads to the pure-imaginary gauge field at the boundary

$$A|_{\text{bdry}} \;=\; i\Phi\mathrm{d}\hat{\tau}\,. \tag{5.132}$$

$\frac{1}{2}\Gamma^{12}$. We have also added a pure-gauge term in the 1-form gauge fields.

Note that although we carried out this analysis for the charged AdS$_7$ black hole solution with no rotations, the results should extend straightforwardly when one turns the rotations back on, as in [21].[24] We will henceforth go back to considering the case with 3-equivalent rotations.

Energy: Translations with respect to the new Euclidean time coordinate $\hat{\tau}$ will have a corresponding charge $\hat{E}$, given by

$$\hat{E} \;=\; E - 3\Omega J \;. \tag{5.133}$$

Utilising this in the quantum-statistical relation (5.113), when formally also including the gauge field for which $A|_{r_+}=0$, leads to

$$I \;=\; \beta\left(\hat{E} + 3(\Omega-\Omega^*)J + 2(A|_{r_+}-\Phi^*)Q\right) - S - 3\omega J - 2\phi Q \;, \tag{5.134}$$

where the term multiplying β is zero via (5.82). However, at the boundary this combination can be interpreted as a supersymmetric Hamiltonian, which can be further simplified to

$$\begin{aligned}\{\mathcal{Q},\mathcal{Q}^\dagger\} \;&=\; \hat{E} + 3(\Omega-\Omega^*)J + 2(A|_{\rm bdry}-\Phi^*)Q \\ &=\; \hat{E} + \frac{1}{\beta}(3\omega J + 2\varphi Q) \;,\end{aligned} \tag{5.135}$$

using (5.132) and the redefined chemical potentials (5.110).

Summary: To summarise, we have derived the following information about the supersymmetric, black hole solution at the boundary of AdS$_7$:

- ◇ It will involve the following metric

$$\begin{aligned}{\rm d}s^2_{\rm bdry} \;&=\; {\rm d}\hat{\tau}^2 + {\rm d}\theta_1^2 + \sin^2\theta_1 {\rm d}\theta_2^2 + \sin^2\theta_1\sin^2\theta_2({\rm d}\hat{\phi}_1 - i\Omega{\rm d}\hat{\tau})^2 \\ &\quad + \sin^2\theta_1\cos^2\theta_2({\rm d}\hat{\phi}_2 - i\Omega{\rm d}\hat{\tau})^2 + \cos^2\theta_1({\rm d}\hat{\phi}_3 - i\Omega{\rm d}\hat{\tau})^2 \;,\end{aligned} \tag{5.136}$$

  which is a nontrivial fibration of S^1_β over S^5.

- ◇ There will be a background gauge field

$$A|_{\rm bdry} \;=\; i\Phi{\rm d}\hat{\tau} \;. \tag{5.137}$$

- ◇ The Killing spinor will satisfy anti-periodic boundary conditions on S^1_β.

[24] For example, rotation is supported by the non-trivial 3-form potential in (5.56) which does not have a component along the time direction and its presence only affects the $(\dots)$ part of the Killing spinor solution (5.125) with the relation (5.126) being unchanged.

◇ At the boundary, the charge associated with translations $\partial/\partial\hat{\tau}$ is given by

$$\beta\hat{E} \;=\; \beta\{\mathcal{Q},\mathcal{Q}^\dagger\} - 3\omega J - 2\varphi Q \;. \tag{5.138}$$

◇ The chemical potentials obey the constraint

$$2\phi - 3\omega \;=\; \pm 2\pi i \;. \tag{5.139}$$

5.5 (2,0) Partition Function on the Boundary

We now shift our attention to the dual field theory. An extremisation principle that reproduces the bulk AdS$_7$ black hole entropy was first proposed in [106], based on an insightful modification of the Casimir-energy result of [121]. Here, we use the bulk calculation of the preceding section to provide a microscopic derivation of [106], in line with expectations from the approach of [21].

5.5.1 Expectations from AdS/CFT

The AdS/CFT correspondence dictates that at large N the on-shell action for the supersymmetric AdS$_7$ black hole solution (5.108) should match the generator of connected correlators in the boundary theory, that is $I = -\log\mathcal{Z}$ [137]. Because of the anti-periodic boundary conditions on the Killing spinors, and assuming usual periodic boundary conditions for the bosons, all fermions will be anti-periodic. Let us encode this information by allowing for general $e^{\pi i n_0}$ periodicity the fermions in the boundary theory with the understanding that we need to set $n_0 = \pm 1$ when comparing with gravity. The partition function is then to be understood as

$$\mathcal{Z} \;\sim\; \mathrm{Tr}_{\mathcal{H}} e^{-\beta\hat{E}} \tag{5.140}$$

since $\hat{E}$ corresponds to translations in the time variable $\hat{\tau}$ and where the trace is over the physical Hilbert space of the flat-space A_{N-1} (2,0) theory in radial quantisation. Through (5.138) it is clear that this is a special case of the index-like quantity

$$\mathbb{I}(\omega_1,\omega_2,\omega_3,\phi_1,\phi_2;n_0) \;=\; \mathrm{Tr}_{\mathcal{H}}(-1)^{F(1+n_0)} e^{-\beta\{\mathcal{Q},\mathcal{Q}^\dagger\}+\beta\sum_{i=1}^3\omega_i J_i+\beta\sum_{j=1}^2\phi_j Q_j} \;, \tag{5.141}$$

where the chemical potentials are subject to the condition

$$\sum_{i=1}^3 \omega_i - \sum_{j=1}^2 \phi_j = \frac{2\pi i n_0}{\beta} \;, \qquad n_0 \in \mathbb{Z} \;. \tag{5.142}$$

In the above, $\mathcal{Q}$ denotes any one of the Poincaré supercharges preserved by the 6D theory, while the $\{\Delta, \omega_i\}$, $\{\phi_j\}$ are Cartan generators (dilatations, orthogonal rotations and R-charges respectively) for the maximal bosonic subalgebra of the 6D superconformal algebra $\mathfrak{so}(2,6) \oplus \mathfrak{sp}(2) \subset \mathfrak{osp}(8^*|4)$. For concreteness, since we will be using the conventions of [121], our chosen supercharge will have charges $Q_1 = Q_2 = \frac{1}{2}$ and $J_1 = J_2 = J_3 = -\frac{1}{2}$. The spin-statistics theorem allows us to express the fermion-number operator as $F = 2J_1$. Note that we have rescaled our chemical potentials as $\{\omega_i, \phi_j\} \to \beta\{\omega_i, \phi_j\}$.

On the one hand, for $n_0 = 0$, the above expression reproduces precisely the definition of the most general 6D superconformal index of [97], as presented in [121]. On the other hand, the case which is of interest to us—as dictated from the gravity calculation—is the one with $\omega_i = \omega$, $J_i = J$, $\phi_j = \phi$, $Q_j = Q$ and $n_0 = \pm 1$. Keeping that in mind, it will be possible to keep all parameters and charges generic for the duration of the following discussion and fix them only at the very end.

Before proceeding further, let us massage Eq. (5.141) by defining a new parameter m through the relations[25]

$$\phi_1 \equiv \frac{1}{2}\sum_{i=1}^{3}\omega_i - m - \frac{\pi i n_0}{\beta}\,, \qquad \phi_2 \equiv \frac{1}{2}\sum_{i=1}^{3}\omega_i + m - \frac{\pi i n_0}{\beta}\,. \tag{5.143}$$

The quantity $\mathbb{I}$ can be rewritten as

$$\begin{aligned}\mathbb{I}(\omega_1,\omega_2,\omega_3,m;n_0) = \mathrm{Tr}_{\mathcal{H}}(-1)^{F(1+n_0)} e^{-\beta\{\mathcal{Q},\mathcal{Q}^\dagger\}+\beta\sum_{i=1}^{3}\omega_i(J_i+\frac{Q_1+Q_2}{2})} \\ \times\, e^{\beta m\frac{Q_2-Q_1}{2}-2\pi i n_0\frac{Q_1+Q_2}{2}}\,.\end{aligned} \tag{5.144}$$

Making use of $2J_1 = F$ leads to

$$\begin{aligned}\mathbb{I}(\omega_1,\omega_2,\omega_3,m;n_0) = \mathrm{Tr}_{\mathcal{H}}(-1)^{F} e^{-\beta\{\mathcal{Q},\mathcal{Q}^\dagger\}+\beta(\omega_1-\frac{2\pi i n_0}{\beta})(J_1+\frac{Q_1+Q_2}{2})} \\ \times\, e^{\beta\sum_{i=2}^{3}\omega_i(J_i+\frac{Q_1+Q_2}{2})+\beta m\frac{Q_2-Q_1}{2}}\,.\end{aligned} \tag{5.145}$$

At this stage one can redefine[26]

$$\tilde{\omega}_1 \equiv \omega_1 - \frac{2\pi i n_0}{\beta}\,, \qquad \tilde{\omega}_2 = \omega_2\,, \qquad \tilde{\omega}_3 = \omega_3\,. \tag{5.146}$$

and write

$$\mathbb{I}(\omega_1,\omega_2,\omega_3,m;n_0) = \mathbb{I}(\tilde{\omega}_1,\tilde{\omega}_2,\tilde{\omega}_3,m;0)\,. \tag{5.147}$$

[25] This paramater m should not be confused with the parameter of the same name appearing in Sec. 5.4. We hope that the repeated use of this symbol will not cause confusion.

[26] By a different assignment of the fermion-number operator, the shifts can also be accommodated in the other chemical potentials.

Therefore, the quantity $\mathbb{I}$ can be thought of as a bona fide superconformal index when associated with the tilded chemical potentials, i.e. it is independent of β. It also has an N-scaling of $O(1)$ as $N \to \infty$; see [21] and also the nice discussion in [108].

Note that when expressed as a supersymmetric path integral, the partition function is expected to factorise into an expression of the form:[27]

$$\mathcal{Z}_{S^5 \times S^1_\beta} \;=\; e^{-\beta \mathcal{F}} \mathbb{I}\,, \tag{5.148}$$

where $\mathcal{F}$ is referred to as the "generalised supersymmetric Casimir energy".[28] Connecting to the gravitational result for the on-shell action requires that $\mathcal{F}$ has a large-N scaling of $O(N^3)$. The evaluation of the RHS for the above equation at large N will be our next goal.

Although analogous partition functions for superconformal theories in three and four dimensions can be directly computed using supersymmetric localisation, this is not the case for the interacting (2,0) theory, which lacks a Lagrangian description. However, for the case where $n_0 = 0$ heroic technical works [116, 117, 118, 101, 119, 120] produced a candidate 6D result from the S^5 partition function of $SU(N)$ 5D MSYM.

Here we will base our calculation on the results of this partition-function calculation at large N following [121]. The key observation is that the indices in (5.147) are expected to be reproduced by the above partition-function calculations in 5D when using the tilded chemical potentials. The answer turns out to be indeed of the form (5.148) where the quantity $\mathcal{F}$ gives back the exact value for the on-shell action predicted by AdS/CFT *including the overall coefficient*, when we take the Cardy-like limit $\omega_i \to 0$.

5.5.2 The S^5 Partition Function at Large N and a Cardy-like Limit

The parameters of the 5D partition function on the (squashed) S^5 can be straightforwardly inherited from the 6D background corresponding to the RHS of (5.147), via dimensionally reducing on S^1_β [138]. The ω_i are associated with the squashing parameters of the five sphere while m plays the role of a mass parameter. The relationship between the (2,0) theory and 5D MSYM also identifies the radius of the thermal circle with the 5D gauge coupling, $2\pi\beta = g^2_{\rm YM}$, with these quantities defined in units of the S^5 radius. The 6D physics is then expected to be recovered in the $\beta \to \infty$ limit, where the M-theory circle can no-longer be neglected.

As argued in [121],[29] to leading order in the large N limit the partition function on S^5 should not receive instanton contributions. This argument significantly simplifies the calculation, as the leading N result in supersymmetric localisation only receives classical

[27] This is indeed the case for cases where the exact supersymmetric path integral can be evaluated directly.

[28] When $n_0 = 0$ this reduces to the supersymmetric Casimir energy of [101].

[29] This argument relies on the results of [139].

contributions from the localising saddle point and one-loop determinant contributions from the $\mathcal{N}=1$ vector multiplet and single adjoint $\mathcal{N}=1$ hypermultiplet.

These one-loop determinants in 5D can be obtained following the procedure of [138]; see also [115, 119]. In that reference, the starting point was precisely (5.141) in 6D for $n_0=0$. The one-loop determinants for 6D $(1,0)$ vector and hypermultiplets were reduced on the thermal circle to produce the 5D $\mathcal{N}=1$ contributions in terms of triple-sine functions, $S_3(x)$. When used in the 5D MSYM calculation of [121], for one vector and one adjoint hypermultiplet, the result is

$$\mathcal{Z}^{n_0=0}_{1-\text{loop}} = \left(\frac{\lim_{x\to 0}S_3(x)/x}{S_3(\tilde{m})}\right)^{N-1}\prod_{i>j}^{N}\frac{S_3(\pm i\lambda_{ij}|\vec{\omega})}{S_3(\tilde{m}\pm i\lambda_{ij}|\vec{\omega})}\,, \tag{5.149}$$

where we are using standard shorthand notation with $S_3(\pm x|\vec{\omega}) = S_3(x|\vec{\omega})S_3(-x|\vec{\omega})$, the equivariant mass is defined as $\tilde{m} = m + \frac{1}{2}(\omega_1+\omega_2+\omega_3)$ and $\lambda_{ij} = \lambda_i - \lambda_j$ are Coulomb-branch parameters. In this expression, the numerators encode fermion contributions from the vector multiplets while the denominators scalar contributions from the hypermultiplets, after supersymmetric cancellations.

It is possible to revisit the derivation of (5.149) from [138] and repeat it for the case of general n_0. We show in App. A.3 that this results in the following modification of the arguments in the triple-sine functions (5.149)

$$\mathcal{Z}^{n_0}_{1-\text{loop}} = \left(\frac{\lim_{x\to 0}S_3(x)/x}{S_3(\frac{\omega_1+\omega_2+\omega_3}{2}-\frac{i\pi n_0}{\beta})}\right)^{N-1}\prod_{i>j}^{N}\frac{S_3(\pm i\lambda_{ij}|\vec{\omega})}{S_3(\frac{\omega_1+\omega_2+\omega_3}{2}-\frac{i\pi n_0}{\beta}\pm i\lambda_{ij}|\vec{\omega})}\,. \tag{5.150}$$

Combining this with the classical contribution from the localising saddle-point, one obtains in the large-N limit [121]

$$\mathcal{Z}^{n_0}_{S^5}(m,\vec{\omega},\vec{\phi},\beta) = \frac{1}{(\omega_1\omega_2)^{\frac{N-1}{2}}}\int\frac{\mathrm{d}^{N-1}\lambda}{N!}e^{-\frac{2\pi^2}{\beta\omega_1\omega_2\omega_3}\sum_i\lambda_i^2}\mathcal{Z}^{n_0}_{1-\text{loop}}(\lambda,\vec{\omega},\vec{\phi},\beta)\,, \tag{5.151}$$

where the integration is over the Coulomb branch parameters λ_i; the scalar vev of the $\mathcal{N}=1$ vector multiplet onto which the path integral localises. It takes values in the Cartan subalgebra of $SU(N)$.

We will now specialise to the case of interest with $\omega_1=\omega_2=\omega_3=\omega$ and $\phi_1=\phi_2=\phi$. The constraint hence reduces to $3\omega-2\phi=\frac{2\pi i n_0}{\beta}$. Using this we can write

$$\mathcal{Z}^{n_0}_{1-\text{loop}} = \left(\frac{\lim_{x\to 0}S_3(x)/x}{S_3(\phi)}\right)^{N-1}\prod_{i>j}^{N}\frac{S_3(\pm i\lambda_{ij}|\vec{\omega})}{S_3(\phi\pm i\lambda_{ij}|\vec{\omega})} \tag{5.152}$$

Performing the matrix integral of (5.151) exactly is challenging. In the $n_0=0$ case the authors of [121] employed the $\beta\to\infty$ limit to simplify the triple-sine functions.

For general n_0 we will use an additional, Cardy-like limit in the spirit of [109] by also considering $\omega \to 0$. We show in App. A.3 that the 1-loop-determinant contribution is then approximated by

$$\mathcal{Z}^{n_0}_{1-\text{loop}} \simeq -\frac{\pi}{\omega^3}\left[\phi^2 \sum_{i>j} \lambda_{ij} + O(\beta,\omega)\right] , \tag{5.153}$$

when the parameters λ are restricted to the Weyl chamber where $\lambda_i > \lambda_j$ for $i > j$ and assumed to be very large while the other parameters remain of order one [121]. The partition function then simplifies to

$$\mathcal{Z}^{n_0}_{S^5}(m,\vec{\omega},\beta) \propto \int \frac{\mathrm{d}^{N-1}\lambda}{N!} e^{-\frac{2\pi}{\omega^3} f(\lambda,\phi,\beta)} , \tag{5.154}$$

where

$$f = \frac{\pi}{\beta}\sum_i^N \lambda_i^2 + \frac{\phi^2}{2}\sum_{i>j}\lambda_{ij} + O(\beta,\omega) . \tag{5.155}$$

The integration in (5.154) can now be carried out using the saddle-point approximation. Note that in our Cardy-like limit the constraint has reduced to $\phi = \frac{\pi i n_0}{\beta}$, which implies that $\phi^2 < 0$. This is crucial to ensure that there exists a saddle point—the λ_i are already ordered. The solution is [121]

$$\lambda_i = -\frac{\beta\phi^2}{4\pi}(2i - N - 1) , \tag{5.156}$$

which when substituted back into the integral leads to the following leading-N expression for the 5D free energy

$$-\log \mathcal{Z}_{S^5} \propto -\frac{\beta\phi^4 N^3}{24\omega^3} + O(\beta^0, \omega^{-2}, N) . \tag{5.157}$$

The claim is that this 5D calculation captures precisely the 6D partition function of the (2,0) theory on $S^5 \times S^1$, Eq. (5.148), and hence that

$$-\log \mathcal{Z}_{S^5} = \beta\mathcal{F} - \log \mathbb{I} . \tag{5.158}$$

In certain limits of the chemical potentials where finite-N calculations can be explicitly performed and the $n_0 = 0$ superconformal-index can be evaluated independently, one sees that the corrections in (5.157) capture $O(N)$ terms in the quantity $\mathcal{F}$ (e.g. coming from instantons) as well as the correct superconformal index contributions $\mathbb{I}$ which are $O(\beta^0, N^0)$ [97, 101, 119, 140, 141].

In the large N limit therefore the expectation is that

$$-\log \mathcal{Z}_{S^5\times S^1} \xrightarrow[\lim_{N\to\infty}]{} \beta\mathcal{F} \tag{5.159}$$

with

$$\beta\mathcal{F} \;=\; -\frac{\beta N^3\phi^4}{24\omega^3} + O(N)\;. \tag{5.160}$$

After setting $n_0 = \pm 1$ as well as converting to gravitational parameters using $N^3 = \frac{3\pi^2}{16g^5G_N}$ we arrive at

$$\beta\mathcal{F} \;=\; -\frac{\beta\pi^2}{128g^5G_N}\frac{\phi^4}{\omega^3} + O(\beta^0,\omega^{-2},N)\;. \tag{5.161}$$

Upon sending $\{\omega,\phi\} \to \beta^{-1}\{\omega,\phi\}$, this expression, which is valid in the Cardy-like limit $\omega \to 0$, exactly reproduces the gravitational on-shell action (5.108) and therefore yields the value of the black hole entropy in AdS$_7$ with the correct normalisation.

Chapter 6

Conclusions

There were two aims of this thesis. The first was to present the results gathered over years of research through varying methods and their applications in the subject of conformal field theories. The other was to present the insight gained by moving between solving problems analytically and numerically. Our aim is that perhaps with the demonstration of these methods and results we can show that all of these tools complement each other and we hope to inspire more theoretical physicists to start using and developing new methodology for numerical methods in these subjects (especially ML). With a growing interest in these areas, we can start bringing machine learning and reinforcement learning out of its infancy in theoretical physics.

6.1 Summary of Results

6.1.1 Learning the Conformal Bootstrap

In Chapter 3 we introduced the use of Reinforcement-Learning techniques into the conformal bootstrap programme. We tested an RL soft Actor-Critic algorithm in the context of several 2D CFTs and showed that the algorithm can perform efficient multi-dimensional searches in the space of scaling dimensions and OPE-squared coefficients. The basic input of our approach is a spin-partition and a window of scaling dimensions, where the search is concentrated. We demonstrated in concrete examples that this minimal input is enough to guide the algorithm towards a CFT of interest and that the obtained numerical values can be sensible even in very rough truncations with only a handful of operators. Our algorithm can be straightforwardly applied to any CFT of arbitrary spacetime dimension. This opens up the very exciting possibility of new non-perturbative results in conformal field theory in a wide range of directions, some of which we plan to explore in the near future.

We view the approach introduced here as largely complementary to the more standard ones that have already been developed to-date in the context of the numerical

conformal bootstrap. We believe that our method is comparatively stronger in performing efficient multi-dimensional searches in arbitrary, a priori selected (unitary or non-unitary) CFTs. Since it is based on statistical and probabilistic techniques, it can be weaker in accuracy, on detecting rigorous bounds and on conclusively rejecting CFT data as inconsistent. The latter is the context where standard numerical conformal-bootstrap approaches have excelled over the last decade. Eventually, one would like to combine all available analytic and numerical methods at their disposal to build a powerful multi-purpose toolbox.

We envisage the most efficient application of our approach in contexts where a CFT can be solved in a parametrically convenient regime (e.g. in a weakly coupled large-N regime or a weakly coupled regime on a conformal manifold). Then, one can use the information of the perturbative solution to set up a well-informed spin-partition, that can in turn be applied adiabatically to a search with gradually changing parameters. By using a gradual update of the CFT data, one should be able to implement the RL algorithm step-by-step and track them from a weak- to a strong-coupling regime. This is a concrete context, where one can try to leverage all available analytic and numerical information. For example, in superconformal field theories, our approach can benefit from many recent developments that use the superconformal structure of the theory in an essential way.

Although our results provide a proof of principle for the usefulness of RL techniques to this class of problems, there are several aspects of our approach that require further investigation and development. The most urgent is to systematically understand how to incorporate reliable errors in our computations. The primary source of error is of an analytic nature and originates from the truncation of the conformal-block expansions. The convergence properties of these expansions, [52], imply that there is a sufficiently high Δ_{max} above which the error will be negligible. It is unclear, however, how to identify this optimal Δ_{max} in a generic theory and for generic four-point functions. Hence, one might initially need to perform a case-by-case analysis in order to explore how our results are affected by an increasing Δ_{max}.

Another source of error, which is sometimes more significant than the error due to the Δ_{max} truncation, comes from the way we reduce the functional dependence of the crossing equations on the cross-ratios to a discrete set of algebraic equations. Here we have chosen to implement this reduction by evaluating the crossing equations on a finite set of cross-ratio values. We noticed experimentally that the sampling of z-points suggested in Sec. 3.1 of [53] works well in our computations. However, we lack a good understanding of whether this is the optimal sampling, or how the calculations are affected by the number of z-points selected. An error can consequently be associated with these effects by varying the sampling (in form and size). Alternatively, one can explore more standard reductions based on Taylor-expansions of the conformal blocks

around some point in z-space. It would be interesting to repeat the computations of this chapter with this alternative approach and compare results.

Other errors have to do with the statistical nature of our approach and the fact that we do not a priori know the minimal possible violation of the truncated crossing equations for a given truncation and reduction. We quantified this violation with a relative measure of accuracy $\mathbb{A}$ and performed runs of the RL algorithm up to the point where the improvement of $\mathbb{A}$ was saturated. An important additional measure of error for each CFT datum is a statistical error obtained by performing the same type of run many times, which we sampled in the case of the $c = 1$ compactified boson CFT on S^1 for the simplest case of $\Delta_{\text{max}} = 2$ in the momentum sector and for $\Delta_{\text{max}} = 8$ in the four-point function of the conserved $U(1)$ current. The evaluation of this type of error would benefit from a fully parallelisable algorithm. As we noted in Sec. 3.4.5, current implementations of the algorithm benefit from the judicious caretaking of the user, which obstructs the full parallelisability of the code. It would be useful to improve this aspect in future work.

We did not make systematic use of the constraints of global symmetries or of the full constraints of unitarity on the OPE-squared coefficients. As we observed in Sec. 3.6.2, multi-dimensional searches can benefit significantly from prior information on the signs of the OPE-squared coefficients. Without such information the agent is allowed to explore cancellations between different conformal blocks that sidetrack the search by increasing the statistical error on certain OPE-squared coefficients, especially so for those at higher scaling dimensions that come naturally with suppressed numerical values.

Finally, we treated the learning algorithm itself as a black box, using the off-the shelf soft Actor-Critic algorithm of [51]. It would be interesting to explore what efficiency and speed gains one can achieve by tuning hyperparameters or choosing the Deep Deterministic Policy Gradient method [60]. We also chose the simplest definition for the reward function (3.52). The choice of an appropriate reward function is crucial in achieving better results for RL algorithms and this is an area that also deserves further investigation.

6.1.2 Brute-Forcing Vacuum Characters

In Chapter 4 we have calculated vacuum characters of rank-one and rank-two VOAs labelled by non-Coxeter, crystallographic complex reflection groups. This involved a brute-force implementation of the algorithms presented in [20] and leads to the Macdonald index of certain 4D $\mathcal{N} = 3$ S-fold SCFTs. Our results were given as an expansion in the fugacity that keeps track of the conformal weight, and were truncated to orders that require short computation times when using a desktop computer; they can be pushed to arbitrary higher orders by allocating appropriate resources. As they stand,

they can already be used as new data for $\mathcal{N} = 3$ SCFTs. E.g. the $\mathsf{G} = \mathbb{Z}_3$ result agrees in the Schur limit with [93].

Our code is customisable. We have clearly signposted where changes would need to be made to return vacuum characters of VOAs labelled by different complex reflection groups, for which the free-field realisation is known. In particular, it would be very interesting to extend this approach to the $\mathcal{N} = 3$ S-fold SCFT of rank two associated with $G(4, 1, 2)$ and the rank-three example $G(3, 3, 3)$; a proposal for the Schur index of the latter was also given in [93]. Unfortunately, finding the free-field realisation for both these VOAs—already needed before identifying the null states—is a challenging task: the simplest anti-chiral strong generator ansatze involve 425 and 2265 undetermined coefficients respectively. It would perhaps be more promising to use the screening-operator approach, upon determining $\mathbb{S}$. Although our screening-operator code is currently more expensive to run, it could benefit from optimisations that parallelise the computations, hence making it significantly faster on multi-core clusters. It will also be interesting to check these results by directly studying the BPS-states of $\mathcal{N} = 3$ theories. One way to do so would be to study three-string junctions in S-fold backgrounds as in [142]. We hope to return to some of these questions in the near future.

6.1.3 AdS_7 Black Holes and 5D MSYM Theory

In Chapter 5 we mainly looked at the how the AdS_7 black hole entropy and the superconformal index of the 6D (2,0) theory were related. In order to do that we first introduced a few ingredients on both sides of the AdS/CFT correspondence. In Sec. 5.2 we introduced the reader to some basic concepts in localisation, and also recreated the famous 3D localisation of the Supersymmetric Chern-Simons theory on S_3 done by [22]. In Sec. 5.4, on the AdS side we generalised the AdS_5 case of [21] for our own research where we took the relatively simple example of a 2-equivalent charge, 3-equivalent rotation non-extremal black hole solution in AdS_7. Just as a remark, we have attempted more complicated solutions (e.g. ones with non-equivalent charges or rotations), but they proved too difficult to generalise to, so we decided to settle on the simpler case in the end. In this section we also imposed the BPS limit on the black hole solutions we considered (supersymmetric and extremal limit) and looked at the thermodynamic quantities in this limit. Then we further analysed the values of certain parameters of the black hole at the outermost horizon which gave us complex values for thermodynamic quantities and also allowed us to write down the relationship $2\phi - 3\omega = \pm 2\pi i$. This relationship between the chemical potentials is analogous to the one in [21] and was paramount to the analysis of the 6D theory.

Before we could begin analysing the (2,0) theory, we had to derive the background for the boundary. We did this by using bulk regularity, that is, finding an ideal coor-

dinate transformation and then taking the limit as $r \to \infty$. This again was done in a similar manner to that of [21], but there was some extra work done to derive the transformations for S^5, which were included in App. A.2. Before moving on we also had to look at what happens to the gauge field. At the boundary there will be a background gauge field, which was pure gauge and imaginary $A|_{\text{bdry}} = i\Phi \mathrm{d}\hat{\tau}$.

In Sec. 5.5 we started considering the boundary CFT side of the correspondence. Since the (2,0) theory is non-Lagrangian, we could not directly calculate the superconformal index using the method of supersymmetric localisation, which we introduced in the review section, directly in 6D. However, there exists a conjecture in which the theory appears from the reduction of a maximally-supersymmetric $\mathcal{N} = 2$ Yang-Mills theory with $SU(N)$ gauge group [115, 116, 117, 118, 101, 119, 120, 121] on a circle from $S^5 \times S^1_\beta$. We then went on to calculate the partition function of this MSYM theory on S^5 in the large N and Cardy-like limit (to simplify the problem further). In order to perform the localisation computation we utilise the procedures of [140, 138] in order to arrive at the result which reproduces the correct N^3 scaling of the supersymmetric Casimir energy as well as matches with the expected value — the gravitational on-shell action— in this limit.

6.2 Final Comments and Outlook

There has been a large variety of research presented in this thesis. All the way from fully numerical — complete with numerical truncations, approximations and novel computational algorithms —; computational brute force, yet still analytic by calculations; and finally fully analytic. It was our aim to showcase the diversity of theoretical physics research taking place at the moment. While analytic solutions still remain the most highly desired in theoretical physics, it is very much the case that computational methods can massively help in verifying conjectures, or even treading into unknown territories on their own.

We have reserved this final section to compare and contrast the methods we used in this thesis in a qualitative way. Let us start with the analytic method of localisation which we employed in the case of the MSYM theory on S^5. Just like with a lot of problems in this area of String theory, usually a direct approach is out of the question, and one has to use a series of convenient limits and/or approximations in order to churn out an answer from the theory being analysed. Usually localising such theories also results in expressions which include large amounts of special functions whose properties must be well considered, which can present a difficulty when analysing the solutions. A great example is in the calculation in appendix A.3 where we had to consider triple sine functions.

We are not trying to justify the use of an analytic solution, since such methods

are already well established. However, computational methods have only really been used in physics perhaps for almost half a century. The 2D VOA case, while perfectly analytically solvable, would have not been efficient to do by hand, if even possible to the level we have shown in Chapter 4. Computers are fast. Trivial to say, but in the future we hope to see a lot of index-like evaluations hopefully being calculated via machines (especially since closed forms are very difficult). Calculating indices from huge sets of operators is definitely not a problem when the algorithm is properly parallelised and potentially running on a high-powered cluster.

Finally, the numerical methods we employed in this thesis also heavily relied on approximations and truncations. In a sense this is somewhat comparable to the analytic computation, since they will both present solutions which are heavily restricted by their assumptions. In the case of our research, our truncations of the crossing equations had to assume that the terms contributing were decaying fast enough to give a good enough approximation if we only included a small, finite amount of operators. Furthermore we also had to put our continuous functions on a grid, and the points we chose to evaluate the functions on also heavily influenced the results. If one has access to high computational power, it is possible to run many iterations of these evaluations in many different grids or assumptions and "integrate (sum) out" the dependence on such trivialities. In our computations we have demonstrated that accurate results can be obtained using such numerical methods and for future directions we will be utilising highly statistical approaches which can eliminate the bias in individual runs of the code and provide a much more robust algorithm, which will also make it easier for the scientific community to replicate results.

In conclusion, the most sensible approach is to utilise all of these methods in conjunction. As it may be, at the moment there is an enormous pool of problems where computational methods could be used to verify existing analytic results, or even help to inspire the use of analytic tools in certain subfields. The increased research into machine learning applications in the String theory landscape, knot theory and also conformal field theories could potentially be the spark of a whole new era in theoretical physics.

Appendix A

Black Hole and S^5 Calculations

A.1 Reality Properties of m

Here we would like to show that the mass parameter appearing in the AdS_7 black hole metric (5.54) becomes complex away from the BPS limit (i.e. when $r_+ > r_*$) and becomes real when the black hole is supersymmetric and extremal (when $r_+ = r_*$).

We can check whether if any solutions of m are complex by looking at the discriminant

$$\Delta \;=\; C_1^2 - 4C_0C_2 \;, \tag{A.1}$$

with $C_i(r_+, r_*, a)$ being the coefficient of the ith power of m_+ in (5.105). The parameter a can be expressed in terms of r_* as

$$a \;=\; \frac{-r_*^2 \pm 2\sqrt{r_*^2(1+r_*^2)}}{4+3r_*^2} \;, \tag{A.2}$$

where we have chosen to set the AdS radius to one, $g = 1$ to simplify the presentation. This expression can be inverted to yield

$$r_* \;=\; \sqrt{\frac{4a^2}{(1+a)(1-3a)}} \;, \tag{A.3}$$

with the positive branch being selected on physical grounds. Reality of the black hole horizon sets a bound on a

$$-1 < a < \frac{1}{3} \tag{A.4}$$

and since this is a radius we can see that a defines the range of r_* to be $[0, \infty)$.

At this stage we should also note that in order to preserve the signature of the metric (5.54), we have to restrict Ξ such that it is always larger than zero. This implies

that

$$\Xi \;=\; 1-a^2>0\,, \tag{A.5}$$

which is always satisfied for a choice in (A.4).

Returning to (A.1), one finds that it can be written as

$$C_1^2-4C_0C_2 \;=\; -\,\frac{1024r_*^4\left(r_+^2-r_*^2\right)^2\left(r_*^2+1\right)\left(4r_+^2\left(-\sqrt{r_*^2\left(r_*^2+1\right)}+r_*^2+1\right)-r_*^2\right)}{9\left(r_*^2-2\sqrt{r_*^2\left(r_*^2+1\right)}\right)^4\left(4\sqrt{r_*^2\left(r_*^2+1\right)}+r_*^2\right)^2}\,. \tag{A.6}$$

All of the above terms are clearly positive, with the exception of

$$\lambda \;\equiv\; 4r_+^2\left(-\sqrt{r_*^2\left(r_*^2+1\right)}+r_*^2+1\right)-r_*^2\,. \tag{A.7}$$

Let us take a part of this and define

$$f(r_*) \;=\; 4(-\sqrt{r_*^2\left(r_*^2+1\right)}+r_*^2+1)\,. \tag{A.8}$$

The range for this function is $2<f(r_*)<4$. This can be seen by taking the infinite limit, or by Laurent expansion. Hence,

$$\lambda>2r_+^2-r_*^2>0\,, \tag{A.9}$$

and the whole of (A.1) is always negative except at the BPS limit. We have therefore shown that the mass is indeed complex for $r_+<r_*$.

A.2 5-sphere Geometry

In this appendix we give the details of the change of coordinates (5.118). Start from $\mathbb{C}^3$ with complex coordinates (z_1,z_2,z_3) and metric

$$\mathrm{d}s_6^2 \;=\; \sum_{i=1}^{3}|\mathrm{d}z_i|^2\,. \tag{A.10}$$

We then restrict to S^5 by imposing the constraint $\sum_{i=1}^3|z_i|^2=1$. Next define coordinates

$$\xi_1 \;=\; \frac{z_1}{z_3}\,,\qquad \xi_2 \;=\; \frac{z_2}{z_3}\,,\qquad z_3 \;=\; |z_3|e^{i\tau}\,, \tag{A.11}$$

and

$$\hat{A} = \frac{i}{2}(1+|\xi_1|^2+|\xi_2|^2)^{-1}\left(\bar{\xi}_1 \mathrm{d}\xi_1 + \bar{\xi}_2 \mathrm{d}\xi_2 - \xi_1 \mathrm{d}\bar{\xi}_1 - \xi_2 \mathrm{d}\bar{\xi}_2\right) . \tag{A.12}$$

Then the 5-sphere metric is

$$\begin{aligned} \mathrm{d}s^2_{S^5} &= (\mathrm{d}\tau - \hat{A})^2 + (1+|\xi_1|^2+|\xi_2|^2)^{-1}(|\mathrm{d}\xi_1|^2+|\mathrm{d}\xi_2|^2) \\ &\quad - (1+|\xi_1|^2+|\xi_2|^2)^{-2}(\bar{\xi}_1\mathrm{d}\xi_1 + \bar{\xi}_2\mathrm{d}\xi_2)^2 . \end{aligned} \tag{A.13}$$

Choosing

$$\begin{aligned} \xi_1 &= \tan\chi \cos\frac{\theta}{2} e^{\frac{i}{2}(\psi+\varphi)} \\ \xi_2 &= \tan\chi \sin\frac{\theta}{2} e^{\frac{i}{2}(\psi-\varphi)} , \end{aligned} \tag{A.14}$$

gives

$$\begin{aligned} \mathrm{d}s^2_{S^5} &= \left(\mathrm{d}\tau + \frac{1}{2}\sin^2\chi(\mathrm{d}\psi + \cos\theta \mathrm{d}\varphi)\right)^2 \\ &\quad + \mathrm{d}\chi^2 + \frac{1}{4}\sin^2\chi\Big[\cos^2\chi(\mathrm{d}\psi+\cos\theta\mathrm{d}\varphi)^2 + \mathrm{d}\theta^2 + \sin^2\theta\mathrm{d}\varphi^2\Big] , \\ &= \mathrm{d}\tau^2 + \sin^2\chi \mathrm{d}\tau(\mathrm{d}\psi+\cos\theta\mathrm{d}\varphi) \\ &\quad + \mathrm{d}\chi^2 + \frac{1}{4}\sin^2\chi\Big[(\mathrm{d}\psi+\cos\theta\mathrm{d}\varphi)^2 + \mathrm{d}\theta^2 + \sin^2\theta\mathrm{d}\varphi^2\Big] . \end{aligned} \tag{A.15}$$

From the choice of ξ's we get

$$\begin{aligned} z_1 &= \sin\chi\cos\frac{\theta}{2}e^{\frac{i}{2}(\psi+\varphi)}e^{i\tau} \\ z_2 &= \sin\chi\sin\frac{\theta}{2}e^{\frac{i}{2}(\psi-\varphi)}e^{i\tau} \\ z_3 &= \cos\chi e^{i\tau} . \end{aligned} \tag{A.16}$$

On the other hand one can take the following Cartesian coordinates for S^5

$$\begin{aligned} x_1 &= \sin\phi_1\sin\theta_1\sin\theta_2 \\ x_2 &= \cos\phi_1\sin\theta_1\sin\theta_2 \\ x_3 &= \sin\phi_2\sin\theta_1\cos\theta_2 \\ x_4 &= \cos\phi_2\sin\theta_1\cos\theta_2 \\ x_5 &= \sin\phi_3\cos\theta_1 \\ x_6 &= \cos\phi_3\cos\theta_1 , \end{aligned} \tag{A.17}$$

and identify

$$\begin{aligned} \tilde{z}_1 &= x_2 + ix_1 &&= e^{i\phi_1}\sin\theta_1\sin\theta_2 \\ \tilde{z}_2 &= x_4 + ix_3 &&= e^{i\phi_2}\sin\theta_1\cos\theta_2 \\ \tilde{z}_3 &= x_6 + ix_5 &&= e^{i\phi_3}\cos\theta_1\,. \end{aligned} \tag{A.18}$$

The metric in these coordinates is

$$\mathrm{d}s^2_{S^5} = \mathrm{d}\theta_1^2 + \sin^2\theta_1\mathrm{d}\theta_2^2 + \sin^2\theta_1\sin^2\theta_2\mathrm{d}\phi_1^2 + \sin^2\theta_1\cos^2\theta_2\mathrm{d}\phi_2^2 + \cos^2\theta_1\mathrm{d}\phi_3^2\,. \tag{A.19}$$

Inserting the coordinate mapping

$$\theta \equiv 2\theta_2\,, \quad \psi \equiv \phi_1+\phi_2-2\phi_3\,, \quad \varphi \equiv -\phi_1+\phi_2\,, \quad \tau \equiv \phi_3\,, \quad \chi \equiv \theta_1\,. \tag{A.20}$$

into (A.15) gives back (A.19).

A.3 5D 1-loop Determinants for General n_0

In this appendix we provide some additional details on the derivation of the 1-loop determinants of 5D MSYM on a squashed S^5 for general n_0 and their simplification in the Cardy-like limit, $\omega \to 0$, which we made use of in Sec. 5.5.2. We will follow both [138] and [121] closely, to which we refer the interested reader for a complete account. The calculation of [138] involves looking at the partition function of a 6D (1,0) theory with vector and hypermultiplets on $S^5 \times S^1$, calculating the 6D one-loop determinants via supersymmetric localisation and then reducing on the circle to get expressions in 5D. Interestingly, even though the 6D theory is not superconformal, the result for the 1-loop determinants can be expressed as a Hamiltonian index. This fact greatly simplifies the organisation of the calculation for $n_0 = 0$ and allows for a straightforward extension to arbitrary n_0.

We begin by setting up notation, as in [138]. There are 5 Cartans left after a choice of localising supercharge $\mathcal{Q}$ in the 6D (1,0) theory

$$H = -\partial_t, \quad Q_V = -i\mathcal{L}_\psi, \quad \tau_3, \quad \lambda_{3,8}\,. \tag{A.21}$$

These Cartans correspond to the bosonic symmetries $\mathbb{R}\times U(1)_V \times SU(3)_V \times SU(2)_R$. We will also make the supercharge we picked manifest, with the associated supersymmetry parameters being

	H	Q_V	τ_3	λ_3	λ_8
ε_1	$+\frac{1}{2}$	$-\frac{3}{2}$	$+1$	0	0
ε_2	$-\frac{1}{2}$	$+\frac{3}{2}$	-1	0	0

With this information, one can formulate the following "index" [138][30]

$$\mathcal{I} = \mathrm{Tr}(-1)^F q^{H-Q_V-2\tau_3} x^{Q_V+\frac{3}{2}\tau_3} y_3^{\lambda_3} y_8^{\lambda_8} \ , \tag{A.22}$$

where $q = e^{-\beta}$, $x = q^{1+iw_0}$ and $y_{3,8} = q^{iw_{3,8}}$. The trace is taken over the Fock space of gauge-invariant states on the squashed S^5. We choose the fermion-number operator as $F = 2Q_V$. This index uses completely independent chemical potentials since the operator on the RHS of (A.22) commutes with the supercharge $\mathcal{Q}$. We note that the chemical potentials $w_{0,3,8}$ are related to the $\omega_{1,2,3}$ that appear in the main part of this paper as

$$(1+iw_0) = \frac{1}{3}\sum_{i=1}^{3}\omega_i \ , \qquad iw_3 = \frac{1}{2}(\omega_2-\omega_1) \ , \qquad iw_8 = \frac{1}{6}(2\omega_3-\omega_1-\omega_2) \tag{A.23}$$

and these are in turn related to the squashing parameters φ_i as $\omega_i = 1 + i\varphi_i$.

Following the discussion in Sec. 5.5.1, one can straightforwardly generalise (A.22) for arbitrary n_0 by shifting one of the chemical potentials, $\omega_1 \to \omega_1 - \frac{2\pi i n_0}{\beta} = \tilde{\omega}_1$

$$\mathcal{I} = \mathrm{Tr}(-1)^F q^{H-Q_V-2\tau_3} \tilde{x}^{Q_V+\frac{3}{2}\tau_3} \tilde{y}_3^{\lambda_3} \tilde{y}_8^{\lambda_8} \ , \tag{A.24}$$

with the fugacities $\tilde{x}, \tilde{y}_{3,8}$ defined as below (A.22) but using the $\tilde{\omega}_i$ of (5.146). From here on we can repeat the calculation of [138] using the tilded chemical potentials. In particular, this means that we will encounter the same bosonic and fermionic cancellations that occur in the calculation of the supersymmetric partition function of [138]. The non-cancelling contributions from the vector multiplet are fermionic modes that can be encoded into the plethystic exponential of the single-letter index

$$\begin{aligned} &-\sum_{\lambda\in\mathrm{adj}}\left[\sum_{k=1}^{\infty} q^{-i\lambda(\sigma)}\tilde{x}^k\chi_{(k,k)}(\tilde{y}_3,\tilde{y}_8)+\sum_{k=0}^{\infty} q^{-i\lambda(\sigma)}\tilde{x}^{(k+3)}\chi_{(k,k)}(\tilde{y}_3,\tilde{y}_8)\right] \\ &=-\sum_{\lambda\in\mathrm{adj}}\left[\sum_{k=1}^{\infty} q^{-i\lambda(\sigma)}\tilde{x}^k\chi_{(k,k)}(\tilde{y}_3,\tilde{y}_8)+\sum_{k=0}^{\infty} q^{-i\lambda(\sigma)+\sum_i\omega_i}\tilde{x}^k\chi_{(k,k)}(\tilde{y}_3,\tilde{y}_8)\right] \ , \end{aligned} \tag{A.25}$$

where the $\chi_{(k,k)}(\tilde{y}_3,\tilde{y}_8)$ is the $SU(3)_V$ character and the $\lambda(\sigma)$ denote an inner product in weight space. The surviving modes from the hypermultiplet in a representation R have a corresponding single-letter index contribution

$$\sum_{\rho\in R}\left[\sum_{k=0}^{\infty} q^{-i\rho(\sigma)}\tilde{x}^{(k+\frac{3}{2})}\chi_{(k,k)}(\tilde{y}_3,\tilde{y}_8)+\sum_{k=0}^{\infty} q^{i\rho(\sigma)}\tilde{x}^{(k+\frac{3}{2})}\chi_{(k,k)}(\tilde{y}_3,\tilde{y}_8)\right] \ . \tag{A.26}$$

[30] When the theory is superconformal this is the standard 6D (1,0) index.

We can use the fact that $n_0 \in \mathbb{Z}$ and recast this as

$$\sum_{\rho\in R}\left[\sum_{k=0}^{\infty} q^{-i\rho(\sigma)+\frac{1}{2}\sum_i \omega_i-\frac{\pi i n_0}{\beta}}\tilde{x}^k\chi_{(k,k)}(\tilde{y}_3,\tilde{y}_8)+\sum_{k=0}^{\infty} q^{i\rho(\sigma)+\frac{1}{2}\sum_i \omega_i+\frac{\pi i n_0}{\beta}}\tilde{x}^k\chi_{(k,k)}(\tilde{y}_3,\tilde{y}_8)\right] . \tag{A.27}$$

By grouping the $q^{\pm(i\rho(\sigma)-\frac{\pi i n_0}{\beta})}$ expressions together in the hypermultiplet, the calculation of the corresponding 1-loop determinants in [138] can be carried out identically. The only point that merits special mention is that the p_i variables of Eq. (79) of that reference are still the ones that are used in the general n_0 case, since

$$\tilde{p}_i = q^{\tilde{\omega}_i} = q^{\omega_i} . \tag{A.28}$$

Following the rest of the arguments in [138], one ends up with the final result for the 1-loop determinants of a 5D $\mathcal{N}=1$ theory with one vector and one hypermultiplet in the representation R

$$\mathcal{Z}_{1-\text{loop}} = \frac{\prod_{\alpha\in\text{roots}} S_3(-i\lambda(\sigma)|\vec{\omega})}{\prod_{\rho\in\text{R}} S_3(-i\rho(\sigma)-\frac{i\pi n_0}{\beta}+\frac{\omega_1+\omega_2+\omega_3}{2}|\vec{\omega})} . \tag{A.29}$$

In the Cardy-like limit $\omega_i \to 0$, the triple-sine functions[31] $S_3(\lambda|\vec{\omega})$ have a simple $\beta\to\infty$ limit if one additionally assumes that the λ scale as β, while the remaining parameters remain of order one [121]

$$\log S_3(i\lambda|\vec{\omega}) \overset{sgn(\lambda)=\pm 1}{\sim} -\frac{\pi}{6\omega_1\omega_2\omega_3}\left(|\lambda|^3+O(\beta^2,\vec{\omega})\right) . \tag{A.30}$$

As a result Eq. (5.152) from the main part of this paper where $\vec{\omega}=(\omega,\omega,\omega)$ becomes

$$\begin{aligned}\mathcal{Z}^{n_0}_{\text{1-loop}} &\propto \prod_{i>j}^{N}\frac{S_3(i\lambda_{ij}|\vec{\omega})S_3(-i\lambda_{ij}|\vec{\omega})}{S_3(\phi+i\lambda_{ij}|\vec{\omega})S_3(\phi-i\lambda_{ij}|\vec{\omega})}\\ &\sim \exp\left(-\frac{\pi}{6\omega^3}\sum_{i>j}\left[2\lambda_{ij}^3-(\lambda_{ij}-i\phi)^3-(\lambda_{ij}+i\phi)^3\right]+O(\beta,\omega)\right)\\ &= \exp\left(-\frac{\pi}{\omega^3}\phi^2\sum_{i>j}\lambda_{ij}+O(\beta,\omega)\right) ,\end{aligned} \tag{A.31}$$

where the absolute values have been dropped because the parameters λ have been restricted to the Weyl chamber where $\lambda_i > \lambda_j$ for $i>j$ and since we have assumed that $\lambda_{ij} \gg i\phi$ because of its β scaling. Note that in the Cardy-like limit $\omega\to 0$ the constraint implies that ϕ is imaginary, so the combination $\lambda_{ij}\pm i\phi$ is real and positive.

[31] For a summary of the properties of triple-sine functions see also [143].

Bibliography

[1] Gergely Kántor, Constantinos Papageorgakis, and Paul Richmond. "AdS_7 black-hole entropy and 5D $\mathcal{N} = 2$ Yang-Mills". In: *JHEP* 01 (2020), p. 017. DOI: 10.1007/JHEP01(2020)017. arXiv: 1907.02923 [hep-th].

[2] Prarit Agarwal et al. "Macdonald indices for four-dimensional $\mathcal{N}$=3 theories". In: *Phys. Rev. D* 103.12 (2021), p. L121701. DOI: 10.1103/PhysRevD.103.L121701. arXiv: 2103.00985 [hep-th].

[3] Gergely Kántor, Vasilis Niarchos, and Constantinos Papageorgakis. "Solving Conformal Field Theories with Artificial Intelligence". In: *Phys. Rev. Lett.* 128.4 (2022), p. 041601. DOI: 10.1103/PhysRevLett.128.041601. arXiv: 2108.08859 [hep-th].

[4] Gergely Kántor, Vasilis Niarchos, and Constantinos Papageorgakis. "Conformal bootstrap with reinforcement learning". In: *Phys. Rev. D* 105.2 (2022), p. 025018. DOI: 10.1103/PhysRevD.105.025018. arXiv: 2108.09330 [hep-th].

[5] Juan Maldacena. In: *International Journal of Theoretical Physics* 38.4 (1999), pp. 1113–1133. DOI: 10.1023/a:1026654312961. URL: https://doi.org/10.1023%2Fa%3A1026654312961.

[6] Ofer Aharony et al. "Large N field theories, string theory and gravity". In: *Physics Reports* 323.3-4 (Jan. 2000), pp. 183–386. DOI: 10.1016/s0370-1573(99)00083-6. URL: https://doi.org/10.1016%2Fs0370-1573%2899%2900083-6.

[7] Justin Kinney et al. "An Index for 4 dimensional super conformal theories". In: *Commun. Math. Phys.* 275 (2007), pp. 209–254. DOI: 10.1007/s00220-007-0258-7. arXiv: hep-th/0510251.

[8] Jyotirmoy Bhattacharya et al. "Indices for superconformal field theories in 3, 5 and 6 dimensions". In: *Journal of High Energy Physics* 2008.02 (Feb. 2008), pp. 064–064. DOI: 10.1088/1126-6708/2008/02/064. URL: https://doi.org/10.1088%2F1126-6708%2F2008%2F02%2F064.

[9] Vasily Pestun. "Localization of Gauge Theory on a Four-Sphere and Supersymmetric Wilson Loops". In: *Communications in Mathematical Physics* 313.1 (May 2012), pp. 71–129. DOI: 10.1007/s00220-012-1485-0. URL: https://doi.org/10.1007%2Fs00220-012-1485-0.

[10] Warren Mcculloch and Walter Pitts. "A Logical Calculus of Ideas Immanent in Nervous Activity". In: *Bulletin of Mathematical Biophysics* 5 (1943), pp. 127–147.

[11] Gordon E. Moore. "Cramming more components onto integrated circuits". In: *Electronics* 38.8 (Apr. 1965).

[12] Richard F. Stark and Tsvi Piran. "Gravitational-Wave Emission from Rotating Gravitational Collapse". In: *Phys. Rev. Lett.* 55 (8 Aug. 1985), pp. 891–894. DOI: 10.1103/PhysRevLett.55.891. URL: https://link.aps.org/doi/10.1103/PhysRevLett.55.891.

[13] Riccardo Rattazzi et al. "Bounding scalar operator dimensions in 4D CFT". In: *JHEP* 12 (2008), p. 031. DOI: 10.1088/1126-6708/2008/12/031. arXiv: 0807.0004 [hep-th].

[14] Yang-Hui He. *Deep-Learning the Landscape*. 2017. DOI: 10.48550/ARXIV.1706.02714. URL: https://arxiv.org/abs/1706.02714.

[15] James Halverson, Brent Nelson, and Fabian Ruehle. "Branes with Brains: Exploring String Vacua with Deep Reinforcement Learning". In: *JHEP* 06 (2019), p. 003. DOI: 10.1007/JHEP06(2019)003. arXiv: 1903.11616 [hep-th].

[16] Kieran Bull et al. "Machine Learning CICY Threefolds". In: *Phys. Lett. B* 785 (2018), pp. 65–72. DOI: 10.1016/j.physletb.2018.08.008. arXiv: 1806.03121 [hep-th].

[17] Yang-Hui He. *The Calabi–Yau Landscape: From Geometry, to Physics, to Machine Learning*. Lecture Notes in Mathematics. May 2021. ISBN: 978-3-030-77561-2, 978-3-030-77562-9. DOI: 10.1007/978-3-030-77562-9. arXiv: 1812.02893 [hep-th].

[18] Matthew J. S. Beach, Anna Golubeva, and Roger G. Melko. "Machine learning vortices at the Kosterlitz-Thouless transition". In: *Phys. Rev. B* 97 (4 Jan. 2018), p. 045207. DOI: 10.1103/PhysRevB.97.045207. URL: https://link.aps.org/doi/10.1103/PhysRevB.97.045207.

[19] Michael R. Douglas. "Machine learning as a tool in theoretical science". In: *Nature Reviews Physics* 4.3 (Feb. 2022), pp. 145–146. DOI: 10.1038/s42254-022-00431-9.

[20] Federico Bonetti, Carlo Meneghelli, and Leonardo Rastelli. "VOAs labelled by complex reflection groups and 4d SCFTs". In: *JHEP* 05 (2019), p. 155. DOI: 10.1007/JHEP05(2019)155. arXiv: 1810.03612 [hep-th].

[21] Alejandro Cabo-Bizet et al. "Microscopic origin of the Bekenstein-Hawking entropy of supersymmetric AdS_5 black holes". In: (2018). arXiv: 1810.11442 [hep-th].

[22] Anton Kapustin, Brian Willett, and Itamar Yaakov. "Exact results for Wilson loops in superconformal Chern-Simons theories with matter". In: *Journal of High Energy Physics* 2010.3 (Mar. 2010). DOI: 10.1007/jhep03(2010)089. URL: https://doi.org/10.1007%2Fjhep03%282010%29089.

[23] P. Di Francesco, P. Mathieu, and D. Senechal. *Conformal Field Theory*. Graduate Texts in Contemporary Physics. New York: Springer-Verlag, 1997. ISBN: 978-0-387-94785-3, 978-1-4612-7475-9. DOI: 10.1007/978-1-4612-2256-9.

[24] David Simmons-Duffin. "The Conformal Bootstrap". In: *Proceedings of the 2015 Theoretical Advanced Study Institute in Elementary Particle Physics*. Ed. by Joseph Polchinski, Pedro Vieira, and Oliver DeWolfe. World Scientific, Jan. 2017, pp. 1–74. DOI: 10.1142/9789813149441_0001. arXiv: 1602.07982 [hep-th].

[25] David Poland, Slava Rychkov, and Alessandro Vichi. "The Conformal Bootstrap: Theory, Numerical Techniques, and Applications". In: *Rev. Mod. Phys.* 91 (2019), p. 015002. DOI: 10.1103/RevModPhys.91.015002. arXiv: 1805.04405 [hep-th].

[26] Shai M. Chester. "Weizmann Lectures on the Numerical Conformal Bootstrap". In: (July 2019). arXiv: 1907.05147 [hep-th].

[27] H. Osborn. "Conformal Blocks for Arbitrary Spins in Two Dimensions". In: *Phys. Lett. B* 718 (2012), pp. 169–172. DOI: 10.1016/j.physletb.2012.09.045. arXiv: 1205.1941 [hep-th].

[28] Eric Perlmutter. "Virasoro conformal blocks in closed form". In: *JHEP* 08 (2015), p. 088. DOI: 10.1007/JHEP08(2015)088. arXiv: 1502.07742 [hep-th].

[29] Christopher Beem et al. "Infinite Chiral Symmetry in Four Dimensions". In: *Commun. Math. Phys.* 336.3 (2015), pp. 1359–1433. DOI: 10.1007/s00220-014-2272-x. arXiv: 1312.5344 [hep-th].

[30] Madalena Lemos. *Lectures on chiral algebras of $\mathcal{N} \geqslant 2$ superconformal field theories*. 2020. DOI: 10.48550/ARXIV.2006.13892. URL: https://arxiv.org/abs/2006.13892.

[31] S. Ferrara, A. F. Grillo, and R. Gatto. "Tensor representations of conformal algebra and conformally covariant operator product expansion". In: *Annals Phys.* 76 (1973), pp. 161–188. DOI: 10.1016/0003-4916(73)90446-6.

[32] A. M. Polyakov. "Nonhamiltonian approach to conformal quantum field theory". In: *Zh. Eksp. Teor. Fiz.* 66 (1974), pp. 23–42.

[33] David Simmons-Duffin. "A Semidefinite Program Solver for the Conformal Bootstrap". In: *JHEP* 06 (2015), p. 174. DOI: 10.1007/JHEP06(2015)174. arXiv: 1502.02033 [hep-th].

[34] Walter Landry and David Simmons-Duffin. "Scaling the semidefinite program solver SDPB". In: (Sept. 2019). arXiv: 1909.09745 [hep-th].

[35] Marten Reehorst et al. "Navigator Function for the Conformal Bootstrap". In: *SciPost Phys.* 11 (2021), p. 072. DOI: 10.21468/SciPostPhys.11.3.072. arXiv: 2104.09518 [hep-th].

[36] Sheer El-Showk et al. "Solving the 3D Ising Model with the Conformal Bootstrap". In: *Phys. Rev. D* 86 (2012), p. 025022. DOI: 10.1103/PhysRevD.86.025022. arXiv: 1203.6064 [hep-th].

[37] Filip Kos, David Poland, and David Simmons-Duffin. "Bootstrapping Mixed Correlators in the 3D Ising Model". In: *JHEP* 11 (2014), p. 109. DOI: 10.1007/JHEP11(2014)109. arXiv: 1406.4858 [hep-th].

[38] Sheer El-Showk and Miguel F. Paulos. "Bootstrapping Conformal Field Theories with the Extremal Functional Method". In: *Phys. Rev. Lett.* 111.24 (2013), p. 241601. DOI: 10.1103/PhysRevLett.111.241601. arXiv: 1211.2810 [hep-th].

[39] Sheer El-Showk and Miguel F. Paulos. "Extremal bootstrapping: go with the flow". In: *JHEP* 03 (2018), p. 148. DOI: 10.1007/JHEP03(2018)148. arXiv: 1605.08087 [hep-th].

[40] Ferdinando Gliozzi. "More constraining conformal bootstrap". In: *Phys. Rev. Lett.* 111 (2013), p. 161602. DOI: 10.1103/PhysRevLett.111.161602. arXiv: 1307.3111 [hep-th].

[41] Wenliang Li. "New method for the conformal bootstrap with OPE truncations". In: (Nov. 2017). arXiv: 1711.09075 [hep-th].

[42] Richard S Sutton and Andrew G Barto. *Reinforcement learning: An introduction*. MIT press, 2018.

[43] HEPML-LivingReview. "A Living Review of Machine Learning for Particle Physics". In: (). URL: https://iml-wg.github.io/HEPML-LivingReview/.

[44] Tom Blum, Taku Izubuchi, and et al. "Machine Learning and Lattice QCD". In: (). SnowMass2021, Computational Frontier 3. URL: https://snowmass21.org/computational/start.

[45] Fabian Ruehle. "Data science applications to string theory". In: *Phys. Rept.* 839 (2020), pp. 1–117. DOI: 10.1016/j.physrep.2019.09.005.

[46] T. R. Harvey and A. Lukas. "Quark Mass Models and Reinforcement Learning". In: *JHEP* 08 (2021), p. 161. DOI: 10.1007/JHEP08(2021)161. arXiv: 2103.04759 [hep-th].

[47] Sven Krippendorf, Rene Kroepsch, and Marc Syvaeri. "Revealing systematics in phenomenologically viable flux vacua with reinforcement learning". In: (July 2021). arXiv: 2107.04039 [hep-th].

[48] Andrei Constantin, Thomas R. Harvey, and Andre Lukas. "Heterotic String Model Building with Monad Bundles and Reinforcement Learning". In: (Aug. 2021). arXiv: 2108.07316 [hep-th].

[49] Akinori Tanaka, Akio Tomiya, and Koji Hashimoto. *Deep Learning and Physics*. Springer Singapore, 2021. DOI: 10.1007/978-981-33-6108-9.

[50] Heng-Yu Chen et al. "Machine Learning Etudes in Conformal Field Theories". In: (June 2020). arXiv: 2006.16114 [hep-th].

[51] Tuomas Haarnoja et al. "Soft Actor-Critic: Off-Policy Maximum Entropy Deep Reinforcement Learning with a Stochastic Actor". In: *CoRR* abs/1801.01290 (2018). arXiv: 1801.01290. URL: http://arxiv.org/abs/1801.01290.

[52] Duccio Pappadopulo et al. "OPE Convergence in Conformal Field Theory". In: *Phys. Rev. D* 86 (2012), p. 105043. DOI: 10.1103/PhysRevD.86.105043. arXiv: 1208.6449 [hep-th].

[53] Alejandro Castedo Echeverri, Benedict von Harling, and Marco Serone. "The Effective Bootstrap". In: *JHEP* 09 (2016), p. 097. DOI: 10.1007/JHEP09(2016)097. arXiv: 1606.02771 [hep-th].

[54] Francesco Caracciolo and Slava Rychkov. "Rigorous limits on the interaction strength in quantum field theory". In: *Physical Review D* 81.8 (Apr. 2010). DOI: 10.1103/physrevd.81.085037. URL: https://doi.org/10.1103%2Fphysrevd.81.085037.

[55] Deepmind. URL: https://deepmind.com/research/case-studies/alphago-the-story-so-far.

[56] David Silver et al. "Mastering the game of Go with deep neural networks and tree search". In: *Nature* 529 (2016), pp. 484–489. DOI: 10.1038/nature16961.

[57] David Silver et al. "Mastering the game of Go without human knowledge". In: *Nature* 550.7676 (2017), pp. 354–359. DOI: 10.1038/nature24270. URL: https://doi.org/10.1038/nature24270.

[58] Volodymyr Mnih et al. "Human-level control through deep reinforcement learning". In: *Nature* 518.7540 (2015), pp. 529–533. DOI: 10.1038/nature14236.

[59] Yannis Flet-Berliac et al. "Adversarially Guided Actor-Critic". In: *CoRR* abs/2102.04376 (2021). arXiv: 2102.04376. URL: https://arxiv.org/abs/2102.04376.

[60] T. Lillicrap et al. "Continuous control with deep reinforcement learning". In: *CoRR* abs/1509.02971 (2016).

[61] Volodymyr Mnih et al. *Playing Atari with Deep Reinforcement Learning*. 2013. DOI: 10.48550/ARXIV.1312.5602. URL: https://arxiv.org/abs/1312.5602.

[62] Vijay R. Konda and John N. Tsitsiklis. "Actor-Critic Algorithms". In: 2000, pp. 1008–1014. URL: http://papers.nips.cc/paper/1786-actor-critic-algorithms.

[63] G. A. Rummery and M. Niranjan. *On-Line Q-Learning Using Connectionist Systems*. Tech. rep. TR 166. Cambridge, England: Cambridge University Engineering Department, 1994.

[64] R. S. Sutton et al. "Policy gradient methods for reinforcement learning with function approximation". In: *Advances in Neural Information Processing Systems 12*. Vol. 12. MIT Press, 2000, pp. 1057–1063.

[65] T. Haarnoja. "Acquiring Diverse Robot Skills via Maximum Entropy Deep Reinforcement Learning". UC Berkeley. ProQuest ID: Haarnoja – Berkeley – 0028E – 18530. Merritt ID: ark : /13030/m5x115n2. PhD thesis. URL: https://escholarship.org/uc/item/25g6573w.

[66] R. J. Williams. "Simple statistical gradient-following algorithms for connectionist reinforcement learning". In: *Machine Learning* 8 (1992), pp. 229–256.

[67] Simone Parisi et al. "TD-regularized actor-critic methods". In: *Machine Learning* 108.8-9 (Feb. 2019), pp. 1467–1501. DOI: 10.1007/s10994-019-05788-0. URL: https://doi.org/10.1007%2Fs10994-019-05788-0.

[68] R. Mertig, M. Bohm, and Ansgar Denner. "FEYN CALC: Computer algebraic calculation of Feynman amplitudes". In: *Comput. Phys. Commun.* 64 (1991), pp. 345–359. DOI: 10.1016/0010-4655(91)90130-D.

[69] Jock McOrist, Ilarion V. Melnikov, and Brian Wecht. "Global symmetries and $\mathcal{N} = 2$ SUSY". In: *Lett. Math. Phys.* 107.8 (2017), pp. 1545–1556. DOI: 10.1007/s11005-017-0952-0. arXiv: 1312.3506 [hep-th].

[70] Vladyslav Shtabovenko, Rolf Mertig, and Frederik Orellana. "New Developments in FeynCalc 9.0". In: *Comput. Phys. Commun.* 207 (2016), pp. 432–444. DOI: 10.1016/j.cpc.2016.06.008. arXiv: 1601.01167 [hep-ph].

[71] Vladyslav Shtabovenko, Rolf Mertig, and Frederik Orellana. "FeynCalc 9.3: New features and improvements". In: *Comput. Phys. Commun.* 256 (2020), p. 107478. DOI: 10.1016/j.cpc.2020.107478. arXiv: 2001.04407 [hep-ph].

[72] Daniel Friedan, Zong-an Qiu, and Stephen H. Shenker. "Superconformal Invariance in Two-Dimensions and the Tricritical Ising Model". In: *Phys. Lett. B* 151 (1985), pp. 37–43. DOI: 10.1016/0370-2693(85)90819-6.

[73] J. Polchinski. *String theory. Vol. 1: An introduction to the bosonic string*. Cambridge Monographs on Mathematical Physics. Cambridge University Press, Dec. 2007. ISBN: 978-0-511-25227-3, 978-0-521-67227-6, 978-0-521-63303-1. DOI: 10.1017/CBO9780511816079.

[74] Philip C. Argyres and Nathan Seiberg. "S-duality in N=2 supersymmetric gauge theories". In: *JHEP* 12 (2007), p. 088. DOI: 10.1088/1126-6708/2007/12/088. arXiv: 0711.0054 [hep-th].

[75] Davide Gaiotto. "N=2 dualities". In: *JHEP* 08 (2012), p. 034. DOI: 10.1007/JHEP08(2012)034. arXiv: 0904.2715 [hep-th].

[76] Christopher Beem et al. "The $\mathcal{N} = 2$ superconformal bootstrap". In: *JHEP* 03 (2016), p. 183. DOI: 10.1007/JHEP03(2016)183. arXiv: 1412.7541 [hep-th].

[77] S. Ferrara, M. Porrati, and A. Zaffaroni. "N=6 supergravity on AdS(5) and the SU(2,2/3) superconformal correspondence". In: *Lett. Math. Phys.* 47 (1999), pp. 255–263. DOI: 10.1023/A:1007592711262. arXiv: hep-th/9810063.

[78] Ofer Aharony and Mikhail Evtikhiev. "On four dimensional N = 3 superconformal theories". In: *JHEP* 04 (2016), p. 040. DOI: 10.1007/JHEP04(2016)040. arXiv: 1512.03524 [hep-th].

[79] Inaki Garcıa-Etxebarria and Diego Regalado. "$\mathcal{N} = 3$ four dimensional field theories". In: *JHEP* 03 (2016), p. 083. DOI: 10.1007/JHEP03(2016)083. arXiv: 1512.06434 [hep-th].

[80] Ofer Aharony and Yuji Tachikawa. "S-folds and 4d N=3 superconformal field theories". In: *JHEP* 06 (2016), p. 044. DOI: 10.1007/JHEP06(2016)044. arXiv: 1602.08638 [hep-th].

[81] Yosuke Imamura and Shuichi Yokoyama. "Superconformal index of $\mathcal{N} = 3$ orientifold theories". In: *J. Phys. A* 49.43 (2016), p. 435401. DOI: 10.1088/1751-8113/49/43/435401. arXiv: 1603.00851 [hep-th].

[82] Reona Arai and Yosuke Imamura. "Finite N Corrections to the Superconformal Index of S-fold Theories". In: *PTEP* 2019.8 (2019), 083B04. DOI: 10.1093/ptep/ptz088. arXiv: 1904.09776 [hep-th].

[83] Philip C. Argyres et al. "Expanding the landscape of $\mathcal{N} = 2$ rank 1 SCFTs". In: *JHEP* 05 (2016), p. 088. DOI: 10.1007/JHEP05(2016)088. arXiv: 1602.02764 [hep-th].

[84] Philip C. Argyres, Antoine Bourget, and Mario Martone. "Classification of all $\mathcal{N} \geq 3$ moduli space orbifold geometries at rank 2". In: *SciPost Phys.* 9 (2020), p. 083. DOI: 10.21468/SciPostPhys.9.6.083. arXiv: 1904.10969 [hep-th].

[85] Abhijit Gadde et al. "Gauge Theories and Macdonald Polynomials". In: *Commun. Math. Phys.* 319 (2013), pp. 147–193. DOI: 10.1007/s00220-012-1607-8. arXiv: 1110.3740 [hep-th].

[86] Thomas Bourton, Alessandro Pini, and Elli Pomoni. "4d $\mathcal{N} = 3$ indices via discrete gauging". In: *JHEP* 10 (2018), p. 131. DOI: 10.1007/JHEP10(2018)131. arXiv: 1804.05396 [hep-th].

[87] Mikhail Evtikhiev. "N = 3 SCFTs in 4 dimensions and non-simply laced groups". In: *JHEP* 06 (2020), p. 125. DOI: 10.1007/JHEP06(2020)125. arXiv: 2004.03919 [hep-th].

[88] Takahiro Nishinaka and Yuji Tachikawa. "On 4d rank-one $\mathcal{N} = 3$ superconformal field theories". In: *JHEP* 09 (2016), p. 116. DOI: 10.1007/JHEP09(2016)116. arXiv: 1602.01503 [hep-th].

[89] Madalena Lemos et al. "Bootstrapping $\mathcal{N} = 3$ superconformal theories". In: *JHEP* 04 (2017), p. 032. DOI: 10.1007/JHEP04(2017)032. arXiv: 1612.01536 [hep-th].

[90] Dražen Adamović. "A REALIZATION OF CERTAIN MODULES FOR THE N = 4 SUPERCONFORMAL ALGEBRA AND THE AFFINE LIE ALGEBRA A2(1)". In: *Transformation Groups* 21.2 (2016), pp. 299–327. DOI: 10.1007/s00031-015-9349-2. eprint: 1407.1527.

[91] Jaewon Song. "Macdonald Index and Chiral Algebra". In: *JHEP* 08 (2017), p. 044. DOI: 10.1007/JHEP08(2017)044. arXiv: 1612.08956 [hep-th].

[92] G. C. Shephard and J. A. Todd. "Finite Unitary Reflection Groups". In: *Canadian Journal of Mathematics* 6 (1954), pp. 274–304. DOI: 10.4153/CJM-1954-028-3.

[93] Gabi Zafrir. "An $\mathcal{N} = 1$ Lagrangian for an $\mathcal{N} = 3$ SCFT". In: *JHEP* 01 (2021), p. 062. DOI: 10.1007/JHEP01(2021)062. arXiv: 2007.14955 [hep-th].

[94] Kris Thielemans. "An Algorithmic approach to operator product expansions, W algebras and W strings". PhD thesis. Leuven U., 1994. arXiv: hep-th/9506159.

[95] A. Fujitsu. "ope.math: Operator product expansions in free field realizations of conformal field theory". In: *Comput. Phys. Commun.* 79 (1994), pp. 78–99. DOI: 10.1016/0010-4655(94)90231-3.

[96] Christian Romelsberger. "Counting chiral primaries in N = 1, d=4 superconformal field theories". In: *Nucl. Phys.* B747 (2006), pp. 329–353. DOI: 10.1016/j.nuclphysb.2006.03.037. arXiv: hep-th/0510060 [hep-th].

[97] Jyotirmoy Bhattacharya et al. "Indices for Superconformal Field Theories in 3,5 and 6 Dimensions". In: *JHEP* 02 (2008), p. 064. DOI: 10.1088/1126-6708/2008/02/064. arXiv: 0801.1435 [hep-th].

[98] Lars Grant et al. "Comments on 1/16 BPS Quantum States and Classical Configurations". In: *JHEP* 05 (2008), p. 049. DOI: 10.1088/1126-6708/2008/05/049. arXiv: 0803.4183 [hep-th].

[99] Chi-Ming Chang and Xi Yin. "1/16 BPS states in $\mathcal{N} = 4$ super-Yang-Mills theory". In: *Phys. Rev.* D88.10 (2013), p. 106005. DOI: 10.1103/PhysRevD.88.106005. arXiv: 1305.6314 [hep-th].

[100] Satoshi Nawata. "Localization of N=4 Superconformal Field Theory on $S^1 x S^3$ and Index". In: *JHEP* 11 (2011), p. 144. DOI: 10.1007/JHEP11(2011)144. arXiv: 1104.4470 [hep-th].

[101] Hee-Cheol Kim and Seok Kim. "M5-branes from gauge theories on the 5-sphere". In: *JHEP* 05 (2013), p. 144. DOI: 10.1007/JHEP05(2013)144. arXiv: 1206.6339 [hep-th].

[102] Jakob Lorenzen and Dario Martelli. "Comments on the Casimir energy in supersymmetric field theories". In: *JHEP* 07 (2015), p. 001. DOI: 10.1007/JHEP07(2015)001. arXiv: 1412.7463 [hep-th].

[103] Benjamin Assel et al. "The Casimir Energy in Curved Space and its Supersymmetric Counterpart". In: *JHEP* 07 (2015), p. 043. DOI: 10.1007/JHEP07(2015)043. arXiv: 1503.05537 [hep-th].

[104] Davide Cassani and Dario Martelli. "The gravity dual of supersymmetric gauge theories on a squashed S^1 x S^3". In: *JHEP* 08 (2014), p. 044. DOI: 10.1007/JHEP08(2014)044. arXiv: 1402.2278 [hep-th].

[105] Seyed Morteza Hosseini, Kiril Hristov, and Alberto Zaffaroni. "An extremization principle for the entropy of rotating BPS black holes in AdS_5". In: *JHEP* 07 (2017), p. 106. DOI: 10.1007/JHEP07(2017)106. arXiv: 1705.05383 [hep-th].

[106] Seyed Morteza Hosseini, Kiril Hristov, and Alberto Zaffaroni. "A note on the entropy of rotating BPS $AdS_7 \times S^4$ black holes". In: *JHEP* 05 (2018), p. 121. DOI: 10.1007/JHEP05(2018)121. arXiv: 1803.07568 [hep-th].

[107] Davide Cassani and Lorenzo Papini. "The BPS limit of rotating AdS black hole thermodynamics". In: (2019). arXiv: 1906.10148 [hep-th].

[108] Finn Larsen, Jun Nian, and Yangwenxiao Zeng. "AdS_5 Black Hole Entropy near the BPS Limit". In: (2019). arXiv: 1907.02505 [hep-th].

[109] Sunjin Choi et al. "Large AdS black holes from QFT". In: (2018). arXiv: 1810.12067 [hep-th].

[110] Sunjin Choi et al. "Entropy functions of BPS black holes in AdS_4 and AdS_6". In: (2018). arXiv: 1811.02158 [hep-th].

[111] Francesco Benini and Paolo Milan. "A Bethe Ansatz type formula for the superconformal index". In: (2018). arXiv: 1811.04107 [hep-th].

[112] Francesco Benini and Paolo Milan. "Black holes in 4d $\mathcal{N} = 4$ Super-Yang-Mills". In: (2018). arXiv: 1812.09613 [hep-th].

[113] Joonho Kim, Seok Kim, and Jaewon Song. "A 4d $N = 1$ Cardy Formula". In: (2019). arXiv: 1904.03455 [hep-th].

[114] Alejandro Cabo-Bizet et al. "The asymptotic growth of states of the 4d N=1 superconformal index". In: (2019). arXiv: 1904.05865 [hep-th].

[115] Guglielmo Lockhart and Cumrun Vafa. "Superconformal Partition Functions and Non-perturbative Topological Strings". In: (2012). arXiv: 1210.5909 [hep-th].

[116] Johan Källén and Maxim Zabzine. "Twisted supersymmetric 5D Yang-Mills theory and contact geometry". In: *JHEP* 05 (2012), p. 125. DOI: 10.1007/JHEP05(2012)125. arXiv: 1202.1956 [hep-th].

[117] Johan Källén, Jian Qiu, and Maxim Zabzine. "The perturbative partition function of supersymmetric 5D Yang-Mills theory with matter on the five-sphere". In: *JHEP* 08 (2012), p. 157. DOI: 10.1007/JHEP08(2012)157. arXiv: 1206.6008 [hep-th].

[118] J. Källén et al. "N^3-behavior from 5D Yang-Mills theory". In: *JHEP* 10 (2012), p. 184. DOI: 10.1007/JHEP10(2012)184. arXiv: 1207.3763 [hep-th].

[119] Hee-Cheol Kim, Joonho Kim, and Seok Kim. "Instantons on the 5-sphere and M5-branes". In: (2012). arXiv: 1211.0144 [hep-th].

[120] Hee-Cheol Kim et al. "The general M5-brane superconformal index". In: (2013). arXiv: 1307.7660 [hep-th].

[121] Nikolay Bobev, Mathew Bullimore, and Hee-Cheol Kim. "Supersymmetric Casimir Energy and the Anomaly Polynomial". In: *JHEP* 09 (2015), p. 142. DOI: 10.1007/JHEP09(2015)142. arXiv: 1507.08553 [hep-th].

[122] Francesco Benini and Alberto Zaffaroni. "A topologically twisted index for three-dimensional supersymmetric theories". In: *JHEP* 07 (2015), p. 127. DOI: 10.1007/JHEP07(2015)127. arXiv: 1504.03698 [hep-th].

[123] Francesco Benini, Kiril Hristov, and Alberto Zaffaroni. "Black hole microstates in AdS_4 from supersymmetric localization". In: *JHEP* 05 (2016), p. 054. DOI: 10.1007/JHEP05(2016)054. arXiv: 1511.04085 [hep-th].

[124] Seyed Morteza Hosseini, Itamar Yaakov, and Alberto Zaffaroni. "Topologically twisted indices in five dimensions and holography". In: *JHEP* 11 (2018), p. 119. DOI: 10.1007/JHEP11(2018)119. arXiv: 1808.06626 [hep-th].

[125] Stefano Cremonesi. "An Introduction to Localisation and Supersymmetry in Curved Space". In: *PoS* Modave2013 (2013), p. 002. DOI: 10.22323/1.201.0002.

[126] Nicole Berline and Michèle Vergne. "Classes caractéristiques équivariantes. Formule de localisation en cohomologie équivariante". In: *CR Acad. Sci. Paris* 295.2 (1982), pp. 539–541.

[127] M. F. Atiyah and R. Bott. "The Moment map and equivariant cohomology". In: *Topology* 23 (1984), pp. 1–28. DOI: 10.1016/0040-9383(84)90021-1.

[128] M. F. Atiyah and I. M. Singer. "The Index of Elliptic Operators: I". In: *Annals of Mathematics* 87.3 (1968), pp. 484–530. ISSN: 0003486X. URL: http://www.jstor.org/stable/1970715 (visited on 06/27/2022).

[129] J. Fuchs and C. Schweigert. *Symmetries, Lie algebras and representations: A graduate course for physicists*. Cambridge University Press, Oct. 2003. ISBN: 978-0-521-54119-0.

[130] Ofer Aharony et al. "The Hagedorn - deconfinement phase transition in weakly coupled large N gauge theories". In: *Adv. Theor. Math. Phys.* 8 (2004). [,161(2003)], pp. 603–696. DOI: 10.4310/ATMP.2004.v8.n4.a1. arXiv: hep-th/0310285 [hep-th].

[131] P. K. Townsend and P. van Nieuwenhuizen. "Gauged Seven-Dimensional Supergravity". In: *Phys. Lett.* B125 (1983), pp. 41–46. DOI: 10.1016/0370-2693(83)91230-3.

[132] Z. -W. Chong et al. "Non-extremal charged rotating black holes in seven-dimensional gauged supergravity". In: *Phys. Lett.* B626 (2005), pp. 215–222. DOI: 10.1016/j.physletb.2005.07.054. arXiv: hep-th/0412094 [hep-th].

[133] David D. K. Chow. "Equal charge black holes and seven dimensional gauged supergravity". In: *Class. Quant. Grav.* 25 (2008), p. 175010. DOI: 10.1088/0264-9381/25/17/175010. arXiv: 0711.1975 [hep-th].

[134] Mirjam Cvetic et al. "Rotating black holes in gauged supergravities: Thermodynamics, supersymmetric limits, topological solitons and time machines". In: (2005). arXiv: hep-th/0504080 [hep-th].

[135] W. Chen, H. Lu, and C. N. Pope. "Mass of rotating black holes in gauged supergravities". In: *Phys. Rev.* D73 (2006), p. 104036. DOI: 10.1103/PhysRevD.73.104036. arXiv: hep-th/0510081 [hep-th].

[136] James T. Liu and Ruben Minasian. "Black holes and membranes in AdS(7)". In: *Phys. Lett.* B457 (1999), pp. 39–46. DOI: 10.1016/S0370-2693(99)00500-6. arXiv: hep-th/9903269 [hep-th].

[137] Edward Witten. "Anti-de Sitter space and holography". In: *Adv. Theor. Math. Phys.* 2 (1998), pp. 253–291. DOI: 10.4310/ATMP.1998.v2.n2.a2. arXiv: hep-th/9802150 [hep-th].

[138] Yosuke Imamura. "Perturbative partition function for squashed S^5". In: *PTEP* 2013.7 (2013), 073B01. DOI: 10.1093/ptep/ptt044. arXiv: 1210.6308 [hep-th].

[139] Daniel L. Jafferis and Silviu S. Pufu. "Exact results for five-dimensional superconformal field theories with gravity duals". In: *JHEP* 05 (2014), p. 032. DOI: 10.1007/JHEP05(2014)032. arXiv: 1207.4359 [hep-th].

[140] Mathew Bullimore and Hee-Cheol Kim. "The Superconformal Index of the (2,0) Theory with Defects". In: *JHEP* 05 (2015), p. 048. DOI: 10.1007/JHEP05(2015)048. arXiv: 1412.3872 [hep-th].

[141] Christopher Beem, Leonardo Rastelli, and Balt C. van Rees. "$\mathcal{W}$ symmetry in six dimensions". In: *JHEP* 05 (2015), p. 017. DOI: 10.1007/JHEP05(2015)017. arXiv: 1404.1079 [hep-th].

[142] Prarit Agarwal and Antonio Amariti. "Notes on S-folds and $\mathcal{N} = 3$ theories". In: *JHEP* 09 (2016), p. 032. DOI: 10.1007/JHEP09(2016)032. arXiv: 1607.00313 [hep-th].

[143] Luigi Tizzano and Jacob Winding. "Multiple sine, multiple elliptic gamma functions and rational cones". In: (2014). arXiv: 1502.05996 [math.CA].